

**Bottom-up Self-Assembly across Hierarchies:
From Triblock Terpolymers to
Patchy Particles to Colloidal (Co-)Polymers**

DISSERTATION

zur Erlangung des akademisches Grades eines Doktors der
Naturwissenschaften (Dr. rer. nat.) im Fach Chemie der Fakultät für
Biologie, Chemie und Geowissenschaften der Universität Bayreuth

vorgelegt von

André H. Gröschel

Geboren in Pegnitz

Bayreuth, 2012

Die vorliegende Arbeit wurde in der Zeit von Januar 2008 bis September 2012 am Lehrstuhl Makromolekulare Chemie II unter der Betreuung von Prof. Dr. Axel H. E. Müller angefertigt.

Vollständiger Abdruck der von der Fakultät für Biologie, Chemie und Geowissenschaften der Universität Bayreuth zur Erlangung des akademischen Grades eines Doktors der Naturwissenschaften genehmigten Dissertation.

Dissertation eingereicht am: 07.10.2012

Zulassung durch die Prüfungskommission: 15.11.2012

Wissenschaftliches Kolloquium: 05.12.2012

Amtierende Dekanin: Prof. Dr. Beate Lohnert

Prüfungsausschuss:

Prof. Dr. Axel H. E. Müller (Erstgutachter)

Prof. Dr. Stephan Förster (Zweitgutachter)

Prof. Dr. Birgit Weber (Vorsitz)

Prof. Dr. Karlheinz Seifert

**“Daß ich erkenne, was die Welt,
im Innersten zusammenhält,...**”

(Faust I)

Anita

Sebastian

Tina

**In besonderem Gedenken an
Klaus Gröschel**

Table of Contents

Summary	1
Zusammenfassung	3
List of Abbreviations	5
1 Introduction	7
1.1 Block Copolymer Self-Assembly.....	10
1.1.1 Diblock Copolymer Morphologies in Solution.....	12
1.1.2 Compartmentalization in Block Copolymer Blends.....	15
1.1.3 Complex Morphologies of ABC Triblock Terpolymers.....	17
1.1.3.1 Multicompartment Micelles by Direct Dispersion.....	19
1.1.3.2 Compartmentalized Structures via Bulk Morphologies.....	23
1.2 Colloidal Self-Assembly.....	25
1.2.1 Superstructures of Janus Particles.....	28
1.2.2 Directed Self-Assembly of ABA Colloids.....	29
1.2.3 Bottom-up Multilevel Hierarchical Self-Assembly.....	31
1.2.4 Co-Assembly.....	34
1.3 Hybrid Materials Based on Self-Assembly.....	37
1.4 Objective of this Thesis.....	42
References.....	42
2 Thesis Overview	51
2.1 Bottom-up Structuring of Patchy Particles and Next Level Self-Assembly.....	52
2.2 Mixed Colloidal Co-Assemblies from Patchy Particles.....	56
2.3 Novel Solution-Based Approach to Janus Micelles via Cross-linking of Spherical Multicompartment Micelles.....	60
2.4 Janus Particle/Multi-Walled Carbon Nanotube Hybrids.....	64
2.5 <i>Individual Contributions to Joint Publications</i>	69
3 Precise Hierarchical Self-Assembly of Multicompartment Micelles	71
4 Guided Hierarchical Co-Assembly of Soft Patchy Nanoparticles	115
5 Facile, Solution-Based Synthesis of Soft, Nanoscale Janus Particles with Tunable Janus Balance	145

6 Janus Particles as Effective Supracolloidal Dispersants for Carbon Nanotubes.....	179
7 List of Publications.....	203
8 Conference Appearances.....	204
9 Acknowledgements.....	205

Summary

In this work the bottom-up self-assembly of compartmentalized particles on multiple hierarchical levels was investigated. The basic building blocks of the lowest level, ABC triblock terpolymers, were directed into nano-scale corona-compartmentalized (patchy) particles via selection of kinetic self-assembly paths using the simplest directing agent, solvent selectivity. An extremely efficient and versatile step-wise self-assembly process was developed offering unique control to nano-engineer the addressable surfaces patches. Thereby, carefully chosen solvent sequences were of outmost importance. Depending on the volume ratio of the core forming blocks, V_A/V_B , two species differing in the geometrical distribution of the patches were identified: for $V_A/V_B > 1$, a Janus-like distribution, with patches A and C emanating from opposing sides of the B core and for $V_A/V_B < 1$ an ABA distribution, with two A patches on opposing sides of the B core, which is protected by an equatorial C corona. The responsive particles were then used as colloidal building blocks (CBBs) that, upon addition of non-solvent for the A patches, underwent next level hierarchical self-assembly. Thereby, AB CBBs self-assemble into homogeneous spherical multicompartment micelles (MCMs) with precise control over aggregation number via the volume ratio, V_A/V_B . In contrast, ABA CBBs grow into extended, worm-like linear colloidal polymers of up to several micrometres in length via a step-growth polymerization process. The cluster size $(AB)_x$ and the worm-length $(ABA)_x$ are both conveniently controlled by the solvent quality for the corona block (expansion/contraction). This dynamic tuning of the corona volume is a unique key feature of the bottom-up approach to soft patchy particles from triblock terpolymers and plays a decisive role in the co-assembly of multiple CBBs.

In a consecutive work, the AB and ABA CBBs were mixed in specific ratios prior to non-solvent addition for the A patches. With both CBBs present, aggregation via mutual A patches into mixed colloidal co-assemblies was accomplished. Colloidal co-assembly is a hierarchical structuring process crossing multiple levels that is primarily driven by the minimization of energetically unfavourable non-solvent/polymer interfaces and critically depends on both the dynamic volumes change of the corona and aggregating patches on solvent polarity. The extraordinary quality of the superstructures is ascribed to the selection of kinetic pathways for self-and co-assembly and similarly, to the dynamic tailoring of patch volume and attractiveness, respectively. Particles with a large C corona, but small attractive A patch are stable over broad a range of solvent/non-solvent compositions for A. On the contrary, particles with a small C corona, but large attractive A patch will start clustering even with the slightest addition of non-solvent for A. Hence, the mismatch of onset of self-assembly is a set screw to either form the colloidal “substrate” first that is decorated

subsequently or vice versa. Both approaches lead to different, well-defined and predictable mixed colloidal co-assemblies comprising colloidal molecules, alternating colloidal co-assemblies, multiblock co-assemblies, telechelic oligomers, ternary co-assemblies and two-dimensional networks, all of which are only accessible with the presented approach.

The spherical MCM consists of CBBs of the AB-type composed of a B-core with a Janus-like distribution of the A and C blocks as a result of symmetry breaking during cluster formation in nonsolvents for A. This phase separation represents a novel and versatile route for the template-free synthesis of terpolymer-based, sub 100 nm Janus particles. The synthesis encompasses simple cross-linking of the patches of spherical MCMs to preserve the phase-separated state of all blocks. This approach to narrowly dispersed Janus particles offers unique handles to nano-engineer the core diameter, the Janus balance (volume ratio of A and C hemispheres) and the chemistry of the patches. The defined formation of MCMs even at very high concentrations of 100 g/L enables high throughput synthesis of soft Janus particles making this novel approach technologically relevant. Beyond that, the Janus balance proved decisive for cluster shape and size when the particles were subjected to a selective solvent for either of the hemispheres.

The Janus particles (JPs) with tailored Janus balance were applied as dispersants for multi-walled carbon nanotubes (MWNTs). Thereby, the JPs attach to the MWNTs with a suitable hydrophobic patch (polystyrene), while facilitating stabilization in the solvent with the other patch. Depending on the Janus balance, i.e., the size ratio of adsorbing to stabilizing patch, dense multilayers were obtained or helical arrangements with defined JP-JP interparticle spacing. In both cases, the quantity of attached JPs was substantial and unparalleled. Besides the known applications of JPs in emulsion polymerization and as compatibilizers in polymer blends, JPs are also effective, non-covalent coatings for MWNTs and may also find application as dispersants for insoluble particulate matter in general.

Zusammenfassung

Im Rahmen dieser Arbeit wurde die Selbstassemblierung von kompartmentierten Partikeln über mehrere hierarchische Ebenen nach dem *Bottom-Up*-Prinzip untersucht. Zunächst wurden oberflächenstrukturierte (patchy) Partikel aus ABC-Triblockterpolymeren aufgebaut, welche Einheiten der niedrigsten Hierarchieebene darstellen. Dies wird über einen kinetischen Selbstassemblierungsprozess über ein selektives Fällungsmittel für den Mittelblock erreicht, gefolgt von Dialyse in ein selektives Lösungsmittel, das nur den C-Block löst. Der hier entwickelte stufenweise Selbstassemblierungsprozess eröffnet eine einzigartige Kontrolle über die Nanostrukturierung adressierbarer Oberflächenpatches. Dabei ist die Lösungsmittelsequenz von entscheidender Bedeutung. Abhängig vom Volumenverhältnis der kernbildenden Blöcke (V_A/V_B) konnten zwei Spezies identifiziert werden, die sich in der geometrischen Anordnung der adressierbaren Segmente unterscheiden. Bei einem Volumenverhältnis von $V_A/V_B > 1$ ordnen sich die Segmente A und C Janus-ähnlich an, d.h. sie befinden sich auf gegenüberliegenden Seiten des B-Kerns (AB-Verteilung der solvophoben Blöcke), wohingegen eine ABA Verteilung der solvophoben Segmente auftritt wenn das Volumenverhältnis $V_A/V_B < 1$ ist. Hier formt B den Kern, jedoch liegen sich die adressierbaren A-Segmente gegenüber und werden von der C-Korona äquatorial abgeschirmt. Diese Partikel wurden als kolloidale Bausteine (*colloidal building blocks* – CBBs) verwendet, die bei Zugabe von Fällungsmittel für die A-Segmente zur nächsten Stufe der hierarchischen Selbstassemblierung führen. Dabei bilden die AB-Bausteine homogene sphärische Multikompartiment-Mizellen (MCMs) aus, wohingegen die ABA-Bausteine über eine Stufenwachstumspolymerisation zu mehreren mikrometerlangen wurmartigen kolloidalen Polymeren heranwachsen. Sowohl die Cluster-Größe $(AB)_x$ als auch die Wurm-Länge $(ABA)_x$ wird durch Zugabe von Fällungs- bzw. Lösungsmittel und die damit zusammenhängende Korona-Expansion bzw. -Kontraktion gesteuert. Diese Kontrolle ist ein wesentliches Element, um mittels des *Bottom-Up*-Prinzips von linearen Triblockterpolymeren zu weichen patchy Partikeln zu gelangen und spielt bei der nachfolgenden Co-Assemblierung verschiedener CBBs eine ausschlaggebende Rolle.

In der Folge wurden AB- und ABA-Bausteine in bestimmten Verhältnissen gemischt was zu kolloidaler Co-Assemblierung führt. Dieser von selbst ablaufende, hierarchische Strukturierungsprozess umfasst mehrere Stufen und wird primär durch die Minimierung der energetisch ungünstigen Fällungsmittel-Polymer-Grenzfläche erreicht und hängt sowohl empfindlich vom dynamischen Volumen der Partikel und der aggregierenden Segmenten ab. Die Qualität dieser Überstrukturen ist auf den verwendeten kinetischen Selbstassemblierungspfad und das dynamisch einstellbare Segmentvolumen sowie deren attraktiver Wechselwirkung zurückzuführen. Besitzen die Partikel eine große C-Korona und ein klei-

nes solvophobes A-Segment, sind diese über einen breiten Bereich von Fällungs-/Lösungsmittel für A stabil, wohingegen Partikel mit großem A-Segment und kleiner C-Korona bei Zugabe von Fällungsmittel für A sofort aggregieren, da die Corona das solvophobe A-Segment nicht mehr ausreichend abschirmt. Der unterschiedliche Beginn der Selbstassemblierung kann ausgenutzt werden, um entweder zuerst das „kolloidale Substrat“ zu schaffen, dass im Anschluss dekoriert wird oder umgekehrt. Beide Ansätze führen zu unterschiedlich gemischten kolloidalen Co-Assemblierungen, wie etwa kolloidale Moleküle, alternierende kolloidale Aggregate, Multiblock Strukturen, telechele Oligomere, ternäre Co-Assemblierungen und zwei-dimensionale Netzwerke. Solch komplexe Strukturen sind ausschließlich mit dem hier vorgestellten Ansatz möglich.

Die sphärischen MCMs bestehen aus Bausteinen des AB-Typs mit einem B-Kern und einer Janus-Verteilung der A und C-Blöcke. Dieser Aufbau ist ein Resultat des Symmetriebruchs während der Clusterbildung durch Zugabe von Fällungsmittel für A. Diese Phasenseparation entspricht einem völlig neuen und vielseitigen Syntheseweg terpolymer-basierter Januspartikel (JP) im sub-100 nm Bereich ohne dass ein Templat benötigt wird. Die Synthese umfasst das Vernetzen der B-Kompartimente der sphärischen MCMs, um sowohl die Janus Partikel als auch die Phasenseparation dauerhaft zu fixieren. Die JP können mit einer engen Größenverteilung hergestellt werden, wobei sich der Kerndurchmesser, die Janus-Balance (d.h. das Größenverhältnis der beiden Koronasegmente) und die Chemie der Koronasegmente präzise steuern lassen. Trotz hoher Konzentrationen (100 g/L) wurden definierte MCMs erhalten, was einen Weg eröffnet JP in großem Maße herzustellen und die technologische Relevanz dieser Methode unterstreicht. Darüber hinaus kann durch Einstellen der Janus-Balance die Clusterform und -größe in selektiven Fällungsmitteln für eine der Koronasegmente vorherbestimmt werden.

Die JP mit maßgeschneiderter Janus-Balance wurden als Dispergierungsmittel für mehrwandige Kohlenstoffnanoröhren (*multi-walled carbon nanotubes* - MWNTs) eingesetzt. Die JP binden sich dabei über physikalische Wechselwirkungen mit einem geeigneten solvophoben Koronasegment (Polystyrol) an die Oberfläche der MWNTs und werden gleichzeitig vom solvophilen Koronasegment stabilisiert. Abhängig von der Janus-Balance bilden sich bei kurzen stabilisierenden Koronasegmenten dichte Multilagen aus oder aber spiralförmige Anordnungen mit einem definierten JP-JP Abstand im Falle eines langen Koronasegmentes. Ungeachtet davon ist die Anzahl der anhaftenden JPs bislang unerreicht und grundlegend für Langzeitstabilität verantwortlich. Dieses Ergebnis zeigt, dass JP neben den bereits bekannten Anwendungen auch als effektive, nicht kovalente Beschichtung für MWNTs dienen können und darüber hinaus generell als Dispergierungsmittel für unlösliche Partikel in Betracht gezogen werden können.

List of Abbreviations

1D, 2D, 3D	one-, two-, three-dimensional
¹H-NMR	proton nuclear magnetic resonance
AAO	anodized aluminium oxide
AFM	atomic force microscopy
ATRP	atom transfer radical polymerization
BCC	body centred cubic
CBB(s)	colloidal building block(s)
CNT	carbon nanotubes
Cryo-TEM	cryogenic transmission electron microscopy
DSC	differential scanning calorimetry
DLS	dynamic light scattering
DMAc	<i>N,N</i> -dimethylacetamide
DNA	deoxyribonucleic acid
DP_n	number-average degree of polymerization
<i>f_x</i>	block weight fraction of block X
GPC	gel permeation chromatography
HCl	hydrogen chloride
IPEC	interpolyelectrolyte complex
JM(s)	Janus micelle(s)
JP(s)	Janus particle(s)
la3d	lyotropic phase
Lucirin TPO[®]	diphenyl(2,4,6-trimethylbenzoyl)phosphine oxide
MCC(s)	multicompartment cylinder(s)
MCM(s)	multicompartment micelle(s)
MWNT(s)	Multi-Walled Carbon Nanotube(s)
MWCO	molecular weight cut-off
MWD	molecular weight distribution
NFC	nanofibrillated cellulose
<i>Nn</i>BEO	PNIPAM- <i>b</i> -P <i>n</i> BA- <i>b</i> -PEO
NP(s)	nanoparticle(s)
OsO₄	osmium tetroxide
P2VP	poly(2-vinylpyridine)
PAA	poly(acrylic acid)
PAm	poly(acryl amide)
PB	polybutadiene
PCE(M)A	poly(2-(cinnamoyloxy)ethyl (meth)acrylate)
PCL	poly(ϵ -caprolactone)
PDI	polydispersity index
PDMAEMA	poly(2-(dimethylamino)ethyl methacrylate)
PDMS	polydimethylsiloxane

PE	polyethylene
PEO	polyethylene oxide
P/B	poly(C ₆ F ₁₃ C ₂ H ₄ S-ethylethylene)
PFG	poly(ferrocenyldimethyl germane)
PFS	poly(ferrocenyldimethyl silane)
PHEMA	poly(2-hydroxyethyl methacrylate)
PMMA	poly(methyl methacrylate)
PMPC	poly(2-(methacryloyloxy) ethylphosphorylcholine)
PnBA	poly(<i>n</i> -butyl acrylate)
PNIPAM	poly(<i>N</i> -isopropylacrylamide)
POEGMA	poly[oligo (ethylene glycol) methyl ether methacrylate]
PTMS-HEMA	poly(2-(trimethylsiloxy)ethyl methacrylate)
PS	polystyrene
PSS	poly(styrenesulfonate), poly(styrenesulfonic acid)
PtBA	poly(<i>tert</i> -butyl acrylate)
PtBMA	poly(<i>tert</i> -butyl methacrylate)
PTFE	poly(tetrafluorethylene)
PtS	poly(4- <i>tert</i> -butoxy-styrene)
PVMeI	poly(2-methylvinyl-pyridinium iodide)
PVP	poly(vinylpyrrolidone)
PXRD	powder X-ray diffractometry
$R_{h,app}$	apparent hydrodynamic radius
RI	refractive index
RuO₄	ruthenium tetroxide
SEC	size exclusion chromatography
SEM	scanning electron microscopy
SBM	PS- <i>b</i> -PB- <i>b</i> -PMMA
SBMAA	PS- <i>b</i> -PB- <i>b</i> -PMAA
SBV	PS- <i>b</i> -PB- <i>b</i> -P2VP
<i>t</i>ACD	PtBA - <i>b</i> -PCEMA- <i>b</i> -PDMAEMA
TCD	PtBMA - <i>b</i> -PCEMA- <i>b</i> -PDMAEMA
TEM	transmission electron microscopy
T_g	glass transition temperature
THF	tetrahydrofuran
TiO₂	titanium dioxide
TMS-HEMA	2-(trimethylsilyloxy)ethyl methacrylate
<i>t</i>SBT	PtS- <i>b</i> -PB- <i>b</i> -PtBMA
TVB	PtBMA- <i>b</i> -P2VP- <i>b</i> -PB
χ_{XY}	Chi-parameter between blocks X and Y

1 Introduction

Modern materials science and soft nanoscience are rapidly evolving fields of high diversity that, over the last two decades, witnessed great progress in miniaturization and functionalization. Inspired by nature's unmatched ability to create and replicate highly complex structures and to optimize structure-property relations via self-organization and self-assembly processes, hierarchical self-assembly established itself as a versatile and powerful tool for the energy efficient bottom-up structuring of bulk materials, surface patterns or nanoobjects in solution.^[1-6] Self-assembly is currently the key tool pushing innovative design towards artificial materials that are "smart",^[7-9] biomimetic,^[10-12] ultra strong,^[13, 14] replace tissue,^[15, 16] revolutionize electronics^[17] or optics^[18-22] and will have, without a doubt, a tremendous impact on our future lives.^[3] Especially responsive, self-healing and self-replicating systems are extremely important on the road to reach one ultimate goal, artificially mimic nature on the cellular level.

The field of self-assembly encompasses the rearrangement of discrete components or building blocks into superstructures with well-defined symmetry, fascinating architecture and often incredibly long-range order. Building blocks may be as small as atoms or molecules such as ions, surfactants and peptides summarized under the term supramolecular self-assembly^[5, 23] or as large as millimetre-sized objects^[24] such as magnets,^[25] beads^[17] or droplets.^[26] Most research interest, however, has been focused on polypeptides and block copolymers,^[27-33] shape anisotropic and patchy nanoparticles,^[34-38] or silica and latex colloids,^[39-43] as promising new effects and properties are eagerly anticipated on these nano-, meso- and micro-scales. Self-assembly and self-organization are concepts that are often interchanged, although one widely accepted definition clearly distinguishes self-organization as a "dynamic self-assembly" process far from equilibrium, continuously dissipating energy to stay "alive", from self-assembly that remains static after the system reached a thermodynamic stable or meta-stable state of equilibrium.^[1] Once self-organized constructs run out of "fuel", they fall apart into their underlying building blocks (metaphorical death). Fuel comes in many forms, e.g., thermal or kinetic energy, magnetic alignment or compounds capable of storing and delivering energy (e.g., adenosine triphosphate in living cells). Once the building blocks are fuelled again, simple systems can be revived and retain its original function. All living and self-replicating systems found in nature such as cells, viruses, bacteria, fish swarms, the weather and eco systems, are, to a certain extent, based on self-organization continuously adapting to the environment. In static self-assembly the building blocks acquire a structure dictated by pre-programmed, geometrically positioned responses and the outcome can be anticipated accordingly. In equilibrium,

they will reside in a predefined geometric form and as long as there is no energy feed, the static structure remains intact. The system preferably settles in the most favourable energetic state (also meta-stable). Static self-assembly is mostly found in crystal growth (atomic, molecular, liquid or colloidal), deposited layers of colloids or polymer (monolayers, membranes or bulk morphologies) and solution-based aggregates (micelles, vesicles, colloidal polymers).

Self-assembly is one of the most frequently used principles in material science, soft matter and nanotechnology, and hence, over the last two decades, a steadily increasing number of publications deal with this subject. In 2011 the article count peaked in almost 9000 publications with about one third specifically in the field of polymer science (Figure 1–1). This is easily understood considering the simplicity with which e.g., block copolymers can be tailored and manipulated to form sophisticated structures. Thereby, the strategy of bottom-up self-assembly is especially interesting as it is not only energy efficient, but also appealing when constructing nanomaterials for biological or biomedical applications, as constructs prepared by this approach are able to fall apart into its individual building blocks if required.

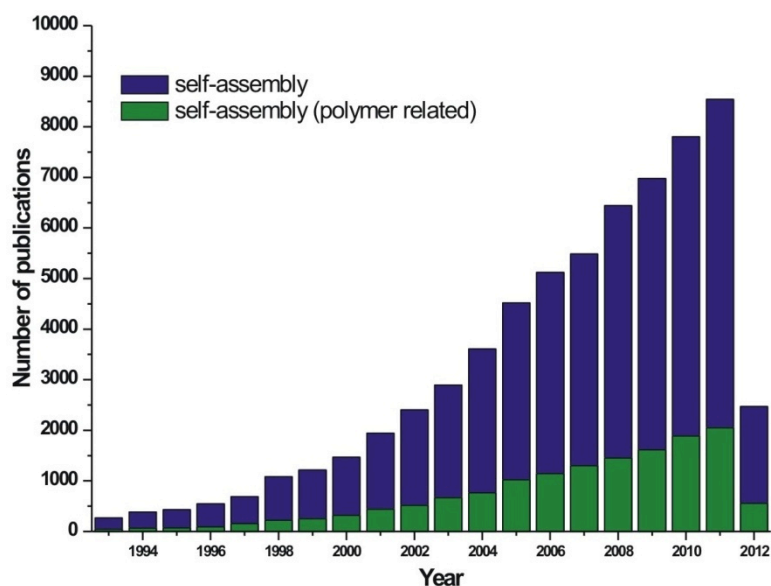


Figure 1–1: Stacked column bars illustrating the immense impact of self-assembly over last 20 years. Publications containing the phrase “self-assembly” in the title (blue) compared to those containing both “polymer” plus “self-assembly” (green).

Although self-assembly happens spontaneously, the outcome can be manipulated into specific directions applying building blocks with orthogonal functionality that start to aggregate when proper external stimuli are applied. Stimuli or directing agents are diverse and basically any change of physical field strength comprising solvent polarity, pH, salinity, electrostatics, photon energy, shear stress, oxidation/reduction, templates, capillary forces or many others.^[9, 38] The production of suitable building blocks and knowledge about driving forces will allow access to multiple hierarchies, level by level, and will be of quintes-

sential importance for structuring of future materials. In an idealized experiment all hierarchical levels would be crossed starting by the smallest possible component. One can imagine mixing very basic molecules or even atoms and self-assembly across all length scales would occur by itself. Monomers (< 1 nm) would polymerize into monodisperse macromolecules with responsive segments or polymer blocks (1 – 10 nm) able to self-assemble into complex particles with attractive surface patches (10 – 100 nm). Some patchy particles aggregate into electrically conducting streaks some into contracting muscle-like strains (μm – mm), while others form vesicular cell mimics and in the end a fully functioning artificial heart would emerge (100 mm). Of course, that such a sophisticated self-assembly process is highly unlikely (not to say impossible), but today, we can already bridge multiple hierarchies by diblock-, triblock or multiblock copolymers, whereas each block may selectively respond to directing agents. Consequently, an increasing number of responses confined within one multiblock copolymer will allow crossing and increasing number of hierarchies, level by level, simply changing one stimulus after the other. For instance, the solution self-assembly of amphiphilic diblock copolymers into spherical micelles by proper choice of solvent polarity mirrors our basic understanding of how randomly distributed building blocks arrange into highly symmetrical spheres. However, for every hierarchy level one selective stimulus needs to be programmed into the building block and it is very desirable to design building blocks capable of self-assembling from one hierarchy into the next, multiple times. Here, directed self-assembly offers elegant means of manipulating block copolymers several nanometres in size into dozens of nanometre patchy particles and further into micrometre long superstructures, whereas without direction usually mere phase separation of multiple blocks into ill-defined aggregates takes place.

This introduction does not encompass all facets of self-assembly, but rather tries to communicate the most important aspects of polymer and colloidal self-assembly to provide a comprehensive understanding of how nanostructuring of 3D objects can be realized. It also tries to extend existing (yet often neglected) parallels between diblock copolymer bulk and solution morphologies and project known concepts on triblock terpolymer system colloidal self-assembly as well. Hopefully these considerations may provide researchers with explanations for puzzling findings or generally alter design criteria for building block architecture. Therefore, this introduction is divided into three major sections with a somewhat unconventional treatment of the subject multicompartment micelles (MCMs). In the first section, the self-assembly of block copolymers is reviewed containing a brief discussion of basics and recent developments in diblock copolymer self-assembly. The following chapters will then treat of MCMs formed by three polymer blocks, i.e., either by blending of two diblock copolymers with one common block or covalently linked triblock terpolymer. This first section then concludes with a brief excerpt about the use of bulk morphologies as a quasi directing or templating method, popularizing de-symmetrized nanoparticles that are otherwise inaccessible. This part also aids as introduction to the second major section: col-

loidal self-assembly. The self-assembly of colloidal building blocks is currently pursued with great emphasis on the preparation of colloidal crystals of shape-anisotropic particles. The decoration of colloidal particles with responsive surface pattern able to undergo hierarchical self-assembly in solution is equally intriguing, whereas the formation of some MCMs mechanistically falls into this category due to reasons that are elaborated in the respective sections. Going beyond self-assembly, co-assembly of multiple polymers and colloids will be briefly introduced at the end of this section. The last section then concludes this introduction presenting functional materials based on self-assembly processes that unify outstanding physical and mechanical properties as well as an assessment of potential future directions in the field.

1.1 Block Copolymer Self-Assembly

A versatile and adaptive self-assembly process involves building blocks that are readily prepared and easily manipulated, preferably with a multitude of selective stimuli. The most important requirement for self-assembly is mobility as otherwise the building blocks cannot rearrange upon the applied stimulus. Best control over the superstructure formation is guaranteed when the stimulus is, above all, selective. Block copolymers, i.e., two or more different polymer blocks with inherent immiscibility covalently linked in a sequential fashion, are very attractive building blocks for any self-assembly process as they combine several advantageous features:

- (i) Simple design and synthesis of diblock, triblock or multiblock copolymers; each block may respond selectively to a specific stimuli;
- (ii) Control over short-range attraction via linkage between the blocks (covalent, coordinating, electrostatic, hydrogen bonding), long-range repulsion by nature of the monomer and immiscibility of the blocks, respectively;
- (iii) Simple tailoring of phase volumes via block lengths;
- (iv) Mobility in solvents and on surfaces/interfaces.

A lot of effort was put into the detailed analysis of which parameters direct block copolymers in bulk and in selective solvents into periodic structures with tuneable symmetry and geometry. Many prominent applications are based on spherical, cylindrical, gyroidal and lamellar morphologies or their solution pendants, micelles, worm-like micelles, bicontinuous networks and vesicles (Figure 1–2).^[31, 32, 44-57] All self-assembly processes in bulk or solution are, to some extent, directed, as solvent selectivity towards blocks already pre-determines the solvophobic core and solvophilic corona. For the preparation of bulk morphologies, block copolymers need to be mobilized in a common solvent for all blocks and thus, the obtained morphologies are typically in thermodynamic equilibrium after drying. Of course, self-assembly relies on block-block immiscibility and in solution especially on the block-solvent incompatibility (selectivity), but striking parallels have been drawn be-

tween morphologies in solution and bulk.^[47, 58, 59] The intermittent lyotropic phases observed in concentrated solutions display similarities of both solution and bulk morphologies,^[60] and may be seen as a transition state between the two extremes corroborating an underlying mechanism of formation.

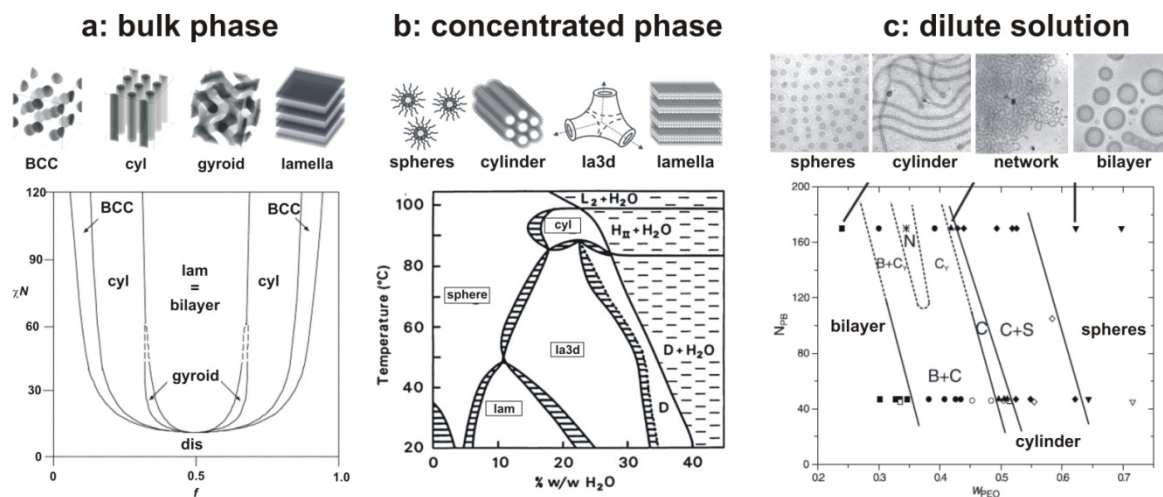


Figure 1–2: Sphere, cylinder, bicontinuous and bilayer morphology. (a) Typically obtained bulk and inverse bulk morphologies of AB diblock copolymers. Adapted from [53]. Reprinted with permission from Elsevier. (b) Schematic of almost identical sphere, hexagonal cylinder, la3d and lamellar morphologies observed for amphiphiles in concentrated lyotropic phases. Adapted from [60]. Reprinted with permission from Royal Society of Chemistry. (c) Transition of micellar morphologies from sphere to vesicle in dilute solutions of an amphiphilic diblock copolymer (PB-*b*-PEO). Adapted from [49]. Reprinted with permission from the American Association for the Advancement of Sciences. Transition states involve cylindrical micelles and dense bicontinuous networks.

An AB diblock copolymer with a volume fraction in favour of block A (e.g., $\phi_A = 0.8$) will form a bulk morphology of B cylinders embedded within an A matrix (Figure 1–2a). In a solvent for A, however, the A corona is strongly swollen, which dramatically increases its volume fraction ($\phi_A \rightarrow 1$) resulting in star-like micelles (Figure 1–2c). Conceptually, the polymer/solvent phase, here A/S, is yet another extremely expanded matrix. Addition of specific non-solvent content for A, dynamically reduces the corona volume (contraction) and simulates bulk conditions by approaching the bulk volume of the A block (back to $\phi_A = 0.8$) and altering the solution morphology to cylindrical micelles. Addition of solvent for the B block and swelling of the B core, respectively, increases ϕ_B and has the same effect. Although these considerations are simplified as other parameters (interfacial tension, surface curvature, chain packing) also play a crucial role in bulk as well as solution, this already demonstrates that dynamic alteration of the volume fractions gives access to a large number of structures in solution that may exist between the two extremes, fully collapsed A blocks in bulk and fully expanded A corona in dilute solutions. As this thesis mostly deals with ABC triblock terpolymers, the immediate question arises, if similar considerations are feasible for terpolymer systems displaying much more complex morphologies, which is discussed in chapter 1.1.3.

1.1.1 Diblock Copolymer Morphologies in Solution

Spherical, worm-like and large compound micelles as well as vesicles are among the simplest and most documented solution morphologies comprehensively described in many ground-breaking works by Eisenberg, Armes, Discher, Förster and many others (Figure 1–3).^[48, 51, 54, 61-69]

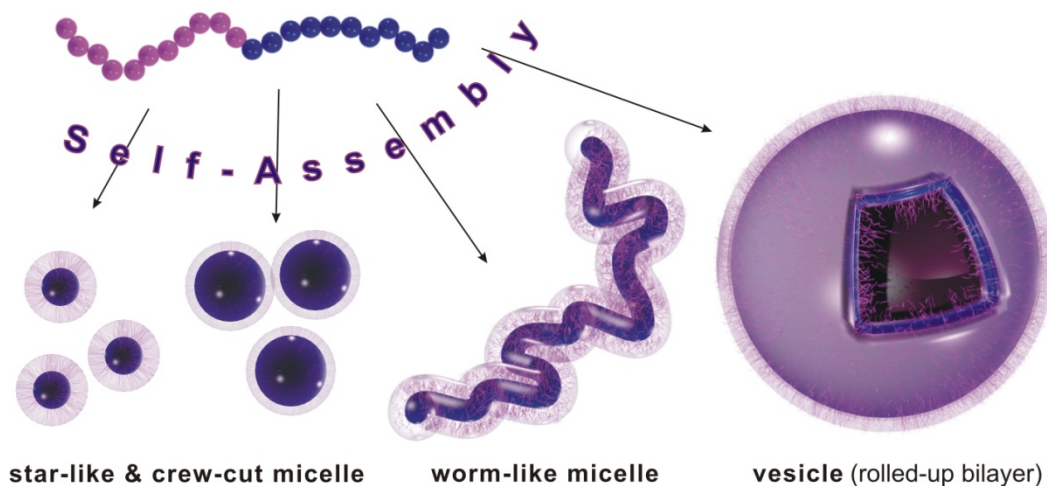


Figure 1–3: Simple diblock copolymer morphologies. Block lengths, interfacial tension and packing parameters of polymer chains in the core and the corona are decisive for surface curvature of the aggregate essentially determining the development of spherical, cylindrical and vesicular morphologies.

Thereby, the choice of solvent can cause several outcomes as e.g., diblock copolymers with large hydrophobic to hydrophilic block ratio may form star-like micelles as small as 10 – 100 nm in organic solvents and at the same time, vesicles as large as 0.1 – 100 μm in water. At first approximation, the block lengths or their ratio is a good reference point to assess the morphology in a specific solvent.^[70] On closer inspection, several delicate interactions fine tune the morphological transitions. The block length of the solvophobic block determines the volume, the aggregation number and chain packing within the core. Block length and block-solvent interaction of the solvophilic block (corona), and especially, the interfacial tension between the core and the corona all contribute to this curvature, essentially responsible for micellar, cylindrical or bilayered/vesicular morphologies. The choice of solvent then finally determines which morphology will be obtained and which one will be preserved, ultimately decided by either kinetic trapping or thermodynamic equilibration. Both mechanisms are eagerly pursued and a unifying theory has yet to be made.

It was only recently that Armes and co-workers were able to visualize the dynamic morphological evolution from spheres to vesicles with unprecedented detail (Figure 1–4a-d).^[71, 72] The experiments provided evidence for a morphological transition that was generally accepted,^[61, 62] but not entirely resolved for almost two decades. In their first work, a water-soluble macroinitiator polymerized the hydrophobic block in a water/methanol mixture. As polymerization continuously extends the second block, unfavourable block/solvent interactions induce phase separation into spherical micelles evolving into worm-like micelles

and finally vesicles. The final morphology is conveniently tuned by the initial monomer concentration that due to full conversion directly translates into the block length ratio (Figure 1–4 a-c).

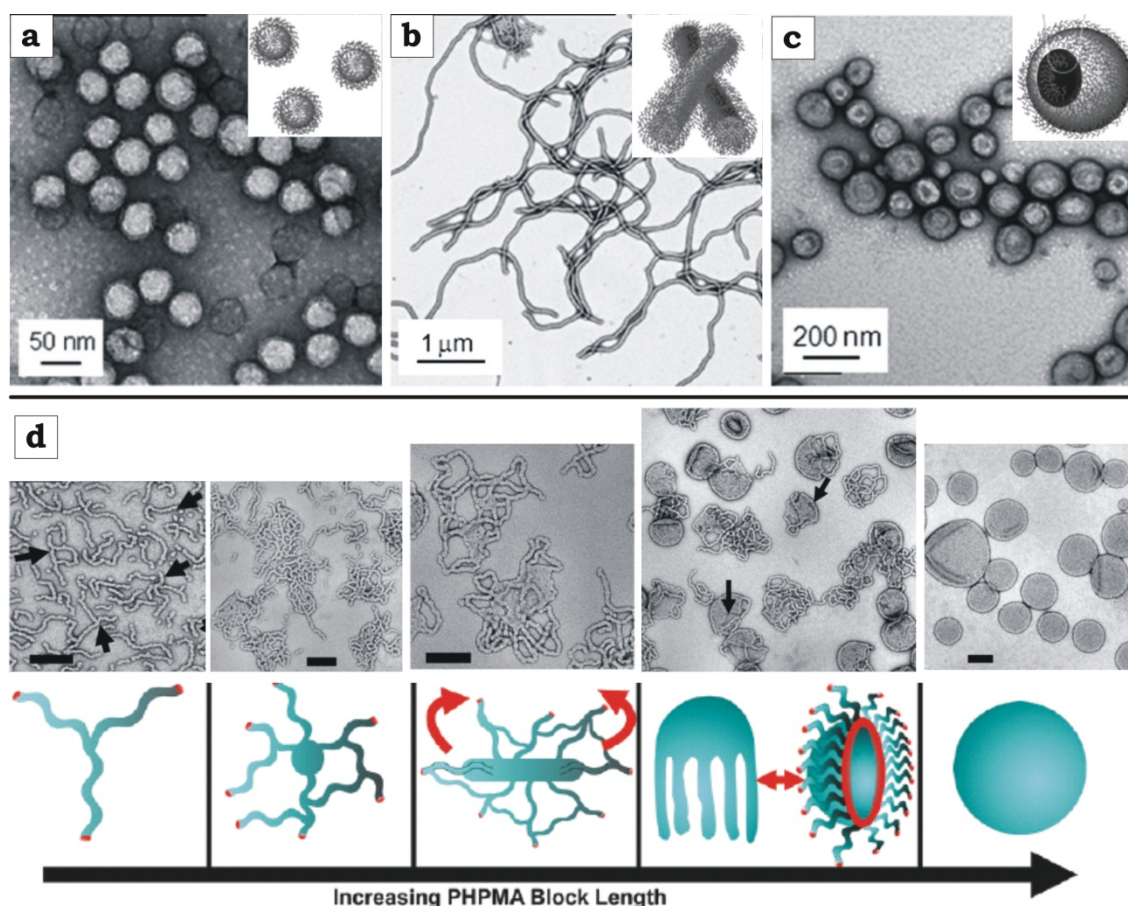


Figure 1–4: Morphological evolution during polymerization of the hydrophobic monomer, 2-hydroxy-propyl methacrylate (HPMA), initiated by the poly(2-(methacryloyloxy)ethyl phosphorylcholine) macroinitiator. Micellar morphologies transform from (a) spherical micelles to (b) cylindrical (worm-like) micelles to (c) vesicles. (d) Structural evolution from worms to vesicles. Adapted from [71] and [72]. Reprinted with permission from the American Chemical Society.

In a consecutive work, the morphological transition of this diblock copolymer was investigated in more detail allowing unprecedented direct visualization of the evolutionary step from worms to vesicles (Figure 1–4d). Especially the evidence for the latter transition was followed with intriguing resolution showing network formation of the worm-like micelles, filling of voids to perforated bilayers, a novel jellyfish morphology and in the end closing of the voids and rolling-up into vesicles. These studies are an excellent example of how mechanistic insight and knowledge of driving forces supports morphological control over the final structure. Nowadays, such systems are so well understood that one can switch between morphologies by design,^[73-76] or fabricate inorganic nanoparticle replicas with surface-functionalized nanoparticles mimicking block copolymer self-assembly.^[77-80]

Among the discussed solution morphologies, vesicles are assigned a special status as they represent capsules capable of carrying solvophilic moieties in the hollow, solvent-filled

interior while storing a solvophobic moiety in the membrane. Thus, vesicles can be considered the simplest compartmentalized structure rendering them attractive as potential gene vectors in drug delivery, as model cells, nanoreactors or for biomedical applications.^[81-84] In general, aggregates bearing solvent filled cavities already present an advancement in complexity compared to the simple core-corona morphologies.^[28] In solution, the dynamic interactions between the single components (polymer blocks and solvent) are delicate and result in morphologies with higher complexity as observed for bulk morphologies. Eisenberg and co-workers documented compartmentalized intermediate structures, i.e., kinetically frozen transitions with broken symmetry of polystyrene-*block*-poly(acrylic acid) (PS-*b*-PAA), encompassing concentrically aligned multilamellar vesicles (onion-like micelles), bicontinuous interpenetrating networks and vesicles with tubular channels in the membrane.^[61, 85] Although, these structures are rarely observed and only appear in a very narrow window of environmental parameters, this clearly demonstrates that there are intermediate morphologies located between thermodynamic equilibrium and kinetic trapping. Broken symmetry is also introduced by, e.g., liquid-crystalline or chiral polymer blocks. Sommerdijk and co-workers relied on hydrophilic/ liquid-crystalline poly(ethylene oxide)-*block*-poly(octadecyl methacrylate) diblock copolymers that self-assemble into cubosomes in water.^[86] The crystalline block adds kinetic control due to the contribution of crystallization driven structure formation. The intricate bicontinuous internal network of these polymersome-like aggregates was resolved using TEM tomography and 3D reconstruction of vitrified films, impressively demonstrating the complexity achieved by single diblock copolymers. Besides liquid-crystalline blocks also polypeptide block copolymers have been intensively investigated due to kinetic obstacles introduced by hydrogen bonding causing the polymers chains to twist and turn. Several reports demonstrated that diblock copolymers bearing a chiral block can arrange into fibres, single, double or triple stranded helices and even a shape reminiscent of nano-flasks.^[87, 88]

A completely different approach to compartmentalized nanoparticles entirely composed of diblock copolymer is the so-called *self-organized precipitation method*, i.e., block copolymer phase separation in concentrated nano-droplets.^[89-93] Here, the dimension of the bulk phase is confined to a spherical droplet consisting of two immiscible homopolymers or of a homopolymer/diblock copolymer blend. It is the confinement and the creation of nano-domains with a large interface that are the driving forces directing self-assembly into diverse morphologies. To produce such a setup, a diblock copolymer or a blend (e.g., PS-*b*-PMMA, PS-*b*-PI/PS/PI) is dissolved in a common solvent for all blocks (THF) and dropped into an immiscible phase (water) under stirring to form droplets. The common solvent is allowed to evaporate inducing polymer concentration and phase separation within the droplet. The particles remain stable and show intriguing internal phase separation into morphologies hardly accessible otherwise, e.g., Janus hemispheres of two homopolymers or spherical, cylindrical and lamella morphologies of block copolymers displaying

lateral instead of concentric orientation towards the particles' centre. "Exfoliation" of lamellae and dispersion of cylinders results in nano-disks and short rods.^[94] Removing the homopolymer minority blended into a sphere morphology produces bucky (or golf) ball particles with a porous network. Beyond that internal organization of both blocks into rings, helices and branched helices has also been reported.

1.1.2 Compartmentalization in Block Copolymer Blends

The comprehensive understanding of polymer-solvent interaction assisted researchers to develop a whole zoo of somewhat exotic, but versatile and multifunctional superstructures. In the previous chapter about diblock copolymer micelles the compartments were, with rare exceptions, solvent filled cavities in a bulk polymer matrix (e.g. vesicles membrane). It is intuitive that blending of two diblock copolymers greatly expands the number of possible block arrangements and can lead to superstructures with polymer/polymer segments stabilized by a corona block. Some very impressive works demonstrated that diblock copolymer blends with proper functionality and mixing ratios can result in highly complex morphologies.^[95-100] Here, examples are reviewed representing important experimental approaches to well-controlled compartmentalized morphologies.

Vesicles with nano-structured membranes demonstrate superior release properties due to persistent channels connecting the interior with the surrounding medium. Control over lateral phase separation within the vesicle membrane from spotted to a entirely phase-separated Janus distribution was achieved by Discher and co-workers via kinetic trapping of diblock copolymer blends (Figure 1-5a).^[95] Mixing of poly(ethylene oxide)-*block*-polybutadiene (PEO-*b*-PB) with poly(acrylic acid)-*block*-polybutadiene (PAA-*b*-PB) in water produces vesicles with a soft, mobile PB membrane and a mixed corona of PEO and PAA. Upon addition of divalent ions such as Ca^{2+} or Cu^{2+} , the PAA chains start to gel and precipitate from solution (kinetic trapping), forming the matrix (depends on the mixing ratio) within the membrane. Fluorescent labelling of PEO-*b*-PB was used to visualize the diblock migration/phase separation within the vesicle membrane into spots or beyond that into Janus hemispheres. With this simple ion trigger, highly complex, tough and nano-structured vesicles were generated at low pH as well as segmented, worm-like superstructures at high pH.

Several attempts were devoted to find a solution-based procedure towards micelles with a Janus distribution of the patches, i.e., corona-compartmentalized micelles. It is a challenging task to overcome the entropic energetic penalty of polymer demixing in solution on the nano-scale. Voets and co-workers were able to fabricate Janus micelles via diblock copolymer mixtures of complementary charged blocks.^[101, 102] Beside the well-documented approach involving bulk morphologies (discussed in chapter 1.1.3.2 in detail), complex co-acervate micelles of poly(acrylic acid)-*block*-poly(acryl amide) (PAA-*b*-PAm) as the poly-

anion and poly(2-methylvinylpyridinium iodide)-*block*-poly(ethylene oxide) (PVMel-*b*-PEO) as the complementary polycation resulted in soft, polymeric Janus micelles (Figure 1–5b). The polymer-polymer immiscibility of the soluble corona blocks, PEO and PAm, promote phase separation overcoming the entropic penalty of demixing, therein. Solution-based approaches to Janus micelles are very rare as de-symmetrisation is challenging without the use of templates and although examples for successful preparation exist, they are limited in several crucial aspects such as scale-up, handling, versatility, feasibility, etc. Chapter 5 of this thesis is dedicated to a simple and versatile solution-based approach to Janus particles developed during my work unifying most advantageous features.

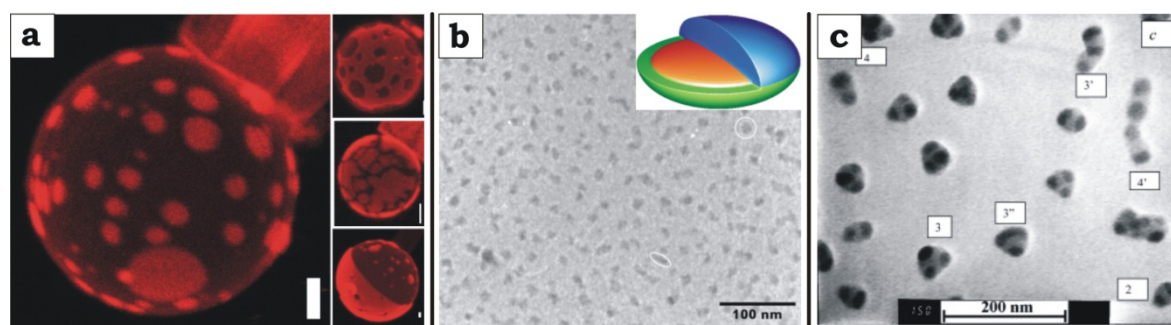


Figure 1–5: Multicompartment structures from diblock copolymer blends. (a) Compartmentalized vesicles in water. Phase separation of fluorescently labelled PEO-*b*-PB and PAA-*b*-PB was induced by gelation of PAA with divalent cations. Adapted from [95]. Reprinted with permission from Nature Publishing Group. **(b)** The two complementary ionic blocks of PAA-*b*-PAm and PVMel-*b*-PEO form the complex co-acervate core with PEO/PAm Janus hemispheres. Adapted from [101]. Reprinted with permission from Wiley-VCH Verlag GmbH & Co. KGaA. **(c)** MCMs with a PS core, two to four patches of chemically stitched blocks containing complementary DNA base-pair derivatives and stabilized by a PtBMA corona. Adapted from [103]. Reprinted with permission from the American Chemical Society.

Besides a compartmentalized corona, Liu and co-workers were also able to generate core-compartmentalized multicompartment micelles (MCMs)^[103-105] via “blending” of block copolymers both carrying a complementary DNA base-pair derivative (adenine and thymine moieties) copolymerized into one of the blocks. This so-called *chemical stitching* of the two diblocks via hydrogen bonding conceptually yields a non-covalently linked triblock terpolymer analogue able to form MCMs with some control over the segment number (Figure 1–5c). Thereby, self-assembly is triggered by transferring the stitched polymer from a common solvent into a selective solvent for the corona block. These “molecular model” MCMs are almost identical to self-assemblies developed during my research, which will be discussed in detail in chapter 3. Despite the similarities of the self-assembly motifs between aggregates shown here and in chapter 3, homogeneity, control over patch number and especially, the understanding of underlying self-assembly mechanisms are unique to the novel approach of chapter 3.

1.1.3 Complex Morphologies of ABC Triblock Terpolymers

Until today, there have been numerous reports on the fabrication on particles on several length scales that fulfil the criteria compartmentalized or nano-structured, but this part of the introduction will focus on bulk morphologies and MCMs based on ABC triblock terpolymers.

The addition of a third block complicates matters as in bulk five independent parameters have to be considered, the polymer-polymer interaction parameters χ_{AB} , χ_{AC} , χ_{BC} and the volume fractions of the blocks ϕ_A , ϕ_B , ϕ_C , the latter being a depended variable ($\phi_C = 1 - (\phi_A + \phi_B)$). On the other hand, the number of block arrangements and morphologies increase many times more.^[27, 29, 106-109] Figure 1–6a illustrates the experimental ternary phase diagram obtained for SBM triblock terpolymers with many reported morphologies depending on the aforementioned parameters. Each bulk morphology has its stability region, whereas e.g., the lamella-lamella phase is often observed in a range of equal weight fractions of all blocks, e.g. $f_C = 0.25-0.35$ and $f_A = f_B = (1 - f_C)/2$. The combined findings of works dealing with triblock terpolymer morphologies in bulk and solution point towards an underlying self-assembly scheme. It stands to reason that known bulk morphologies can be targeted in solution as well by approaching the proper volume ratios and stability regions, respectively. In C-selective solvents, A and B phase separate (as in bulk) and tuning of the solvent quality (addition of non-solvent) can be used to balance the corona volume between contracted (mimics bulk conditions) and sufficiently solubilised to stabilise the aggregates. Thus, beyond the possibility to replicate bulk morphologies in solution, the dynamic swelling/contraction of the corona may allow tailoring of the interfacial tension and curvature, and ultimately switching between morphologies. Such switching has already been demonstrated for diblock copolymers by inducing growth of spherical micelles into extended worm-like micelles. Although, over the years, a number of similarities surfaced that suggest parallels for manipulating diblock co- and triblock terpolymer aggregates in solution, true unifying mechanisms have still to be uncovered.

Figure 1-6b illustrates a suggestion for a ternary phase diagram in dependence of the volume ratios instead of the commonly applied weight fractions. Using volumes is more adequate in solution, not only for estimating the dimensions of solvophobic domains, but especially, to describe the extent of the solubilised corona volume (block length plus swelling). Hillmyer and Lodge proposed such an approach for miktoarm star terpolymers as will be discussed in the next chapter. From the diagram in Figure1–6b it becomes clear that the corona volume is a function of the used solvent and inverse morphologies can only be obtained by switching the solvent e.g., from C- to A-selective. Some of the solution morphologies that are schematically depicted in Figure 1–6b have already been documented and are commonly referred to as MCMs throughout the literature. The similarities to bulk morphologies are striking as the type of phase separation also strongly depends on the volume

fractions of the blocks, the interfacial tension at the block/block interface and the interaction parameter. In solution surface curvature and interfacial tension at the core/solvent interface have to be considered as well raising the total of structuring parameters to eight (the ones as in bulk plus χ_{AS} , χ_{BS} , χ_{CS}). This interaction is again strongly dependent on the interaction parameter or more simplified, on the difference in polarity. In solution triblock terpolymers offer many possibilities for the blocks to arrange into MCMs, which, at first, may appear to be accompanied by a lot of uncertainty and loss of control over block positioning, but also increases the number of possible functional materials that may be deduced from one single type of triblock terpolymer. The simplest positioning of the blocks, frequently found at the outset of this research direction, was core-shell-corona or core-corona-corona self-assemblies (Figure 1–6b).^[111]

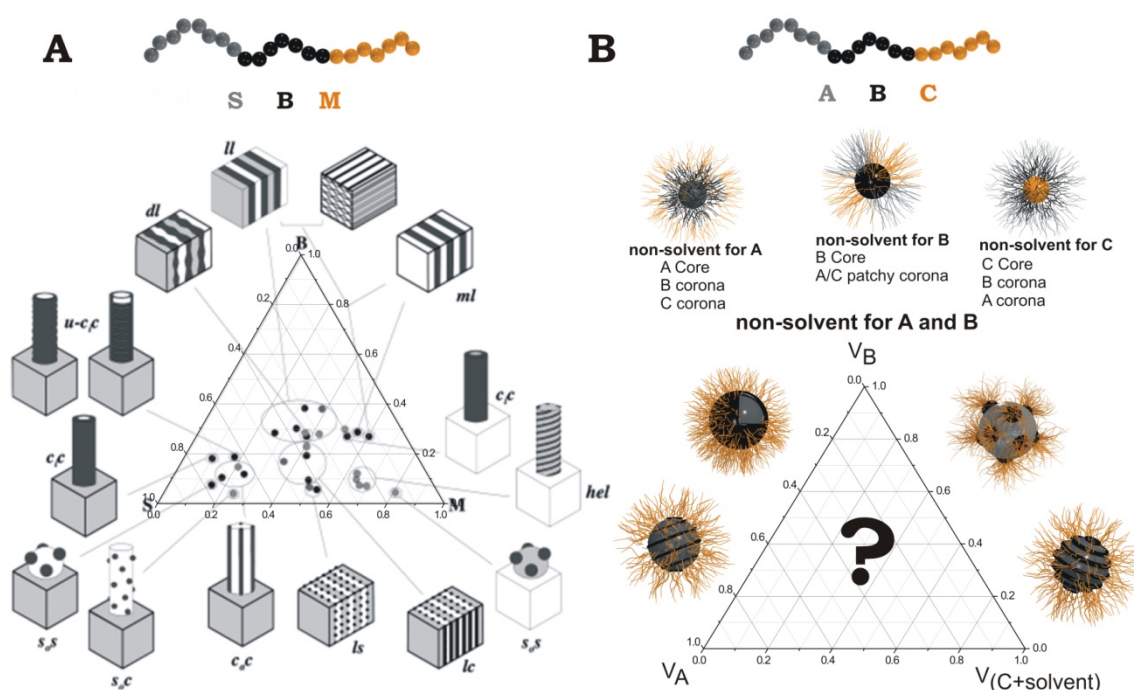


Figure 1–6: Ternary phase diagram of SBM triblock terpolymers in bulk and schematic diagram in solution. (a) Known terpolymer morphologies in dependence of the weight fractions of S, B and M.^[110] **(b)** Suggestion of a ternary phase diagram of an ABC triblock terpolymer in solvent S in dependence of volume fractions V_A , V_B and $V_{C+solvent}$.

Triblock terpolymers also demonstrate the known morphological transitions from spherical aggregates to cylinders to vesicles, whereas these morphologies need to be further subcategorized as now two connected, immiscible blocks form a phase-separated solvophobic core (apart from the core-shell-corona morphology). Exemplified on spherical aggregates, subcategories could be sphere-on-sphere, sphere-on-cylinder and sphere-on-lamella (sphere-on-vesicle) morphologies and many others considering the known bulk morphologies (helix-on-cylinder, ring-on-cylinder, gyroid, etc.). Indeed, quite a number of terpolymer morphologies have already been realized in solution (e.g. sphere-on-sphere, sphere-on-cylinder, helix-on-cylinder),^[112-115] but a unifying concept to the morphological puzzle is

still missing. In the following sections strategies are explored and experimental evidence discussed for a multitude of diverse compartmentalized systems.

1.1.3.1 Multicompartment Micelles by Direct Dispersion

Although, from the synthetic point of view, diblock copolymers are clearly advantageous over triblock terpolymers, there is always the necessity to introduce orthogonal functionality into one of the blocks to direct self-assembly into well-ordered structures. The number of orthogonal functions is limited and may demand special conditions considerably reducing the number of possible materials. The self-assembly of triblock terpolymers generally yields more defined MCMs as observed for e.g., diblock copolymer blends, because all three blocks are covalently linked and cannot evade each other. Thus, the three blocks will always form phase-separated nanostructures in selective solvents.^[27-29] There are several directing agents facilitating control over phase separation on the nanoscale^[116, 117] and among of these, selective solvents are by far the simplest, yet the direct dispersion of linear block copolymers in a selective solvent for one block is a general, frequently recurring method spawning morphologies with intriguing nanostructure.^[118-122]

Thereby, the self-assembly of ABC miktoarm star terpolymers is one of the most prominent approaches for the formation of compartmentalized nanostructures.^[123] Miktoarm star terpolymers consist of three polymer blocks covalently linked at one single junction point. Hillmyer and Lodge documented the self-assembly of a fluorocarbon/ hydrocarbon miktoarm stars in water stabilized by a poly(ethylene oxide) corona block (Figure 1–7a). The unique miktoarm architecture does not allow the blocks to arrange into a core-shell-corona sequence, as often observed for linear triblock terpolymers, and thus, a core segmented structure is energetically favoured. The miktoarm star terpolymer first forms frustrated disc-like segments with a lateral corona emanating from the bilayered core. However, without full protection of the hydrophobic core, the unfavoured core/water interface is then minimized by stacking of the micelles via mutual patches into a variety of frequently reoccurring core-compartmentalized superstructures, some of which termed “raspberry”, “hamburger” and core-segmented worm-like MCMs (Figure 1–7b, c). These results marked a cornerstone in MCM research, as this was the first time the internal structure was convincingly visualized *in-situ* by cryogenic transmission electron microscopy (cryo-TEM).

The morphology of multiblock copolymers depends on many parameters (see chapter 1.1.3) which can be summarized in a comprehensive ternary phase diagram with a plethora of MCMs in solution with a rich repertoire of core geometries (Figure 1–7d).^[124, 125] From the phase diagram it was extracted that the volume fractions of the hydrophobic blocks control aggregation of the core segments and that the corona volume controls the degree of association of the “hamburger” MCMs (Figure 1–7e, f).^[126] An interesting mechanistic insight into the morphological evolution from spheres to cylinders was obtained by mixing

a miktoarm star terpolymer with a long corona block into worm-like MCMs inducing depolymerisation into small fragments due to additional stabilization and the smaller hydrophobic to hydrophilic volume ratio, respectively. Such sophisticated switching between colloidal building block and colloidal polymers is an elegant structuring feature that will be recapitulated in chapter 3. Beyond these early mechanistic insights, over the years, many more morphologies were identified such as sphere-on-cylinders, laterally segmented vesicles and perforated sheets.^[127-132]

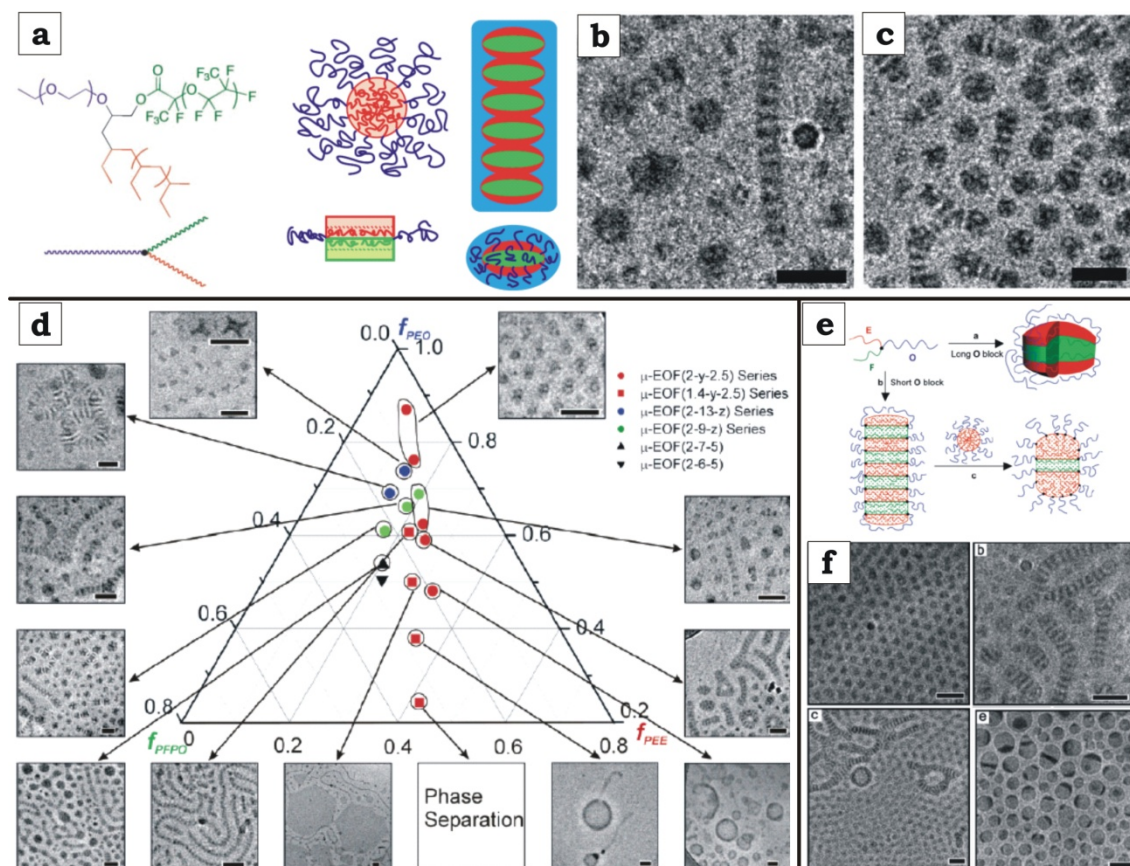


Figure 1-7: Miktoarm star terpolymers in water. (a) Schematic of miktoarm star terpolymer architectures and proposed aggregation into laterally phase-separated disks. (b, c) Cryo-TEM of segmented worm-like and raspberry-like MCMs. Adapted from [123]. Reprinted with permission from the American Association for the Advancement of Sciences. (d) Comprehensive phase diagram of one type of miktoarm star terpolymer encompassing spherical and worm-like micelles, laterally structured hexagons and vesicles. Adapted from [124]. Reprinted with permission from the American Chemical Society. (e, f) Schematic and TEM images of the depolymerisation of worm-like MCMs by blending with “hamburger” MCMs. Adapted from [126]. Reprinted with permission from the American Chemical Society.

The synthesis of miktoarm star terpolymers, in particular, can be very cumbersome and for some block combinations also unlikely. On the other hand, procedures for the preparation of linear ABC triblock terpolymers are state-of-the-art accomplished with many polymerisation techniques.^[133-136] In fact, countless linear triblock terpolymers have been reported offering a multitude of possibilities, one of the main driving force for many research efforts in the field and also for this thesis.

Similarly to Hillmyer/Lodge, Laschewsky and co-workers demonstrated in several studies that linear triblock terpolymers with hydrocarbon/fluorocarbon blocks are also capable to form raspberry-like MCMs in water stabilized by a PEO corona (Figure 1–8a).^[113, 137-140] The strong segregation and the pronounced interfacial energies between the highly immiscible blocks in the core cause de-wetting of the shell and induce a morphological transition from core-shell-corona to MCMs with spherical patches located on the core. Until then, the raspberry-like MCMs of linear triblock terpolymers were only found as sphere-on-sphere morphology in bulk by Stadler and Ritzenthaler.^[141, 142] Schacher and co-workers demonstrated that spontaneous self-assembly of more common and functional polymer blocks polybutadiene-*block*-poly(2-vinylpyridine)-*block*-poly(*tert*-butyl methacrylate) (PB-*b*-P2VP-*b*-PtBMA) also results in the sphere-on-sphere morphology in acetone (Figure 1–8b).^[114] The extraordinary high χ -parameter between PB and P2VP induces de-wetting of the P2VP shell into spheres that reside on the spherical PB core. Hydrolysis of the PtBMA block to PMAA and quaternization of P2VP spawned several types of MCMs with a hydrophobic PB core and complex co-acervate patches of oppositely charged blocks via dialysis of the now polybutadiene-*block*-(2-methylvinyl-pyridinium iodide)-*block*-poly(methacrylic acid) from a common solvent for all blocks (dioxane) into water with pH > 6.^[143] The intra-polyelectrolyte complexes (IPECs)^[144] are formally charge neutral, i.e. hydrophobic, and thus collapsed onto the hydrophobic PB core, but mixing is suppressed due to the extraordinary high χ -parameter. The excess PMAA block length then stabilizes the MCMs. The functions of the polymer blocks comprise cross-linking of the core and loading of the IPEC with gold nanoparticles towards catalytic carrier systems.^[145] In consecutive works Synatschke *et al.* extended the system to core-shell-shell-corona micelles, i.e. an increased number of compartments, via IPEC formation with of the excess polyanionic corona with a cationic homopolymer (e.g. poly(2-(dimethylamino)ethyl methacrylate) (PDMAEMA), P2VP) and a double hydrophilic diblock copolymer (e.g. PEO-*b*-PDMAEMA, PEO-*b*-P2VP), respectively.^[146]

The quality of phase separation and the geometry of the domains in bulk morphology strongly depend on the interfacial tension and polymer-polymer interaction parameters (Flory-Huggins), but most importantly on the volume fractions. Thus, it is not surprising that for triblock terpolymers in solution an equivalent evolution from spherical to cylindrical aggregates is observed. Liu and co-workers were able to produce MCMs with spherical patches on a cylindrical core by adequate choice of the solvophobic block lengths (Figure 1–8c).^[115] The domains of the sphere-on-cylinder morphology are represented by a cylindrical liquid crystalline poly(perfluorooctylethyl methacrylate) core, spherical poly(2-cinnamoyloxyethyl methacrylate) patches and a poly(acrylic acid) corona. Each block was attributed to the respective phase via the combined results of TEM and AFM imaging. Again this morphology was found earlier in bulk by Stadler or Schacher underlining the notion that in solution more parameters have to be considered determining the final mor-

phology complicating the formation of homogeneous samples, therein. Liu and co-workers also prepared sphere-on-cylinders in solution capable of further self-assembly via spherical patches that were selectively switched solvophobic.^[149] They noticed that sphere-on-cylinder MCMs of poly(glyceryl monomethacrylate)-*block*-poly(2-cinnamoyloxyethyl methacrylate)-*block*-poly(*tert*-butyl acrylate) triblock terpolymers started to twist and curl into an almost α -helical secondary structure. This “secondary structure” is reminiscent of, e.g., the secondary backbone conformation of cellulose chains.

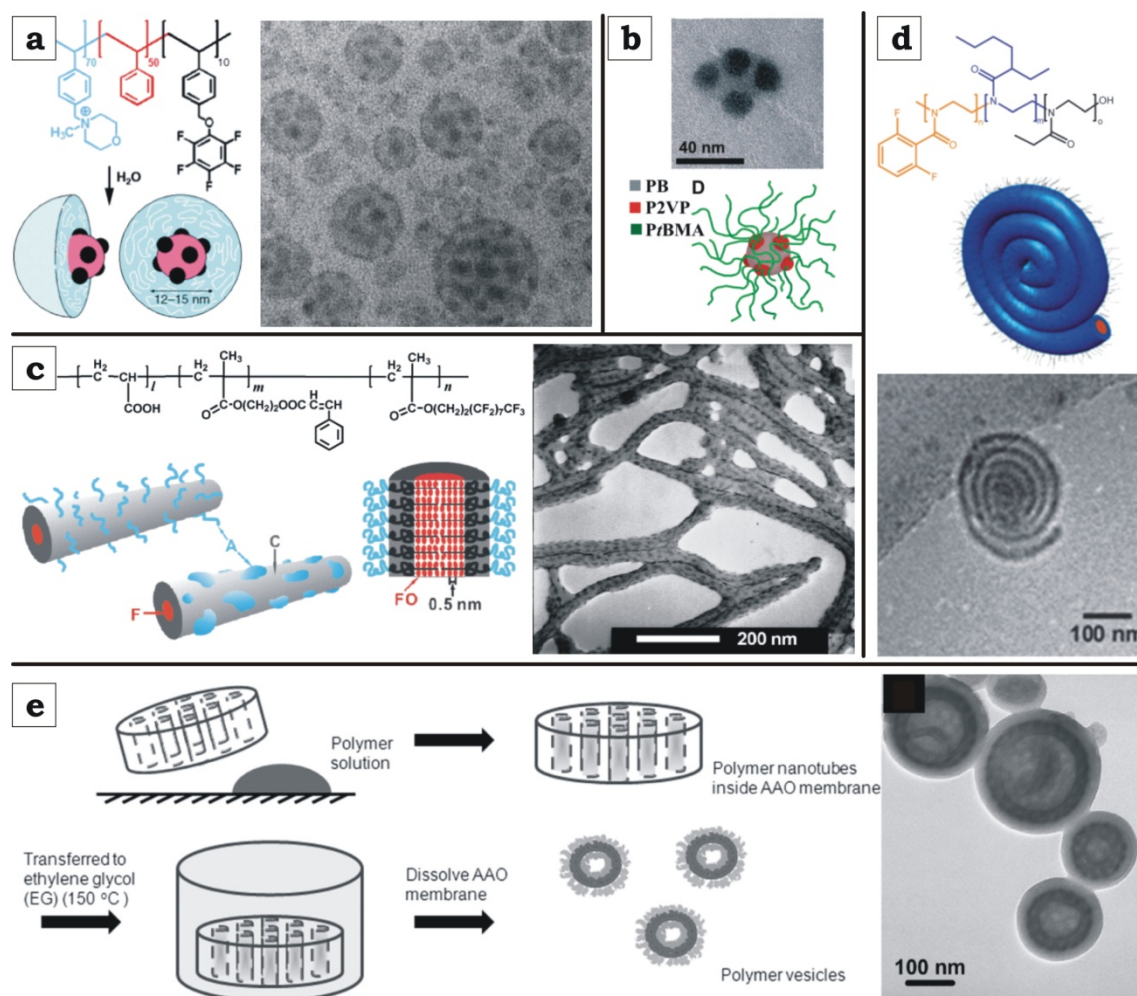


Figure 1-8: Complex MCMs prepared via direct dispersion of ABC triblock terpolymers in C selective solvents. (a) Raspberry-like MCMs in water with a fluorocarbon/hydrocarbon core and PEO corona. Adapted from [113]. Reprinted with permission from Royal Society of Chemistry. **(b)** The same morphology formed by PB-*b*-P2VP-*b*-PtBMA in organic solvents. Adapted from [114]. Reprinted with permission from the American Chemical Society. **(c)** Sphere-on-cylinder morphology by adequate choice of block length and monomers. Adapted from [115]. Reprinted with permission from the American Chemical Society. **(d)** Exotic morphology of rolled-up cylinders via surface attractions. Adapted from [147]. Reprinted with permission from Royal Society of Chemistry. **(e)** Template assisted formation of nano-structured vesicles. Adapted from [148]. Reprinted with permission from the American Chemical Society.

Instead of folding, Schubert and co-workers observed curling and rolling-up of cylindrical micelles into flat spirals as the secondary structure (Figure 1-8d).^[147] Similarly to triblock terpolymers reported by Laschewsky, here, three different oxazoline derivatives were polymerized forming a phase-separated fluorocarbon/hydrocarbon core stabilized by a hydro-

philic corona block. The rolling-up to flat spirals is thought to be a metastable sheet-like intermediate on the morphological evolution from cylindrical micelles to vesicle. This has not been observed, e.g., in the previously discussed works of Armes on diblock copolymers, as here three instead of two blocks need to rearrange to minimize unfavourable interfacial energies. Hence, simple aggregation of the cylindrical cores of the micelles into a continuous 2D sheet is not possible, but instead a sheet interrupted by the third block is observed.

The further transition to phase-separated vesicles is not entirely resolved with pure bottom-up self-assembly in solution, yet. Russel and co-workers demonstrated structures with mesh-like membranes formed by polyisoprene-*block*-polystyrene-*block*-poly(2-vinyl pyridine) (PI-*b*-PS-*b*-P2VP) triblock terpolymer with the aid of anodic aluminium oxide (AAO) templates (Figure 1–8e).^[148] Dissolved in toluene at moderately high concentrations and spread on a glass substrate the polymer solution is pulled into the tubular nanochannels of the AAO template ($d \approx 100 - 200$ nm) via capillary forces. As the polymer solution moves through the channels, the arising shear forces enhance and direct phase separation into the mesh-like or gyroidal morphology of the membrane. To find a general synthetic strategy towards sub-structured vesicles is very desirable, because loading/release protocols could be significantly improved for these prominent delivery vehicles if permanent channels between the in- and outside were reversibly accessible. So far, only few examples treat of triblock terpolymer-based vesicles and, except for the presented case, lack of convincing visualization and characterization. Nevertheless, Russell and co-workers impressively demonstrated how directing agents, here structuring using surface templates, can guide block copolymers into nanostructures far from equilibrium.

1.1.3.2 Compartmentalized Structures via Bulk Morphologies

The structuring via bulk morphologies can, by itself, not be considered as a templating process, because directing effects of the substrate immediately abate after a few nano-domain repetitions. From there on, the triblock terpolymer minimizes the interfacial energy exclusively among the blocks. However, the polymer chains require mobility to be able to rearrange into the desired phases. Solvent casting, shear alignment of polymer melts and alignment in electric fields are frequently used means of manipulation. All cases are directed, even solvent casting as slight variations in solvent-polymer interactions still influence the development of the morphology by premature nano-domain formation during concentration. As already pointed out in the penultimate chapters the structuring in bulk shows many similarities to solution morphologies and strongly depend on the volume fractions of all blocks, their polymer-polymer interaction parameters (Flory-Huggins parameter) and the tension at the domain interfaces. Today, many morphologies are known,^[27, 53, 150-152] whereas lamella morphologies are especially attractive as they are pursued as the source for Janus particles. These particles feature exactly two hemispheres differing in

chemical and/or physical properties, which is the origin of their extraordinary interfacial activity. Over the years Müller and co-workers have targeted and classified many different triblock terpolymer morphologies among of which the lamella-sphere, lamella-cylinder and the lamella-lamella morphology of PS-*b*-PB-*b*-PMMA gave rise to Janus micelles,^[153] cylinders^[154] and discs^[155] via the cross-linking of the inter-lamella PB phase (Figure 1–9a).

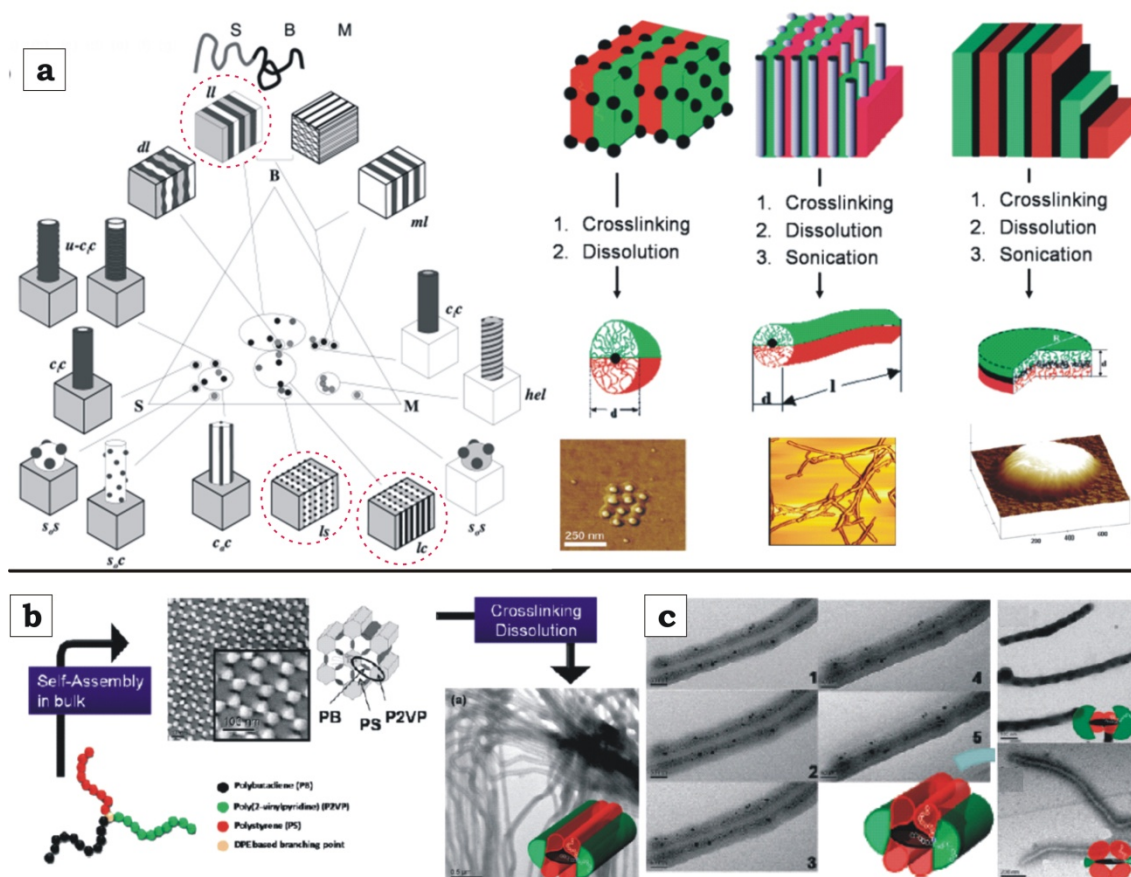


Figure 1–9: Compartmentalized superstructures via bulk morphologies. (a) Comprehensive phase diagram of SBM triblock terpolymers. The block weight fractions determine the morphology. The lamella-sphere, lamella-cylinder and lamella-lamella morphology are highlighted with red circles, resulting in Janus spheres, cylinders and disks. Adapted from [153], [154], [155]. Reprinted with permission from the American Chemical Society. (b) Bulk morphology of a miktoarm star terpolymer with polystyrene, polybutadiene and poly(2-vinylpyridine) arms and MCCs after cross-linking and re-dispersion in THF. (c) Directed compartment swelling in selective solvents and tilt-angle cryo-TEM images (0° – 60°) after loading with inorganic particles. Adapted from [159]. Reprinted with permission from the American Chemical Society.

In the case of terpolymer-based Janus particles, the bulk morphology is a necessary tool to break the symmetry, because the hemispheres do not spontaneously form in solution due to entropic penalties upon total de-mixing of two coronal polymer blocks. The Janus character, i.e., two completely phase-separated hemispheres, is of special interest as it is the origin of the extraordinary interfacial activity. Several theoretical and empirical studies devoted their efforts to investigate the relation between the size and geometry of Janus particles and their desorption energy on liquid-liquid, liquid-air and solid-liquid interfaces.^[156, 157] Janus particles are not only of academic significance, but also technologically attractive as future surfactants, compatibilizers or as drug delivery vehicles, capable to un-

dergo reversible self-assembly/disassembly processes (chapter 1.2.1). Some technological-ly appealing aspects of Janus particles will be discussed in chapter 1.3 of this Introduction: “Hybrid Materials Made by Self-Assembly”.

Preserving bulk morphologies via cross-linking is generally pursued as a source for soft nanoparticles (spheres, cylinders, sheets), also with intriguing fine structure (rings-on-cylinders, helix-, double helix-on-cylinders, perforated lamellae etc.).^[141, 151, 160-162] Particularly miktoarm star terpolymers are well-known for their rich morphological diversity exceeding that of linear triblock terpolymers.^[27] Cross-linking of these bulk morphologies is an elegant approach to fabricate highly anisotropic, compartmentalized and responsive structures with high precision (Figure 1–9b). Walther *et al.* showed that polystyrene-*b*-polybutadiene-*b*-poly(2-vinylpyridine) miktoarm star terpolymers (μ -SBV) undergo sophisticated phase separation into hexagonal pattern, which, after cross-linking of the PB phase and re-dispersion in a common solvent for all blocks, revealed multicompartment cylinders (MCCs) with a ribbon-like PB core flanked by P2VP patches in plane and PS patches on top and below the PB ribbon (Figure 1–9c).^[159] In selective solvents, the opposing PS (toluene) and P2VP (ethanol) patches expand/contract and are used to adjust the position and distance of inorganic particles coordinated by the P2VP phase. The perfect spatial separation of both inorganic “highways” by the hydrophobic isolating PB ribbon qualifies this structure as a bidirectional electric conductor. One can easily imagine that the contracting patches, at brink of precipitation, may be used for hierarchical self-assembly into next higher level. The next section will discuss possibilities of hierarchical self-assembly of colloidal particles with emphasis on surface isotropic particles with surface asymmetry.

1.2 Colloidal Self-Assembly

The last few years witnessed great progress in the self-assembly of colloidal particles.^[39, 163, 164] The key element for defect-free hierarchical self-assembly are homogeneous particles that are mostly prepared via top-down approaches such as covalent functionalization, “stamping”, surface coordination or glancing-angle deposition of metal layers onto specific surface areas of two-dimensional arrays of silica or latex particles. Ever since van Blaaderen popularized the term “Colloidal Molecules”^[40] the idea to correlate physical and physicochemical effects in approximation to much smaller systems sparked immediate interest in many research groups.^[165] As a result, numerous theoretical and practical studies were dedicated to this idea. Although theoretical considerations predict a great variety of particles suitable to form colloidal molecules, polymers or crystals, until now, mostly inorganic particles, latex colloids and inorganic/latex hybrids have been reported to undergo hierarchical self-assembly. Besides isotropic particles, shape anisotropic (mostly inorganic)

and shape isotropic particles with surface anisotropy (or asymmetry) have shifted into the focus as CBBs for hierarchical self-assembly (Figure 1–10).

As a great part of this thesis deals with the synthesis and self-assembly of soft patchy particles, general achievements in the field of colloidal self-assembly will be discussed shortly. For more elaborate information on this subject, comprehensive reviews can be found elsewhere.^[37-39, 165-167]

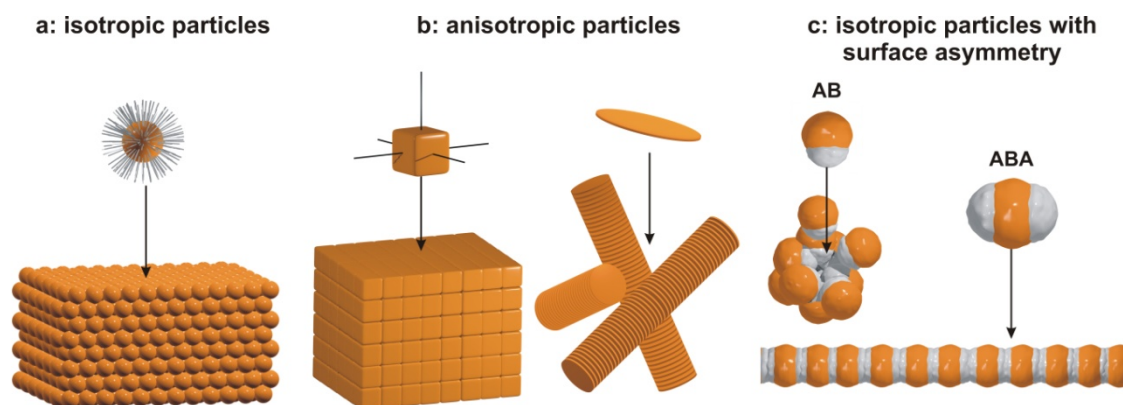


Figure 1–10: Classes of colloidal particles suitable for self-assembly. (a) Isotropic particles without preferential self-assembly direction result in colloidal crystals of infinite dimension with dense sphere packing. (b) Anisotropic particles have less freedom to self-assemble, e.g., six directions for cubes, but still mostly form colloidal crystals mirroring the geometry of the underlying CBB. Only strong anisotropy finally adds a direction as observed for disc-shaped particles. (c) Isotropic particles with surface asymmetry display pre-programmed self-assembly direction with at least one finite dimension. AB particles form spherical clusters of finite size and ABA particles grow into extended linear aggregates with defined width.

Spherical particles, i.e., completely isotropic particles, is the simplest design for colloidal building blocks. As there are no restricting or directing forces, self-assembly of these particles is undirected (isotropic) and results mostly in colloidal crystals of infinite size.^[168-170] Clusters with well-defined, finite size were achieved via droplet assisted cohesion of multiple particles. Thereby, poly(styrene sulfonate) (PSS) latex particles are dispersed in water containing 1 – 10 μm droplets of toluene.^[171] The surface charged colloids act as emulsifiers and locate at the toluene/water droplet interface. During toluene evaporation the particles are drawn together due to the raising surface tension of the deforming droplets and start to self-assemble into clusters of defined size. The number-disperse clusters are gravimetrically separated according to their size via centrifugation in a solution with a density gradient. With this approach fifteen different cluster geometries were obtained in high yield and with extraordinary homogeneity (Figure 1–11a), the first seven of which are surprisingly similar to fluorine containing atom clusters dictated by the Lennard-Jones potential. These similarities lead to the expression “Colloidal Molecules”.

Although synthesis is more challenging, shape-anisotropic CBBs demonstrate excellent control over the superstructure’s geometry usually reflecting the shape of the underlying

CBB.^[36, 43, 172-175] Despite a few exceptions,^[176-178] shape anisotropic polyhedra also form colloidal crystals with indefinite dimension. This it is not surprising as anisotropy is not very pronounced for polyhedra that, conceptually, are spheres (indefinite number of facets) with a lower resolution, i.e. lower number of facets, whereas tetraeder have the lowest possible number of facets for 3D objects (4 facets).^[174] Only if particles are extreme shape-deformed (e.g. discs), the growth direction experiences a strong preference along one facet. Among other shape-anisotropic particles, cubic colloids form crystals with long range order on 2D and 3D scales (Figure 1–11b).^[179] The adhesion of two approaching cubic particles originates from an osmotic pressure imbalance induced by the overlap of exclusion zones, i.e. the volume defined by the cubes surface and the radius of gyration of the polymer coil, an effect called depletion interaction. With this simple CBB design almost defect-free crystals with long-range order are accessible. Shape anisotropic colloids are also capable of multilevel self-assembly as recently proven by the directed super-structure formation with octapods (Figure 1–11c).^[180-182] The extreme anisotropy of these CBBs induces interlocking of the single crystals into linear strings on the first hierarchy level that undergo pronounced 3D crystal formation on the second one. Although theoretic-cal calculations predict a plethora of shape-anisotropic colloids (polyhedra) forming super-lattices with properties ranging from liquid to plastic crystals,^[174] these octapods are among very rare examples demonstrating multilevel self-assembly from 0D CBB to 1D strings and 3D crystal lattices.

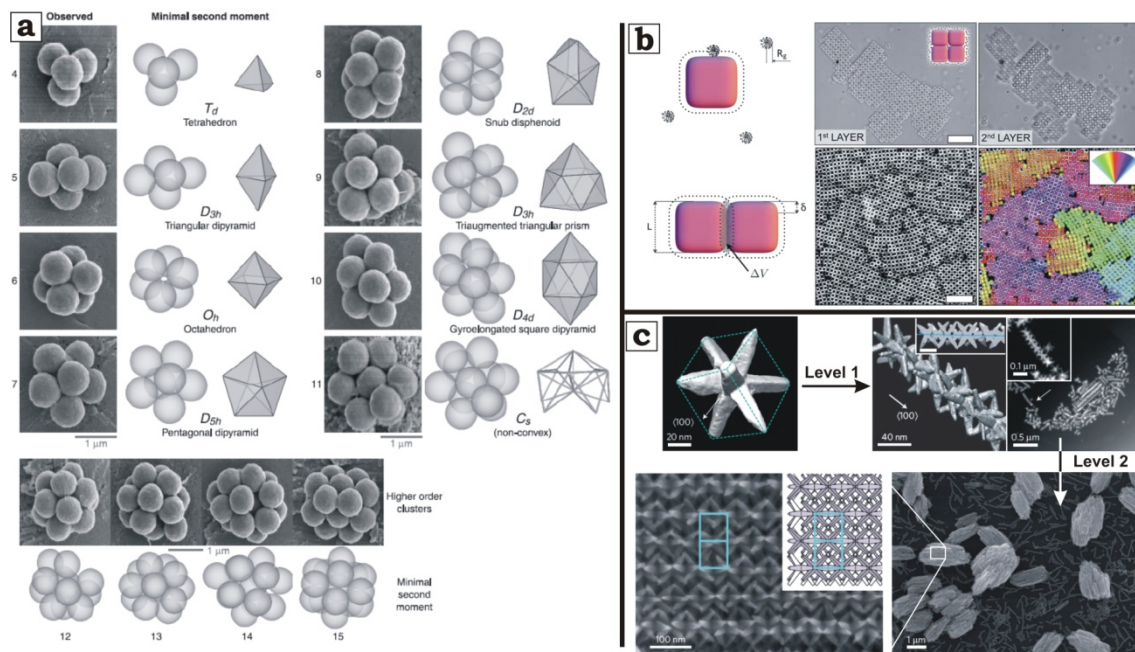


Figure 1–11: Colloidal homo-assemblies. (a) Geometric clusters of isotropic hard spheres obtained by evaporation induced self-assembly and gravitational separation. Adapted from [171]. Reprinted with permission from the American Association for the Advancement of Sciences. (b) Self-assembly of shape-anisotropic colloidal cubes into two- and three-dimensional sheets and cubic crystals, respectively. Adapted from [179]. Reprinted with permission from Royal Society of Chemistry. (c) Multilevel self-assembly of colloidal octapods into linear chains and subsequent higher-level aggregation into colloidal crystals. Adapted from [172]. Reprinted with permission from Nature Publishing Group.

Beyond the geometric shape, tailoring of the surface chemistry of shape isotropic particles allows to control particle positioning, growth direction and shape of the self-assemblies. The geometrical distribution of responsive patches gives access to directionality adding another level of control. These patchy particles are in focus of colloidal self-assembly^[43, 158, 183-191] and comprise a rapidly evolving field of great diversity allowing functionalization, compartmentalization and bottom-up structuring of hierarchical superstructures. The discovery of highly complex aggregation pattern in solution and on surfaces using micro-metre-sized patchy colloids received tremendous attention only recently.^[192-194] The ability of “simple” building blocks to rearrange into complex patterns is already encoded within the distribution of surface patches of the particles that will acquire their position accordingly, if proper stimuli are applied. However, easier visualization of this distribution and the produced superstructures, and especially, simpler crafting of the surface patches are the main reasons self-assembly is preferentially studied on this scale. It simply poses a major challenge to find proper synthetic means for surface functionalization on the sub 100 nm scale. The most prominent directing agents in this regard are solvent polarity or the use of complementary DNA strands.^[195-199]

1.2.1 Superstructures of Janus Particles

Janus particles (JPs) are a special type of surface-anisotropic particles with two strictly phase-separated hemispheres differing in their chemical and/or physical properties. These particles are of immense interest for a variety of applications due to their superior surface and interfacial activity compared to homogeneous particles.^[156] Janus particles come in all sizes from sub-nm Janus fullerols^[200] to millimetre-sized “eyeballs”^[11] and all shapes from spherical,^[153] cylindrical,^[154] matchsticks,^[196, 201] discs^[155] to even Janus walls.^[202] Despite the tremendous progress in the field and the numerous reports on synthesis and applications of this special type of particle,^[158, 166, 196, 203-212] the self-assembly has been rarely addressed in the literature.^[206, 213-216] As this part of the introduction primarily focuses on self-assembly of the colloids the most relevant examples will be discussed.

In the early beginnings of research on polymeric Janus micelles, Erhardt *et al.* studied the self-assembly behaviour of polystyrene-*block*-polybutadiene-*block*-poly(methyl methacrylic acid) (SBMAA) JMs in selective solvents (Figure 1–12a).^[216] These highly amphiphilic particles were obtained via hydrolysis of its non-polar pendant SBM. A mixture of methanol/dioxane yielded unimeric dispersions and self-assembly was induced by changing the solvent quality for the PS hemisphere via dialysis into pure water. Aggregation occurred along the collapsing PS patches into spherical clusters with a hydrodynamic radius of around 60 nm, stabilized by the PMAA corona patches. However, some larger aggregates of several hundred nanometres were also identified and termed supermicelles. These studies marked the outset of colloidal self-assembly with highly dynamic corona patches capable of adjusting their volume with respect to the solvent quality.

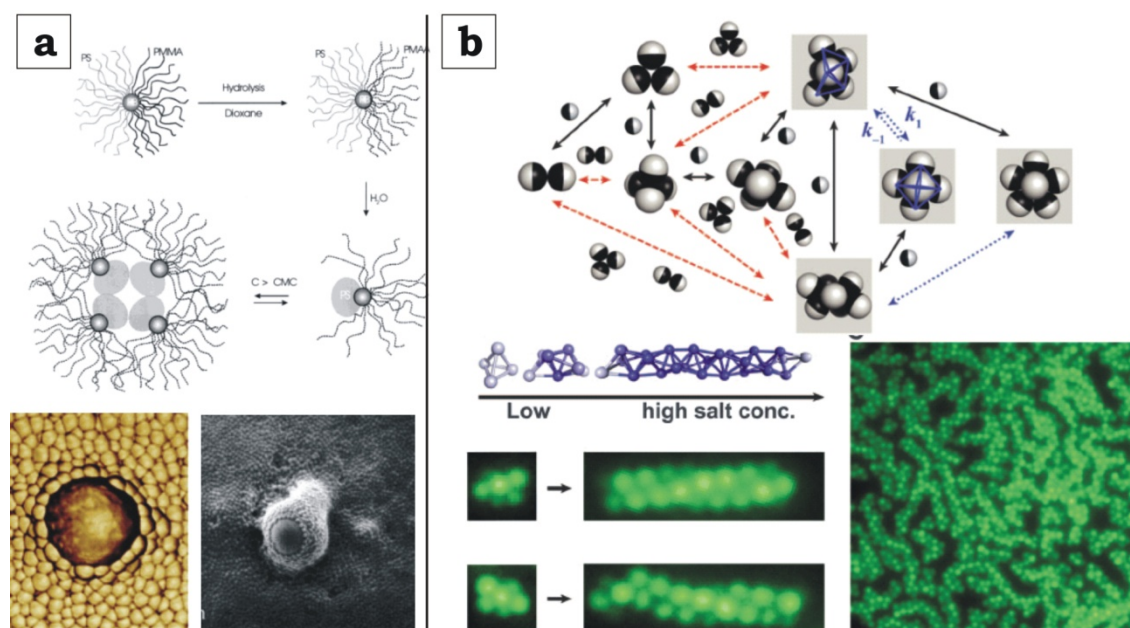


Figure 1–12: Spherical and helical clusters formed by AB type Janus particles. (a) Self-assembly of SBMAA Janus micelles into spherical clusters and supermicelles triggered by exchanging the solvent. Adapted from [216]. Reprinted with permission from the American Chemical Society. (b) Clustering possibilities of fluorescently labelled PS latex particles with a poly(styrene sulfonate) and an octadecyl hemisphere and complex triple helices found in aqueous solutions of high salinity. Adapted from [193]. Reprinted with permission from the American Association for the Advancement of Sciences.

In contrast to the dynamic JMs on the nano-scale, fluorescently labelled PSS Janus particles exhibit a more static character of the amphiphilic surface patches. (Figure 1–12b).^[193] One hemisphere of the particles ($d \approx 1 \mu\text{m}$) were covered with a 2 nm titania (TiO_2) layer, followed by a 25 nm topping layer of gold (glancing angle deposition) and successive thiolation with octadecanethiol to obtain two hemispheres of different polarity. Surprisingly, these Janus particles showed very sophisticated self-assembly behaviour by arranging into intricate helical arrangements. The supracolloidal self-assembly kinetics thereby revealed clusters matching theoretical predictions. The study of the self-assembly kinetics may aid to fundamentally understand driving forces behind complex aggregation behaviour and will advance the development of defect-free, large area supracolloidal networks with interesting optical properties, superior selectivity in particle separation, as biomaterials or lightweight hybrids.

1.2.2 Directed Self-Assembly of ABA Colloids

The patch distribution of the second frequently recurring type of patchy colloids is described by two attractive patches (“poles”) at opposing sides of an inert segment often covered by an equatorial repulsive patch. This setup basically is the advancement of the Janus distribution by an additional attractive patch, yet dramatically altering the growth direction from spherical clustering to extended linear growth via a step-growth polymerization analogous end-to-end addition. The aggregation behaviour of such difunctional ABA colloids

has been reported for a number of inorganic nanoparticles and inorganic-polymer hybrids.^[177, 217-222]

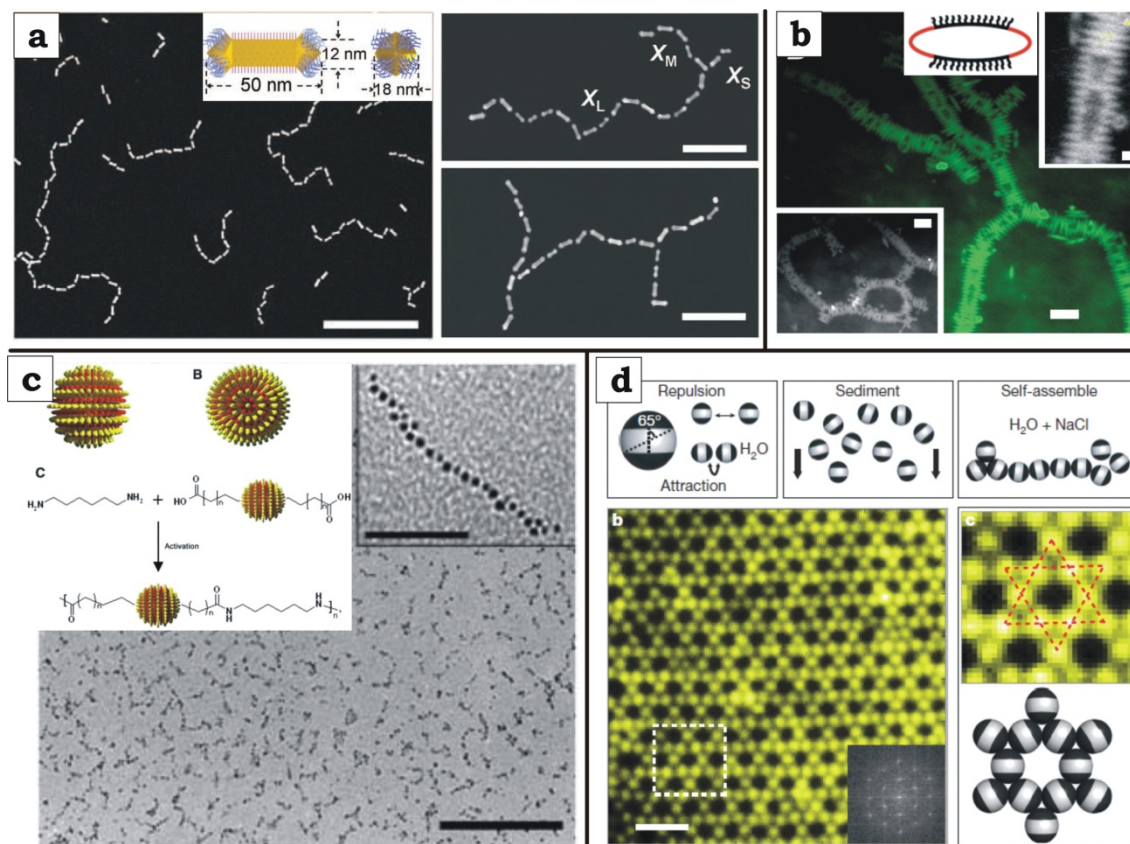


Figure 1–13: Self-assembly of difunctional ABA colloidal building blocks. (a) Linear step-growth polymerization of PS end-functionalized gold nano-rods. Adapted from [223]. Reprinted with permission from the American Association for the Advancement of Sciences. **(b)** Self-assembly of ABA building blocks directed sideways into parallel streaks. Adapted from [228]. Reprinted with permission from the American Chemical Society. **(c)** Step-growth-polymerization of difunctional gold monomer mimics into linear chains. Adapted from [229]. Reprinted with permission from the American Association for the Advancement of Sciences. **(d)** Kagome lattice formed by ABA building blocks. Patch distribution and interaction by sedimentation process leading to the formation of defect free, large area Kagome lattices composed of neighbouring triangles and hexagons. Adapted from [192]. Reprinted with permission from Nature Publishing Group.

Kumachva and co-workers realized step-growth polymerization of PS-gold-PS colloids (ABA) and visualized each steps of the growth kinetic at specific time intervals (Figure 1–13a).^[223] This is an unthinkable undertaking for molecular monomers, but easily done via TEM imaging of nano-sized gold particles with strong contrast. The ABA configuration was achieved by selective end-decoration of the rod-like gold nano-particles with PS polymer chains selectively attached to the “arrowheads”. This was possible due to the different reactivity of etched {111} facets of the arrowheads of the gold particles compared to the {000} facets of the longitudinal sides.^[224] Thereby, the recorded growth kinetics of the nanoparticles can be described extremely well by known step-growth polymerization kinetics cementing an underlying scheme for the “reaction” of di-functional units, irrespective of their nature (particulate or organic compound). Beyond end-to-end aggregation into chains and rings also consecutive side-to-side and end-to-end self-assembly resulted in

spheres, vesicles and multi-string chains simply by switching first the longitudinal sides insoluble followed by the PS located at the arrowheads.^[224-227]

A quite similar way to obtain ABA CBBs was found for the functionalization of organic particles.^[228] PMMA latex particles were co-cast with polydimethylsiloxane (PDMS) that was subsequently cross-linked and deformed at temperatures above the T_g of PMMA. The particles adapt an ellipsoidal shape and after cooling below the T_g this shape is preserved. Surprisingly, the surface coating (poly(12-hydroxystearic acid)) of the PMMA ellipsoids is more susceptible to hydrolysis at the tips than on the longitudinal sides and thus, surface patterning in dependence on the curing time allows creating attractive patches either located at the tips for end-to-end aggregation or on the sides for stacking into columns (Figure 1–13b).

Methods of finding spots with diverse reactivity are rare and thus it is especially surprising that nanoparticles can be functionalized to yield ABA type building blocks with the responsive patch being as small as a single molecule.^[229] Such a patch resolution is unmatched and originates from an effect based on the “hairy ball theorem”, basically stating that the homogeneous self-assembly of a ligand monolayer on a curved nanoparticle surface is not possible, but instead always causes at least two defects (Figure 1–13c). If two strongly immiscible ligands span up this monolayer, a curved surface will cause decoration with alternating ring-like phases dramatically increasing the probability ($p \rightarrow 1$) that the poles of the nanoparticle are functionalized with the same molecule. Placing 11-mercaptopundecanoic acid at the poles renders the particle bifunctional and a two-phase polycondensation with 1,6-diaminohexane results in linear nanoparticle chains. These chains very recently applied as ultrasensitive sensors for toxic cations, e.g., for CH_3Hg^+ over an extreme concentration range of 18 orders of magnitude down to an unprecedented attomolar detection limit.^[230]

Among the many extraordinary examples in literature, Granick and co-workers presented a distinguished study with sophisticated control over the aggregation of micron-scale ABA colloids (Figure 1–13d).^[192, 231, 232] Metal vapour deposition under varying angles allowed adjusting the hydrophobic/hydrophilic surface area of the PSS particles with octadecylthiol covered gold caps. If brought into water dynamic regulation of the hydrophilic, equatorial corona drives the ABA colloids to self-assemble into highly ordered geometric Kagome pattern upon sedimentation (highly symmetrical pattern of repeating hexagons interconnected by triangles) simply by adjusting the salinity of the medium.

1.2.3 Bottom-up Multilevel Hierarchical Self-Assembly

Although this seems to be yet another chapter on terpolymer self-assembly, the preparation and underlying mechanisms are entirely different from the previously discussed MCMs of chapter 1.1.3.1. In most reports, the triblock terpolymer is directly dispersed in a solvent

selective for one block and as the solvophobic blocks cannot tackle with kinetic obstacles, random geometries with ill-defined core segmentation are the dominant species. Nevertheless defined and reproducible morphologies have also been reported, e.g., raspberry-like multicompartment micelles (MCMs), in analogy to the sphere-on-sphere morphology, are often the outcome of the direct dispersion of a linear ABC triblock terpolymer in C selective solvents. However, in recent years, a new step-wise self-assembly protocol evolved, involving preformed patchy particles and solvent sequences. This procedure was either deliberately implemented or used by accident, but either way, the homogeneity of the morphologies observed with this step-wise approach improved to a great extent.^[112, 149, 233-235] It can be very difficult to classify MCMs solely by their morphology. Conceptually raspberry-like MCMs fabricated by the de-wetting of core-shell-corona micelles or via clustering of patchy particles cannot be distinguished after self-assembly is completed. As these mechanisms are clearly different, this part about MCMs from triblock terpolymers is separated from chapter 1.1.3.1 and instead, located within the chapter on colloidal self-assembly. Here, self-assembly processes are discussed that cross more than one hierarchy level via the formation of patchy particles from triblock terpolymers and their subsequent self-assembly into colloidal superstructures.

A step-wise procedure may sound more cumbersome at first, but the control over fine structure, size distribution and positioning of the blocks is often unparalleled. First, the triblock terpolymer is either directly dispersed in a non-solvent for the middle block or portions of non-solvent are added to precipitate the middle block. The thermodynamic control is guaranteed by annealing for hours to weeks depending of the polymers used. This procedure gives rise to thermodynamically equilibrated B core, A/C corona micelles. Thermodynamic equilibration of these CBBs is crucial to fabricate uniform species, as irregularities will amplify throughout the hierarchy levels. In a subsequent step the CBBs are self-assembled in a kinetically controlled process, where the solvent quality is changed to only match one of the two corona blocks A or C. The collapsing block forms a new patch with an unfavoured block/solvent interface and thus serves as mutual contact point for the CBBs. The newly formed multicompartment structure then consists of multiple building blocks and is more defined than with other experimental approaches.

All examples in this chapter follow this principle, some with complete convergence and some with small deviation. It may be noted that details about similarities and parallels between the formation mechanisms may not be explicitly discussed in the cited articles. As described for diblock copolymer micelles, the transition from spherical to worm-like micelle to vesicle is well understood and therefore, it is not surprising that similar transitions have also been observed for micelles with a non-uniform de-symmetrised corona composed of patches of different chemistries. Since these environments respond to different stimuli a transition from spherical to worm-like topology can be anticipated and has in fact been reported for several cases. Here, the key difference is the arrangement of the respec-

tive blocks. In contrast to diblock copolymer micelles that simply fuse together to an elongated homogeneous core and a homogeneous corona, patchy micelles aggregate via mutual patches. The core of the newly formed cylindrical micelle is then composed of two immiscible segments. Figure 1–14 shows some examples where worm-like MCMs are obtained from patchy spherical micelles.

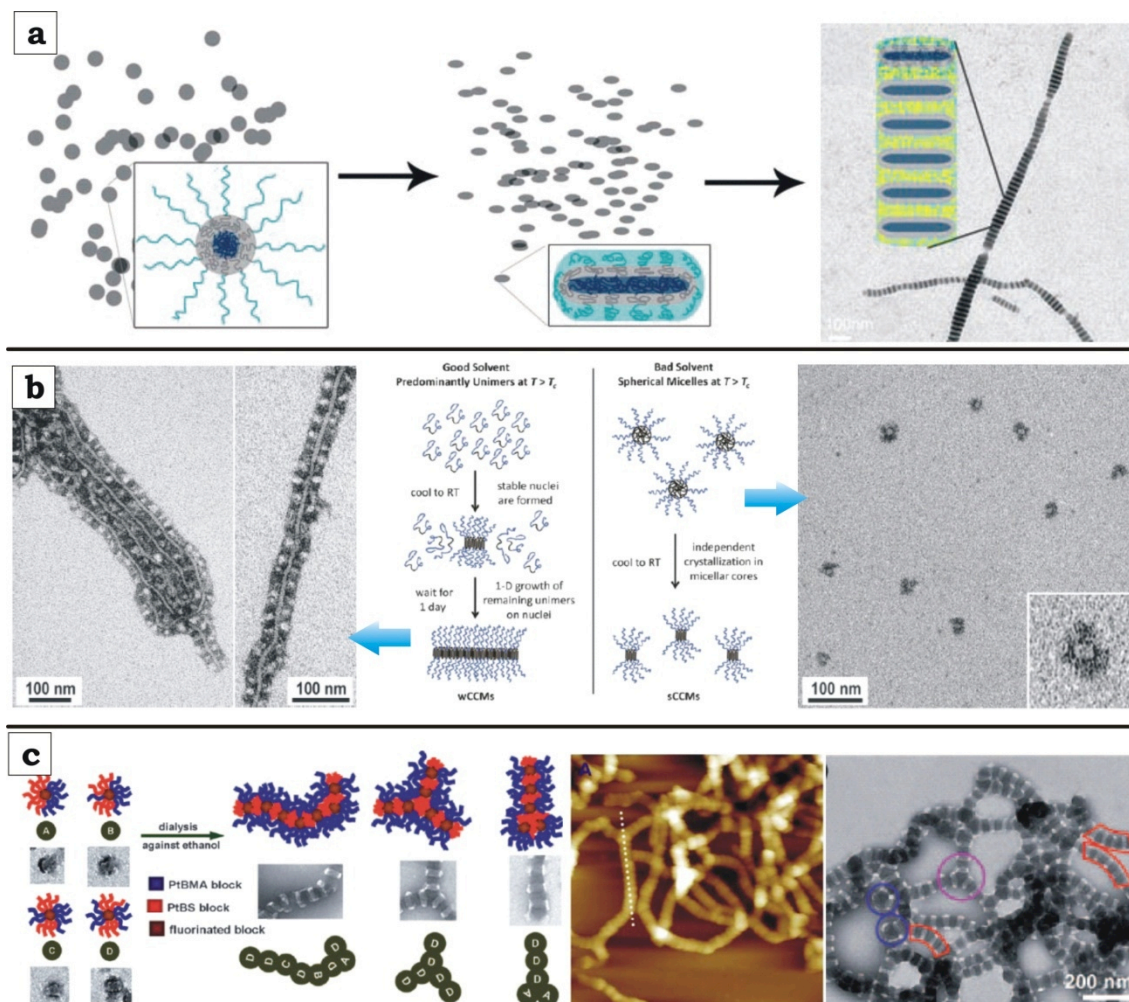


Figure 1–14: Linear superstructures based on very similar step-wise procedures. (a) Stacking of disk-like PS-*b*-PMA-*b*-PAA micelles into extended segmented worm-like micelles. Adapted from [236]. Reprinted with permission from the American Association for the Advancement of Sciences. **(b)** Worm-like micelles with a crystalline core and a segregated corona were obtained from PS-*b*-PE-*b*-PMMA triblock terpolymers driven by crystallization in good solvents for the core. Adapted from [241]. Reprinted with permission from the American Chemical Society. **(c)** MCMs prepared by step-wise self-assembly of PtS-*b*-P/B-*b*-PtBMA micelles after fluorination of the middle block. Adapted from [242]. Reprinted with permission from Wiley-VCH Verlag GmbH & Co. KGaA.

The common theme in all cases is the formation of B core, A/C corona micellar building blocks in a first self-assembly level that aggregate into 1D worm-like MCMs on a second level. This transition is realized in different ways. Wooley, Pochan and co-workers^[236] demonstrated core-shell-corona formation of polystyrene-*block*-poly(methyl acrylate)-*block*-poly(acrylic acid) (PS-*b*-PMA-*b*-PAA) triblock terpolymers that are anisotropically deformed to disks upon addition of an organic diamine controlled by delicate THF/water

mixtures. The disks stack into one-dimensional worm-like structures due to the preferential orientation of the flat sides and are then interlocked via interpolyelectrolyte formation between the cationic diamine and the anionic PAA corona. This self-assembly is a very delicate process as slightest variations of any parameter result in diverse superstructures such as stacked lamellae or toroids.^[237-240]

Schmelz *et al.* reported anisotropic worm-like micelles with a compartmentalized corona and a crystalline core by the crystallization driven assembly of polystyrene-*block*-polyethylene-*block*-poly(methyl methacrylate) (PS-*b*-PE-*b*-PMMA) triblock terpolymers (Figure 1–14b).^[241, 243] When heated above the melting point of the PE block the terpolymer chains were molecularly dissolved. Cooling below the crystallization temperature then triggered self-assembly into either complex 1D worm-like micelles with a crystalline core and incompatible corona patches of PS/PMMA in good solvents for all blocks (THF) or spherical patchy particles in bad solvents for PE. Although this example does not strictly conform with the self-assembly of ABA type colloids, the micellar seeds exclusively undergo linear aggregation via the crystalline facets that are distributed in an ABA manner. Similar concepts will be discussed in chapter 1.2.4 “Co-Assembly”.

One of the most influential works for this thesis was published by Fang *et al.* who prepared core segmented worm-like MCMs from a poly(4-*tert*-butoxystyrene)-*b*-polybutadiene-*b*-poly(*tert*-butyl methacrylate) (PtS-*b*-PB-*b*-PtBMA) triblock terpolymer (Figure 1–14c).^[242] The PB middle block was functionalized with 1-mercapto-1*H*,1*H*,2*H*,2*H*-perfluorooctane *via* thiol-ene click reaction to alter its volume and to enhance incompatibility with the solvents and other blocks. Dispersion in dioxane and annealing over night resulted in patchy particles with a P/B core and a patchy PtS/PtBMA corona. The patch distribution of PtS on these precursor micelles equalled ABA CBBs and subsequent dialysis into ethanol triggered the self-assembly via insoluble PtS patches into undulated bamboo-like MCMs reaching lengths of several micrometres. Chapter 3 of this thesis presents the advancement to this approach by developing a generic and more versatile procedure applicable to any linear triblock terpolymer.

1.2.4 Co-Assembly

The co-assembly of multiple colloids or polymers is an exciting field, which requires a sophisticated level of control in many aspects. Since co-assembly of colloids inherits cluster and compartment formation, here, we will define similar rules for polymer and colloidal co-assembly namely the formation of more than two core and/or corona compartments. Some prominent examples in solution are discussed in more detail.

A well-known step-by-step co-assembly process comprehensively studied by Ian Manners and co-workers is the crystallization driven co-assembly of polyferrocenylsilane block copolymers such as polyferrocenylsilane-*block*-polydimethylsiloxane (PFS-*b*-PDMS) and

polyisoprene-*block*-poly(ferrocenyldimethyl-germane) (PI-*b*-PFG) into alternating core and corona segments (Figure 1–15a).^[244–249] The extension to ABC ter-micelles was the first true example of self-assembly across multiple hierarchies (Figure 1–15b, c), realized by the fabrication of difunctional cylindrical A micelles that were extended on both ends yielding BAB block co-micelles.^[250] The B part carried a cross-linkable corona and after cross-linking, the terminal crystalline core segments are blocked for further growth. Dissolving the A part then provides a micellar species that exhibits only one accessible facet. The sequential crystallization of two more block copolymers differing in the corona block then yielded ABC ter-micelles able to undergo higher hierarchical self-assembly into supermicelles via the insoluble corona of the terminal segment.

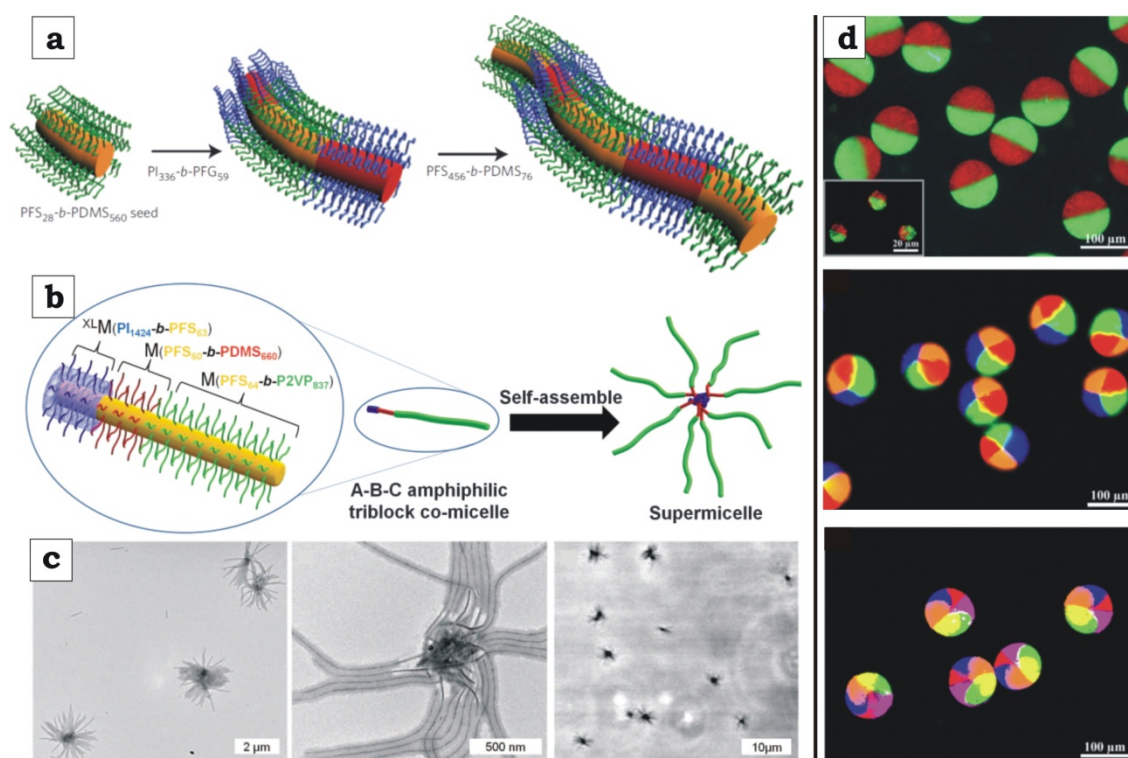


Figure 1–15: Two examples of rarely observed polymer co-assembly into compartments. (a) Schematic representation of the crystallization driven step-wise co-assembly of two diblock copolymers into alternating co-core and co-corona MCMs. Adapted from [246]. Reprinted with permission from Nature Publishing Group. **(b)** Sequential addition of blocks to yield ter-micelles and **(c)** TEM images of supermicelles composed of the linear ABC ter-micelles. Adapted from [250]. Reprinted with permission from the American Association for the Advancement of Sciences. **(d)** Microfluidic of multiple fluorescently labelled sodium alginate solutions gelled by calcium dichloride into rainbow coloured co-assemblies. Adapted from [251]. Reprinted with permission from Wiley-VCH Verlag GmbH & Co. KGaA.

Microfluidic is an entirely different approach providing an elegant platform to continuously produce compartmentalized droplets usually in the range of 10 μm - 1000 μm with near-monodisperse size distributions. For many years, this method was also used to synthesize Janus droplets by co-emulsifying two incompatible fluids or polymerizable monomers with the same stabilizer. This concept was recently extended to unify up to six different compartments within one single droplet. The incorporation of multiple fluorescent dyes into the

single compartments of these beach balls allows clearly distinguishing and following the fusion into spatially separated compartments (Figure 1–15d).^[251]

Block copolymer co-assembly is a challenging task as it can be difficult to find the proper conditions that satisfy sufficient phase separation and co-aggregation into the same superstructure. Methods for colloidal self- and co-assembly achieve outstanding results on the micron-scale, but are mostly not applicable to manipulate polymer self-assembly. For instance, colloidal particles form regular pattern on surfaces and interfaces due to capillary forces or coalesce due to Van-der-Waals forces. This can be exploited to generate 2D and 3D colloidal (co-)crystals on surfaces with interesting optical properties or in solution upon evaporation induced self-assembly in drying colloid loaded droplets.^[252-254] Size-constrained or finite particle arrangements are often realized by particle dispersion in droplets as demonstrated earlier in Figure 1–11a. The co-assembly of two particles applying this method was presented with tremendous precision of particle positioning (Figure 1–16a).^[255-258] The same principle can also be exploited to produce colloidal co-assemblies as demonstrated by the co-dispersion of micrometer-sized PS and gold nanoparticles in water droplets.^[259] Self-assembly into colloids is induced by evaporation of water on super hydrophobic surfaces. Both particles densely pack into opalescent shimmering spheres whereas the pole collapses to finally yield rainbow-coloured doughnuts.^[260]

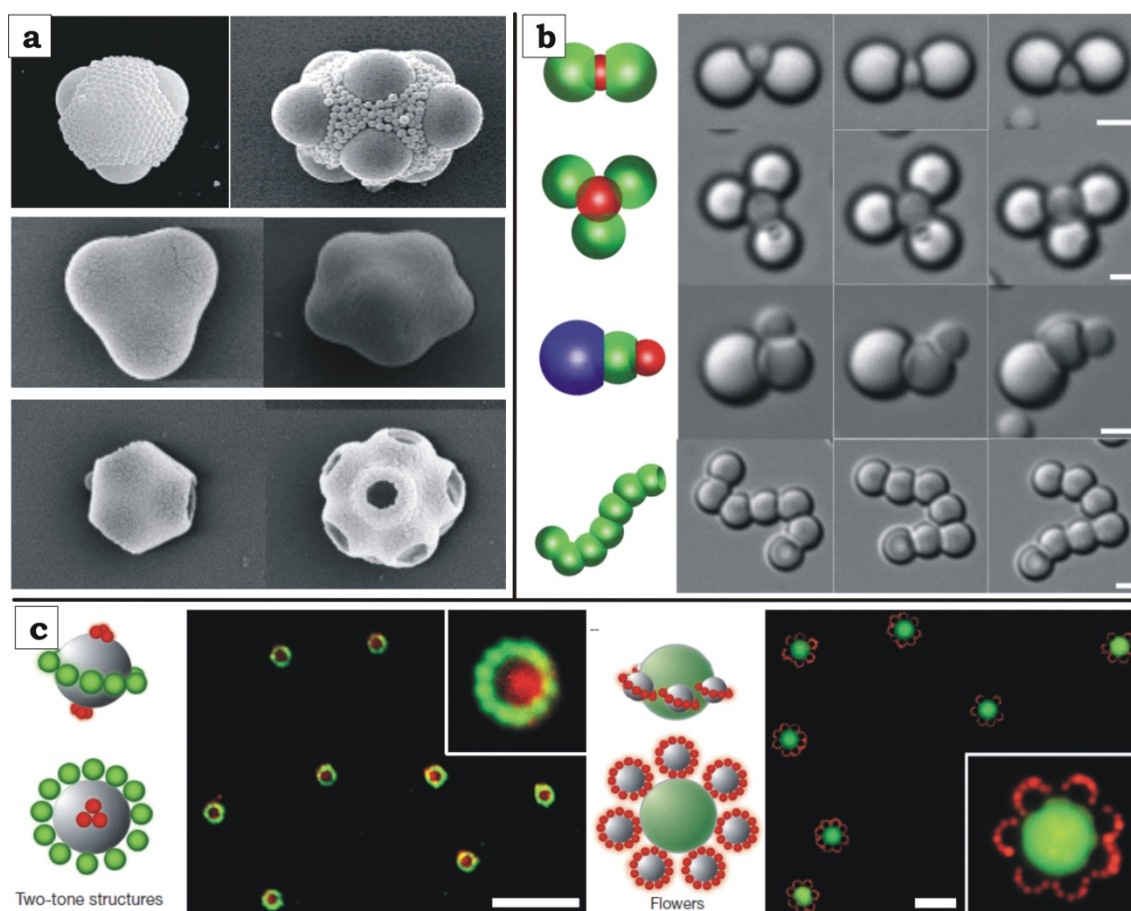


Figure 1–16: Colloidal co-assembly. (a) Evaporation induced co-assembly of silica-silica particle mixtures, PS-silica particle mixtures and selective dissolution of PS to yield silica scaffolds. Adapted from [258]. Re-

printed with permission from American Chemical Society. **(b)** Lock-and-key recognition as the directing and depletion interaction as the coalescing force. Adapted from [41]. Reprinted with permission from Nature Publishing Group. **(c)** Colloidal co-assembly of multiple particles directed by magnetic field. Adapted from [261]. Reprinted with permission from Nature Publishing Group.

The principle of depletion interaction was also already introduced for the formation of cubic crystals (Figure 1–11b) and recently combined with deterministic control of multiple species of a novel type of colloidal particle reminiscent of lock-and-key recognition (Figure 1–16b).^[41, 164, 262] Thereby, the key colloids are spherical particles of varying size and chemistry (PS or silica), and the lock particles are PS latex particles with precisely defined cavities. The cavities are the result of buckling instabilities during emulsion polymerization.^[179] If lock and key are in close proximity coalescence can be directed into co-assemblies with “bond angles” of two or more colloidal species, simply by clever choice of particle size and shapes. The lock and key principle is based on depletion interaction induced by small polymer chains evading the two approaching and essentially matching surfaces. This method can be even further developed to only use lock colloids that will form ice-cones or strings.

Alignment of magnetic particles in magnetic fields offers elegant directing possibilities and with the right choice of components also yields highly complex self-assemblies when multiple colloids are involved (Figure 1–16c).^[261] Magnetic colloids dispersed in a ferrofluid, e.g., a water phase with a specific concentration of magnetite nanoparticles (Fe_3O_4) and subjected to a magnetic field display extraordinary self-assembly potential. The largest colloid is a paramagnetic particle with a diameter of around 10 μm and represents the “planet”, whereas the smaller particles (red/green) are non-magnetic and represent the satellites. Co-assembly of all three species occurs due to the orientation of the magnetite particles to the surface of the non-magnetic colloids inducing magnetization, therein. At a specific magnetite concentration, the medium is less magnetic than the smallest, magnetite-covered colloids (red), which move towards the poles of the giant paramagnetic particle (same sense), but is stronger magnetized than the mid-sized green colloids that now have the opposite sense and acquire equatorial orientation.

1.3 Hybrid Materials Based on Self-Assembly

Downscaling, control and structuring are optimization processes towards potential applications and technological relevance. Desired physical properties and functionality suiting application needs have to be an essential design criterion for any self-assembly process. To replicate model systems, refined and improved by nature in (sometimes) millions of evolutionary optimization steps, is a reliable concept for the material development. We take advantage of nature’s ability to adapt to any environmental condition and perfect structure-property relations, pick materials with outstanding performances from a variety of proper-

ties and put a lot of effort in mimicking these materials artificially or combine multiple materials to outsmart nature.

Hybrid materials or composites usually unify otherwise incompatible physical properties e.g., material's strength combined with energy dissipation components to enhance toughness. In other cases the dispersion of immiscible matter needs compatibilization or control over particle-particle distance in solution^[263] and polymer matrices^[264] towards discovering novel effects (e.g. tailoring plasmon resonance of gold nanoparticles). Moffitt and co-workers designed responsive particles by coating CdSe with a PS-*b*-PMAA-*b*-PMMA triblock terpolymer (Figure 1–17a).^[265] Thereby, the PMAA middle block exchanges to the ligand on the nanoparticle's surface, essentially generating an inorganic block copolymer mimic. Self-assembly then is induced according to a complementary process as discussed in chapter 1.1.3.1 by change of solvent quality for one of the blocks of the coating. In case of the CdSe nanoparticles, the PMMA blocks were hydrolysed to PMAA (the first PMAA block was derived from *Pt*BMA) and self-assembly was induced by transfer into water as the selective solvent. The transient configuration of the mimics was described by a Janus character and aggregation via the collapsed PS blocks resulted in diverse hybrid morphologies such as large compound micelles, segmented worm-like micelles and vesicles. As a special feature of this approach the nanoparticles are exclusively located in spatially separated domains with precise interparticle distance on multiple levels, i.e., the particles are separated by a polymer coating of defined thickness (~nm) and by the domains of the superstructure (> 10 nm).

When dealing with block copolymer self-assembly drug delivery is almost always the primary argument. Vesicles are very prominent structures for the delivery of water-soluble agents, as artificial cell mimics or hybrid protein/polymer cell prototypes. The structural configuration of multicompartment micelles is ideally suited to deliver compatible cargo separately stored in the incompatible compartments. The simultaneous loading of two fluorescent compounds into the compartments of one MCM was demonstrated by Hillmyer and Lodge (Figure 1–17b).^[266] Thereby, miktoarm star terpolymers were used to form hamburger MCMs in water with hydrocarbon/fluorocarbon core segments, each selectively loaded with a naphthalene bearing a fluorocarbon tail and pyrene, respectively. The measured absorbance confirmed the synergetic absorbance of both compounds matching theoretical predictions extremely well. As the naphthalene derivative does not show significant intensity at 300 nm if located in a hydrocarbon environment, the synergetic absorbance at this wavelength can only be achieved if this compound is stored in the fluorocarbon segment.

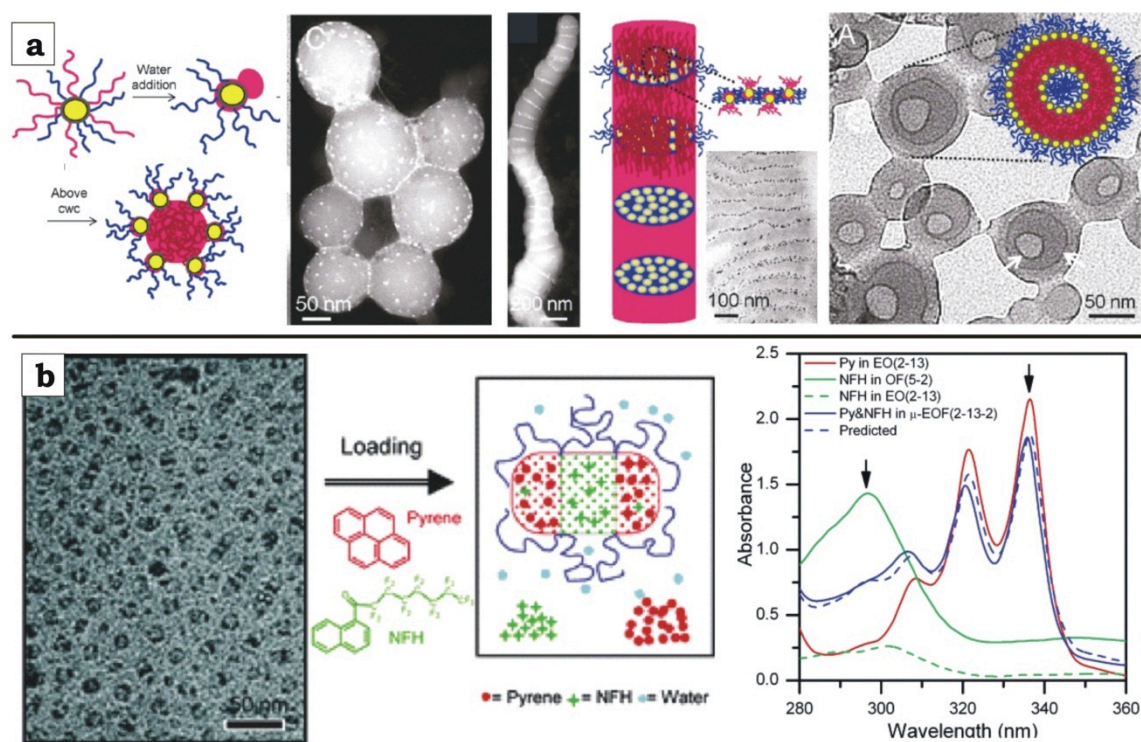


Figure 1–17: Hybrid materials based-on block copolymer self-assembly in solution. (a) The surface coating of CdSe nanoparticles with amphiphilic PS/PMAA patches creates particles capable of higher level self-assembly induced by transfer into water. Sophisticated clustering into hybrid large compound micelles, segmented cylinders and even vesicles, depending on the block weight fractions. **(b)** Multicompartment micelles from mikroarm star terpolymer with core compartments selectively loaded with two different dyes quantified by UV absorption measurements. Adapted from [265] and [266]. Reprinted with permission from the American Chemical Society.

Janus particles have been synthesized via numerous methods and were studied with respect to their superior interfacial properties. Over the years these asymmetric particles shifted into the focus of diverse applications involving interfaces, some of which are discussed here. Walther *et al.* utilized polymeric SBMAA Janus particles as “super surfactants” for stabilization of styrene droplets in water (Figure 1–18a).^[267] Thereby, only a small weight fraction (< 5 wt %) of particles was required to form a stable emulsion, whereas each Janus particle was calculated to stabilize around one hundred times the interface compared to its own size. The emulsion polymerization of these droplets generated PS latex particles (< 500 nm) with an extremely narrow size distributions becoming also evident from BCC packing of the spheres upon deposition on surfaces. In the face of the discussed similarities on solution and in bulk, it is not surprising that soft Janus particles could also be used to facilitate to blending of to homopolymers that match the hemisphere chemistry of the Janus particles (Figure 1–18b).^[268] In this work, SBM Janus particles are compounded together with PS/PMMA powder under melt conditions. After extrusion, the blend exhibits very small (\approx 250 nm) and narrowly distributed PMMA domains in a PS matrix with the Janus particles located at the PS/PMMA interface as small black dots. Thereby, the Janus particles demonstrate superior performance compared to block copolymer compatibilizers due to increased desorption energies. Although the interfacial activity can be expected the

pronounced orientation towards the interfaces at elevated temperatures in highly viscous melts still is a surprising accomplishment.

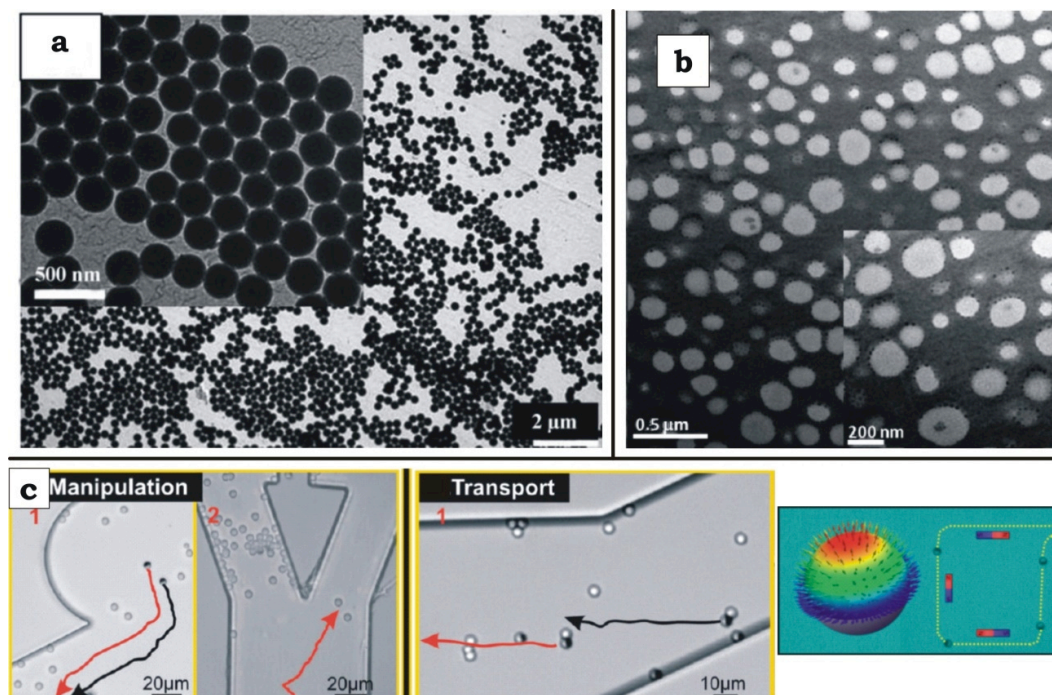


Figure 1–18: Application of Janus particles from 10 nm to several micrometers in size. (a) Soft 10 nm sized SBMAA Janus particles used as stabilizers in the emulsion polymerization of PS latex particles. The addition of only 0.5wt% JPs results in monodisperse PS spheres. Adapted from [267]. Reprinted with permission from Wiley-VCH Verlag GmbH & Co. KGaA.. **(b)** SBMMA JPs are also capable compatibilizers when added to PS/PMMA polymer blends. The droplet size of the minority phase, here PMMA, is considerably reduced with the addition of the SBMMA JPs. Adapted from [268]. Reprinted with permission from the American Chemical Society. **(c)** Heterogeneous JPs with one CoPt hemisphere are capable of directional movement and cargo pick-up, transportation and release. The bimetallic hemisphere is responsible for both propulsion via the catalytic reduction of hydrogen peroxide and dictating the direction via attractive magnetic steering. Adapted from [269]. Reprinted with permission from the American Chemical Society.

Catalytic particulate motors are a very active field frequently utilizing Janus particles. The nanomotors usually consist of a metal or metal alloy surface catalyzing the reaction with the surrounding medium causing propulsion and motion of the particle, respectively (Figure 1–18c).^[270-275] The generic design concept is simple and explains why Janus particles are ideally suited for this task. The propulsion combined with the Janus character offers elegant cargo pickup and delivery possibilities in 2D space.^[269] Baraban *et al.* designed colloidal Janus particles with one hemisphere catalytically converting hydrogen peroxide for propulsion and one hemisphere for deterministic motion via magnetic direction. Thereby, the magnetically active hemisphere was chosen to be a CoNi-alloy the exhibits magnetization perpendicular to the particles surface enabling the controlled steering of the particle. These particles are capable to perform complex activities such as start/stop, approaching and picking up magnetic cargo as well as transport and release. These magnetic swimmers are model particles for separating and purifying particulate matter with microscale precision.

From a material point of view novel materials often mimic nature with artificial components. The work of Ikkala and co-workers is renowned for the preparation of biomimetic materials such as fibres from nanofibrillated cellulose (NFC), approaching the tensile strength of steel or ultrastrong nanopaper of layered clay/polymer composites with a tensile strength comparable to that of nacre.^[14] The self-assembly and positioning of the underlying materials plays a very important role for sufficient energy dissipation, while preserving the structural integrity and preventing catastrophic failure. An intriguing example of how to create such a material from ultra strong components is the combination of NFC with exfoliated graphene sheets mediated by the Janus-like protein, hydrophobin (Figure 1–19a). NFC and graphene are among the strongest known materials^[276-278] and exhibit characteristic surface chemistries. Thereby, the Janus protein hydrophobin has a strong hydrophobic side perfectly suited to attach to the graphene sheets, whilst the other side of the protein can be altered to react with the NFC fibres. The result is a layered nanopaper displaying extraordinary tensile strength.

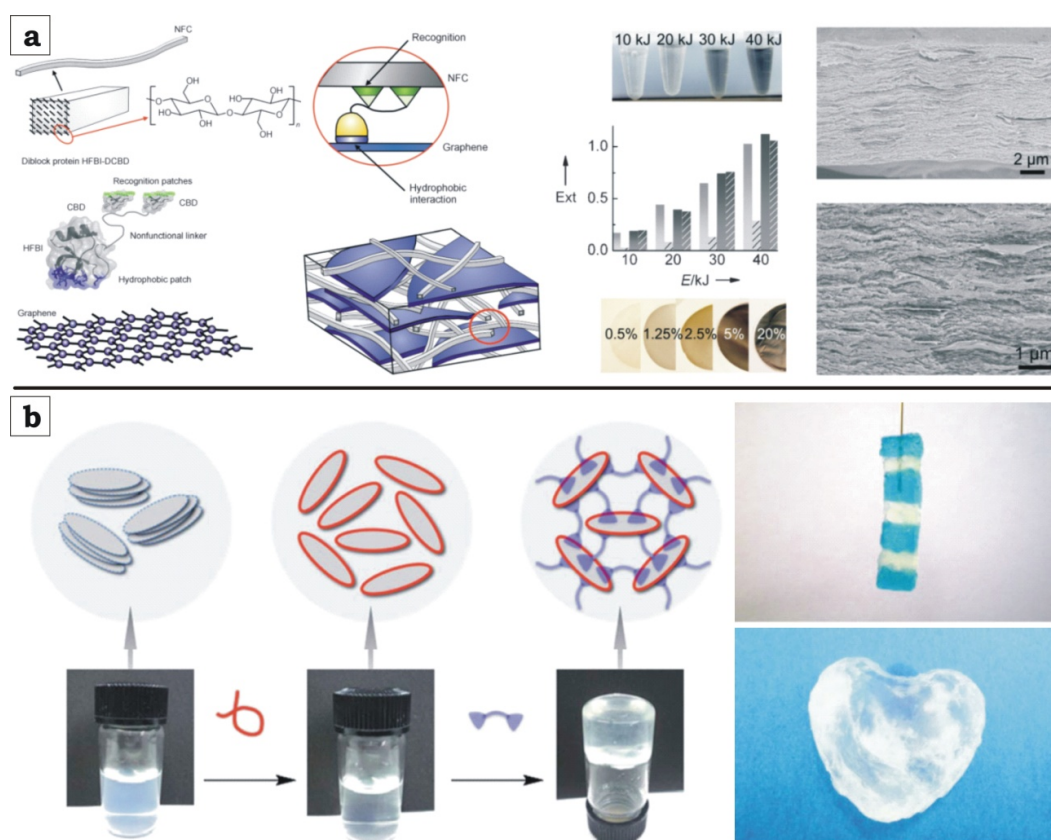


Figure 1–19: Functional materials based on self-assembly. (a) Self-assembly of nanofibrillated cellulose fibres and graphene sheets mediated by a perfectly suited Janus protein (hydrophobin) that selectively binds to both materials. Ultra strong nanopaper with exceptional mechanical properties is the result. Adapted from [14]. Reprinted with permission from Wiley-VCH Verlag GmbH & Co. KGaA. (b) Self-assembly of well-defined anionic clay (laponite) and a cationic dendrimer results in self-healing and strong hydrogels with shape memory. The generation 2 dendrimer consists of a well-defined number of cationic anchor groups on the linked by a poly(ethylene oxide) spacer. Adapted from [5]. Reprinted with permission from Nature Publishing Group.

Hydrogels are attractive materials capable of suiting diverse applications depending on the components used.^[279] Aida and co-workers were able to generate hydrogels with remarkable strength with rapid self-healing properties by the self-assembly of commercially available clay with homopolymer and a dendrimer (Figure 1–19b).^[8] Thereby, the process is extremely simple: (i) vortex stirring of clay facilitates dispersion; (ii) addition of a polyanion compensates the edge charges to complete exfoliation; (iii) non-covalent network formation via multifunctional cationic dendrons. The overall process takes less than 5 min and yields hydrogels with outstanding properties. More importantly this demonstrates that knowledge of interactions on the molecular and particle level allows manipulating matter to unify contradictive physical properties within one material.

1.4 Objective of this Thesis

The aim of this thesis was to derive a novel, generic self-assembly approach to multicompartment micelles which are mostly acknowledged as exotic. A unifying concept would broaden the existing field of polymer and colloidal self-assembly considerably beyond the reach of today's compartmentalized superstructures. Thereby, access to hierarchical self-assembly across multiple length scales is especially attractive with the ultimate goal to create colloidal co-assemblies.

On a series of linear ABC triblock terpolymers common features in self-assembly behaviour should be investigated to find a general self-assembly motif applicable to any linear triblock terpolymer. Control over fine structure and/or geometry are most desirable and even more preferably, control over the positioning of the respective blocks within the superstructure. Depending on the degree of control that is achieved in the preparation of building blocks, the gained knowledge was to be used in attempts to produce building blocks to form unprecedented soft colloidal copolymers. If possible the self-assembly was to be optimized to gain control over size distribution, positioning and sequence of the colloids.

Also depending on the homogeneity of the produced superstructures and the quality of block-block phase separation in the segmented compartmentalized cores, the possibility of developing a universal concept to produce soft, nanometre-sized Janus particles from solution was to be investigated. This transformation from uniform spherical MCM to Janus particles is intuitive and would represent the first feasible application of this fascinating soft material.

References

- [1] G. M. Whitesides, B. Grzybowski, *Science* **2002**, *295*, 2418-2421.
- [2] R. D. Kamien, *Science* **2003**, *299*, 1671-1673.

-
- [3] J. A. Pelesko, *Self-Assembly: The Science of Things That Put Themselves Together*, Taylor & Francis Group New York and London. **2007**.
- [4] S. Mann, *Nat. Mater.* **2009**, *8*, 781-792.
- [5] T. Aida, E. W. Meijer, S. I. Stupp, *Science* **2012**, *335*, 813-817.
- [6] A. H. E. Müller, O. V. Borisov, *Self Organized Nanostructures of Amphiphilic Block Copolymers I + II*, Springer Berlin/Heidelberg, **2011**.
- [7] O. Ikkala, G. ten Brinke, *Science* **2002**, *295*, 2407-2409.
- [8] Q. Wang, J. L. Mynar, M. Yoshida, E. Lee, M. Lee, K. Okuro, K. Kinbara, T. Aida, *Nature* **2009**, *463*, 339-343.
- [9] M. A. C. Stuart, W. T. S. Huck, J. Genzer, M. Muller, C. Ober, M. Stamm, G. B. Sukhorukov, I. Szleifer, V. V. Tsukruk, M. Urban, F. Winnik, S. Zauscher, I. Luzinov, S. Minko, *Nat. Mater.* **2010**, *9*, 101-113.
- [10] V. H. Ebron, Z. Yang, D. J. Seyer, M. E. Kozlov, J. Oh, H. Xie, J. Razal, L. J. Hall, J. P. Ferraris, A. G. MacDiarmid, R. H. Baughman, *Science* **2006**, *311*, 1580-1583.
- [11] J. R. Millman, K. H. Bhatt, B. G. Prevo, O. D. Velev, *Nat. Mater.* **2005**, *4*, 98-102.
- [12] National Research Council, *Inspired by Biology: From Molecules to Materials to Mechanics*, National Academies Press, **2008**.
- [13] P. Podsiadlo, A. K. Kaushik, E. M. Arruda, A. M. Waas, B. S. Shim, J. Xu, H. Nandivada, B. G. Pumplun, J. Lahann, A. Ramamoorthy, N. A. Kotov, *Science* **2007**, *318*, 80-83.
- [14] P. Laaksonen, A. Walther, J.-M. Malho, M. Kainlauri, O. Ikkala, M. B. Linder, *Angew. Chem. Int. Ed.* **2011**, *50*, 8688-8691.
- [15] B. V. Slaughter, S. S. Khurshid, O. Z. Fisher, A. Khademhosseini, N. A. Peppas, *Adv. Mater.* **2009**, *21*, 3307-3329.
- [16] Z. Tang, Y. Wang, P. Podsiadlo, N. A. Kotov, *Adv. Mater.* **2006**, *18*, 3203-3224.
- [17] D. H. Gracias, J. Tien, T. L. Breen, C. Hsu, G. M. Whitesides, *Science* **2000**, *289*, 1170-1172.
- [18] A. Kuzyk, R. Schreiber, Z. Fan, G. Pardatscher, E.-M. Roller, A. Hogele, F. C. Simmel, A. O. Govorov, T. Liedl, *Nature* **2012**, *483*, 311-314.
- [19] O. Benson, *Nature* **2011**, *480*, 193-199.
- [20] Y. Kang, J. J. Walish, T. Gorishnyy, E. L. Thomas, *Nat. Mater.* **2007**, *6*, 957-960.
- [21] S.-H. Kim, S. Y. Lee, S.-M. Yang, G.-R. Yi, *NPG Asia Mater.* **2011**, *3*, 25-33.
- [22] M. Veiga-Gutiérrez, M. Woerdemann, E. Prasetyanto, C. Denz, L. De Cola, *Adv. Mater.* **2012**, *24*, 5199-5204.
- [23] K. Oohora, S. Burazerovic, A. Onoda, Y. M. Wilson, T. R. Ward, T. Hayashi, *Angew. Chem. Int. Ed.* **2012**, *51*, 3818-3821.
- [24] D. Yan, Y. Zhou, J. Hou, *Science* **2004**, *303*, 65-67.
- [25] N. Bowden, A. Terfort, J. Carbeck, G. M. Whitesides, *Science* **1997**, *276*, 233-235.
- [26] R. Cademartiri, C. A. Stan, V. M. Tran, E. Wu, L. Friar, D. Vulis, L. W. Clark, S. Tricard, G. M. Whitesides, *Soft Matter* **2012**.
- [27] N. Hadjichristidis, H. Iatrou, M. Pitsikalis, S. Pispas, A. Avgeropoulos, *Prog. Polym. Sci.* **2005**, *30*, 725-782.
- [28] S. J. Holder, N. A. J. M. Sommerdijk, *Polym. Chem.* **2011**, *2*, 1018-1028.
- [29] A. O. Moughton, M. A. Hillmyer, T. P. Lodge, *Macromolecules* **2012**, *45*, 2-19.
- [30] T. Smart, H. Lomas, M. Massignani, M. V. Flores-Merino, L. R. Perez, G. Battaglia, *Nano Today* **2008**, *3*, 38-46.
- [31] F. H. Schacher, P. A. Rugar, I. Manners, *Angew. Chem. Int. Ed.* **2012**, *51*, 7898-7921.
- [32] Y. Mai, A. Eisenberg, *Chem. Soc. Rev.* **2012**, *41*, 5969-5985.
- [33] R. C. Hayward, D. J. Pochan, *Macromolecules* **2010**, *43*, 3577-3584.
- [34] K. Liu, N. Zhao, E. Kumacheva, *Chem. Soc. Rev.* **2011**, *40*, 656-671.
-

- [35] E. Duguet, A. Desert, A. Perro, S. Ravaine, *Chem. Soc. Rev.* **2011**, *40*, 941-960.
- [36] S. C. Glotzer, M. J. Solomon, *Nat. Mater.* **2007**, *6*, 557-562.
- [37] K. Zhang, M. Jiang, D. Chen, *Progr. Polym. Sci.* **2012**, *37*, 445-486.
- [38] M. Grzelczak, J. Vermant, E. M. Furst, L. M. Liz-Marzán, *ACS Nano* **2010**, *4*, 3591-3605.
- [39] F. Li, D. P. Josephson, A. Stein, *Angew. Chem. Int. Ed.* **2011**, *50*, 360-388.
- [40] A. van Blaaderen, *Science* **2003**, *301*, 470-471.
- [41] S. Sacanna, W. T. M. Irvine, P. M. Chaikin, D. J. Pine, *Nature* **2010**, *464*, 575-578.
- [42] A. van Blaaderen, *Nature* **2006**, *439*, 545-546.
- [43] J. Yoon, K. J. Lee, J. Lahann, *J. Mater. Chem.* **2011**, *21*, 8502-8510.
- [44] L. Zhang, A. Eisenberg, *Science* **1995**, *268*, 1728-1731.
- [45] P. Alexandridis, B. Lindman, *Amphiphilic Block Copolymers: Self-Assembly and Applications*, Elsevier, Amsterdam, **2000**.
- [46] C. Allen, D. Maysinger, A. Eisenberg, *Colloids Surf., B* **1999**, *16*, 3-27.
- [47] S. Förster, T. Plantenberg, *Angew. Chem. Int. Ed.* **2002**, *41*, 688-714.
- [48] D. E. Discher, A. Eisenberg, *Science* **2002**, *297*, 967-973.
- [49] S. Jain, F. S. Bates, *Science* **2003**, *300*, 460-464.
- [50] C. Park, J. Yoon, E. L. Thomas, *Polymer* **2003**, *44*, 6725-6760.
- [51] P. Lim Soo, A. Eisenberg, *J. Polym. Sci. Part B: Polym. Phys.* **2004**, *42*, 923-938.
- [52] D. J. Pochan, Z. Chen, H. Cui, K. Hales, K. Qi, K. L. Wooley, *Science* **2004**, *306*, 94-97.
- [53] V. Castelletto, I. W. Hamley, *Curr. Opin. Solid State Mater. Sci.* **2004**, *8*, 426-438.
- [54] A. Blanazs, S. P. Armes, A. J. Ryan, *Macromol. Rapid Commun.* **2009**, *30*, 267-277.
- [55] H. Yu, W. Jiang, *Macromolecules* **2009**, *42*, 3399-3404.
- [56] H. Cui, Z. Chen, K. L. Wooley, D. J. Pochan, *Soft Matter* **2009**, *5*, 1269-1278.
- [57] E. B. Zhulina, O. V. Borisov, *Macromolecules* **2012**, *45*, 4429-4440.
- [58] K. P. Davis, T. P. Lodge, F. S. Bates, *Macromolecules* **2008**, *41*, 8289-8291.
- [59] G. S. Attard, M. Edgar, C. G. Göltner, *Acta Materialia* **1998**, *46*, 751-758.
- [60] C. V. Kulkarni, W. Wachter, G. Iglesias-Salto, S. Engelskirchen, S. Ahualli, *Phys. Chem. Chem. Phys.* **2011**, *13*, 3004-3021.
- [61] S. Burke, H. Shen, A. Eisenberg, *Macromol. Symp.* **2001**, *175*, 273-284.
- [62] A. Choucair, A. Eisenberg, *Eur. Phys. J. B* **2003**, *10*, 37-44.
- [63] F. Liu, A. Eisenberg, *J. Am. Chem. Soc.* **2003**, *125*, 15059-15064.
- [64] S. Yu, T. Azzam, I. Rouiller, A. Eisenberg, *J. Am. Chem. Soc.* **2009**, *131*, 10557-10566.
- [65] J. Ding, G. Liu, *Macromolecules* **1998**, *31*, 6554-6558.
- [66] A. Rank, S. Hauschild, S. Förster, R. Schubert, *Langmuir* **2009**, *25*, 1337-1344.
- [67] M. Antonietti, S. Förster, *Adv. Mater.* **2003**, *15*, 1323-1333.
- [68] N. Ali, S.-Y. Park, *Langmuir* **2008**, *24*, 9279-9285.
- [69] L. Zhang, A. Eisenberg, *Macromolecules* **1999**, *32*, 2239-2249.
- [70] Y. Yu, L. Zhang, A. Eisenberg, *Macromolecules* **1998**, *31*, 1144-1154.
- [71] S. Sugihara, A. Blanazs, S. P. Armes, A. J. Ryan, A. L. Lewis, *J. Am. Chem. Soc.* **2011**, *133*, 15707-15713.
- [72] A. Blanazs, J. Madsen, G. Battaglia, A. J. Ryan, S. P. Armes, *J. Am. Chem. Soc.* **2011**, *133*, 16581-16587.
- [73] S. Kessel, C. N. Urbani, M. J. Monteiro, *Angew. Chem. Int. Ed.* **2011**, *50*, 8082-8085.
- [74] T. Owen, R. Pynn, J. S. Martinez, A. Butler, *Langmuir* **2005**, *21*, 12109-12114.
- [75] A. O. Moughton, R. K. O'Reilly, *Chem. Commun.* **2010**, *46*, 1091-1093.

- [76] L. Wang, X. Yu, S. Yang, J. X. Zheng, R. M. Van Horn, W.-B. Zhang, J. Xu, S. Z. D. Cheng, *Macromolecules* **2012**, *45*, 3634-3638.
- [77] R. J. Hickey, A. S. Haynes, J. M. Kikkawa, S.-J. Park, *J. Am. Chem. Soc.* **2011**, *133*, 1517-1525.
- [78] J. Hu, T. Wu, G. Zhang, S. Liu, *J. Am. Chem. Soc.* **2012**, *134*, 7624-7627.
- [79] J. Song, J. Zhou, H. Duan, *J. Am. Chem. Soc.* **2012**, *134*, 13458-13469.
- [80] J. Song, L. Cheng, A. Liu, J. Yin, M. Kuang, H. Duan, *J. Am. Chem. Soc.* **2011**, *133*, 10760-10763.
- [81] M.-H. Li, P. Keller, *Soft Matter* **2009**, *5*, 927-937.
- [82] G. Fuks, R. Mayap Talom, F. Gauffre, *Chem. Soc. Rev.* **2011**, *40*, 2475-2493.
- [83] R. P. Brinkhuis, F. P. J. T. Rutjes, J. C. M. van Hest, *Polym. Chem.* **2011**, *2*, 1449-1462.
- [84] S. F. Fenz, K. Sengupta, *Integr. Biol.* **2012**, *4*, 982-995.
- [85] K. Yu, A. Eisenberg, *Macromolecules* **1998**, *31*, 3509-3518.
- [86] B. E. McKenzie, F. Nudelman, P. H. H. Bomans, S. J. Holder, N. A. J. M. Sommerdijk, *J. Am. Chem. Soc.* **2010**, *132*, 10256-10259.
- [87] M. Ueda, A. Makino, T. Imai, J. Sugiyama, S. Kimura, *Soft Matter* **2011**, *7*, 4143-4146.
- [88] C.-K. Chen, S.-C. Lin, R.-M. Ho, Y.-W. Chiang, B. Lotz, *Macromolecules* **2010**, *43*, 7752-7758.
- [89] Z. Lu, G. Liu, F. Liu, *Macromolecules* **2001**, *34*, 8814-8817.
- [90] X. Jiang, Y. Wang, W. Zhang, P. Zheng, L. Shi, *Macromol. Rapid Commun.* **2006**, *27*, 1833-1837.
- [91] Y. Zhang, H. Tan, H. Li, Y.-Q. Liu, F. C. Kartawidjaja, Z.-C. Yang, J. Wang, *Chem. Mater.* **2011**, *23*, 2745-2752.
- [92] R. Deng, S. Liu, J. Li, Y. Liao, J. Tao, J. Zhu, *Adv. Mater.* **2012**, *24*, 1889-1893.
- [93] S. Qin, H. Li, W. Z. Yuan, Y. Zhang, *Soft Matter* **2012**, *8*, 2471-2476.
- [94] T. Higuchi, A. Tajima, K. Motoyoshi, H. Yabu, M. Shimomura, *Angew. Chem. Int. Ed.* **2009**, *48*, 5125-5128.
- [95] D. A. Christian, A. Tian, W. G. Ellenbroek, I. Levental, K. Rajagopal, P. A. Janmey, A. J. Liu, T. Baumgart, D. E. Discher, *Nat. Mater.* **2009**, *8*, 843-849.
- [96] S. Yang, X. Yu, L. Wang, Y. Tu, J. X. Zheng, J. Xu, R. M. Van Horn, S. Z. D. Cheng, *Macromolecules* **2010**, *43*, 3018-3026.
- [97] N. V. Salim, Q. Guo, *J. Phys. Chem. B* **2011**, *115*, 9528-9536.
- [98] J. Zhu, R. C. Hayward, *Macromolecules* **2008**, *41*, 7794-7797.
- [99] D. J. Pochan, J. Zhu, K. Zhang, K. L. Wooley, C. Miesch, T. Emrick, *Soft Matter* **2011**, *7*, 2500-2506.
- [100] Y. Han, W. Jiang, *J. Phys. Chem. B* **2011**, *115*, 2167-2172.
- [101] I. K. Voets, A. de Keizer, P. de Waard, P. M. Frederik, P. H. H. Bomans, H. Schmalz, A. Walther, S. M. King, F. A. M. Leermakers, M. A. Cohen Stuart, *Angew. Chem. Int. Ed.* **2006**, *45*, 6673-6676.
- [102] I. Voets, F. Leermakers, A. de Keizer, M. Charlaganov, M. Stuart, A. H. E. Müller, O. Borisov, *Vol. 241*, Springer Berlin / Heidelberg, pp. 163-185.
- [103] X. Yan, G. Liu, J. Hu, C. G. Willson, *Macromolecules* **2006**, *39*, 1906-1912.
- [104] R. Zheng, G. Liu, X. Yan, *J. Am. Chem. Soc.* **2005**, *127*, 15358-15359.
- [105] J. Hu, G. Liu, *Macromolecules* **2005**, *38*, 8058-8065.
- [106] L. Wang, J. Lin, *Soft Matter* **2011**, *7*, 3383-3391.
- [107] Y. Zhu, H. Yu, Y. Wang, J. Cui, W. Kong, W. Jiang, *Soft Matter* **2012**, *8*, 4695-4707.
- [108] R. M. Holmes, D. R. M. Williams, *Macromolecules* **2011**, *44*, 6172-6181.
- [109] T. Jiang, L. Wang, S. Lin, J. Lin, Y. Li, *Langmuir* **2011**, *27*, 6440-6448.

- [110] C. Auschra, R. Stadler, *Macromolecules* **1993**, *26*, 2171-2174.
- [111] R. K. O'Reilly, C. J. Hawker, K. L. Wooley, *Chem. Soc. Rev.* **2006**, *35*, 1068-1083.
- [112] J. Dupont, G. Liu, K.-i. Niihara, R. Kimoto, H. Jinnai, *Angew. Chem. Int. Ed.* **2009**, *48*, 6144-6147.
- [113] S. Kubowicz, J.-F. Baussard, J.-F. Lutz, A. F. Thünemann, H. von Berlepsch, A. Laschewsky, *Angew. Chem. Int. Ed.* **2005**, *44*, 5262-5265.
- [114] F. Schacher, A. Walther, M. Ruppel, M. Drechsler, A. H. E. Müller, *Macromolecules* **2009**, *42*, 3540-3548.
- [115] Y. Gao, X. Li, L. Hong, G. Liu, *Macromolecules* **2012**, *45*, 1321-1330.
- [116] Z. Wang, W. Jiang, *Chem. Phys. Lett.* **2010**, *487*, 84-87.
- [117] J. Zhu, W. Jiang, *Macromolecules* **2005**, *38*, 9315-9323.
- [118] M. Uchman, M. Štěpánek, K. Procházka, G. Mountrichas, S. Pispas, I. K. Voets, A. Walther, *Macromolecules* **2009**, *42*, 5605-5613.
- [119] Z. Ma, H. Yu, W. Jiang, *J. Phys. Chem. B* **2009**, *113*, 3333-3338.
- [120] J. Du, S. P. Armes, *Soft Matter* **2010**, *6*, 4851-4857.
- [121] J.-F. Gohy, C. Ott, S. Hoepfener, U. S. Schubert, *Chem. Commun.* **2009**, 6038-6040.
- [122] J.-F. Lutz, A. Laschewsky, *Macromol. Chem. Phys.* **2005**, *206*, 813-817.
- [123] Z. Li, E. Kesselman, Y. Talmon, M. A. Hillmyer, T. P. Lodge, *Science* **2004**, *306*, 98-101.
- [124] Z. Li, M. A. Hillmyer, T. P. Lodge, *Langmuir* **2006**, *22*, 9409-9417.
- [125] Z. Li, M. A. Hillmyer, T. P. Lodge, *Nano Lett.* **2006**, *6*, 1245-1249.
- [126] C. Liu, M. A. Hillmyer, T. P. Lodge, *Langmuir* **2008**, *24*, 12001-12009.
- [127] N. Saito, C. Liu, T. P. Lodge, M. A. Hillmyer, *ACS Nano* **2010**, *4*, 1907-1912.
- [128] N. Saito, C. Liu, T. P. Lodge, M. A. Hillmyer, *Macromolecules* **2008**, *41*, 8815-8822.
- [129] C. Liu, M. A. Hillmyer, T. P. Lodge, *Langmuir* **2009**, *25*, 13718-13725.
- [130] J. Xia, C. Zhong, *Macromol. Rapid Commun.* **2006**, *27*, 1110-1114.
- [131] S.-H. Chou, H.-K. Tsao, Y.-J. Sheng, *J. Chem. Phys.* **2006**, *125*, 194903-194906.
- [132] A. Walther, A. H. E. Müller, *Chem. Commun.* **2009**, 1127-1129.
- [133] H. L. Hsieh, R. P. Quirk, *Marcel Dekker Inc., New York* **1996**.
- [134] K. Matyjaszewski, N. V. Tsarevsky, *Nat. Chem.* **2009**, *1*, 276-288.
- [135] A. H. E. Müller, K. Matyjaszewski, *Controlled and Living Polymerizations: From Mechanisms to Applications*, Wiley-VCH Verlag Weinheim, **2009**.
- [136] K. Matyjaszewski, *Macromolecules* **2012**, *45*, 4015-4039.
- [137] A. Kotzev, A. Laschewsky, P. Adriaensens, J. Gelan, *Macromolecules* **2002**, *35*, 1091-1101.
- [138] H. v. Berlepsch, C. Böttcher, K. Skrabania, A. Laschewsky, *Chem. Commun.* **2009**, 2290-2292.
- [139] K. Skrabania, H. v. Berlepsch, C. Böttcher, A. Laschewsky, *Macromolecules* **2009**, *43*, 271-281.
- [140] J.-N. I. Marsat, M. Heydenreich, E. Kleinpeter, H. v. Berlepsch, C. Böttcher, A. Laschewsky, *Macromolecules* **2011**, *44*, 2092-2105.
- [141] U. Breiner, U. Krappe, T. Jakob, V. Abetz, R. Stadler, *Polym. Bull.* **1998**, *40*, 219-226.
- [142] S. Ritzenthaler, F. Court, L. David, E. Girard-Reydet, L. Leibler, J. P. Pascault, *Macromolecules* **2002**, *35*, 6245-6254.
- [143] F. Schacher, A. Walther, A. H. E. Müller, *Langmuir* **2009**, *25*, 10962-10969.
- [144] D. V. Pergushov, A. H. E. Müller, F. H. Schacher, *Chem. Soc. Rev.* **2012**.
- [145] F. Schacher, E. Betthausen, A. Walther, H. Schmalz, D. V. Pergushov, A. H. E. Müller, *ACS Nano* **2009**, *3*, 2095-2102.

- [146] C. V. Synatschke, F. H. Schacher, M. Fortsch, M. Drechsler, A. H. E. Müller, *Soft Matter* **2011**, *7*, 1714-1725.
- [147] K. Kempe, R. Hoogenboom, S. Hoepfner, C.-A. Fustin, J.-F. Gohy, U. S. Schubert, *Chem. Commun.* **2010**, *46*, 6455-6457.
- [148] W. Zhao, D. Chen, Y. Hu, G. M. Grason, T. P. Russell, *ACS Nano* **2011**, *5*, 486-492.
- [149] S. Zhong, H. Cui, Z. Chen, K. L. Wooley, D. J. Pochan, *Soft Matter* **2008**, *4*, 90-93.
- [150] S. Ludwigs, A. Böker, V. Abetz, A. H. E. Müller, G. Krausch, *Polymer* **2003**, *44*, 6815-6823.
- [151] F. Schacher, J. Yuan, H. G. Schoberth, A. H. E. Müller, *Polymer* **2010**, *51*, 2021-2032.
- [152] M. C. Orilall, U. Wiesner, *Chem. Soc. Rev.* **2011**, *40*, 520-535.
- [153] R. Erhardt, A. Böker, H. Zettl, H. Kaya, W. Pyckhout-Hintzen, G. Krausch, V. Abetz, A. H. E. Müller, *Macromolecules* **2001**, *34*, 1069-1075.
- [154] Liu, V. Abetz, A. H. E. Müller, *Macromolecules* **2003**, *36*, 7894-7898.
- [155] A. Walther, X. André, M. Drechsler, V. Abetz, A. H. E. Müller, *J. Am. Chem. Soc.* **2007**, *129*, 6187-6198.
- [156] B. P. Binks, P. D. I. Fletcher, *Langmuir* **2001**, *17*, 4708-4710.
- [157] H. Xu, R. Erhardt, V. Abetz, A. H. E. Müller, W. A. Goedel, *Langmuir* **2001**, *17*, 6787-6793.
- [158] A. Walther, A. H. E. Müller, *Soft Matter* **2008**, *4*, 663-668.
- [159] A. Walther, J. Yuan, V. Abetz, A. H. E. Müller, *Nano Lett.* **2009**, *9*, 2026-2030.
- [160] F. H. Schacher, T. Rudolph, M. Drechsler, A. H. E. Müller, *Nanoscale* **2011**, *3*, 288-297.
- [161] F. H. Schacher, H. Sugimori, S. Hong, H. Jinnai, A. H. E. Müller, *Macromolecules* **2012**.
- [162] A. Sperschneider, F. Schacher, M. Gawenda, L. Tsarkova, A. H. E. Müller, M. Ulbricht, G. Krausch, J. Köhler, *Small* **2007**, *3*, 1056-1063.
- [163] Y. Min, M. Akbulut, K. Kristiansen, Y. Golan, J. Israelachvili, *Nat. Mater.* **2008**, *7*, 527-538.
- [164] S. Sacanna, D. J. Pine, *Curr. Opin. Colloid Interface Sci.* **2011**, *16*, 96-105.
- [165] Z. Mao, H. Xu, D. Wang, *Adv. Funct. Mater.* **2010**, *20*, 1053-1074.
- [166] A. B. Pawar, I. Kretzschmar, *Macromol. Rapid Commun.* **2010**, *31*, 150-168.
- [167] K. J. Lee, J. Yoon, J. Lahann, *Curr. Opin. Colloid Interface Sci.* **2011**, *16*, 195-202.
- [168] K. E. Davis, W. B. Russel, W. J. Glantsching, *Science* **1989**, *245*, 507-510.
- [169] E. Lauga, M. P. Brenner, *Phys. Rev. Lett.* **2004**, *93*, 238301.
- [170] J. Zhu, M. Li, R. Rogers, W. Meyer, R. H. Ottewill, W. B. Russel, P. M. Chaikin, *Nature* **1997**, *387*, 883-885.
- [171] V. N. Manoharan, M. T. Elsesser, D. J. Pine, *Science* **2003**, *301*, 483-487.
- [172] Z. Quan, J. Fang, *Nano Today* **2010**, *5*, 390-411.
- [173] D. Baranov, L. Manna, A. G. Kanaras, *J. Mater. Chem.* **2011**, *21*, 16694-16703.
- [174] P. F. Damasceno, M. Engel, S. C. Glotzer, *Science* **2012**, *337*, 453-457.
- [175] G. Lee, Y.-S. Cho, S. Park, G.-R. Yi, *Korean J. Chem. Eng.* **2011**, *28*, 1641-1650.
- [176] S. Srivastava, A. Santos, K. Critchley, K.-S. Kim, P. Podsiadlo, K. Sun, J. Lee, C. Xu, G. D. Lilly, S. C. Glotzer, N. A. Kotov, *Science* **2010**, *327*, 1355-1359.
- [177] Z. Tang, N. A. Kotov, M. Giersig, *Science* **2002**, *297*, 237-240.
- [178] Z. Tang, Z. Zhang, Y. Wang, S. C. Glotzer, N. A. Kotov, *Science* **2006**, *314*, 274-278.
- [179] L. Rossi, S. Sacanna, W. T. M. Irvine, P. M. Chaikin, D. J. Pine, A. P. Philipse, *Soft Matter* **2011**, *7*, 4139-4142.
- [180] S. Deka, K. Miszta, D. Dorfs, A. Genovese, G. Bertoni, L. Manna, *Nano Lett.* **2010**, *10*, 3770-3776.
- [181] K. Miszta, J. de Graaf, G. Bertoni, D. Dorfs, R. Brescia, S. Marras, L. Ceseracciu, R. Cingolani, R. van Roij, M. Dijkstra, L. Manna, *Nat. Mater.* **2011**, *10*, 872-876.

- [182] W. Qi, J. d. Graaf, F. Qiao, S. Marras, L. Manna, M. Dijkstra, *Nano Lett.* **2012**.
- [183] Zhang, S. C. Glotzer, *Nano Letters* **2004**, *4*, 1407-1413.
- [184] G. Zhang, D. Wang, H. Möhwald, *Angew. Chem. Int. Ed.* **2005**, *44*, 7767-7770.
- [185] A. M. Jackson, Y. Hu, P. J. Silva, F. Stellacci, *J. Am. Chem. Soc.* **2006**, *128*, 11135-11149.
- [186] C. Singh, Y. Hu, B. P. Khanal, E. R. Zubarev, F. Stellacci, S. C. Glotzer, *Nanoscale* **2011**, *3*, 3244-3250.
- [187] A. J. Williamson, A. W. Wilber, J. P. K. Doye, A. A. Louis, *Soft Matter* **2011**, *7*, 3423-3431.
- [188] I. C. Pons-Siepermann, S. C. Glotzer, *ACS Nano* **2012**, *6*, 3919-3924.
- [189] I. C. Pons-Siepermann, S. C. Glotzer, *Soft Matter* **2012**, *8*, 6226-6231.
- [190] Z. He, I. Kretzschmar, *Langmuir* **2012**, *28*, 9915-9919.
- [191] F. Romano, F. Sciortino, *Nat. Commun.* **2012**, *3*, 975.
- [192] Q. Chen, S. C. Bae, S. Granick, *Nature* **2011**, *469*, 381-384.
- [193] Q. Chen, J. K. Whitmer, S. Jiang, S. C. Bae, E. Luijten, S. Granick, *Science* **2011**, *331*, 199-202.
- [194] Q. Chen, S. C. Bae, S. Granick, *J. Am. Chem. Soc.* **2012**, *134*, 11080-11083.
- [195] C. A. Mirkin, R. L. Letsinger, R. C. Mucic, J. J. Storhoff, *Nature* **1996**, *382*, 607-609.
- [196] S. Park, J.-H. Lim, S.-W. Chung, C. A. Mirkin, *Science* **2004**, *303*, 348-351.
- [197] R. J. Macfarlane, B. Lee, M. R. Jones, N. Harris, G. C. Schatz, C. A. Mirkin, *Science* **2012**, *334*, 204-208.
- [198] S. Angioletti-Uberti, B. M. Mognetti, D. Frenkel, *Nat. Mater.* **2012**, *11*, 518-522.
- [199] M. G. Warner, J. E. Hutchison, *Nat. Mater.* **2003**, *2*, 272-277.
- [200] Y. Liu, G. Zhang, L. Niu, L. Gan, D. Liang, *J. Mater. Chem.* **2011**, *21*, 14864-14868.
- [201] K. Chaudhary, Q. Chen, J. J. Juárez, S. Granick, J. A. Lewis, *J. Am. Chem. Soc.* **2012**, *134*, 12901-12903.
- [202] H. Yoon, A. Ghosh, J. Y. Han, S. H. Sung, W. B. Lee, K. Char, *Adv. Funct. Mater.* **2012**, *22*, 3723-3728.
- [203] J. Du, R. K. O'Reilly, *Chem. Soc. Rev.* **2011**, *40*, 2402-2416.
- [204] A. Perro, S. Reculosa, S. Ravaine, E. Bourgeat-Lami, E. Duguet, *J. Mater. Chem.* **2005**, *15*, 3745-3760.
- [205] Q. Chen, J. Yan, J. Zhang, S. C. Bae, S. Granick, *Langmuir* **2012**.
- [206] S. Jiang, Q. Chen, M. Tripathy, E. Luijten, K. S. Schweizer, S. Granick, *Adv. Mater.* **2010**, *22*, 1060-1071.
- [207] F. Wurm, A. F. M. Kilbinger, *Angew. Chem. Int. Ed.* **2009**, *48*, 8412-8421.
- [208] I. Kretzschmar, J. H. Song, *Curr. Opin. Colloid Interface Sci.* **2011**, *16*, 84-95.
- [209] M. Lattuada, T. A. Hatton, *Nano Today* **2011**, *6*, 286-308.
- [210] J. Hu, S. Zhou, Y. Sun, X. Fang, L. Wu, *Chem. Soc. Rev.* **2012**, *41*, 4356-4378.
- [211] G. Loget, A. Kuhn, *J. Mater. Chem.* **2012**, *22*, 15457-15474.
- [212] L. Zhang, Y. Zhu, *Langmuir* **2012**, *28*, 13201-13207.
- [213] A. Walther, M. Drechsler, A. H. E. Müller, *Soft Matter* **2009**, *5*, 385-390.
- [214] A. Walther, M. Drechsler, S. Rosenfeldt, L. Harnau, M. Ballauff, V. Abetz, A. H. E. Müller, *J. Am. Chem. Soc.* **2009**, *131*, 4720-4728.
- [215] L. Hong, A. Cacciuto, E. Luijten, S. Granick, *Nano Lett.* **2006**, *6*, 2510-2514.
- [216] R. Erhardt, M. Zhang, A. Böker, H. Zettl, C. Abetz, P. Frederik, G. Krausch, V. Abetz, A. H. E. Müller, *J. Am. Chem. Soc.* **2003**, *125*, 3260-3267.
- [217] A. Figuerola, I. R. Franchini, A. Fiore, R. Mastroia, A. Falqui, G. Bertoni, S. Bals, G. Van Tendeloo, S. Kudera, R. Cingolani, L. Manna, *Adv. Mater.* **2009**, *21*, 550-554.
- [218] L. Xu, H. Kuang, L. Wang, C. Xu, *J. Mater. Chem.* **2011**, *21*, 16759-16782.

- [219] Z. Zhao, Z. Shi, Y. Yu, G. Zhang, *Langmuir* **2012**, *28*, 2382-2386.
- [220] T. Mokari, E. Rothenberg, I. Popov, R. Costi, U. Banin, *Science* **2004**, *304*, 1787-1790.
- [221] J.-Y. Wang, Y. Wang, S. S. Sheiko, D. E. Betts, J. M. DeSimone, *J. Am. Chem. Soc.* **2012**, *134*, 5801-5806.
- [222] L. J. Hill, M. M. Bull, Y. Sung, A. G. Simmonds, P. T. Dirlam, N. E. Richey, S. E. DeRosa, I.-B. Shim, D. Guin, P. J. Costanzo, N. Pinna, M.-G. Willinger, W. Vogel, K. Char, J. Pyun, *ACS Nano* **2012**, *6* (10), 8632-8645.
- [223] K. Liu, Z. Nie, N. Zhao, W. Li, M. Rubinstein, E. Kumacheva, *Science* **2010**, *329*, 197-200.
- [224] Z. Nie, D. Fava, E. Kumacheva, S. Zou, G. C. Walker, M. Rubinstein, *Nat. Mater.* **2007**, *6*, 609-614.
- [225] Z. Nie, A. Petukhova, E. Kumacheva, *Nat. Nanotech.* **2010**, *5*, 15-25.
- [226] Z. Nie, E. Kumacheva, *Nat. Mater.* **2008**, *7*, 277-290.
- [227] D. Fava, Z. Nie, M. A. Winnik, E. Kumacheva, *Adv. Mater.* **2008**, *20*, 4318-4322.
- [228] Z. Zhang, P. Pfliegerer, A. B. Schofield, C. Clasen, J. Vermant, *J. Am. Chem. Soc.* **2011**, *133*, 392-395.
- [229] G. A. DeVries, M. Brunnbauer, Y. Hu, A. M. Jackson, B. Long, B. T. Neltner, O. Uzun, B. H. Wunsch, F. Stellacci, *Science* **2007**, *315*, 358-361.
- [230] E. S. Cho, J. Kim, B. Tejerina, T. M. Hermans, H. Jiang, H. Nakanishi, M. Yu, A. Z. Patashinski, S. C. Glotzer, F. Stellacci, B. A. Grzybowski, *Nat. Mater.* **2012**, *11*, 978-985.
- [231] Q. Chen, E. Diesel, J. K. Whitmer, S. C. Bae, E. Luijten, S. Granick, *J. Am. Chem. Soc.* **2011**, *133*, 7725-7727.
- [232] F. Romano, F. Sciortino, *Soft Matter* **2011**, *7*, 5799-5804.
- [233] J. Hu, G. Njikang, G. Liu, *Macromolecules* **2008**, *41*, 7993-7999.
- [234] A. Walther, C. Barner-Kowollik, A. H. E. Müller, *Langmuir* **2010**, *26*, 12237-12246.
- [235] R. Ma, B. Wang, Y. Xu, Y. An, W. Zhang, G. Li, L. Shi, *Macromol. Rapid Commun.* **2007**, *28*, 1062-1069.
- [236] H. Cui, Z. Chen, S. Zhong, K. L. Wooley, D. J. Pochan, *Science* **2007**, *317*, 647-650.
- [237] K. Hales, Z. Chen, K. L. Wooley, D. J. Pochan, *Nano Lett.* **2008**, *8*, 2023-2026.
- [238] Z. Li, J. Ma, N. S. Lee, K. L. Wooley, *J. Am. Chem. Soc.* **2011**, *133*, 1228-1231.
- [239] J. L. Sorrells, Y.-H. Tsai, K. L. Wooley, *J. Polym. Sci. Part A: Polym. Chem.* **2010**, *48*, 4465-4472.
- [240] H. Cui, Z. Chen, K. L. Wooley, D. J. Pochan, *Macromolecules* **2006**, *39*, 6599-6607.
- [241] J. Schmelz, M. Karg, T. Hellweg, H. Schmalz, *ACS Nano* **2011**, *5*, 9523-9534.
- [242] B. Fang, A. Walther, A. Wolf, Y. Xu, J. Yuan, A. H. E. Müller, *Angew. Chem. Int. Ed.* **2009**, *48*, 2877-2880.
- [243] J. Schmelz, A. E. Schedl, C. Steinlein, I. Manners, H. Schmalz, *J. Am. Chem. Soc.* **2012**, *134*, 14217-14225.
- [244] X. Wang, G. Guerin, H. Wang, Y. Wang, I. Manners, M. A. Winnik, *Science* **2007**, *317*, 644-647.
- [245] F. He, T. Gädt, I. Manners, M. A. Winnik, *J. Am. Chem. Soc.* **2011**, *133*, 9095-9103.
- [246] T. Gadt, N. S. Jeong, G. Cambridge, M. A. Winnik, I. Manners, *Nat. Mater.* **2009**, *8*, 144-150.
- [247] H. Wang, A. J. Patil, K. Liu, S. Petrov, S. Mann, M. A. Winnik, I. Manners, *Adv. Mater.* **2009**, *21*, 1805-1808.
- [248] J. Qian, G. Guerin, Y. Lu, G. Cambridge, I. Manners, M. A. Winnik, *Angew. Chem. Int. Ed.* **2011**, *50*, 1622-1625.
- [249] P. A. Rugar, G. Cambridge, M. A. Winnik, I. Manners, *J. Am. Chem. Soc.* **2011**, *133*, 16947-16957.
- [250] P. A. Rugar, L. Chabanne, M. A. Winnik, I. Manners, *Science* **2012**, *337*, 559-562.

- [251] K. Maeda, H. Onoe, M. Takinoue, S. Takeuchi, *Adv. Mater.* **2012**, *24*, 1340-1346.
- [252] Z. Dai, Y. Li, G. Duan, L. Jia, W. Cai, *ACS Nano* **2012**, *6*, 6706-6716.
- [253] S. Pichler, M. I. Bodnarchuk, M. V. Kovalenko, M. Yarema, G. Springholz, D. V. Talapin, W. Heiss, *ACS Nano* **2012**, *5*, 1703-1712.
- [254] Z. Chen, J. Moore, G. Radtke, H. Sirringhaus, S. O'Brien, *J. Am. Chem. Soc.* **2007**, *129*, 15702-15709.
- [255] D. Sen, J. Bahadur, S. Mazumder, S. Bhattacharya, *Soft Matter* **2012**, *8*, 10036-10044.
- [256] J. Bahadur, D. Sen, S. Mazumder, B. Paul, H. Bhatt, S. G. Singh, *Langmuir* **2012**, *28*, 1914-1923.
- [257] D. J. Kraft, W. S. Vlug, C. M. van Kats, A. van Blaaderen, A. Imhof, W. K. Kegel, *J. Am. Chem. Soc.* **2008**, *131*, 1182-1186.
- [258] Y.-S. Cho, G.-R. Yi, J.-M. Lim, S.-H. Kim, V. N. Manoharan, D. J. Pine, S.-M. Yang, *J. Am. Chem. Soc.* **2005**, *127*, 15968-15975.
- [259] V. Rastogi, S. Melle, O. G. Calderón, A. A. García, M. Marquez, O. D. Velev, *Adv. Mater.* **2008**, *20*, 4263-4268.
- [260] V. Rastogi, A. A. García, M. Marquez, O. D. Velev, *Macromol. Rapid Commun.* **2010**, *31*, 190-195.
- [261] R. M. Erb, H. S. Son, B. Samanta, V. M. Rotello, B. B. Yellen, *Nature* **2009**, *457*, 999-1002.
- [262] S. Sacanna, W. T. M. Irvine, L. Rossi, D. J. Pine, *Soft Matter* **2011**, *7*, 1631-1634.
- [263] Y. Mai, A. Eisenberg, *Acc. Chem. Res.* **2012**, *45* (10), 1657-1666.
- [264] S. Fischer, A. Salcher, A. Kornowski, H. Weller, S. Förster, *Angew. Chem. Int. Ed.* **2011**, *50*, 7811-7814.
- [265] Y. Guo, S. Harirchian-Saei, C. M. S. Izumi, M. G. Moffitt, *ACS Nano* **2011**, *5*, 3309-3318.
- [266] T. P. Lodge, A. Rasdal, Z. Li, M. A. Hillmyer, *J. Am. Chem. Soc.* **2005**, *127*, 17608-17609.
- [267] A. Walther, M. Hoffmann, A. H. E. Müller, *Angew. Chem. Int. Ed.* **2008**, *47*, 711-714.
- [268] A. Walther, K. Matussek, A. H. E. Müller, *ACS Nano* **2008**, *2*, 1167-1178.
- [269] L. Baraban, D. Makarov, R. Streubel, I. Mönch, D. Grimm, S. Sanchez, O. G. Schmidt, *ACS Nano* **2012**, *6*, 3383-3389.
- [270] Y. Wang, R. M. Hernandez, D. J. Bartlett, J. M. Bingham, T. R. Kline, A. Sen, T. E. Mallouk, *Langmuir* **2006**, *22*, 10451-10456.
- [271] P. M. Wheat, N. A. Marine, J. L. Moran, J. D. Posner, *Langmuir* **2010**, *26*, 13052-13055.
- [272] S. J. Ebbens, J. R. Howse, *Langmuir* **2011**, *27*, 12293-12296.
- [273] R. A. Pavlick, S. Sengupta, T. McFadden, H. Zhang, A. Sen, *Angew. Chem. Int. Ed.* **2011**, *50*, 9374-9377.
- [274] S. Sengupta, M. E. Ibele, A. Sen, *Angew. Chem. Int. Ed.* **2012**, *51*, 8434-8445.
- [275] W. Gao, A. Pei, J. Wang, *ACS Nano* **2012**, *6*, 8432-8438.
- [276] A. K. Geim, *Science* **2009**, *324*, 1530-1534.
- [277] A. K. Geim, K. S. Novoselov, *Nat Mater* **2007**, *6*, 183-191.
- [278] M. Henriksson, L. A. Berglund, P. Isaksson, T. Lindström, T. Nishino, *Biomacromolecules* **2008**, *9*, 1579-1585.
- [279] J.-Y. Sun, X. Zhao, W. R. K. Illeperuma, O. Chaudhuri, K. H. Oh, D. J. Mooney, J. J. Vlassak, Z. Suo, *Nature* **2012**, *489*, 133-136.

2 Thesis Overview

This thesis contains 4 articles, presented in chapters 3 to 6.

The central theme, connecting all chapters of this thesis, is the bottom-up hierarchical self-assembly of linear ABC triblock terpolymers into colloidal building blocks (CBBs) and their further self-assembly across multiple length scales. Self-assembly in nature and in synthetic materials is the ultimate bottom-up strategy for the energy-efficient structuring of future complex materials with advanced functionality. They find applications from nanolithography to targeted drug delivery, where precise control of the structure is of utmost importance. The main aim was to investigate possibilities to structure soft patchy nanoparticles with control of geometric positioning of responsive surface patches. Consecutively they were used as CBBs capable to further aggregate into complex colloidal (co-)polymers. The successful preparation of micron-scale multicompartment micelles (MCMs), patchy colloids and co-colloids via directed self-assembly of nanoscale triblock terpolymers presents a major advancement in the field of polymer and colloidal self-assembly.

Amphiphilic block copolymers are among of the simplest and smallest building blocks for hierarchical self-assembly with the size of a single coiled block copolymer chain usually in the range of 10 nm (10-100 kg/mol). The main aim of this thesis is to explore ways of utilizing multiple responses confined into triblock terpolymers to produce patchy nanoparticles that can further self-assemble into higher hierarchies. The self-assembly via selective solvents for one of the blocks paved the way to moderately simple surface compartmentalized nanoparticles with AB and ABA distribution of the responsive surface patches, which are motifs reported in the literature and considered self-assembly of “Hierarchy Level 1”. My research efforts were devoted to turn self-assembly of “Hierarchy Level 2”, commonly perceived as exotic, into state of the art by simple and proper means of terpolymer manipulation in solution. The obtained results prove that simple sequential solvent sequences with changing quality pave the way to a large variety of structurally different MCMs with unprecedented homogeneity. In a subsequent step Hierarchy Level 2 was advanced even further and paradigms were set for the controlled self- and co-assembly of triblock terpolymers to first surface compartmentalized nanoparticles and further into, e.g., particle decorated cylindrical colloidal co-assemblies corresponding to the bridging of multiple hierarchies. Not only could the positioning of the respective colloids be predicted and controlled, but also the length and dispersity of the worm-like co-assemblies by interrupting the step-growth polymerization process by introducing tailored patchy nanoparticles as end-cappers.

This thesis is divided into three main sections. The major contribution is located in Chapter 3 and 4 encompassing the directed self-assembly of triblock terpolymers into patchy nanoparticles, rarely observed MCM architectures (Level 1) with controllable aggregation number (Level 2) and unprecedented co-assembly of multiple patchy nanoparticles (Level 2.5). In chapter 5 the spherical MCMs of chapter 3 find application in a novel solution-based route to Janus particles giving access to, so far, unattainable structural features such as control of core diameter, Janus balance and modulation of corona chemistries. The tuneable Janus balance provides a versatile platform to study aggregation behaviour of Janus particles in selective solvents for either one of the corona patches. The Janus particles of Chapter 5 were in turn applied in chapter 6 to study the effect of Janus balance on stabilization capabilities of carbon nanotubes. The next few sections summarize the most relevant results of each chapter.

2.1 Bottom-up Structuring of Patchy Nanoparticles and Next Level Self-Assembly

MCMs formed by linear ABC triblock terpolymers are fascinating soft patchy nanoparticles that can adopt a rich repertoire of core geometries and internal segregation, and have emerged as remarkable class of nanostructured self-assemblies in solution where true hierarchies exist. Up to now, reports on compartmentalized particles were mostly found in combination with complicated polymer architectures such as miktoarm star terpolymers, with strongly phase separating fluorocarbon and/or hydrocarbon blocks or with the aid of additives. Even then, the geometry and fine-structure of these aggregates were random, unpredictable and highly disperse as a comprehensive understanding (thermodynamics and kinetics) and a straightforward concept for controlling MCM architectures for simple and readily accessible terpolymer topologies does not exist. In this project, I developed an approach that opens a new direction for hierarchical self-assembly of complex superstructures from readily accessible linear ABC triblock terpolymers. Proper sequenced changes of the solvent quality facilitate the formation of a multitude of MCMs from one single type of triblock terpolymer with unprecedented homogeneity. Figure 2–1 schematically depicts the mechanism with which the first selective solvent precipitates the middle block of the ABC triblock terpolymer, creating B-core micelles with a patchy A/C corona, therein. In a subsequent step, the corona-compartmentalized nanoparticles are transferred into a non-solvent for B and A where self-assembly is triggered via the solvophobic A patches into a variety of MCMs with surprisingly narrow dispersity. The MCMs are always constituted of a segmented A/B core and a stabilizing C corona.

The underlying mechanism of the self-assembly process is clearly different from what most articles described before. Usually the terpolymer is directly dispersed in a selective solvent for one block only, resulting in spontaneous arrangement of all three blocks according to their block/block and block/solvent interactions, interfacial tension and curva-

ture at the interface. In this study, however, the terpolymer was directed step-by-step into its final superstructure allowing us to determine the position of the respective block within the MCMs by choosing the solvent sequence accordingly. Besides the possibility to generate a large plethora of MCMs from the same type of linear triblock terpolymer, especially spherical MCMs can be obtained in extraordinary homogeneity. Exemplified on what we specified as "Clover" MCM the evaluation of 500 specimens peaked in over 92% identical particles with 3 compartments geometrically positioned in an angle of $\alpha \approx 120^\circ$. The remaining 8% were equally distributed between 2 and 4 compartments. In summary, this results in an extremely narrow distribution ($PDI < 1.05$) of core segments per MCM.

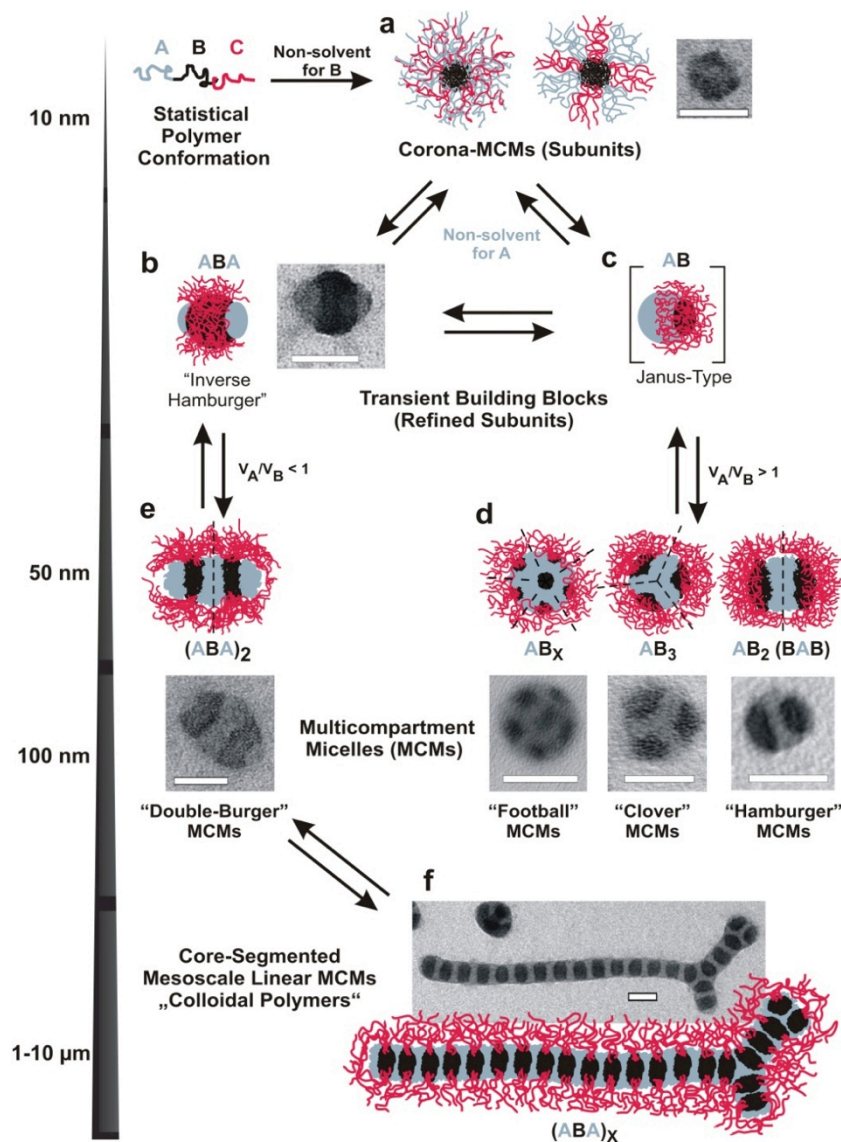


Figure 2–1: Schematic of MCM formation using a carefully chosen solvent sequence to direct the self-assembly of linear ABC triblock terpolymers. The series of TEM images shows the mechanism behind MCM formation exemplified on SBM triblock terpolymers. The process starts with the dispersion of the triblock terpolymer in a nonsolvent for B yielding corona-MCMs with a patchy corona. Subsequent change of the solvent quality for B and A evokes collapse of the A patches and triggers aggregation into spherical or wormlike MCMs according to V_A/V_B . (OsO₄ staining: PB black, PS gray and PMMA not visible due to *e*-beam degradation).

Beyond that, the volume ratios of the core forming blocks V_A/V_B were determined to be the crucial parameter for self-assembly to proceed into spherical or worm-like MCMs (also colloidal polymers). With long A blocks and a high $V_A/V_B > 1$, respectively, the patchy corona-MCMs (subunits) aggregate into spherical MCMs with larger aggregation numbers the higher the value for V_A/V_B . This is attributed to the dominant solvophobic core fraction that needs to be stabilized by corona. Thus, swelling and contracting the corona via addition of good or bad solvent allows manipulating the aggregation number of subunits per MCM.

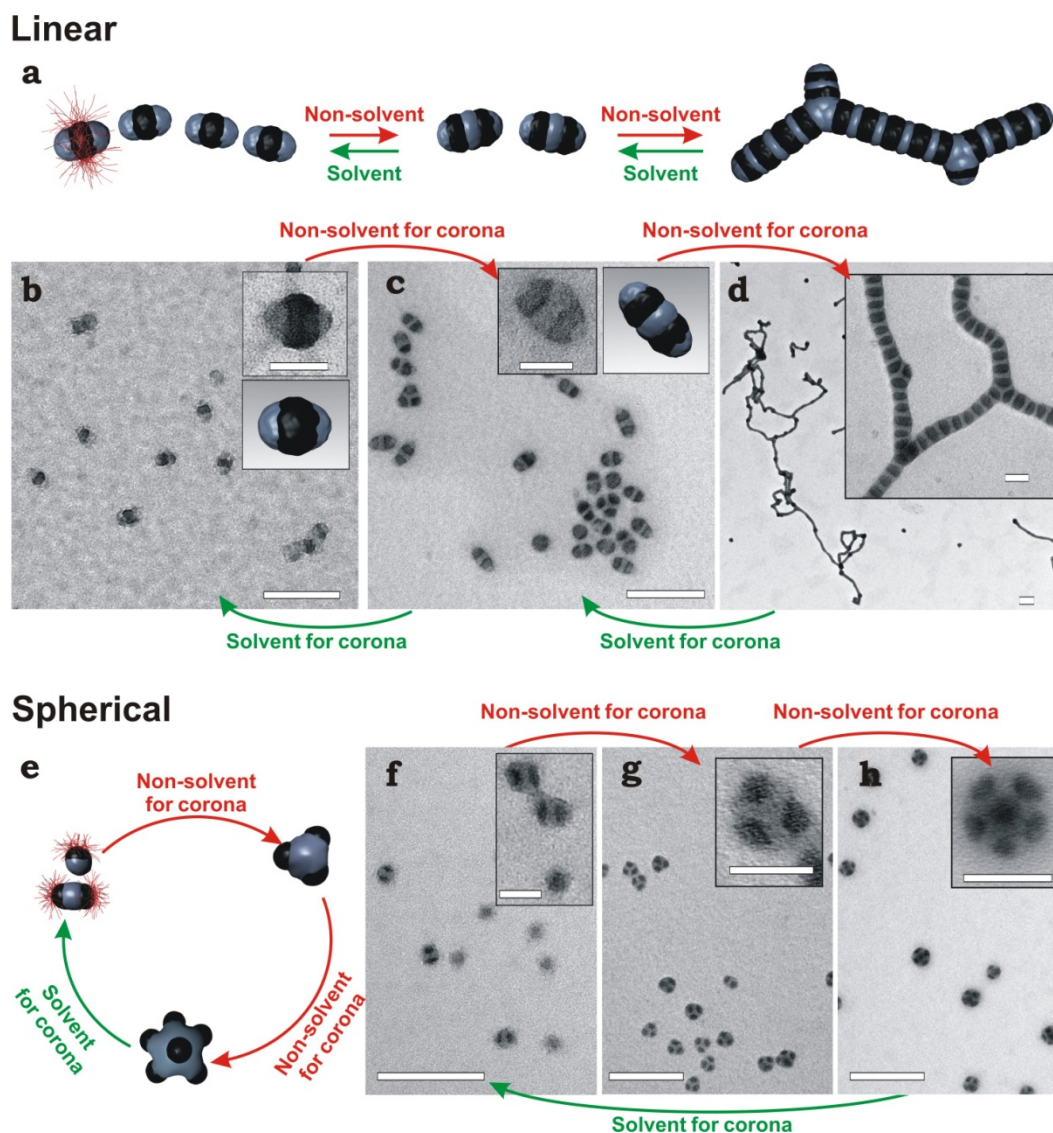


Figure 2–2: Switching between step-growth polymerization and de-polymerization of linear ABA building blocks and spherical AB building blocks. TEM images show MCMs exemplified on SBM terpolymers with polymer phases after OsO_4 staining: PS grey, PB black and PMMA invisible due to e-beam degradation.

In a similar manner, the self-assembly mechanism allows control of both the growth into linear MCMs ($V_A/V_B < 1$) and the degree of polymerization by choosing the solvent quality for the corona accordingly. For instance, instead of using one single selective solvent for the M corona of SBM triblock terpolymers (e.g. glycol ethers), a solvent mixture was cho-

sen (acetone/isopropanol) to be able to adjust the corona volume by design. The addition of solvent (acetone) causes depolymerisation of the colloidal polymer due to the expanding corona protecting the solvophobic A patches. Increasing the non-solvent content (isopropanol) results in polymerization due to the contracting corona, unfavourable exposure of the solvophobic core and further aggregation (Figure 2–2). The effect of polymerization/depolymerisation is very pronounced and can lead to growth into extended worm-like MCMs up to several micrometres and fragmentation of the same into 100 nm dimers. This concept enabled to understand and direct the hierarchical step-growth polymerization of MCMs into micron-scale segmented supracolloidal polymers as an example of programmable meso-scale colloidal hierarchies via well-defined patchy nanoparticles.

The general applicability of this concept was demonstrated for a multitude of linear and easily synthesized ABC triblock terpolymers with widely different physical/chemical properties. Especially the latter, demonstrate elegant pH-programmable, reversible aggregation/decay of small MCM bricks into extended chains (Figure 2–3).

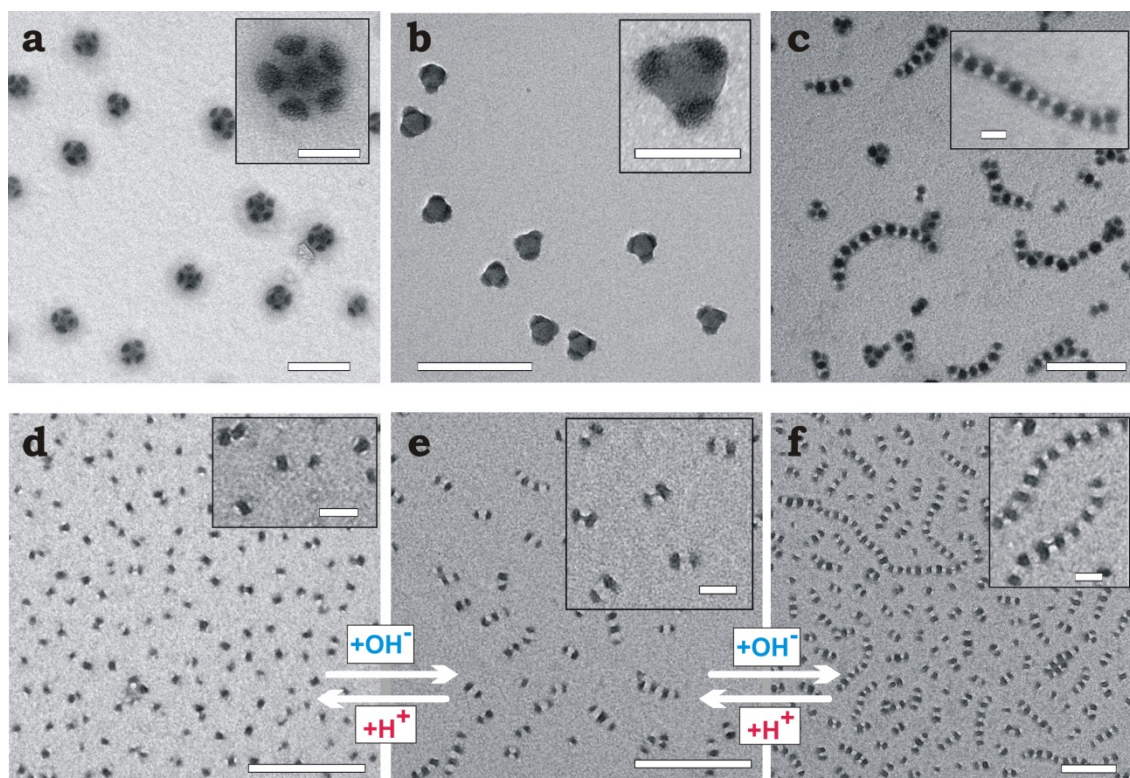


Figure 2–3: General validity of the concept - MCMs of different triblock terpolymers. (a) polystyrene-*block*-polybutadiene-*block*-poly(2-vinylpyridine) SBV in acetone/isopropanol 20/80. (b) polystyrene-*block*-polybutadiene-*block*-poly(*tert*-butyl methacrylate) SBT2 in ethanol. (c) poly(*tert*-butyl methacrylate)-*block*-poly(2-vinylpyridine)-*block*-polybutadiene TVB1 in dodecane. (d-f) pH-programmable colloidal polymerization of poly(*tert*-butyl methacrylate)-*block*-poly(2-cinnamoyloxyethyl methacrylate)-*block*-poly(2-(dimethylamino)ethyl methacrylate) TCD in water: (d) pH = 3 completely protonated, (e) pH = 6 partially protonated, and (f) pH = 10 deprotonated corona. (Scale bars are 200 nm and 50 nm in insets).

2.2 Mixed Colloidal Co-Assemblies from Patchy Nanoparticles

In this consecutive work on the step-wise self-assembly of linear ABC triblock terpolymers, patchy nanoparticles (corona-MCMs in chapter 3) were investigated upon their ability to not only form clusters and self-assemblies, but also colloidal co-assemblies. Therefore, two triblock terpolymers, SBM and SDM, act as the building blocks of (the lowest) hierarchy level 0 that yield CBBs of the next higher hierarchy level 1, SB^{M} and SD^{M} S. If both species are kept separate and the solvent quality is reduced for A, the described self-assembly of chapter 3 into “football” MCMs $(\text{SB}^{\text{M}})_x$ and linear colloidal polymers $[\text{SD}^{\text{M}}\text{S}]_m$ is observed, depending on the volume ratio of the core forming blocks ($V_{\text{S}}/V_{\text{B}} > 1$ and $V_{\text{S}}/V_{\text{D}} < 1$). These colloidal co-assemblies correspond to a structuring on hierarchy level 2.

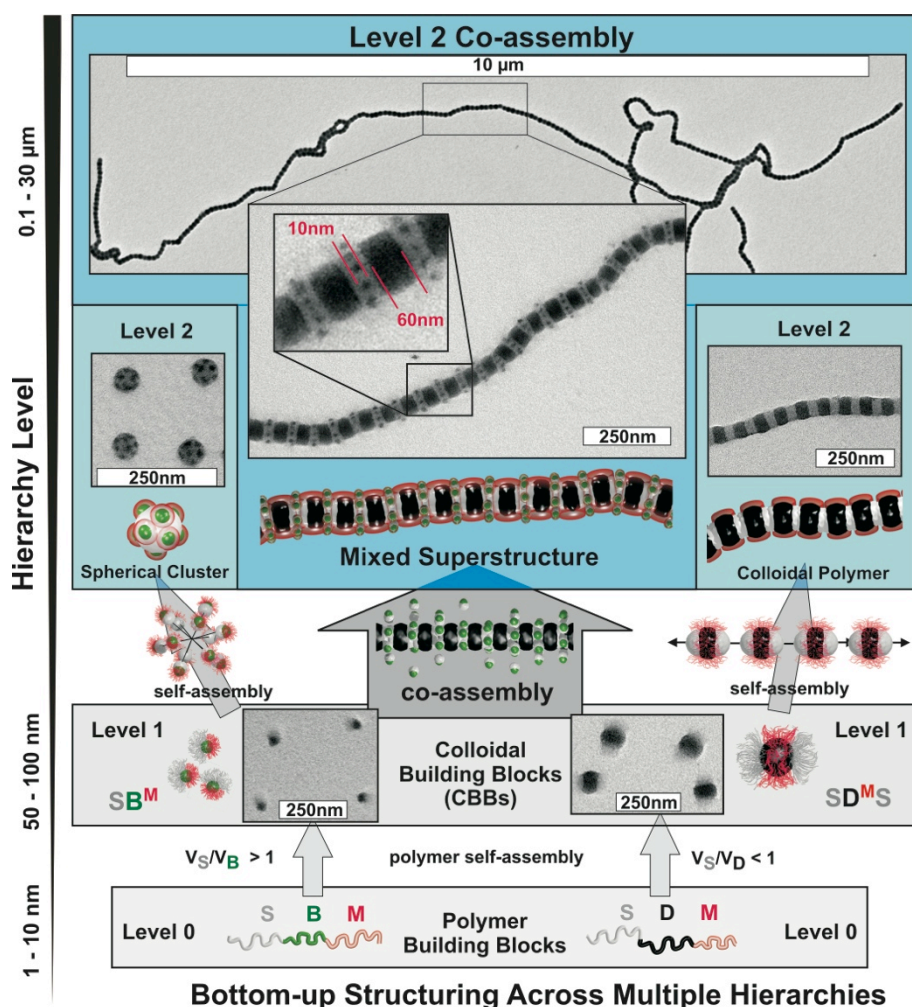


Figure 2–4: Schematic of multilevel homo- and co-assembly. The ABC triblock terpolymers from Hierarchy Level 0 form the AB^{C} and $\text{AB}^{\text{C}}\text{A}$ units of hierarchy level 1 in dependence of the volume ratios $V_{\text{A}}/V_{\text{B}}$ of the core forming blocks. Separately, the AB^{C} and $\text{AB}^{\text{C}}\text{A}$ CBBs undergo further self-assembly into colloidal clusters and polymers on hierarchy level 2. Upon mixing, both CBBs self-assemble to 100% into colloidal co-assemblies. (OsO₄ staining: PB black, PS gray and PMMA not visible due to e-beam degradation). Adapted from *Nature*, 2013, doi:10.1038/nature12610. Reprinted with permission from Nature Publishing Group.

However, if both species are mixed prior to lowering the solvent quality for A, both CBBs co-assemble along the mutual solvophobic S-patches into the same superstructure (hierarchy level 2 co-assembly). It is evident that the superstructure in Figure 2–4 is composed of two different CBB species, a fact which is further supported by grey scale analysis. The cyan diagram shows maxima and minima corresponding to the S and D segments of the used **SDS** units and in addition local minima within the peaks attributed to the **SB** units selectively attached to the –S– segments of the colloidal co-assembly.

The size of the **SB** units has a dramatic effect on the final composition of the superstructure. The –S– segments are able to accommodate an average of 7-9 of the smallest **SB** units, whereas larger particles either fit exactly once or are even too large to attach laterally (Figure 2–5A-C). Interestingly, the mid-sized particles (Figure 2–5B) displace their own volume within the –S– segments and induce a strong kink. This kink causes the colloidal co-assembly to wrinkle, which changes its stiffness and room for manoeuvre. The largest particles share a similar S-patch interface as the **SDS** units and both particles co-assemble simultaneously. Not only are the largest **SB** particles exclusively observed at terminal positions of the colloidal copolymer, but they also interrupted the end-to-end growth of the **SDS** units by blocking the attractive positions (end capping).

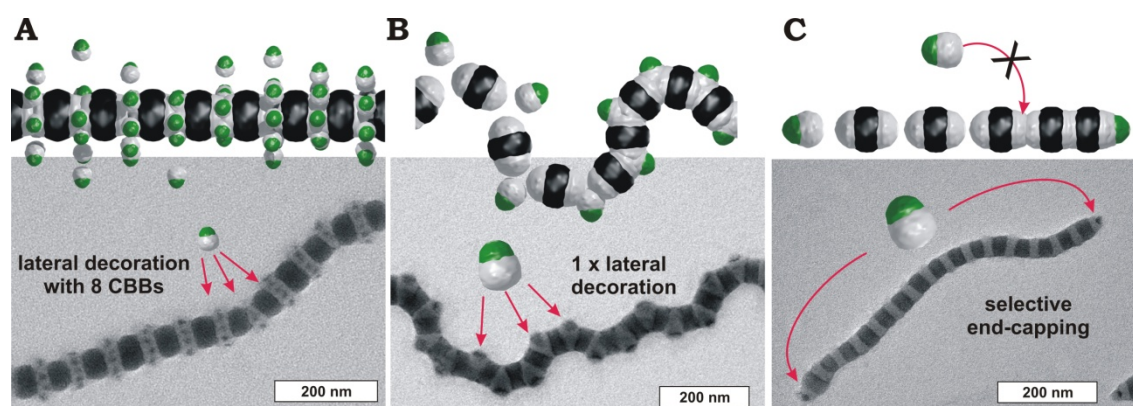


Figure 2–5: Co-assembly of CBBs of different sizes. (A) The smallest **AB** building block that was used decorated the colloidal co-assembly 7-9 times laterally. (B) Larger **AB** building blocks only fit once into the S rich segments and displace a larger volume. As a result, the growth direction is disturbed visible as a strong kink. (C) Even larger particles do not fit laterally into the colloidal polymer but only once to the terminal positions. This end capping of the growing colloidal self-assembly is highly selective and can be used to control the co-assembly length. (OsO₄ staining: PB black, PS grey and PMMA not visible due to *e*-beam degradation). Adapted from *Nature*, **2013**, doi:10.1038/nature12610. Reprinted with permission from Nature Publishing Group.

This end-capping behaviour and its capability to manipulate the length of the colloidal assemblies were further studied by mixing the **SDS** units and the largest **SB** units in various ratios prior to solvent exchange (Figure 2–6A-D). Without any end-capper added, the **SDS** units grow into extremely extended structures with lengths of up to 30 μm consisting of 500-600 units (Figure 2–6A). The addition of **SB** end-cappers in specific ratios then shortens the colloidal polymer due to terminal blocking suppressing growth. Evaluating 250 co-assemblies for all mixing ratios, frequency distributions for each ratio were obtained,

which can be described by a Flory-Schulz frequency distribution for step-growth polymerization. The effect of shortening became more pronounced for increasing end-capper concentration. In fact, the final number average of the repeating units, N_n , correlate well to the initial mixing ratios corroborated by the linear trend when plotting five different **SB:SDS** mixing ratios against the repeating units.

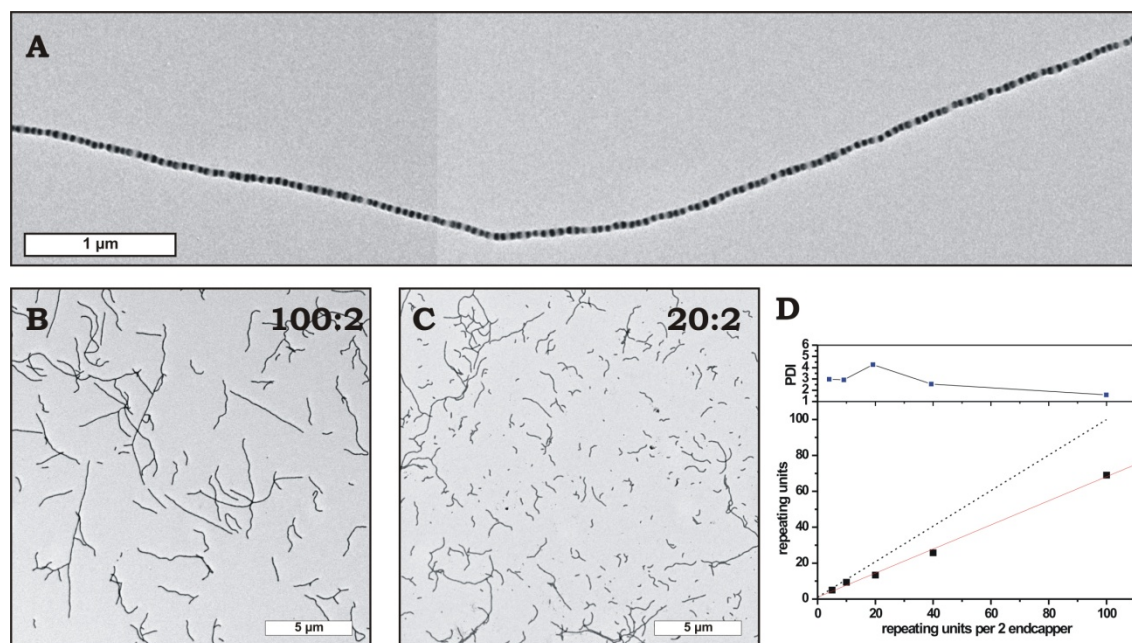


Figure 2-6: Control of degree of polymerization of the colloidal assembly via addition of end-cappers. (A) Without end-cappers the colloidal assemblies grow into extremely extended superstructures composed of several 100 **SDS** units. The depicted colloidal assembly is a cutout from a linear superstructure 30 μm in length and a degree of polymerization of 500-600 units. (B) Mixing **SDS** units and end-cappers in a ratio of 100:2 results in shorter colloidal assembly with a number average of 64 repeating units. (C) Increasing the end-cappers concentration (**SB:SDS** = 20:2) significantly decreases the length to oligomeric aggregates. (D) Plot of repeating units against five different mixing ratios shows a linear dependence of colloidal assembly length on the mixing ratio. (OsO_4 staining: PB black, PS grey and PMMA not visible due to e -beam degradation). Adapted from *Nature*, 2013, doi:10.1038/nature12610. Reprinted with permission from Nature Publishing Group.

Having a modular co-assembly approach at hand, several hybrid materials were prepared and well-known polymer architectures replicated to demonstrate the versatility of the concept (Figure 2-7A-E). Up to now the co-assembly consisted of multiple nano environments within the core determining the structures flexibility and stiffness. However, for some applications the corona is more attractive due to easier access. Hence, a colloidal copolymer was fabricated (Figure 2-7A) unifying five compartments, three core segments (S, B and D) and two alternating, ring-like corona segments of PMMA (M) and *Pt*BMA (T). Surprisingly, the T corona can be utilized to stabilize the entire colloidal copolymer in solvents the **SDS** self-assembly immediately precipitates. Also de-protection of T is a straightforward polymer analogue reaction towards PMAA corona segments suitable for a variety of functionalization. The presented multilevel self-assembly process can be modified at each stage which we use to prepare magnetically responsive hybrid **SDS** colloidal co-assembly with

selectively loaded D compartments (Figure 2–7B). This was achieved by loading the CBBs during self-assembly the SDM triblock terpolymer (from level 1 to 2). As the D segments do not interfere with higher level self-assembly, this procedure gives access to colloidal assemblies with the possibility to precisely load specific compartments.

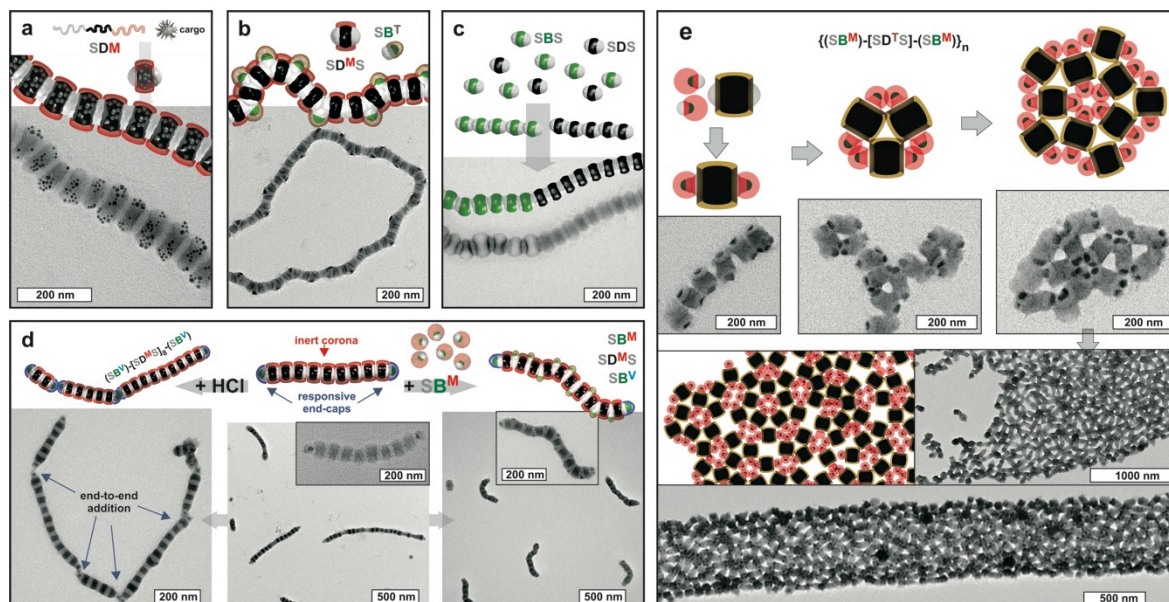


Figure 2–7: Potential of step-wise self-assembly demonstrated on several colloidal co-assembly architectures. (a) Example of a colloidal co-core & co-corona co-assembly polymer unifying five chemically different nanoenvironments. (b) Magnetically responsive colloidal co-assembly. The D compartments are selectively loaded during terpolymer self-assembly. (c) Telechelic colloidal oligomers of **SDS** selectively end-capped with **SB^V** units. Addition of HCl protonates the V corona at the termini of the colloidal co-assemblies inducing aggregation via these patches. (d) Example of a colloidal block co-assembly consisting of oligomeric segments of **SBS** and **SDS** units. (e) Combining preparative steps gives access to ternary colloidal co-assembly. (OsO₄ staining: B black, S gray, V dark gray and M and T not visible due to *e*-beam degradation). Adapted from *Nature*, 2013, doi:10.1038/nature12610. Reprinted with permission from Nature Publishing Group.

Beyond the decoration of colloidal assemblies, assembly architectures were mimicked with CBBs as depicted in Figure 2–7C and D. Here, two bifunctional CBBs of comparable size were co-assembled resulting in a block-like sequence of **SDS** and **SBS** units. The selective end-capping behaviour can also be exploited to generate telechelic colloidal oligomers. This was realized by end-capping **SDS** units with **SB^V** units during step-growth polymerization. The **SB^V** units are CBBs with a poly(2-vinylpyridin) corona patch and due to their similar size to **SDS**, simultaneous aggregation and selective end-capping of $[\text{SDS}]_m$ was observed. The V-patches are clearly visible as a gray area surrounding the black B core of the end-cap. Again the initial mixing ratio determined the average aggregation number. Addition of equimolar amounts of HCl protonates V-patches and the collapse in organic solvents induces linear aggregation of the telechelic colloidal oligomers. In a similar manner ternary co-assemblies were generated by first end capping **SDS** colloidal polymers with **SB^V** units and subsequent decoration with **SB** units (Figure 2–7E). Colloidal networks with defined pore sizes and nearest neighbours per link have been fabricated from **SD^TS/SB^M**

colloidal molecules as an example of hierarchy level 3 colloidal co-assemblies and as final demonstration for the complexity that can be reached with the hierarchical bottom-up concept.

2.3 Novel Solution-Based Approach to Janus Micelles via Cross-linking of Spherical Multicompartment Micelles

In chapter 3 and 4 of this thesis, triblock terpolymers were self-assembled into CBBs, whereas a volume ratio of the core forming blocks $V_S/V_B > 1$ resulted in spherical clusters with precise control of the cluster size. In chapter 5, I explored methods to utilize the unique morphology of the near-monodisperse and readily accessible spherical MCMs for the preparation of soft, nanometre-sized Janus particles (JPs) in the sub-100 nm range. This size regime has remained difficult to access with other solution-based protocols for JPs synthesis. The herein developed process is a general, large-scale approach and uses simple self-assembly of ABC triblock terpolymers in selective solvents and facile cross-linking reactions.

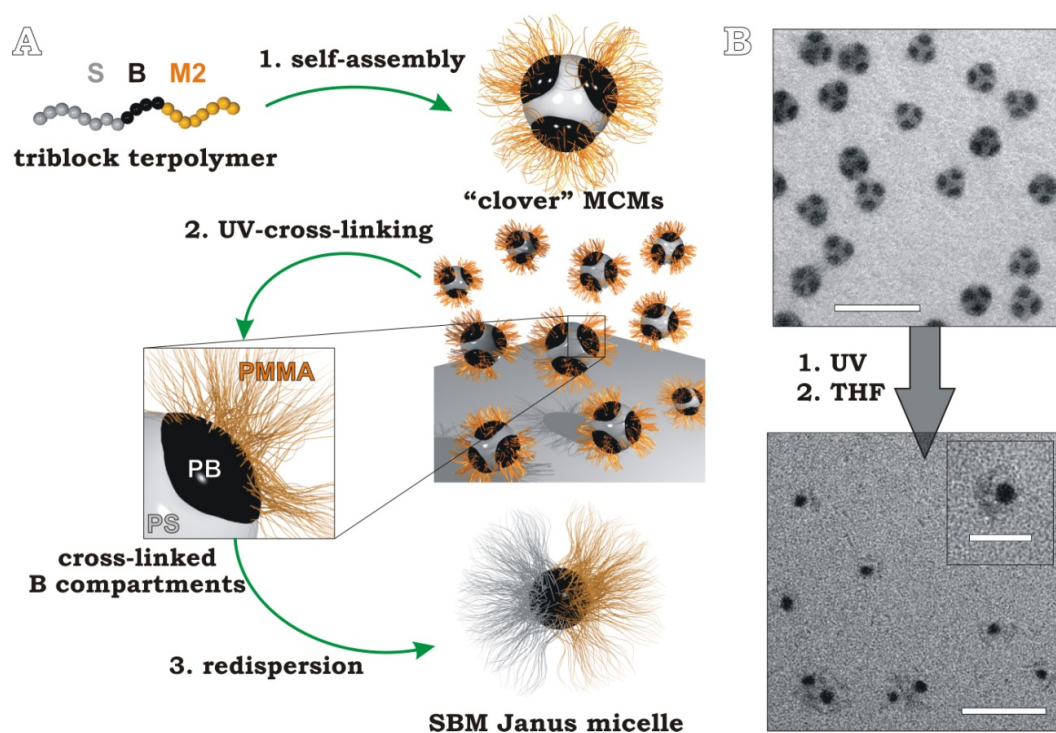


Figure 2–8: Preparation of SBM Janus micelles from SBM triblock terpolymers. (A) Systematic approach comprising the self-assembly of SBM triblock terpolymer into homogeneous “clover” MCMs. After cross-linking, the MCMs are re-dispersed in a good solvent for all blocks which breaks up the MCM and releases SBM JPs. (B) TEM image of clover MCMs drop coated from acetone/isopropanol (70:30 v/v) and single JPs from THF solutions. (OsO₄ staining: B black, S grey and M not visible due to *e*-beam degradation). Adapted from *J. Am. Chem. Soc.* **2012**, *134*, 13850-13860. Reprinted with permission from the American Chemical Society.

Exemplified of SBM triblock terpolymers, the near-monodisperse spherical MCMs can be seen as clusters formed by SB Janus-type particles as we learned from the underlying self-

assembly mechanism (Figure 2–8). Thereby, S forms the MCM core and B the compartments sandwiched between core and the M corona. Within the MCMs all polymer blocks are entirely phase-separated either due to polymer-polymer incompatibility (e.g. S and B) or to polymer solubility/insolubility (S and B precipitated and M soluble). Cross-linking of B preserves the phase-separated state and transfer into a good solvent for all blocks then breaks up the MCMs into single JPs. Figure 2–8B unambiguously illustrates the Janus character of the freed particles as the grey S hemisphere only emanates from one side of the black B core. This approach does not require any additional template as symmetry breaking happens during MCM formation. The self-assembly into MCMs is a necessary measure to completely break the symmetry as otherwise cross-linking of particles with a patchy S/M corona merely result in ill-defined aggregates and precipitation during solvent exchange.

This novel approach allows nano engineering with unprecedented structural control inaccessible otherwise. The Janus particles exhibit a narrow size distribution due to near monodisperse MCMs, whereas the overall size can be controlled by the total molecular weight. The core of the JPs is a direct result of the polymer block length and can adopt weight fractions of up to 30 wt.-%. As a comparison, the well-established cross-linking of lamella-sphere bulk morphology can only produce Janus particles with weight fractions of the core of up to ca. 10 wt.-% as otherwise morphological transformation occurs (15 wt.-% cylinder and 25 wt.-% lamella morphology). A larger core may be beneficial as softener in e.g. polymer blends.

Another intriguing aspect of the presented method is the possibility to tune the Janus balance, i.e., the size ratio of both corona patches. It was theoretically predicted that the Janus balance would have a dramatic effect on stabilization properties, but it is also intuitive that uneven corona patches of different chemistry may form clusters of diverse geometry in selective solvents. A set of SBM JPs with the Janus balance varying from dominant S to even S/M to dominant M-patch size ratios was synthesized with the novel approach. The JPs with the dominant S-patch show especially promising self-assembly behaviour after M was hydrolysed to poly(methacrylic acid) (MAA) for improved solvent selectivity of the corona patches. We find that competing timescales for different processes during the self-assembly can induce kinetic selection into non-equilibrium structures. Studies of Janus particle self-assembly in dependence of the Janus balance are rare and cannot be found elsewhere for sub 100 nm Janus particles.

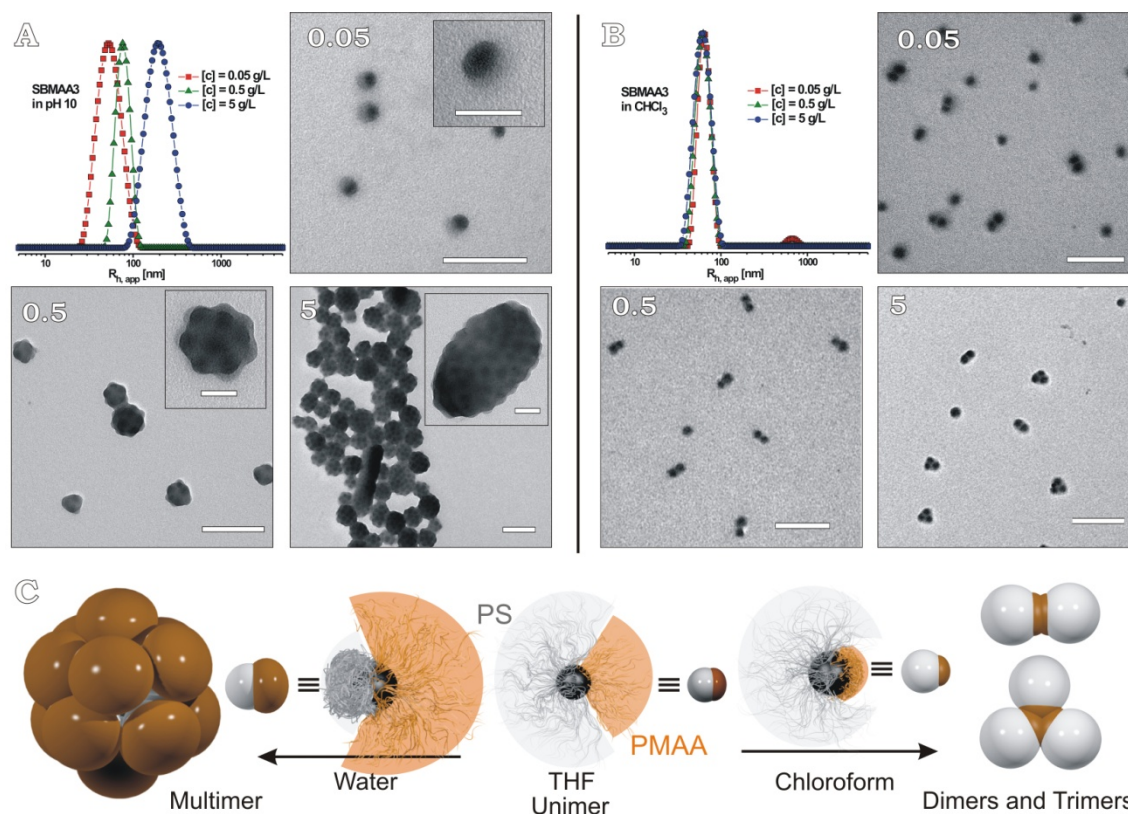


Figure 2–9: DLS and TEM studies of concentration dependent superstructure formation of poly(styrene)-*b*-poly(butadiene)-*b*-poly(methacrylic acid) (SBMAA) JPs with a dominant S-patch. The solvents used are water (selective for MAA) and chloroform (selective for S). (OsO₄ staining: B black, S grey and M not visible due to *e*-beam degradation). Adapted from *J. Am. Chem. Soc.* **2012, *134*, 13850–13860. Reprinted with permission from the American Chemical Society.**

Figure 2–9 presents DLS size distributions and corresponding TEM images of a concentration series of SBMAA in water pH 10 (selective for MAA) and Chloroform (selective for S). With increasing initial concentration of SBMAA JPs in THF, the cluster size dramatically increases after solvent exchange to water pH 10 (Figure 2–9A). At a concentration of 0.05 g/L single JPs are the dominant species, whereas the Janus character is clearly visible as the collapsed grey S-patch only emanates from one side of the B core. With increasing JP concentration the clusters grow into football and raspberry-like aggregates consisting of around 20 and over 50 JPs, respectively. DLS and TEM analysis shows a completely different evolution for SBMAA JPs in chloroform (Figure 2–9B). Collapse of the minor MAA-patch merely results in concentration independent dimer- or trimers protected by the very large S-corona. Figure 2–9C illustrates schematically the dynamic volume change of both corona patches in dependence of the solvent and the corresponding clustering. These studies revealed that corona patches able to dynamically reorganize to size ratio self-assemble into clusters.

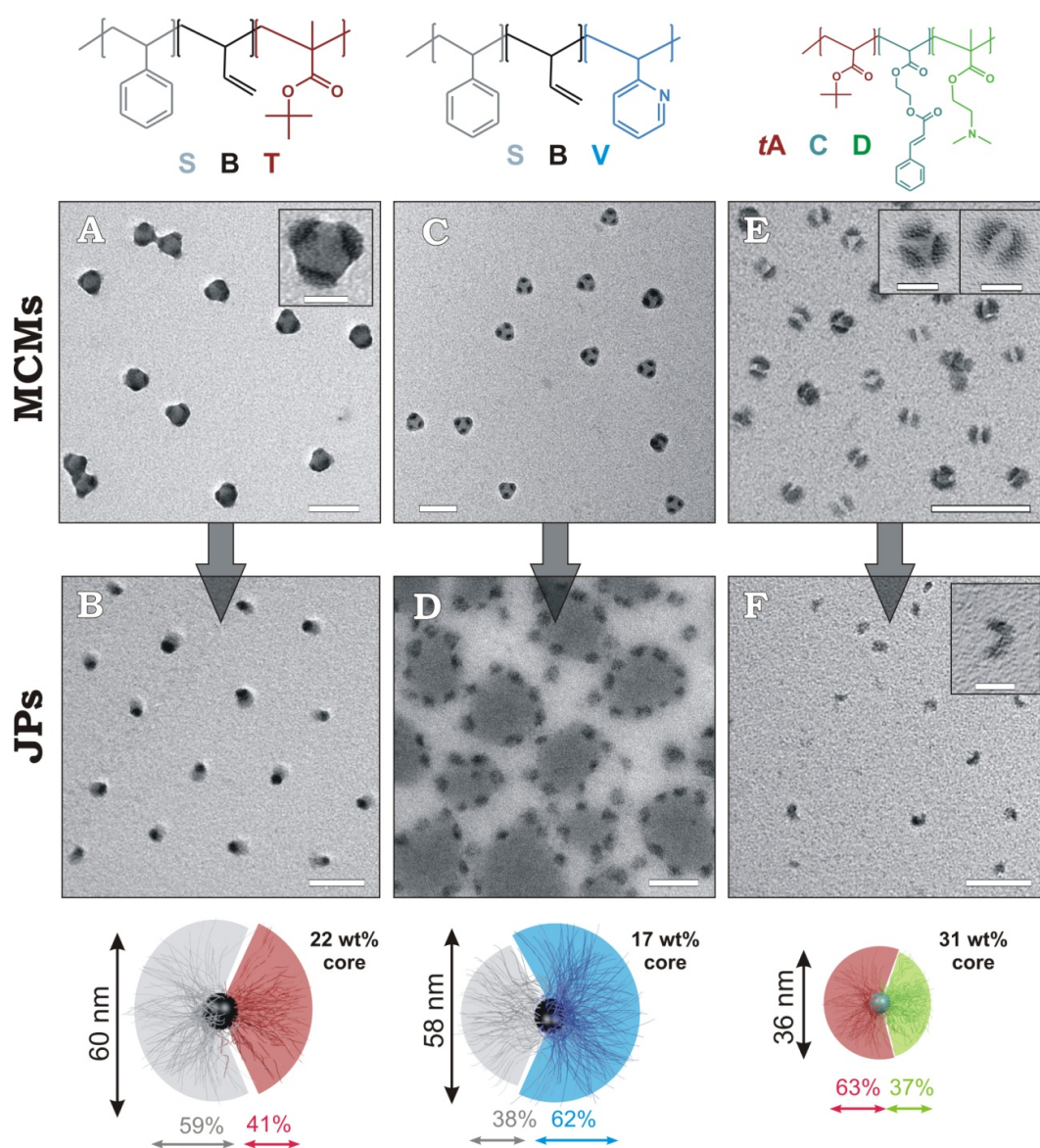


Figure 2–10: Generality of the solution-based concept. (A, B) “Clover” MCMs of SBT in ethanol and single JPs in DMAc after cross-linking. The Janus character is clearly visible and the random orientation of the S patch excludes drying artefacts. (C, D) “Clover” MCMs of SBV in isopropanol and corresponding JPs in DMAc (OsO₄ staining: B black, S gray and M and T not visible due to *e*-beam degradation). (E, F) “Hamburger” and “Clover” MCMs of *t*ACD in water pH 10 and corresponding JPs in water pH 3 (RuO₄ staining: B bright, S black and D not visible due to *e*-beam degradation). Adapted from *J. Am. Chem. Soc.* **2012**, *134*, 13850-13860. Reprinted with permission from the American Chemical Society.

Beyond nanoengineering of structural features the presented approach also proved to be very flexible considering polymer block chemistries (Figure 2–10). Several different triblock terpolymers were self-assembled into MCMs (mostly “clover”) and transformed into JPs with increased amphiphilicity of the corona patches (M→T→V), higher functionality (V coordinates metal ions or nanoparticles) or entirely composed of methacrylates. Especially the latter paves the way to completely new JP compositions as all-methacrylate terpolymers can be easily realized with standard laboratory equipment (ATRP) and lesser requirements have to be met (e.g., only one polymer-polymer incompatibility instead of three). Not only is the incompatibility of polymer blocks relevant, but also the interfacial

tension between the phases and thus S/T corona hemispheres (SBT) are exclusively accessible with the solution-based method due to spreading of B in bulk morphologies.

Another central aspect of this chapter was the development of a procedure that can be readily up-scaled for technological applications. This was realized by using extremely high terpolymer concentrations of up to 10 wt.-% that resulted in spherical MCMs of acceptable quality. Surprisingly, the self-assembly process and terpolymer mobility was not noticeably disturbed by the strong viscosity increase. Although, a higher number and broader number distribution of compartments per MCMs was observed, JPs are always obtained after cross-linking of the compartments as long as all polymer blocks are entirely phase-separated. Monitoring the exchange rate of the solvents per $^1\text{H-NMR}$ revealed that dialysis was completed within hours for most solvents and thus, one a gram scale production cycle of JPs could be accomplished within 1 day.

2.4 Janus Particle/Multi-Walled Carbon Nanotube Hybrids

In this chapter Janus micelles (JMs) were studied upon their ability to attach to multi-walled carbon nanotubes (MWNTs) and form hybrid materials stable in various media. Therefore, SBM JMs were prepared via the solution-based approach of chapter 5, were mixed with MWNTs in acetone and sonified for 5 minutes resulting in a stable dispersion. In acetone the JMs cluster via the insoluble PS-patch while the strongly solvophobic MWNT are bundled minimizing the high specific solvent/surface area, therein (Figure 2–11). Strong pulses of ultrasound “open” up both aggregates releasing single JMs and MWNTs. Switching off agitation after 5-10 min then allows the materials to reassemble and preferential attachment of JMs onto the MWNTs surface is observed. The JM coating then stabilize each MWNT with the soluble/repulsive M corona suppressing rebundling. TEM, SEM and AFM analysis clearly demonstrated an unparalleled quantity of JMs as dense packing on the MWNTs. Surprisingly, if less JMs are present than would fit onto the surface of the disentangled MWNTs, no JMs clusters are detected anymore, but all JMs are exclusively adsorbed to the tube’s surface. This observation suggests a preferential orientation of the JMs towards the MWNTs lowering the unfavoured surface energy of the entire system. The hybrid materials were then systematically studied to elucidate the effect of JM concentration and Janus balance on the aggregation pattern of JMs on the MWNTs. It was found that generally higher JM concentrations result in denser packing until the entire surface of the MWNTs is covered. Thereby, the Janus balance had a dramatic effect on the packing density. SBM1 JMs with a dominant S patch were able to form extremely dense coatings and due to the comparably small repulsive M corona increasing JM concentrations led to multi-layer coatings. Even growth of JM clusters from the surface was observed (Figure 2–12 SBM1).

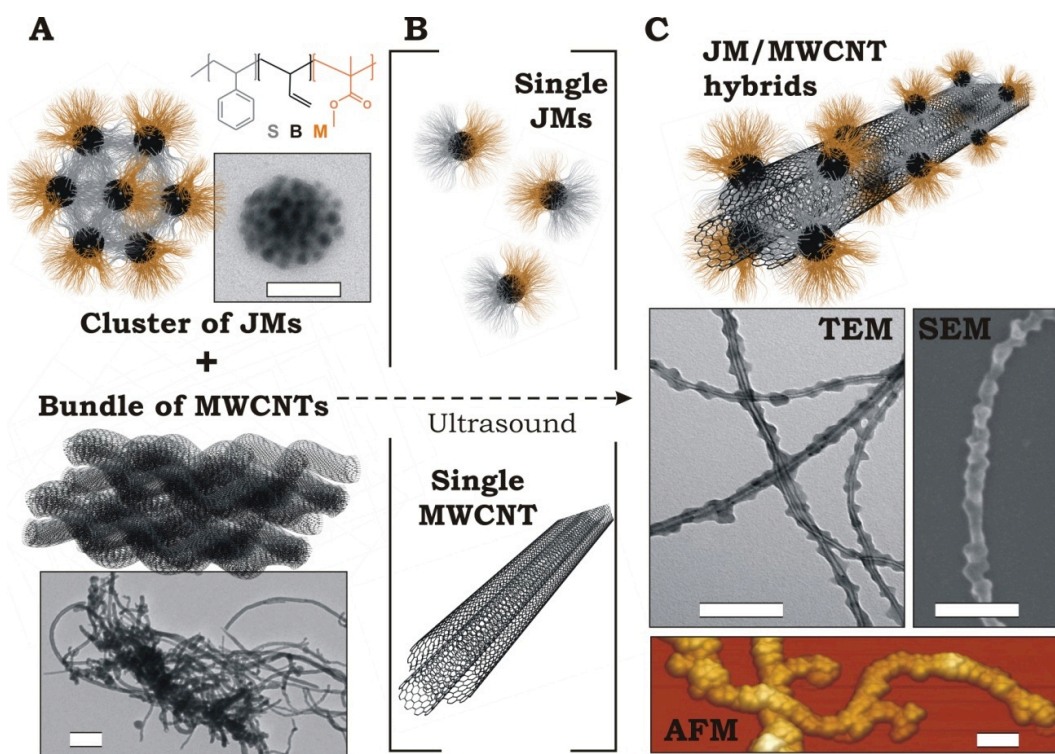


Figure 2–11: Preparative steps to hybrids material composed of Janus micelles and multi-walled carbon nanotubes (JM/MWNT) (A) In acetone, the JMs aggregate into clusters along the insoluble S hemisphere and the MWNTs bundle in virtue of the very high solvophobicity. (B) Sonication temporarily disassembles the JM clusters and the MWNT bundles. (C) Both materials preferably re-assemble with each other. The soluble M corona hemisphere acts as compatibilizers stabilizing the MWNTs. TEM, SEM and AFM all prove dense coating of the MWNT surface with JMs. Adapted from *Angew. Chem. Int. Ed.* **2013**, *52*, 3602–3606. Reprinted with permission from Wiley-VCH Verlag GmbH & Co. KGaA.

The situation changed using SBM2 JMs with evenly sized S/M corona patches. Still massive adsorption onto the surface was evident from TEM imaging, but the single layers were less dense as observed for SBM1. Although an increasing concentration of JMs led to complete coverage of the tubes, JM clusters were also identified in the background. This was attributed to the larger M corona acting repulsive towards other incoming JMs preventing multi-layer coating, therein. This effect becomes even more pronounced for SBM3 JMs exhibiting a dominant M corona patch. Already at comparably low mixing ratios single JMs and JM clusters are found adjacent to the MWNTs who themselves are sparsely covered. Irrespective of the concentration the coating density remains low. This is not surprising as the large highly swollen M corona, which is not visible in TEM imaging, requires a lot of space blocking the surface around each JM for other particles. Thus it was concluded that the Janus balance significantly alters the adsorption patterns and the amount of particles per MWNT, respectively.

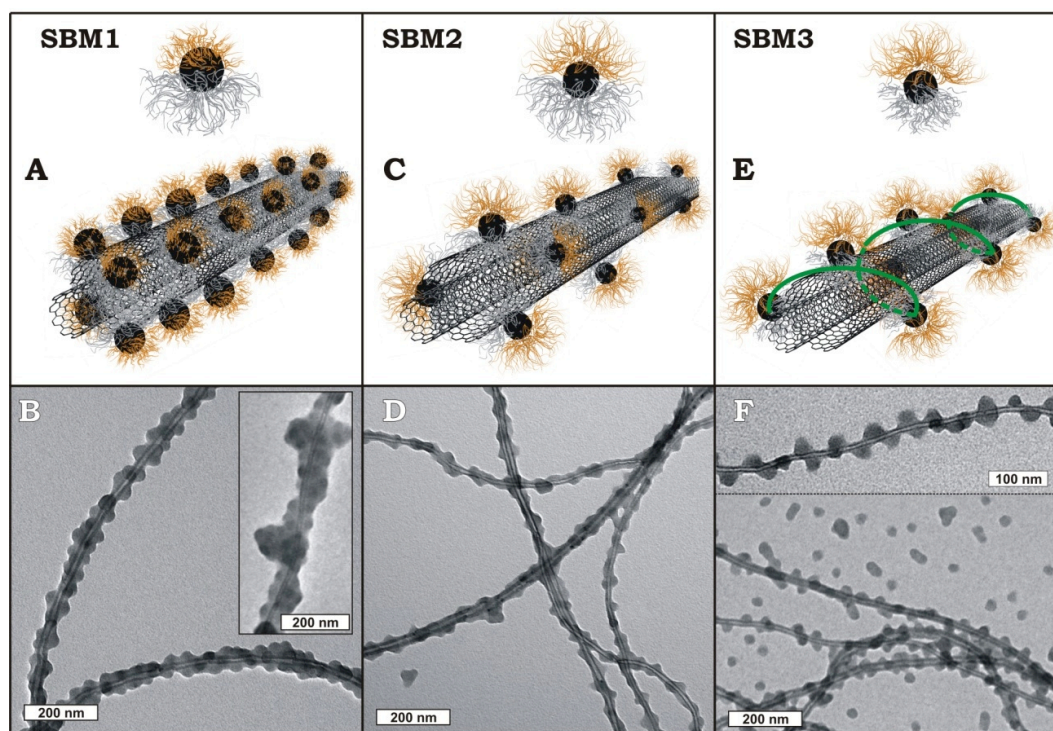


Figure 2–12: Systematic study of the effect of concentration and Janus balance on JM aggregation pattern on the surface of MWNTs. JMs, SBM1-3, with S/M corona size ratios ranging from dominant S (SBM1) to equal sized (SBM2) to dominant M (SBM3) corona patches. Adsorption patterns were investigated at mixing ratios of JP/MWNT = 1:1. Adapted from *Angew. Chem. Int. Ed.* **2013**, 52, 3602-3606. Reprinted with permission from Wiley-VCH Verlag GmbH & Co. KGaA.

Finally JMs with an S corona patch and varying stabilizing patches (T, V and MAA) were used to form stable dispersions in media with increasing polarity. Thereby, a T corona patch allowed the transfer of JM/MWNT hybrids to protic organic media such as isopropanol and ethanol (Figure 2–13A), a V corona patch to acidic water (pH < 4; Figure 2–13B) and a MAA corona patch (after de-protection of M) to basic water (pH > 5; Figure 2–13C). The V and MMA corona patches are still responsive as changing the pH results in reversible precipitation/re-dispersion of the hybrids. The effect of Janus balance is best visualized with SBMAA JMs in water pH 10 (Figure 2–13D). As it turned out, the amount of adsorbed JMs is not a measure for the stability of the hybrid material, but rather the ratio of stabilizing corona per particle, because where the pristine MWNTs float (lower density as water), those densely coated with SBMAA1 particles settle to the bottom. The MAA corona is too small to provide insufficient stabilization to balance to the increase weight. SBMAA3 coated MWNTs on the other hand showed best stability as the gain in stabilization easily counteracts the additional weight. The Janus balance is crucial design criterion that in case of stabilization of particulate matter has to be in favour of the stabilizing patch.

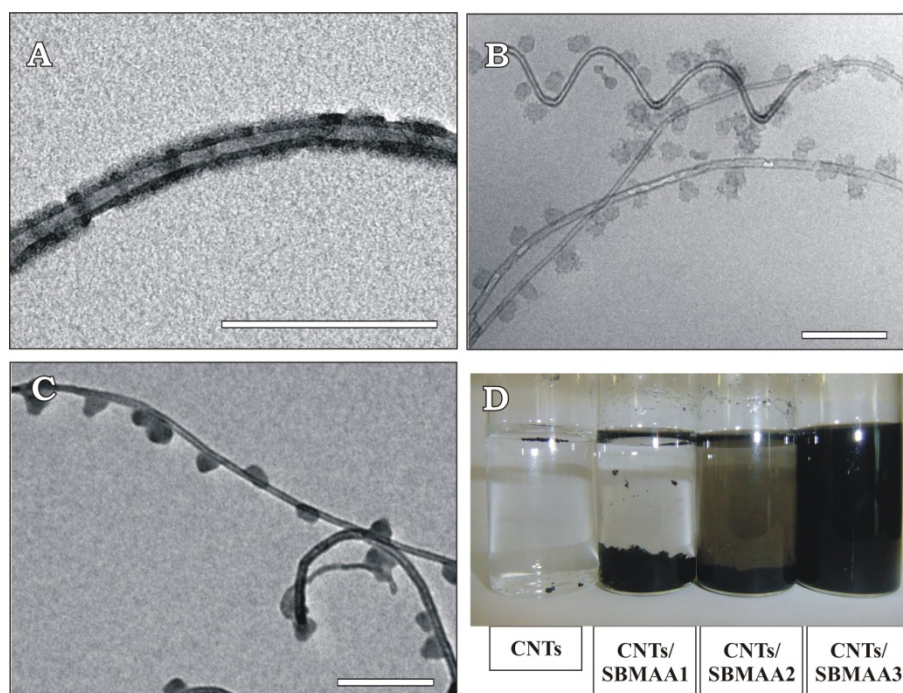


Figure 2–13: JM/MWNTs stabilized by different corona patches. (A) SBT JMs stabilize the MWNTs in ethanol, (B) SBV JMs in acidic water ($\text{pH} < 4$) and (C) SBMAA in basic water ($\text{pH} > 4$). (D) Comparison of the stability of pristine MWNTs, MWNTs coated with JMs with a minor MAA corona (SBMAA1), equally-sized corona patches (SBMAA2) and a dominant MAA patch (SBMAA3). Adapted from *Angew. Chem. Int. Ed.* **2013**, 52, 3602-3606. Reprinted with permission from Wiley-VCH Verlag GmbH & Co. KGaA.

2.5 Individual Contributions to Joint Publications

The results presented in this thesis were obtained in close collaboration with others and published as indicated below. In the following, the contributions of all the co-authors to the different publications are specified. The asterisk denotes the corresponding author(s).

Chapter 3

This work is published in *Nature Communications* **2012**, 3:710 under the title:

“Precise Hierarchical Self-Assembly of Multicompartment Micelles”

by André H. Gröschel, Felix H. Schacher, Holger Schmalz, Oleg V. Borisov, Ekaterina B. Zhulina, Andreas Walther,* and Axel H. E. Müller*

I conceived the project, conducted all experiments and measurements, and wrote the publication. Exceptions are as follows:

F. H. Schacher was involved in scientific discussions.

H. Schmalz provided some polymers and was involved in discussing the results.

O. V. Borisov and E. B. Zhulina derived the scaling theory from discussed results.

A. Walther and A. H. E. Müller were involved in scientific discussions and writing the manuscript.

Chapter 4

This work will be published in *Nature*, **2013**, DOI 10.1038/nature12610 under the title:

“Guided Hierarchical Co-Assembly of Soft Patchy Nanoparticles”

by André H. Gröschel*, Andreas Walther, Tina I. Löbbling, Felix H. Schacher, Holger Schmalz, Axel H. E. Müller*

I conceived the project, conducted most experiments and measurements, and wrote the publication. Exceptions are as follows:

A. Walther was involved in writing the manuscript and scientific discussions.

T. I. Löbbling conducted some experiments and performed TEM measurements.

F. H. Schacher was involved in discussing the results.

H. Schmalz provided polymers and was involved in discussing the results.

A. H. E. Müller was involved in scientific discussions and correcting the manuscript.

Chapter 5

This work is published in the *Journal of the American Chemical Society* **2012**, *134*, 13850-13860 under the title:

“Facile, Solution-Based Synthesis of Soft, Nanoscale Janus Particles with Tunable Janus Balance”

by André H. Gröschel*, Andreas Walther, Tina I. Löbling, Joachim Schmelz, Andreas Hanisch, Holger Schmalz, Axel H. E. Müller*

I conceived the project, conducted most experiments and measurements, and wrote the publication. Exceptions are as follows:

A. Walther was involved in correcting the manuscript and scientific discussions.

T. I. Löbling conducted some experiments and performed TEM measurements.

J. Schmelz provided some polymers.

A. Hanisch provided some polymers.

H. Schmalz provided some polymers and was involved in discussing the results.

A. H. E. Müller was involved in scientific discussions and correcting the manuscript.

Chapter 6

This work was published in submitted to *Angewandte Chemie International Edition* **2013**, *52 (13)*, 3602-3606; *Angewandte Chemie* **2013**, *125 (13)*, 3688-3693 under the title:

“Janus Micelles as Effective Supracolloidal Dispersants for Carbon Nanotubes”

by André H. Gröschel*, Tina I. Löbling, Petar D. Petrov, Markus Müllner, Christian Kuttner, Florian Wieberger, Holger Schmalz, Axel H. E. Müller*

I conducted most experiments and measurements, and wrote the publication. Exceptions are as follows:

P. D. Petrov conducted some experiments and was involved in correcting the manuscript.

T. I. Löbling conducted some experiments and performed TEM measurements.

M. Müllner performed AFM measurements.

F. Wieberger performed SEM measurements.

H. Schmalz provided polymers.

C. Kuttner performed Raman spectroscopic measurements.

A. H. E. Müller was involved in scientific discussions and correcting the manuscript.

Chapter 3

Precise Hierarchical Self-Assembly of Multicompartment Micelles

André H. Gröschel, Felix H. Schacher², Holger Schmalz, Oleg V. Borisov^{3,4},
Ekaterina B. Zhulina⁴, Andreas Walther^{1*} & Axel H. E. Müller^{*}

Makromolekulare Chemie II, Universität Bayreuth, D-95440 Bayreuth, Germany

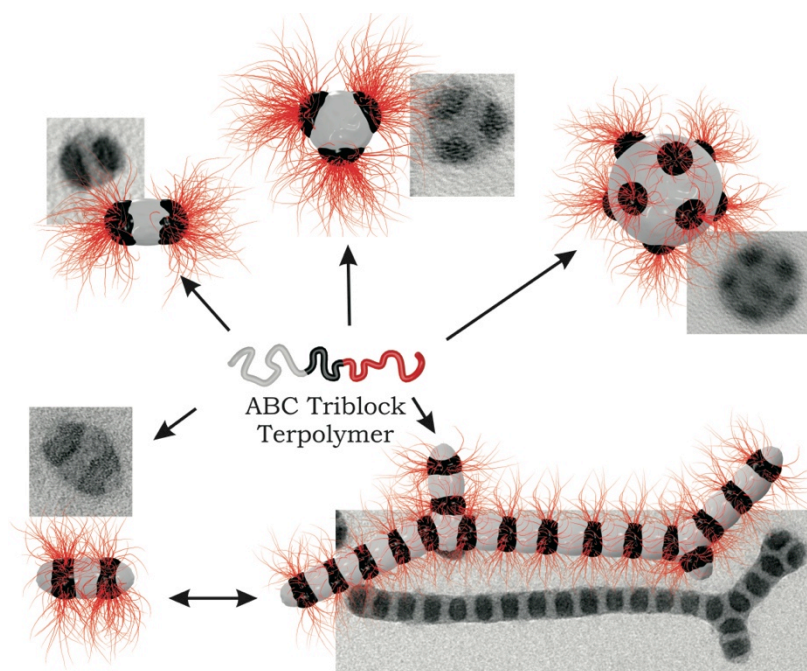
walther@dwf.rwth-aachen.de; axel.mueller@uni-bayreuth.de

¹ DWI at the RWTH Aachen University, 52056 Aachen, Germany

² Institut für Organische Chemie und Makromolekulare Chemie and Jena Center for Soft Matter,
Friedrich Schiller Universität Jena, D-07743 Jena, Germany

³ Institut Pluridisciplinaire de Recherche sur l'Environnement et les Matériaux UMR 5254
CNRS/UPPA, F-64053 Pau, France

⁴ Institute of Macromolecular Compounds of the Russian Academy of Sciences, 199004 St. Petersburg,
Russia



Published in *Nature Communications* **2012**, 3, 710-717.

Abstract

Hierarchical self-assembly offers elegant and energy-efficient bottom-up strategies for the structuring of complex materials. For block copolymers, the last decade witnessed great progress in diversifying the structural complexity of solution-based assemblies into multicompartment micelles. However, a general understanding of what governs multicompartment micelle morphologies and polydispersity, and how to manipulate their hierarchical superstructures using straightforward concepts and readily accessible polymers remains unreached. Here we demonstrate how to create homogeneous multicompartment micelles with unprecedented structural control via the intermediate pre-assembly of subunits. This directed self-assembly leads to a step-wise reduction of the degree of conformational freedom and dynamics and avoids undesirable kinetic obstacles during the structure build-up. It yields a general concept for homogeneous populations of well-defined multicompartment micelles with precisely tuneable patchiness, while using simple linear ABC triblock terpolymers. We further demonstrate control over the hierarchical step-growth polymerization of multicompartment micelles into micronscale segmented supracolloidal polymers as an example of programmable mesoscale colloidal hierarchies via well-defined patchy nanoobjects.

Introduction

Nature fascinates with the rich functionality it creates from hierarchically self-organized complex architectures. The precision with which biology forms near monodisperse proteins or enzymes from polypeptides is unparalleled. In man-made self-assemblies we pursue complex functional hierarchies with the ultimate goal to replace top-down approaches for the elegant and energy-efficient structuring of advanced materials.^[1-8] Irrespective of the physical interaction used for achieving complex multilevel self-assemblies, there is an increasing bottleneck of precision engineering when constructing across length scales. The build-up of hierarchies requires control of the homogeneity of the subunits that order into the next higher level, as polydispersity can amplify throughout the process. With increasing size and complexity of the self-assembling building blocks, the kinetic obstacles become significant and trapping of meta-stable species can occur, preventing well-defined solution hierarchies of low polydispersity on an appropriate time-scale.^[9, 10]

Here, however, biology inspires a strategy to overcome this bottleneck as it teaches that the precise folding of peptides involves prefolded intermediates prior to furnishing monodisperse, perfectly functioning proteins or enzyme complexes. Thus, a step-wise restriction of the degrees of freedoms occurs^[11] along a directional energy landscape, similar to a funnel (Fig. 3–1).^[12, 13] This calls for directing the self-assembly of synthetic bricks when increasingly complex hierarchical structures are targeted, especially when competing interactions and slow dynamics are involved.

In soft-matter nanotechnology, multicompartment micelles (MCMs) and their superstructures, formed by block copolymers, have emerged as a remarkable class of complex self-assemblies that allow to fundamentally understand the bottom-up structuring of solution-based hierarchies.^[14-32] They are an intriguing class of responsive nanoobjects as they combine—similar to proteins—different physical nanoenvironments in well-segregated compartments and allow transporting different payloads simultaneously. Either the core or the corona can be compartmentalized, where we will concentrate on multicompartment-*core* micelles. We distinguish these further into spherical and linear MCMs according to their geometric dimensions. Here, early studies reported on the formation of spherical MCMs with raspberry appearance formed by ABC triblock terpolymers, containing hydrocarbon, fluorocarbon and hydrophilic blocks. In recent years, Lodge and Hillmyer largely extended the space of morphologies by exploring the structures formed by ABC miktoarms in selective solvents, in which spherical MCMs, substructured vesicles and linear worm-like MCMs were identified.^[32-34] Furthermore, the kinetically controlled (non-equilibrium) aggregation of solvent-swollen spherical micelles formed by ABC triblock terpolymers into linear substructured strands was achieved by complexation of the corona with oppositely charged complexing agents. Importantly, MCMs can bridge several length scales from segmented polymer chains (~10 nm) over substructured individual MCMs (25 – 100 nm) into extended superstructured cylinders (0.1 – 10 μm). So far, there has been best

diversification of structures by promoting specific systems with non-linear polymer topologies or polymer-specific additives and processes.^[35-37] However, looking at these systems, one can identify that it has remained challenging to establish a general concept, in particular for simple linear ABC triblock terpolymers, and more importantly, a scheme to predict and manipulate the architecture (patch distribution, geometry, linear vs. spherical aggregates) of the resulting MCMs as a function of the polymer composition. For instance, football (aka raspberry) MCMs with various patches ($n \approx 5 - 10$) are the most common and also widely observed MCM morphology for triblock terpolymers.^[15, 17, 31, 38-42] However, it can be anticipated that there must be stable regions for MCMs possessing smaller amounts of patches (e.g. 2,3,4) as such MCMs can be identified in polydisperse populations in present literature.^[31, 35, 36, 43, 44]

Consequently, the major question arises to how can these distinct patch numbers be obtained in high monodispersity? Also, what governs the aggregation into isolated spherical MCMs vs. extended linear MCM strings? In the future, the self-assembly of block copolymers in solution will move to the second level of hierarchy, meaning that it becomes increasingly important to use MCMs as bricks to construct higher level aggregates (2nd level), whereas present approaches mostly deal with the aggregation of block copolymers into micelles (MCMs, 1st level). Success in this direction however, critically depends on controlling patch distributions and achieving high monodispersity for MCMs so that they can serve as reliable bricks for the self-assembly into higher orders.^[23]

Herein, we will demonstrate a general concept of what governs the amount of patches and how to achieve very homogeneous distributions of MCMs. Reasonably, only shallow differences in the free energy of MCMs with various patches can be expected and the challenge is to selectively target one specific morphology. Therefore, various MCMs in Figure 3-1 are depicted on similar levels of free energy and we expect near-equilibrium structures when one is realized over the other. With the aim of avoiding undesirable kinetic traps, we take a different look at the structure formation and apply the concept of directed self-assembly by step-wise reduction of the degrees of freedom for the MCM formation of readily accessible linear ABC triblock terpolymers. This largely contrasts present approaches using one-step dissolution (or direct dialysis), and – as we will show – has a decisive influence on achieving superior control. Instead of considering MCMs as single entities with intact structures, we identify the essential pre-assembled subunits and target their formation in a dedicated first step. Using suitable solvents we first construct well defined micellar subunits with a collapsed but dynamic B core and a mixed or compartmentalized corona of blocks A/C (first reduction of conformational freedom). We chose to specifically direct the self-assembly via these intermediates as it assures the mechanistic pathway with high confidence and allows to sequentially reduce the dynamics from soluble to collapsed blocks. By lowering the solvent quality for block A, these subunits serve as bricks for the next-level assembly into various well-defined spherical MCMs with A core, B patches and

C corona (second reduction of conformational freedom). This surprisingly simple step-wise approach allows maintaining significant dynamics for the subunits and directs the kinetic pathway during the self-assembly into unusually homogeneous MCMs. We regard this analogous to funnelling the structure formation along an energy landscape into final well-defined hierarchical architectures. With the aid of this approach, we demonstrate unique structural control over spherical MCMs.

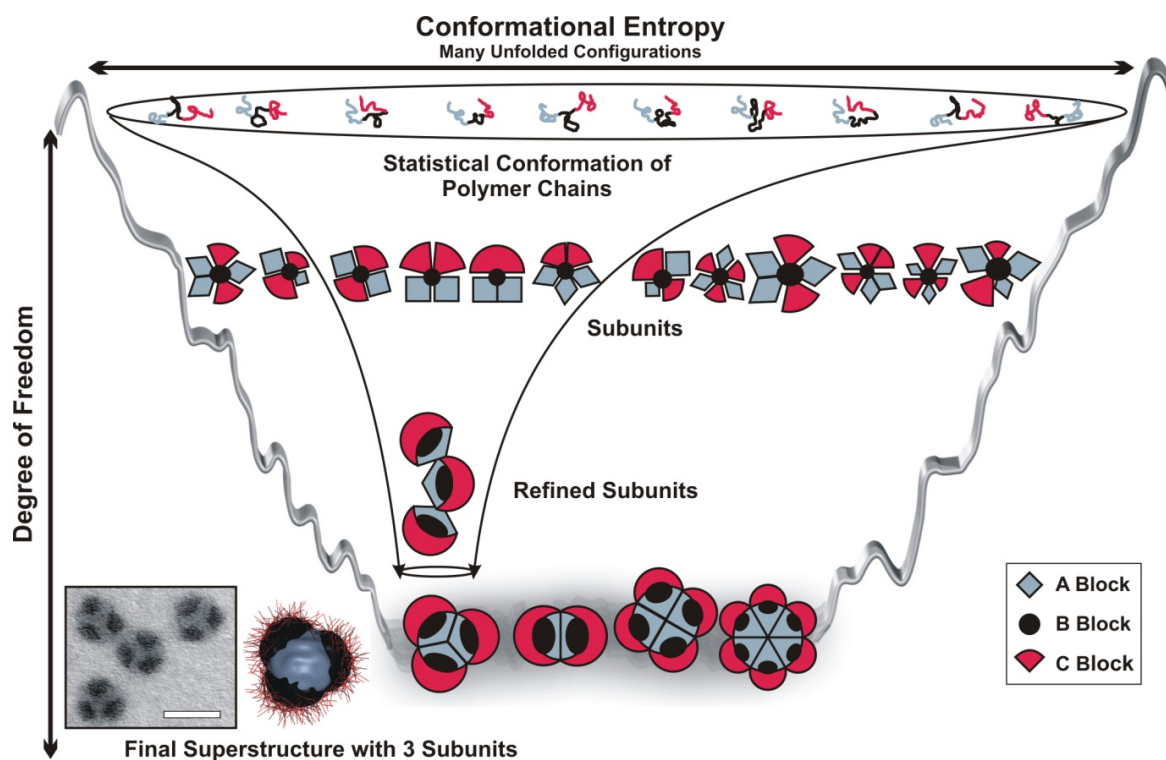


Figure 3–1: Funnel concept for the directed, hierarchical self-assembly of ABC triblock terpolymers in solution. Minimization of kinetic traps is realized by step-wise reduction of conformational freedom via pre-assembled subunits. In the first step, triblock terpolymers self-assemble into subunits, i.e. pre-assembled intermediates, in a nonsolvent for the middle block B (black), leaving different corona conformations of A (red) and C (grey). In the second step, the collapse of block A is triggered by exposure to a nonsolvent for A and B, and higher level assembly of the subunits occurs into the final superstructure. The process is accompanied by a refinement of the initial corona structure of A and C, and the conformational space narrows down into MCM superstructures of low polydispersity (Scale bar is 50 nm).

Moreover, we define conditions for which instead of spherical MCMs linear ones with alternating A and B segments will form via colloidal step-growth polymerization into mesoscale superstructures (colloidal polymers), as an example of colloidal LEGO[®] based on well-defined patchy nanoobjects. This progress is accomplished with one of the simplest starting materials, i.e. linear ABC triblock terpolymers, without the need of post-modifications or complexing agents. In combination with a herein developed scaling theory, we establish the stability criteria of different MCM morphologies and validate the general applicability by extending it to five types of terpolymers with widely different physical characteristics (Fig. 3–2, Table 3–1).

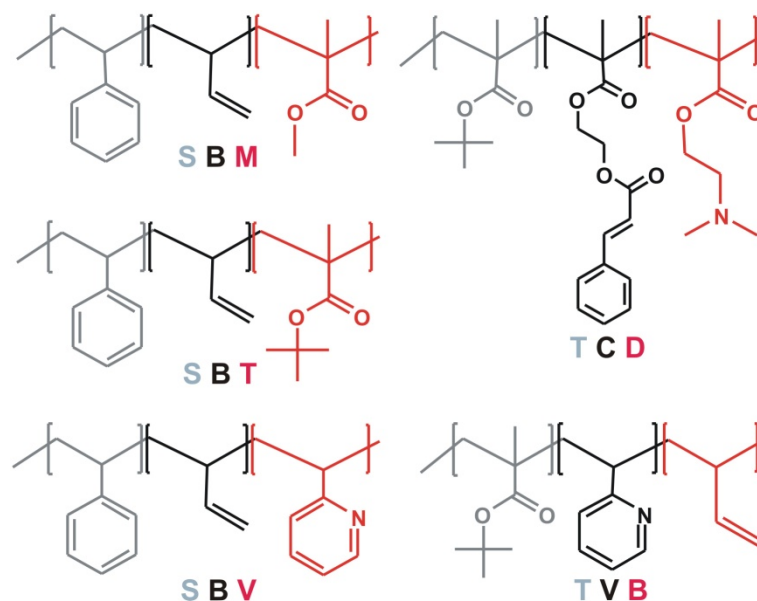


Figure 3–2: Structures of linear ABC triblock terpolymers. S = polystyrene, B = polybutadiene, M = poly(methyl methacrylate), T = poly(*tert*-butyl methacrylate), V = poly(2-vinylpyridine), D = poly(2-(dimethylamino)ethyl methacrylate), C = poly(2-(cinnamoyloxy)ethyl methacrylate). In each case the red block builds up the corona.

Results

Influence of volume ratio of core-forming blocks. We start with a series of polystyrene-*block*-polybutadiene-*block*-poly(methyl methacrylate)s (PS-*b*-PB-*b*-PMMA; SBM1-12; Fig. 3–2, Table 3–1), differing in the volume ratio of PS and PB blocks, $V_{\text{PS}}/V_{\text{PB}}$, and the molar ratio of coronal versus PS + PB units, $r_{\text{PMMA}} = N_{\text{PMMA}}/(N_{\text{PS}} + N_{\text{PB}})$. We apply a two-step process for the directed self-assembly. The terpolymer is first dissolved in a nonsolvent for the middle block PB, followed by dialysis into a nonsolvent for both blocks PS and PB. Annealing of the subunits in the first solvent ensures near-equilibrium conformations at this stage. Dissolution of SBMs in DMAc (*N,N*-dimethylacetamide, nonsolvent for PB, $c = 1$ g/L) yields spherical micelles with a PB core and a mixed or compartmentalized corona of PS and PMMA, *termed* subunits. This is the first reduction of the degrees of conformational freedom in the directed self-assembly process. Dynamic Light Scattering (DLS) confirms their formation with small hydrodynamic radii of $R_{\text{h,app}} = 9 - 14$ nm (Fig. 3–3a-c, Supplementary Fig. S3–1 and Table S3–1).^[47] In a second step to direct the structure formation, dialysis against an acetone/isopropanol mixture (60/40 v/v) triggers the collapse of the PS block within the corona and induces higher-level aggregation of the subunits into the final multicompartment-core micelles (MCMs, Fig. 3–1). Rearrangements and phase-segregation between PS and PMMA occur during this process, equalling a refinement of the subunits. Acetone is a nonsolvent for PB, a near- Θ solvent for PS and a good solvent for PMMA. Isopropanol is a near- Θ solvent for PMMA and a nonsolvent for both PS and PB. Hence, PB remains insoluble at all times, its chains yet mobile enough to allow for rearrangements during the process of subunit aggregation into the final MCMs. The importance of a dynamic PB-core is underscored by the fact that freezing the segmen-

tal dynamics of the subunits via crosslinking the PB-core results in ill-defined MCMs (see Supplementary Fig. S3–2).

Table 3–1 Molecular and micellar characteristics of employed ABC triblock terpolymers

Code ^a	Polymer ^c	$\frac{V_A}{V_B}$ ^d	$r_c = \frac{N_C}{N_A + N_B}$	MCM morphology
SBM1	S ₃₅₄ B ₁₄₈ M ₃₅₂ ⁸⁰	4.20	0.70	spherical
SBM2	S ₃₀₆ B ₁₅₁ M ₃₄₀ ⁷⁴	3.57	0.75	spherical
SBM3	S ₃₃₇ B ₃₃₃ M ₃₆₉ ⁹⁰	1.78	0.54	spherical
SBM4	S ₆₆₀ B ₆₇₄ M ₃₅₀ ¹⁴⁰	1.72	0.26	spherical
SBM5	S ₆₁₁ B ₆₃₅ M ₂₉₂ ¹²⁷	1.69	0.23	spherical
SBM6	S ₂₇₇ B ₃₃₃ M ₄₃₀ ⁹⁰	1.46	0.70	spherical
SBM7	S ₃₂₅ B ₆₈₁ M ₇₆₄ ¹⁴⁷	0.84	0.76	linear
SBM8	S ₃₆₃ B ₇₆₅ M ₃₈₉ ¹¹⁸	0.84	0.35	linear
SBM9	S ₂₈₃ B ₅₉₆ M ₃₀₄ ⁹²	0.84	0.35	linear
SBM10	S ₃₇₄ B ₈₁₉ M ₅₀₉ ¹³⁴	0.80	0.43	linear
SBM11	S ₁₄₁ B ₃₄₅ M ₁₅₇ ⁴⁹	0.72	0.32	linear
SBM12	S ₂₈₃ B ₇₀₀ M ₃₇₈ ¹⁰⁵	0.71	0.38	linear
SBV	S ₃₅₈ B ₃₇₈ V ₅₉₄ ¹²⁰	1.67	0.81	spherical
SBT1 ^b	S ₅₈₀ B ₁₂₄ T ₄₇₂ ¹³⁴	8.23	0.67	spherical
SBT2 ^b	S ₅₂₀ B ₅₃₈ T ₃₄₃ ¹³²	1.70	0.32	spherical
TVB1 ^b	T ₃₈₀ V ₃₀₇ B ₄₄₈ ¹¹⁰	1.77	0.64	linear
TVB2 ^b	T ₆₄₃ V ₂₉₃ B ₄₄₈ ¹⁴⁵	3.00	0.46	linear
TVB3 ^b	T ₇₉₀ V ₂₈₆ B ₄₄₈ ¹⁶⁵	3.68	0.40	linear
TCD	T ₂₈₀ C ₁₃₅ D ₂₅₅ ¹¹¹	1.17	0.62	linear
<i>t</i> SfBT	<i>t</i> S ₄₅₂ fB ₅₁₃ T ₄₆₃ ³⁹²	0.62	0.45	linear
N <i>n</i> BEO	N ₁₇₈ <i>n</i> B ₁₀₅ EO ₁₁₄ ³⁹	1.22	0.40	linear

^a SBM = polystyrene-*block*-polybutadiene-*block*-poly(methyl methacrylate), SBV = polystyrene-*block*-polybutadiene-*block*-poly(2-vinylpyridine), SBT = polystyrene-*block*-polybutadiene-*block*-poly(*tert*-butyl methacrylate), TVB = poly(*tert*-butyl methacrylate)-*block*-poly(2-vinylpyridine)-*block*-polybutadiene, TCD = poly(*tert*-butyl methacrylate)-*block*-poly(2-(cinnamoyloxy)ethyl methacrylate)-*block*-poly(2-(dimethylamino)ethyl methacrylate), *t*SfBT = Poly(*tert*-butoxy styrene)-*block*-poly(C₆F₁₃C₂H₄S-ethylethylene)-*block*-poly(*tert*-butyl methacrylate)^[45] and N*n*BEO = Poly(N-isopropyl acrylamide)-*block*-poly(*n*-butyl acrylate)-*block*-poly(ethylene oxide).^[46]

^b Fraction of 1,4-butadiene units ca. 10 mol%, otherwise 90 mol%.

^c Subscripts denote number average degrees of polymerization of each block, N_A , N_B , N_C ; Superscripts give overall molecular weight in kg/mol.

^d Volume fractions V_A and V_B calculated from polymer densities.

Figures 3d-k depict TEM-micrographs of MCMs formed by various SBMs after OsO₄ staining (PS grey, PB black, PMMA invisible due to e-beam degradation). We observe

spherical MCMs with PS core and distinct numbers (2—12) of PB patches for SBM1-6 (Fig. 3–3d-i). In contrast, SBM7-12 (Fig. 3–3j,k) show linear, partially segmented worm-like MCMs. The morphology (spherical vs. linear) is determined by the volume ratio of the two insoluble blocks V_{PS}/V_{PB} .

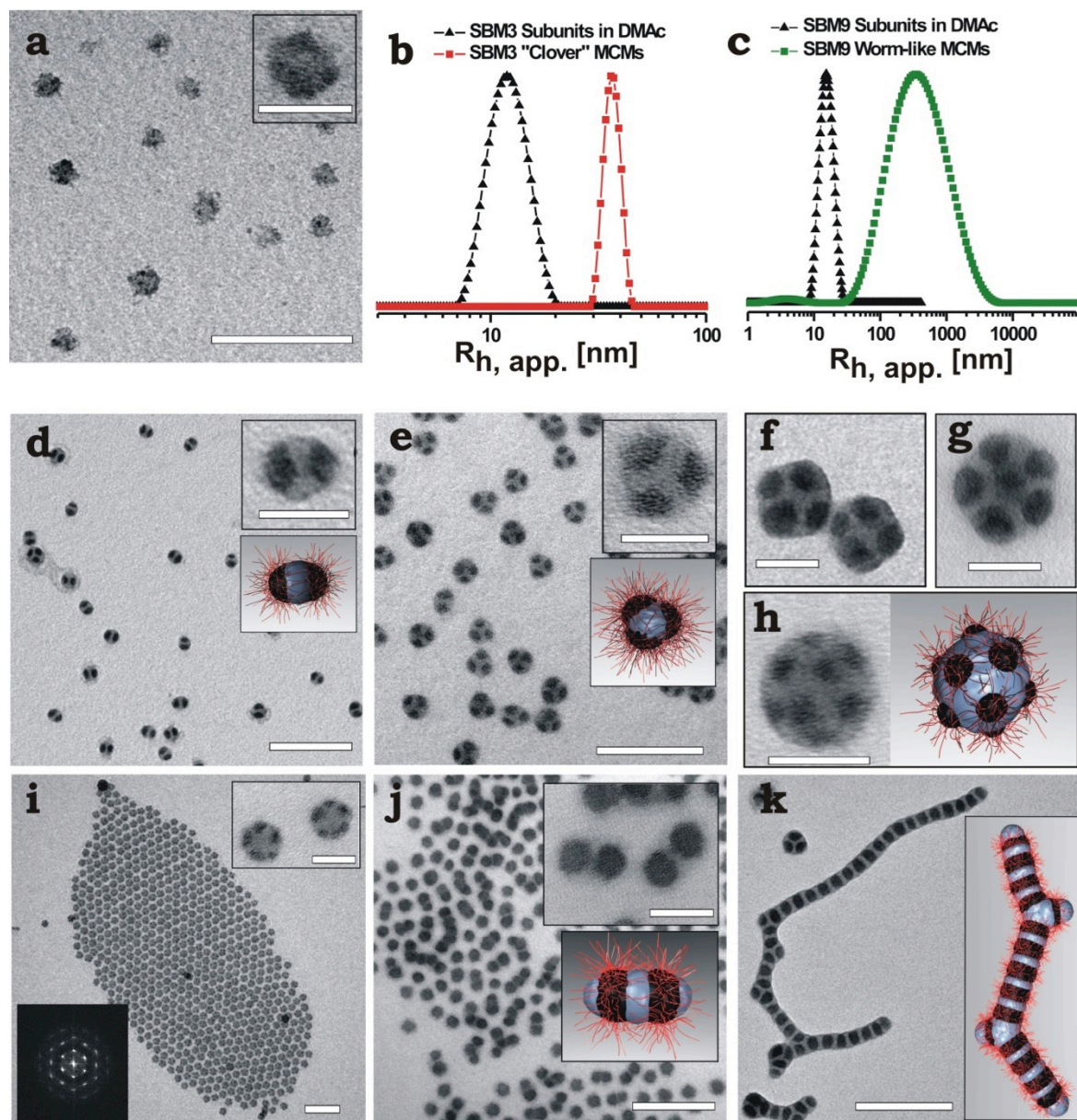


Figure 3–3: TEM images of SBM9 subunits in DMAc, spherical and linear MCMs formed by SBMs with various core volume ratios (V_{PS}/V_{PB}) and DLS data for SBM3 and SBM9 in the stage of subunits and MCMs. MCMs were prepared by dialysis of subunits with mixed- or compartmentalized PS/PMMA corona and PB core in DMAc into acetone/isopropanol (60/40 v/v). Staining was achieved with OsO₄ (PB black, PS grey, PMMA corona invisible). **Subunits:** (a) Weakly phase-segregated corona of PS and PMMA of SBM9 subunits with a PB core in DMAc. (b–c) DLS CONTIN plots of pre-assembled subunits and final MCMs of SBM3 and SBM9. **MCMs:** (d) SB₂ (BSB) “hamburgers” of SBM6; (e) SB₃ “clovers” of SBM3; (f) SB₄ “Maltese crosses” of SBM4; (g) SB₇ “footballs” of SBM5; (h, i) SB_{*x*} “footballs” of SBM1 and SBM2. The inset (lower right, i) depicts the Fourier transform of the TEM micrograph; (j) SBSBS = (SBS)₂ “double-burgers” of SBM7 (see also Supplementary Fig. S3); (k) (SBS)_{*x*} linear MCM colloidal polymers of SBM9. The kinks in the colloidal polymers will be discussed below (Scale bars are 200 nm and 50 nm in insets).

We find that SBM terpolymers with $V_{PS}/V_{PB} > 1$ form spherical MCMs, whereas those with $V_{PS}/V_{PB} \leq 1$ aggregate into linear MCMs. We will discuss the influence of the corona block later. In accordance to TEM, DLS confirms a 4-fold increase in hydrodynamic dimension for discrete spherical MCMs vs. their preceding subunits (Fig. 3–3b and Supplementary Fig. S3–1). For example, SBM3 subunits exhibit $R_{h,app} = 11 \pm 2$ nm in DMAc and $R_{h,app} = 43 \pm 9$ nm for the MCMs in acetone/isopropanol (60/40 v/v). Similarly, the radii dramatically increase to several μm for SBM7-12 caused by the progressing step-growth polymerization of micellar building blocks into segmented chains (Fig. 3–3c).

The dominant population in SBM6 (Fig. 3–3d) are “hamburgers” with a BSB core, which are different from SBM7 “double-burgers” with an SBSBS = (SBS)₂ core sequence. Note the tendency of the “double-burgers” to undergo linear growth via end-to-end attachment in concentrated areas on the TEM grid (Fig. 3–3j). A detailed TEM grey-scale analysis in Supplementary Figure S3–3 clearly reveals a step on each end of the “double-burger”, which is absent for “hamburgers”, and confirms terminal PS-compartments. These double-burgers undergo step-growth polymerization into linear chains (Fig. 3–3k) for suitable corona volumes as will be shown below. From these experiments, we identify two key features. First, we generate a previously inaccessible diversity of well-defined MCM morphologies with remarkable control over the number of patches. Just using one simple triblock copolymer system, we are able to reproduce the established classes of MCMs, open pathways to rarely observed morphologies such as “clovers”^[44] and provide completely new core geometries like “Maltese crosses” (Fig. 3–3e, f). Most importantly, we find homogeneous populations and not just single events among polydisperse mixtures.^[31, 35, 36, 38, 39, 43, 44] This is significant, considering the delicate interplay of various thermodynamic factors and the shallow differences in free energy between the MCMs with various patches. For instance, SBM3 forms more than 92 % “clover” MCMs with 3 patches, whereas SBM6 forms above 90 % “hamburger” MCMs. Overall, the extent of controlled structure formation into homogeneous populations is unprecedented and a unique feature of our process. Secondly, in particular the spherical MCMs are not only homogeneous in number of patches but also remarkably monodisperse in size. This is evidenced by the formation of hexagonally ordered 2D lattices exhibiting third order reflections in the corresponding Fourier-transform image (Fig. 3–3i).

The advantage of the herein developed directed self-assembly process with step-wise reduction of conformational freedom can be demonstrated by omitting the first dedicated reduction of conformational freedom (i.e. the confinement into subunits). Common approaches to prepare MCMs include direct dissolution in the final solvent with very long equilibration times (days to weeks)^[35, 43, 48] or one-step dialysis^[15, 39]. Direct dissolution of SBM into acetone/isopropanol only leads to polydisperse or even ill-defined aggregates for polymers with a large solvophobic fraction. During a single-step, direct dialysis from a common solvent (THF), a pre-assembly into subunits can also take place but remains “hid-

den” and uncontrolled while passing the various solvent compositions. On the one hand this complicates an experimental analysis and mechanistic understanding. But, moreover, the final MCMs are also increasingly polydisperse and for large solvophobic fractions, meaning slower dynamics, only ill-defined agglomerates can be found. Detailed results on both are presented in Supplementary Figs S3–5, S3–6 and Supplementary Notes 1 and 2. It may also be noted that our two step process (dissolution in a nonsolvent for PB, followed by dialysis) is similarly fast compared to direct dialysis and substantially faster and potentially more reliable than direct dissolution and prolonged equilibration. Consequently, clear advantages of the step-wise procedure can be identified in rapid preparation and the access to unique architectures with highly homogeneous populations. These advantages are most pronounced for systems containing large solvophobic/insoluble parts and, hence, slower dynamics.

The extent of compartmentalization of the A and C corona depends on the interaction parameters between A and C and polymer/solvent.^[49] Subsequent addition of a nonsolvent for A induces its collapse. This collapse occurs slowly during the dialysis and leads to consecutive refinement of the A/C corona structure of the intermediate subunits (Fig. 3–4b,c) due to an enforced phase segregation of A and C. Rearrangements are allowed due to the dynamic B core. Classical core-shell-corona micelles are not observed under these conditions. At some point, the insufficiently swollen C blocks cannot stabilize the refining subunits anymore and secondary aggregation is triggered by the unfavourable exposure of solvophobic A patches. Consequently, initial subunits serve as building blocks for the MCMs (Fig. 3–4d-f). A *transient AB Janus structure* (Fig. 3–4c) is assumed during the merging of various subunits into spherical MCMs, thus forming distinct geometries.

Suitable polymers form “inverse hamburger” ABA micelles with two A patches (Fig. 3–4b) under good solvent conditions for C and moderate solvent conditions for A. These are the crucial transient subunits for colloidal step-growth polymerization into linear “double-burger” dimers (Fig. 3–4e), oligomers, and colloidal polymers (Fig. 3–4f). They possess sticky terminal A compartments (if unprotected by an undersized corona), as the stabilizing corona chains only emerge from the non-terminal B patches. This supra-micellar polymerization of “inverse hamburgers” via “double-burgers” into colloidal mesoscale chains is the soft-matter analogue to a recent approach for gold nanorods.^[50]

Detailed mechanism of directed self-assembly. Figure 3–4 illustrates mechanistic details of the process. Here, we use the general ABC nomenclature as it applies to all triblock terpolymers. Dissolution in a nonsolvent for B leads to micellar subunits (Fig. 3–4a).

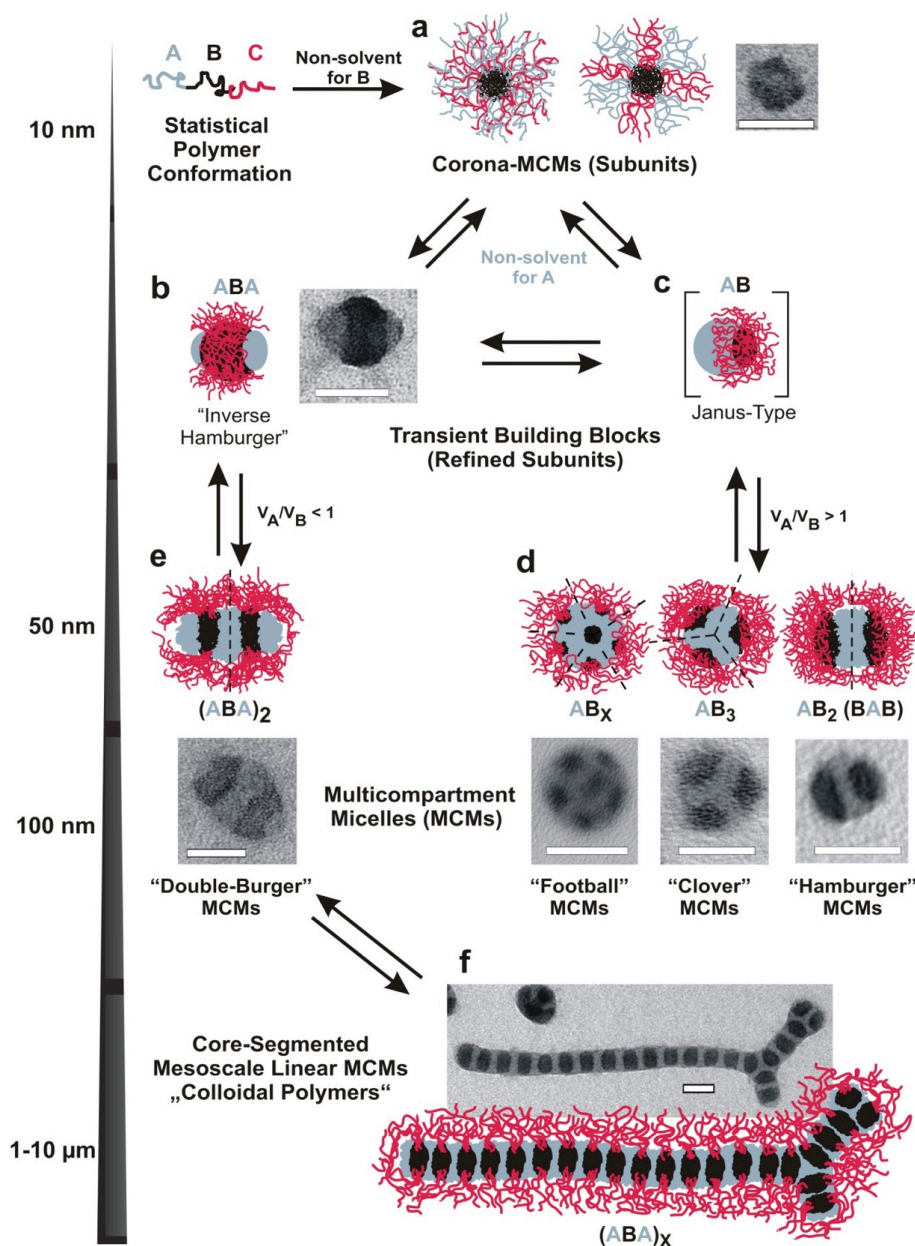


Figure 3–4: Detailed mechanism for the preparation and directed hierarchical self-assembly of well-defined MCMs. First, the ABC triblock terpolymers are forced into (a) corona MCMs via dissolution in a nonsolvent for B (termed subunits). Upon dialysis into a nonsolvent for A and B, these subunits self-assemble further via a refinement of the corona structure (b, c) into various MCMs with well-defined number of patches (d, e). (f) Under suitable conditions, the colloidal polymerization into segmented worms can be triggered (TEM images, OsO₄-stained: PS grey, PB black and PMMA not visible due to e-beam degradation; Scale bars are 50nm).

Scaling Theory. We rationalize the thermodynamic stability criteria of MCM morphologies using the scaling approach, where we derive power law dependences for the MCM structures as a function of the degrees of polymerization, N_A, N_B, N_C , of the segments and the solvent quality for the corona block C (see Supplementary Fig. S3–11 and Supplemen-

tary Note 3 for details). We start from micellar subunits with B core and A/C corona. Switching to poor solvent conditions for the A block induces its collapse. Two different scenarios of subunit aggregation are envisioned: strongly asymmetric, $V_A/V_B \gg 1$, and nearly symmetric, $V_A/V_B \approx 1$, core block volume ratios. For $V_A/V_B \gg 1$, *starlike or crew-cut spherical MCMs* with $n \gg 1$ B-patches on the spherical A core are formed. A continuous B shell is unstable when the interfacial tension between the solvophobic blocks becomes $\gamma_{AB} \geq \gamma_{AS} - \gamma_{BS}$, where S denotes the solvent.

In the limiting case of *starlike* micelles ($d_{corona} = R_{micelle} - R_{core} \gg R_{core}$) the number of patches, n , is

$$n \equiv (N_A v_A / N_B v_B)^{4/5} (\gamma_{AS} / \tilde{\gamma}_{BS})^{6/5} \ln^{-6/5} (R_{micelles} / R_{core}) \quad (3-1a)$$

$$\text{where } \frac{R_{micelle}}{R_{core}} \equiv \begin{cases} 1 N_C^{3/5} \tau_C^{1/5} (N_A v_A)^{-11/25} \gamma_{AS}^{-4/25}, & \text{for good solvent} \\ 1 N_C^{1/2} (N_A v_A)^{-2/5} \gamma_{AS}^{-1/10}, & \text{for near-}\Theta \text{ solvent} \end{cases} \quad (3-1b)$$

Here, l is the length of one monomer unit, $\tau_C \equiv 1/2 - \chi_{CS}$ quantifies the solvent strength for the coronal block C, v_A and v_B are the volumes of the corresponding monomer units and $\tilde{\gamma}_{BS} \approx \gamma_{BS} (1 - \cos\theta)^{2/3} (1 + \frac{\cos\theta}{2})^{1/3}$, where $\cos\theta = (\gamma_{AS} - \gamma_{AB}) / \gamma_{BS}$ is the contact angle of B patches on the core. Since $V_A/V_B \gg 1$, N_B is neglected in Eq. 3-1b.

In the limiting case of *crew-cut MCMs* ($d_{corona} \ll R_{core}$), the number of patches is given by

$$n \equiv (N_A v_A)^2 (N_B v_B)^{4/5} \tilde{\gamma}_{BS}^{6/5} \begin{cases} (\gamma_{AS} / l^{5/3} N_C \tau_C^{1/3})^{18/11}, & \text{for good solvent} \\ (\gamma_{AS} / l^{-2} N_C)^{3/2}, & \text{for near } \Theta\text{-solvent} \end{cases} \quad (3-2)$$

as long as the inter-patch distance $h_{patch} \leq d_{corona}$.

The experimental reality lies between these extremes. The number of B-patches, n , increases with $V_A/V_B \equiv v_A N_A / v_B N_B$ and decreases with the solvent strength, τ_C , and the length of the C block, N_C . This theoretical prediction is in good agreement with our experimental results.

For $V_A/V_B \approx 1$ or $V_A/V_B \leq 1$ the collapse of the A blocks only leads to a moderate increase in the overall solvophobicity of the terpolymers and, as a result, to a moderate growth of the (multicompartment) core. Aggregation of the micellar subunits into spherical MCMs (“hamburger”, BAB) is not favoured (Fig. 3-4). Gain in the overall interfacial energy promotes switching from BAB to ABA (“inverse hamburger”, linear) favoured for

$$V_A/V_B \leq [1 + const \cdot (\gamma_{AS} - \gamma_{BS}) / \gamma_{AB}]^{-1} \quad (3-3)$$

, where *const* is of the order of unity. When $\gamma_{AS} < \gamma_{BS}$, the core shape switching occurs at $V_A/V_B > 1$. This leads to a stability region of ABA “inverse hamburger”, capable of linear

polymerization. Considering the ABA "inverse hamburgers" or the $(ABA)_2 = ABABA$ "double-burger" MCMs as monomers and dimers, respectively, for colloidal polymers, we estimate the number average degree of polymerization, as a mesoscale analogue to the chain-length distribution of supramolecular polymers or step-growth polymerization in synthetic polymers. A model for non-cooperative polymerization^[51] yields:

$$\bar{n} \sim (Kc)^{1/2} : c^{1/2} \exp[-E / 2k_B T] \quad (3-4)$$

Here, c is the concentration and K denotes the equilibrium association constant between two MCMs, which depends on the excess free energy of one end of the worm-like MCM, E . K and E rise when decreasing the length or solvent quality for the corona, inducing longer supramicellar chains.

Switching aggregate morphologies via corona volume. As predicted by theory, the degree of subunit assembly of spherical and linear MCMs is also controlled by the corona volume (Eq. 3-1, 2 and 4). This can be manipulated by the degree of polymerization of the C block, N_C , or the solvent quality expressed by the excluded volume parameter, $\tau_C \cong 1/2 - \chi_{CS}$. The latter can also be elegantly tuned in stimuli-responsive corona blocks. Below, we demonstrate all of these possibilities. The basic reasoning is that a corona of insufficient expansion cannot effectively shield the underlying MCM subunits against aggregation via their exposed insoluble patches. Figure 3-5 depicts the growth of linear (SBM9) and spherical (SBM3) MCMs by changing the solvent quality for the corona block. In DMAc, the initial subunits of SBM9 showed a weakly phase-separated PS/PMMA-corona (Fig. 3-3a).^[30] Dialysis into acetone/isopropanol (90/10) induces a contraction of PS and a refinement of the structure as visible by the grey patches on the opposite sides of the PB-core (Fig. 3-5b), i.e. the formation of SBS "inverse hamburger" MCMs (refined subunit). The increasing solvophobicity of the PS-domains of these symmetrical building blocks and the concomitant contraction of the PMMA-corona trigger the following dimerization and step-growth polymerization. Upon addition of further nonsolvent (80/20) "double burger" dimers, $(SBS)_2$, are formed as dominant species (Fig. 3-5c). A distribution of oligomers cannot be found here and thus we attribute their intermediate stability to a rearranged corona that is large enough to protect the terminal PS compartments, suppressing further growth (compare Fig. 3-4e). At higher isopropanol content (70/30) slightly extended 1D oligomers are formed, followed by several μm long (60/40) and increasingly branched colloidal polymers (50/50; Fig. 3-5d). Branches and kinks are caused by fusion/assembly of three SBS-"inverse hamburgers" into an $(SBS)_3$ branching point with one common PS domain in the centre.

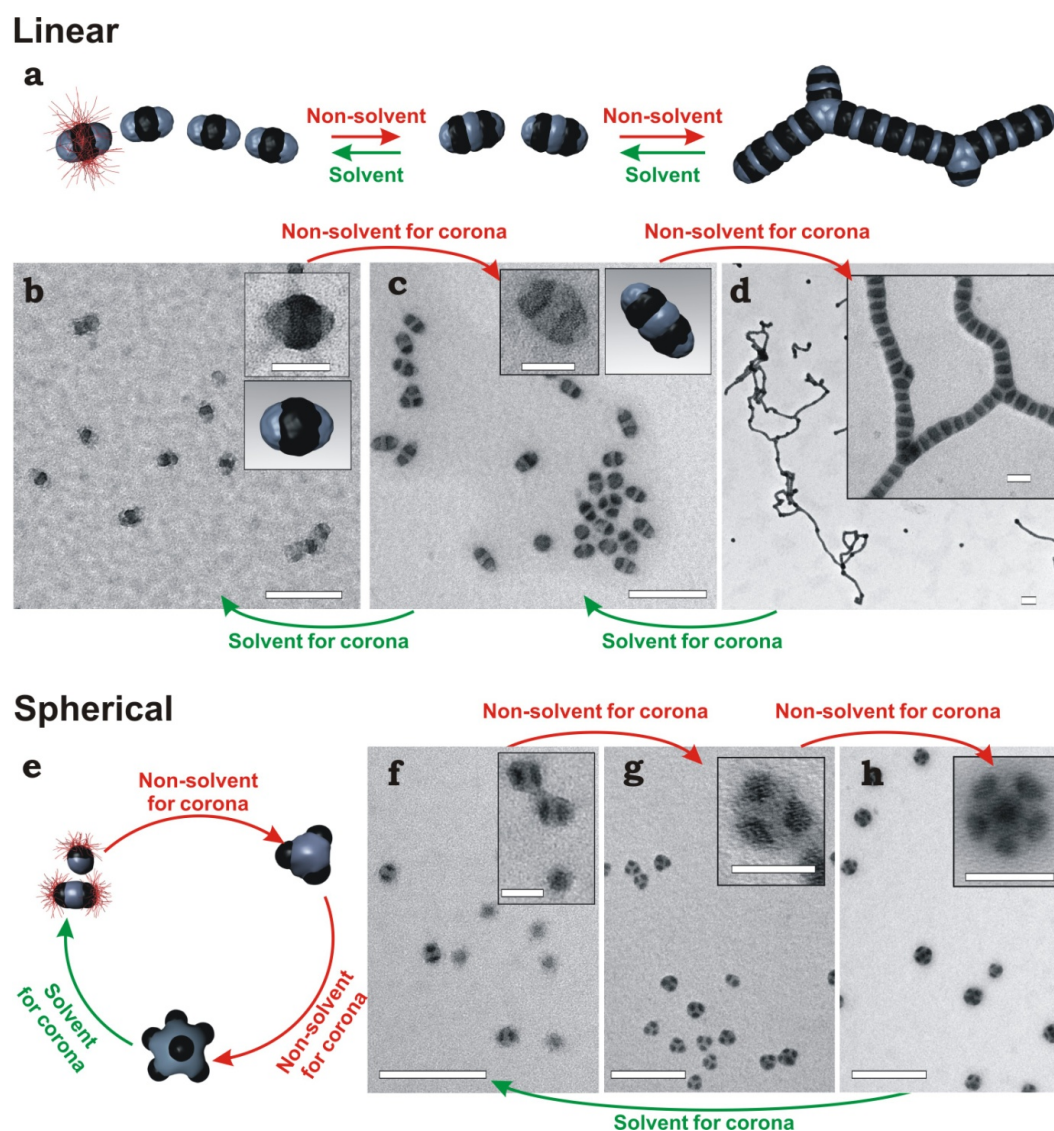


Figure 3–5: Mesoscale polymerization of linear MCMs and subunit exchange of spherical MCMs promoted by changing the corona volume. The red corona chains emerge from the black compartments, but are mostly omitted for clarity (TEM images, OsO₄-staining except (b) RuO₄, acetone/isopropanol fractions are given in v/v). **(a)** Scheme for reversible mesoscale colloidal polymerization (SBM9). Note that the branching points are composed of (SBS)₃ centers. **(b)** SBS refined subunits in acetone/isopropanol (90/10), **(c)** (SBS)₂ “double burgers” formed by two SBS in acetone/isopropanol (80/20) and their polymerization **(d)** in acetone/isopropanol (50/50). **(e)** Scheme for reversible exchange of refined subunits in spherical MCMs (SBM3). **(f–h)** *In-situ* switching of spherical MCMs. **(f)** “Hamburgers” and refined subunits successively merge into **(g)** “clovers” and **(h)** “footballs” triggered by reduction of the solvent quality for the corona (addition of isopropanol from 90/10 to 60/40 to 50/50). Refined subunits clearly reappear upon the expansion of the corona (addition of acetone from 50/50 to 90/10). Scale bars are 200 nm and 50 nm in insets.

The drop in solvent quality contracts the corona and corresponds to an increase of the equilibrium association constant, K , as expressed in Eq. 3–4 and explains the formation of longer mesoscale colloidal polymers (DLS in Fig. 3–3c and Supplementary Fig. S3–4). Even higher isopropanol contents result in network formation and precipitation, caused by the increasing end-to-side addition, possible at stronger corona contraction. The polymerization is fully reversible by changing the solvent quality, e.g. from 80/20 to 50/50 and back. Loosely related are results from Lodge and Hillmyer who observed that addition of

diblock copolymer micelles to MCM worms can induce a shortening of the worms via fusion/fission event.^[43]

The same principle of selective switching between high and low aggregation numbers can be applied to spherical MCMs (SBM3, Fig. 3–5e-h). Decreasing the solvent quality for the corona block forces geometry changes into higher patch numbers and vice-versa, in good accordance with theory. The process is fully reversible. Importantly, subunits, “hamburgers”, “clovers” and “football” MCMs show near identical average PB-compartment sizes between 16.1 ± 0.6 nm (evaluations given in Supplementary Fig. S3–7), thus supporting the exchange/release of intact refined subunits/individual patches.

General Validity of the Concept. In the last part we demonstrate the general validity of our concept by applying it to vastly different block terpolymer systems. Those differ in (i) the selection of monomers, leading to different incompatibilities and solubilities, (ii) the polarity of the final solvent (dodecane/alcohols/water), (iii) the dynamics of the intermediate subunits as expressed by the bulk glass transition temperature, T_g , of the middle block, varying from -51 °C to $+100$ °C. Furthermore, we exploit the stimuli-responsiveness of a “smart” polymer (PDMAEMA in TCD) to control colloidal superstructures by simply triggering a pH switch. Table 3–1 and Figure 3–6 display the investigated terpolymers: SBV (Fig. 3–6a), SBT2 (Fig. 3–6b), TVB1 (Fig. 6c) and TCD (Fig. 3–6d-f) and also two polymers from our earlier work that conform to our concept (*t*SfBT and *Nn*BEO).^[45, 46]

Let us first change to different end blocks (C) and solvents, while keeping the same inner blocks. PS-*block*-PB-*block*-poly(2-vinylpyridine) (SBV) is dialyzed from DMAc into isopropanol (selective solvent for P2VP) resulting in 86 % “hamburger” MCMs (see Supplementary Fig. S3–8). The large P2VP corona ($r_{P2VP} = 0.81$) provides sufficient stabilization and the slightly asymmetric volume ratio ($V_{PS}/V_{PB} = 1.67$) favours spherical MCMs. As expected, a nonsolvent for P2VP (addition of acetone to yield isopropanol/acetone 80/20) increases the degree of aggregation of subunits towards narrowly distributed “football” MCMs (Fig. 3–6a). Next, PS-*block*-PB-*block*-(*tert*-butyl methacrylate) (SBT2) is dialyzed from DMAc into ethanol (selective for P*t*BMA), leading to “clover” MCMs (Fig. 3–6b), almost identical to SBM3, and in very good agreement with theoretical expectations, as SBT2 exhibits a comparable molar ratio of the corona units ($r_{P*t*BMA} = 0.32$) and the same slightly asymmetric core volume ratio $V_{PS}/V_{PB} = 1.70$. Furthermore, upon changing the composition to the range of SBM1/2, SBT1 exhibits “football” MCMs (not shown here) due to a higher molar ratio of the corona units ($r_{P*t*BMA} = 0.67$) and a strongly asymmetric core volume ratio $V_{PS}/V_{PB} = 8.23$.

The TVB series (see Table 3–1) broadens the concept to a completely new monomer sequence, very non-polar solvents and to a centre block with a much higher T_g near 100 °C. The dialysis sequence from THF/cyclohexane (20/80; P2VP insoluble) to dodecane (selective for PB) yields linear MCMs (Fig. 3–6c). TVB1 forms extended linear structures due to

the comparably small corona-forming block ($r_{PB} = 0.64$). Branching in these mesoscopic worms occurs for higher ratios of V_{PtBMA}/V_{P2VP} (see Supplementary Figs. S3–9 and S3–10). Thus, even a high bulk glass transition temperature does not pose kinetic obstacles for the formation of well-defined MCMs in our step-wise process. Interestingly, all TVBs self-assemble into linear and branched MCMs despite their large core asymmetry ($V_{PtBMA}/V_{P2VP} > 1$), in apparent contrast to the other polymers. However, as derived in Eq. 3–3, the condition $\gamma_{AS} < \gamma_{BS}$, here $\gamma_{PtBMA/S} < \gamma_{P2VP/S}$, is fulfilled, i.e., the surface tension of P2VP towards dodecane is higher as compared to PtBMA.

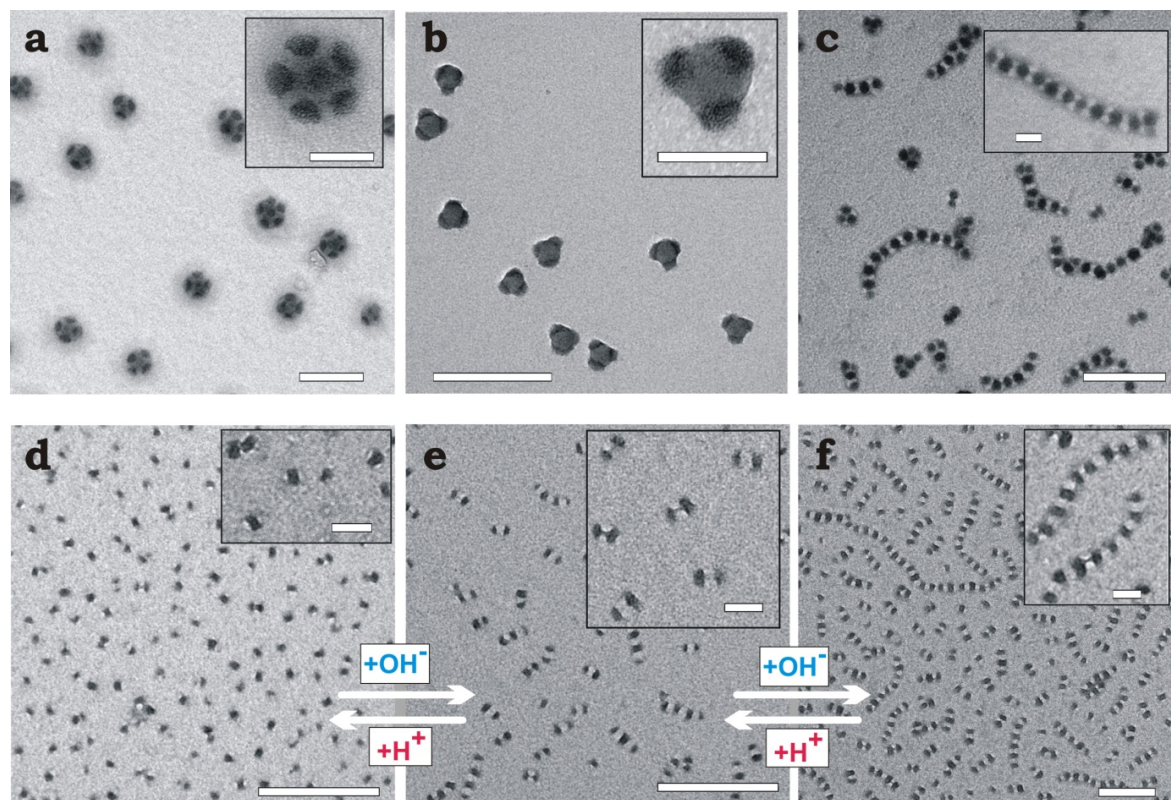


Figure 3-6: General validity of the concept - MCMs of different triblock terpolymers. (TEM images, OsO_4 -stained if not mentioned otherwise; scale bars are 200 nm and 50 nm in insets). **(a) SBV** in acetone/isopropanol 20/80 (PB black, PS bright grey, P2VP corona grey). **(b) SBT2** in ethanol (PB black, PS grey, PtBMA invisible due to e-beam degradation). **(c) TVB1** in dodecane (I_2 staining; P2VP black, PtBMA white). **(d-f) pH-programmable colloidal polymerization of TCD in water:** **(d)** pH = 3 completely protonated, **(e)** pH = 6 partially protonated, and **(f)** pH = 10 deprotonated PDMAEMA corona (RuO_4 staining; PCEMA black, PtBMA bright grey, PDMAEMA corona not visible).

Finally, the herein developed understanding enables us to command mesoscale micellar superstructures via a stimuli-responsive terpolymer, poly(*tert*-butyl methacrylate)-*block*-poly(2-(cinnamoyloxy)ethyl methacrylate)-*block*-poly(2-(dimethylamino)ethyl methacrylate) (TCD), in water. TCD has a high T_g middle block and a pH- and temperature-sensitive, water-soluble PDMAEMA end block with $pK_a = 6.2$ ^[52] (Fig. 3–6d-f). Micellar subunits are first formed in isopropanol, which is a nonsolvent for PCEMA. Subsequent dialysis against water (pH = 3) leads to TCT “inverse hamburger” refined subunits (Fig. 3–6d, $V_{PtBMA}/V_{PCEMA} = 1.17$) stabilized by the fully protonated corona ($r_{PDMAEMA} = 0.62$ in

Table 1 underestimates its real extension). Next, we can exploit the smart corona to elegantly manipulate the colloidal self-assembly into linear MCMs, as the pH value regulates the corona swelling. At pH = 6, the PDMAEMA corona is partially protonated, stretched and still occupies a moderately large volume. Hence, it provides good coverage of the compartmentalized core and “double-burger” MCMs and linear oligomers are formed (Fig. 3–6e). At pH = 10, the PDMAEMA corona is uncharged and contracted, thus inducing polymerization into extended linear mesoscale-MCM polymers (Fig. 3–6f). The pH-induced contraction of the PDMAEMA corona corresponds to an increase in the association constant, K (Eq. 3–4). This is a particularly elegant example of how to organize interactive polymer structures into nanostructured aggregates and harness their intelligent properties, as encoded via polymer chemistry, to control aggregation across several length scales, i.e., from the polymer sequence to micrometer-long segmented worms. Such well-defined pH-programmable hierarchies drastically rely on highly defined colloidal building blocks of low polydispersity.

Discussion

We demonstrated the precise prediction of substructure, morphology, size, and superstructures of self-assembled MCM hierarchies based on readily accessible linear triblock terpolymers. Therein, a directed step-wise self-assembly via pre-assembled subunits and sequential reductions of the degrees of freedom proved to be the key steps to reliably generate thermodynamically labile morphologies of MCMs with extremely homogeneous structure. This is not only expressed in the overall narrow size distribution but also manifests in a striking control over the number of patches. The latter is a substantial contribution and promising approach to the quest for well-defined patchy organic and inorganic nanoobjects.^[1, 3, 23, 53] In particular for low patch numbers, the resulting MCMs exhibit control of the geometry (angle and interpatch distance), wherein the dimensions can be tailored to potentially suit for sensing applications or the patterning of surfaces via nanolithographic procedures. For instance, the selective loading of patches with inorganics can lead to distinct spatial and tunable geometries of functional materials within ordered compartments. We also foresee that removal of the corona blocks (e.g., when connected via supramolecular bonds) can be used to fabricate well-defined soft patchy nanoparticles not conceivable by other techniques. Interestingly, the switching of the geometries and patchiness of spherical MCMs, as well as the reversible aggregation of linear MCMs across length-scales during the step-growth polymerization from monomers into mesoscale chains, is enabled by the straightforward manipulation of the corona volume fraction. Such a high precision in structure and tuneability contributes in satisfying the pressing need for homogeneous building blocks for the fabrication of future bottom-up materials. Our comprehensive development can be widely applied to other polymer systems and introduces a new paradigm

for the design of polymer-based solution superstructures following surprisingly simple guidelines.

Beyond that, our strategy answers the important challenge of how to induce selectivity in hierarchical structure formation of complex self-assemblies with wide conformational space and shallow energy landscape. Therefore, the discussed considerations of directing the self-assembly pathway with dedicated processes may well serve as inspiration for other self-assembling hierarchies where large length scales with slow dynamics are approached and opens possibilities to overcome obstacles towards reliable structure formation therein.

Looking out to the future, our understanding lays the cornerstones for the rational design of new generations of tuneable and functional multicompartment solution-based hierarchies. Moreover, the accomplished comprehensive picture of the kinetics and pathways of MCM self-assembly into defined near-equilibrium structures establishes the necessary foundation for targeting defined non-equilibrium self-organized superstructures in the next steps. In consequence, the herein introduced concept paves the way for programmable particle hierarchies using anisotropic soft nanoobjects, where the balance of kinetics and thermodynamics can lead to new levels of complexity with superstructures also stable far from equilibrium.

Methods

Materials. The preparation and characterization of SBM, SBV, SBT, and TVB triblock terpolymers were reported in detail previously.^[54-58] Important parameters are summarized in Table 1 and Supplementary Table S3–1. All solvents used were of analytical grade. Dialysis tubes of regenerated cellulose with a MWCO of 12.000 – 14.000 g/mol were purchased from Roth, equilibrated in deionized water for 30 min and washed with excess dioxane before use.

Preparation of subunits. SBM, SBV and SBT terpolymers were dissolved in *N,N'*-dimethylacetamide (DMAc), TCD in isopropanol, and TVB in a mixture of cyclohexane/THF (80/20 v/v). All polymer solutions were prepared at an initial concentration of 1 g/L. The as-prepared micellar solutions of SBM, SBV and SBT were annealed overnight at 70 °C, TCD and TVB at 50 °C to guarantee an equilibrated system. Afterwards, the resulting structures were investigated by both dynamic light scattering (DLS) and transmission electron microscopy (TEM).

Self-Assembly of MCMs. In all cases, 5 mL of the micellar solution ($c = 1\text{g/L}$) were dialyzed against 5 L of selective solvent for the corona block. The solvent exchange was monitored by ¹H-NMR. Micellar solutions of SBM terpolymers were dialyzed against acetone/isopropanol mixtures, whereas in case of SBT terpolymer ethanol, and for SBV isopropanol (or an isopropanol/acetone mixture) was used. TCD was dialyzed from isopropanol

nol against water with pH values of 3, 6, and 10 and. TVB terpolymers were dialyzed from cyclohexane/THF (80/20 v/v) mixtures into dodecane.

For the determination of compartment size, size distribution and invariance of compartment size throughout assembly-disassembly steps, a quantity of at least 150 compartments were measured in TEM images, plotted as statistical histograms and evaluated to yield diameter distributions and average diameters.

Dynamic Light Scattering (DLS). DLS measurements were performed at a scattering angle of 90° or multiple angles ranging from 30°-150° in 10° steps on an ALV DLS/SLS-SP 5022F equipment consisting of an ALV-SP 125 laser goniometer, an ALV 5000/E correlator, and a He-Ne laser operating at a wavelength of $\lambda = 632.8$ nm. The CONTIN algorithm was applied to analyze the obtained correlation functions. Apparent hydrodynamic radii were calculated according to the Stokes-Einstein equation. All CONTIN plots are intensity-weighted. Prior to the light scattering measurements, all sample solutions were filtered twice through a PTFE filter with a pore size of 5 μm . The dynamic viscosities of acetone/isopropanol mixtures were calculated according to Ubbelohde,

$$\eta = \nu\rho = K(t - \nu)[w_1\rho_1 + (1 - w_1)\rho_2],$$

, where ν is the kinematic viscosity, K is the viscometer constant, t is the measurement time, ν is the Hagenbach capillary correction factor, w_1 is the weight fraction of acetone and, ρ_i are the corresponding densities.

Transmission Electron Microscopy (TEM). TEM was performed in bright-field mode on Zeiss CEM 902 and LEO 922 OMEGA electron microscopes operated at 80kV and 200kV, respectively. The samples were prepared by placing one drop of the polymer solution (0.01 g/L) onto carbon-coated copper grids. Excess solvent was instantly absorbed by a filter paper. For selective staining, the TEM specimens were exposed to RuO₄ vapour for 15 min (stains aromatics: PS, P2VP, PCEMA and partially PB), OsO₄ vapour for 2 h (stains double bonds: PB) or I₂ vapour for 4 h (stains amines: P2VP, PDMAEMA).

References

- [1] Q. Chen, S. C. Bae, S. Granick, *Nature* **2011**, *469*, 381-384.
- [2] G. M. Whitesides, B. Grzybowski, *Science* **2002**, *295*, 2418-2421.
- [3] M. Grzelczak, J. Vermant, E. M. Furst, L. M. Liz-Marzán, *ACS Nano* **2010**, *4*, 3591-3605.
- [4] M. A. Kostianen, O. Kasyutich, J. J. L. M. Cornelissen, R. J. M. Nolte, *Nature Chem.* **2010**, *2*, 394-399.
- [5] V. Percec, D. A. Wilson, P. Leowanawat, C. J. Wilson, A. D. Hughes, M. S. Kaucher, D. A. Hammer, D. H. Levine, A. J. Kim, F. S. Bates, K. P. Davis, T. P. Lodge, M. L. Klein, R. H. DeVane, E. Aqad, B. M. Rosen, A. O. Argintaru, M. J. Sienkowska, K. Rissanen, S. Nummelin, J. Ropponen, *Science* **2010**, *328*, 1009-1014.
- [6] D. A. Christian, A. Tian, W. G. Ellenbroek, I. Levental, K. Rajagopal, P. A. Janmey, A. J. Liu, T. Baumgart, D. E. Discher, *Nature Mater.* **2009**, *8*, 843-849.

- [7] S. I. Stupp, V. LeBonheur, K. Walker, L. S. Li, K. E. Huggins, M. Keser, A. Amstutz, *Science* **1997**, *276*, 384-389.
- [8] S. Mann, *Nature Mater.* **2009**, *8*, 781-792.
- [9] S. Park, J.-H. Lim, S.-W. Chung, C. A. Mirkin, *Science* **2004**, *303*, 348-351.
- [10] D. J. Hill, M. J. Mio, R. B. Prince, T. S. Hughes, J. S. Moore, *Chem. Rev.* **2001**, *101*, 3893-4012.
- [11] C. Levinthal, *J. Chim. Phys.* **1968**, *65*, 44-45.
- [12] C. M. Dobson, *Nature* **2003**, *426*, 884-890.
- [13] M. S. Cheung, L. L. Chavez, J. N. Onuchic, *Polymer* **2004**, *45*, 547-555.
- [14] N. Hadjichristidis, H. Iatrou, M. Pitsikalis, S. Pispas, A. Avgeropoulos, *Progr. Polym. Sci.* **2005**, *30*, 725-782.
- [15] S. Kubowicz, J.-F. Baussard, J.-F. Lutz, A. F. Thünemann, H. Berlepsch, A. Laschewsky, *Angew. Chem. Int. Ed.* **2005**, *44*, 5262-5265.
- [16] T. Gadt, N. S. Jeong, G. Cambridge, M. A. Winnik, I. Manners, *Nature Mater.* **2009**, *8*, 144-150.
- [17] F. Schacher, A. Walther, M. Ruppel, M. Drechsler, A. H. E. Müller, *Macromolecules* **2009**, *42*, 3540-3548.
- [18] D. E. Discher, A. Eisenberg, *Science* **2002**, *297*, 967-973.
- [19] N. Houbenov, N. Antti, I. Hermis, H. Nikos, R. Janne, F. J. F. Charl, I. Olli, *Adv. Funct. Mater.* **2008**, *18*, 2041-2047.
- [20] L. Wang, J. Lin, *Soft Matter* **2011**, *7*, 3383-3391.
- [21] S. Sacanna, W. T. M. Irvine, P. M. Chaikin, D. J. Pine, *Nature* **2010**, *464*, 575.
- [22] E. Duguet, A. Desert, A. Perro, S. Ravaine, *Chem. Soc. Rev.* **2011**, *40*, 941-960.
- [23] S. C. Glotzer, M. J. Solomon, *Nature Mater.* **2007**, *6*, 557-562.
- [24] R. C. Hayward, D. J. Pochan, *Macromolecules* **2010**, *43*, 3577-3584.
- [25] S. C. Glotzer, *Science* **2004**, *306*, 419-420.
- [26] A. van Blaaderen, *Nature* **2006**, *439*, 545-546.
- [27] Q. Chen, J. K. Whitmer, S. Jiang, S. C. Bae, E. Luijten, S. Granick, *Science* **2011**, *331*, 199-202.
- [28] I. Kretzschmar, J. H. Song, *Curr. Opin. Colloid Interface Sci.* **2011**, *16*, 84-95.
- [29] D. J. Pochan, J. Zhu, K. Zhang, K. L. Wooley, C. Miesch, T. Emrick, *Soft Matter* **2011**, *7*, 2500-2506.
- [30] J. Schmelz, M. Karg, T. Hellweg, H. Schmalz, *ACS Nano* **2011**, DOI: 10.1021/nn202638t.
- [31] J.-N. Marsat, M. Heydenreich, E. Kleinpeter, H. v. Berlepsch, C. Böttcher, A. Laschewsky, *Macromolecules* **2011**, *44*, 2092-2105.
- [32] C. Liu, M. A. Hillmyer, T. P. Lodge, *Langmuir* **2008**, *24*, 12001-12009.
- [33] Z. Li, M. A. Hillmyer, T. P. Lodge, *Langmuir* **2006**, *22*, 9409-9417.
- [34] N. Saito, C. Liu, T. P. Lodge, M. A. Hillmyer, *ACS Nano* **2010**, *4*, 1907-1912.
- [35] Z. Li, E. Kesselman, Y. Talmon, M. A. Hillmyer, T. P. Lodge, *Science* **2004**, *306*, 98-101.
- [36] J. Dupont, G. Liu, *Soft Matter* **2010**, *6*, 3654-3661.
- [37] H. Cui, Z. Chen, S. Zhong, K. L. Wooley, D. J. Pochan, *Science* **2007**, *317*, 647-650.
- [38] J.-F. Gohy, E. Khouzakoun, N. Willet, S. K. Varshney, R. Jérôme, *Macromol. Rapid Commun.* **2004**, *25*, 1536-1539.
- [39] H. v. Berlepsch, C. Böttcher, K. Skrabania, A. Laschewsky, *Chem. Commun.* **2009**, *17*, 2290-2292.
- [40] R. Zheng, G. Liu, X. Yan, *J. Am. Chem. Soc.* **2005**, *127*, 15358-15359.
- [41] S. Ritzenthaler, F. Court, L. David, E. Girard-Reydet, L. Leibler, J. P. Pascault, *Macromolecules* **2002**, *35*, 6245-6254.

- [42] S. Ritzenthaler, F. Court, E. Girard-Reydet, L. Leibler, J. P. Pascault, *Macromolecules* **2002**, *36*, 118-126.
- [43] Z. Li, M. A. Hillmyer, T. P. Lodge, *Macromolecules* **2005**, *39*, 765-771.
- [44] X. Yan, G. Liu, J. Hu, C. G. Willson, *Macromolecules* **2006**, *39*, 1906-1912.
- [45] B. Fang, A. Walther, A. Wolf, Y. Xu, J. Yuan, A. H. E. Müller, *Angew. Chem. Int. Ed.* **2009**, *48*, 2877-2880.
- [46] A. Walther, C. Barner-Kowollik, A. H. E. Müller, *Langmuir* **2010**, *26*, 12237-12246.
- [47] C. M. Fernyhough, D. Pantazis, S. Pispas, N. Hadjichristidis, *Eur. Polym. J.* **2004**, *40*, 237-244.
- [48] A. Walther, P.-E. Millard, A. S. Goldmann, T. M. Lovestead, F. Schacher, C. Barner-Kowollik, A. H. E. Müller, *Macromolecules* **2008**, *41*, 8608-8619.
- [49] M. Charlaganov, O. V. Borisov, F. A. M. Leermakers, *Macromolecules* **2008**, *41*, 3668-3677.
- [50] K. Liu, Z. Nie, N. Zhao, W. Li, M. Rubinstein, E. Kumacheva, *Science* **2010**, *329*, 197-200.
- [51] D. Zhao, J. S. Moore, *Org. Biomol. Chem.* **2003**, *1*, 3471-3491.
- [52] F. A. Plamper, M. Ruppel, A. Schmalz, O. Borisov, M. Ballauff, A. H. E. Müller, *Macromolecules* **2007**, *40*, 8361-8366.
- [53] T. M. Hermans, A. C. Broeren Maarten, N. Gomopoulos, S. P. van der, H. P. van Genderen Marcel, A. J. M. Sommerdijk Nico, G. Fytas, E. W. Meijer, *Nature Nanotech.* **2009**, *4*, 721-726.
- [54] C. Auschra, R. Stadler, *Polymer Bulletin* **1993**, *30*, 257-264.
- [55] E. Giebel, R. Stadler, *Macromolecular Chemistry and Physics* **1997**, *198*, 3815-3825.
- [56] A. Walther, X. André, M. Drechsler, V. Abetz, A. H. E. Müller, *J. Am. Chem. Soc.* **2007**, *129*, 6187-6198.
- [57] F. Schacher, J. Yuan, H. G. Schoberth, A. H. E. Müller, *Polymer* **2010**, *51*, 2021.
- [58] H. Ruckdäschel, J. K. W. Sandler, V. Altstädt, C. Rettig, H. Schmalz, V. Abetz, A. H. E. Müller, *Polymer* **2006**, *47*, 2772-2790.

Acknowledgments

This work was supported by the *Deutsche Forschungsgemeinschaft* within SFB 840 (TP A1 and A2). We thank Sandrine Tea, Andreas Hanisch and Joachim Schmelz for providing some polymers.

Author contributions

A.H.G. conceived the project, performed all experiments, was involved in the project planning and in writing the manuscript. F.H.S. synthesized some of the polymers and co-designed the experiments. H.S. synthesized the SBM polymers. O.V.B. and E.B.Z. performed the theoretical calculations. A.W. co-designed the experiments and wrote the manuscript. A.H.E.M. co-designed the experiments and was involved in writing the manuscript. All authors jointly discussed the results and commented on the manuscript.

Additional information

Supplementary Information accompanies this paper at <http://www.nature.com/ncomms>

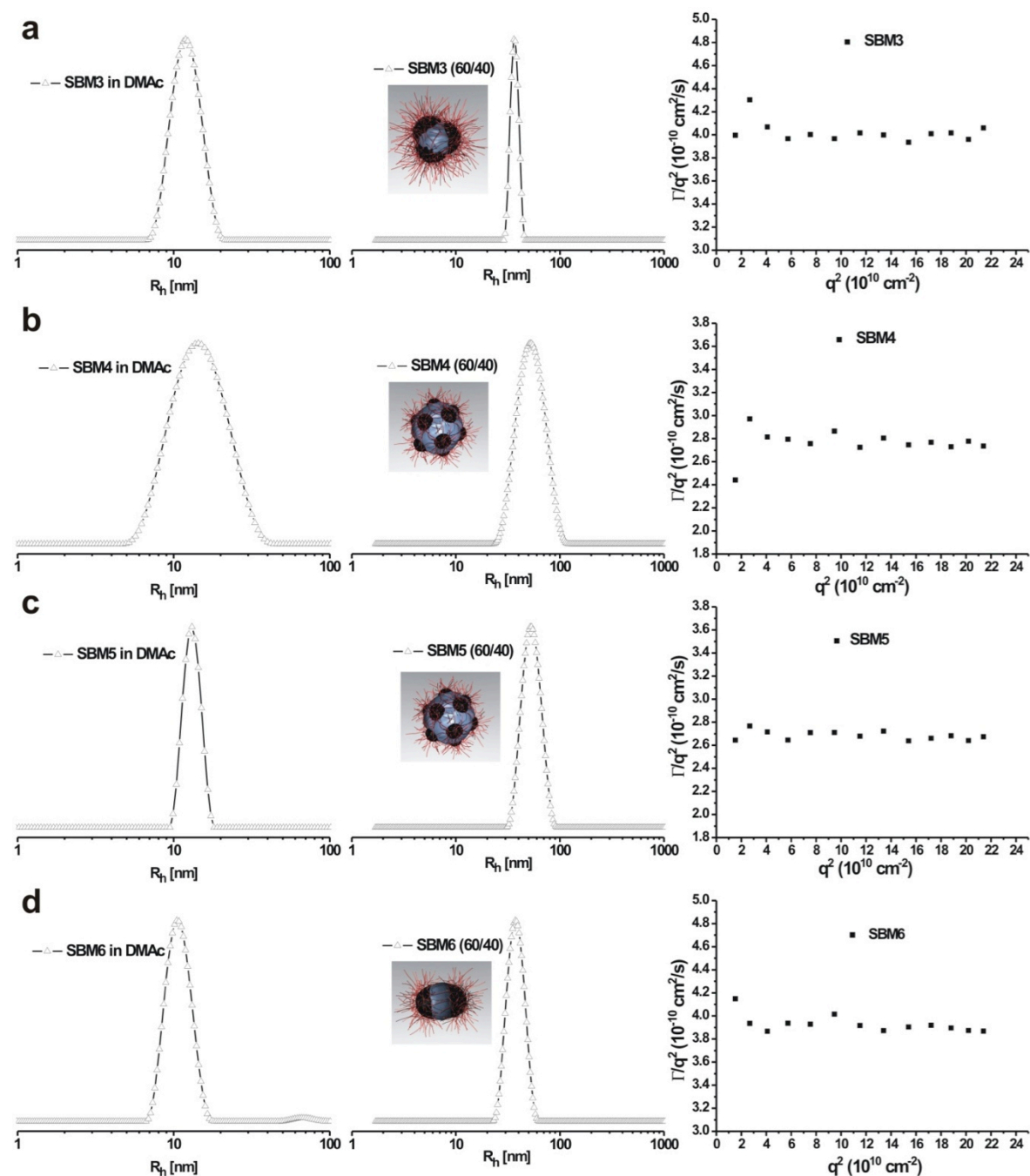
Competing financial interests: The authors declare no competing financial interests.

Supporting Online Material

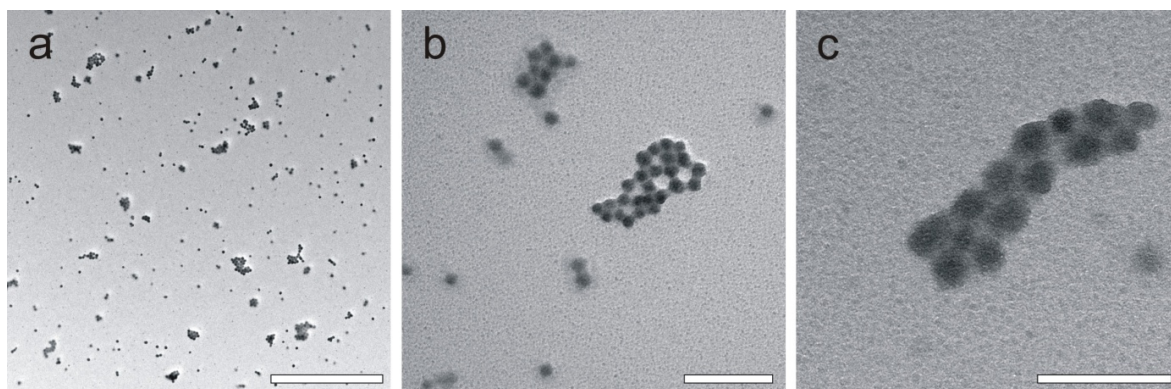
to

Precise Hierarchical Self-Assembly of Multicompartment Micelles

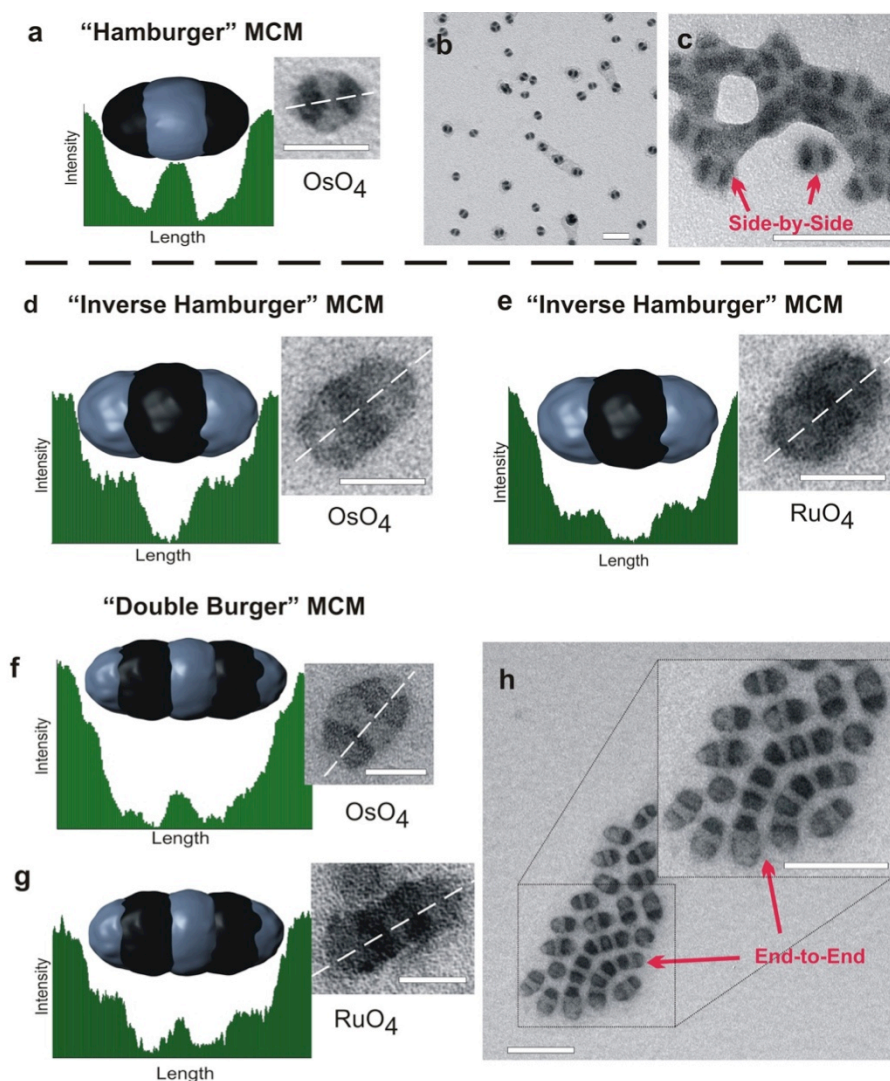
**André H. Gröschel, Felix H. Schacher, Holger Schmalz, Oleg V. Borisov,
Ekaterina B. Zhulina, Andreas Walther*, Axel H. E. Müller***



Supplementary Figure S3–1: Dynamic light scattering CONTIN plots of subunits and corresponding spherical MCMs of polystyrene-*block*-polybutadiene-*block*-poly(methyl methacrylate) triblock terpolymers (SBM3-6). In DMAc, well-defined subunits with hydrodynamic radii in the range of $R_{h,app} = 11 \text{ nm} - 14 \text{ nm}$ can be found (left column). A clear shift in the dimensions is observed after dialysis against acetone/isopropanol (60/40 v/v) with values ranging from $R_{h,app} = 36 \text{ nm} - 54 \text{ nm}$, depending on the morphology of the formed spherical MCMs (middle column). The absence of an angular dependence of the DLS data by plotting the reduced decay rate, Γ/q^2 , as a function of the squared scattering vector, q^2 , and almost constant values for Γ/q^2 in all cases confirm spherical MCMs with very narrow size distribution (right column). Polydispersity and anisotropy typically lead to the observation of a curved plot (see Supplementary Figure S3–4, see also Supplementary Table S3–1 for terpolymer characteristics).

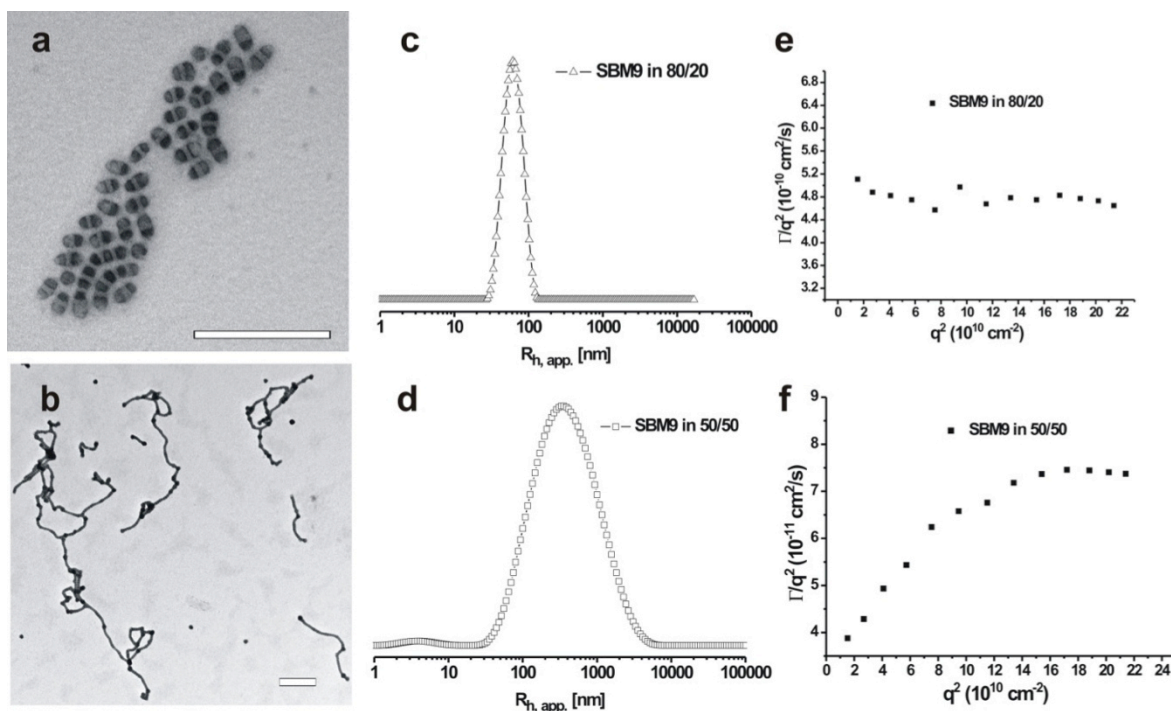


Supplementary Figure S3–2: Influence of core mobility on MCM formation as demonstrated by cross-linking of the subunits. To investigate the importance of a dynamic core, the PB cores of SBM9 micellar subunits were crosslinked in DMAc with the photo-cross-linker 2,4,6-trimethylbenzoyl-diphenylphosphine oxide (Lucirin TPO[®], $\lambda_{\text{max}} = 360\text{nm}$, obtained from BASF SE) by UV irradiation for 1 h. Any corona restructuring (i.e. refinement) during the aggregation of the subunits also requires a drastic rearrangement of chains in the micellar core. **(a-c)** After cross-linking in DMAc and subsequent dialysis into acetone/isopropanol (60/40 v/v), no defined MCMs can be observed (TEM images, OsO₄ stained with increasing magnification; scale bars are 1 μm **(a)**, 200 nm **(b)**, 100 nm **(c)**). For comparison, SBM9 forms well-defined mesoscale colloidal polymers in this solvent mixture without crosslinking (see Figure 3–4e,f and Figure 3–5a-d in the main text). Those can clearly not be found. Instead, core crosslinked micelles and their ill-defined aggregates appear. This clearly demonstrates that the presence of a dynamic core during structural rearrangements and fusion of subunits into final MCMs is necessary. Large-scale corona restructuring is only possible for dynamic cores.

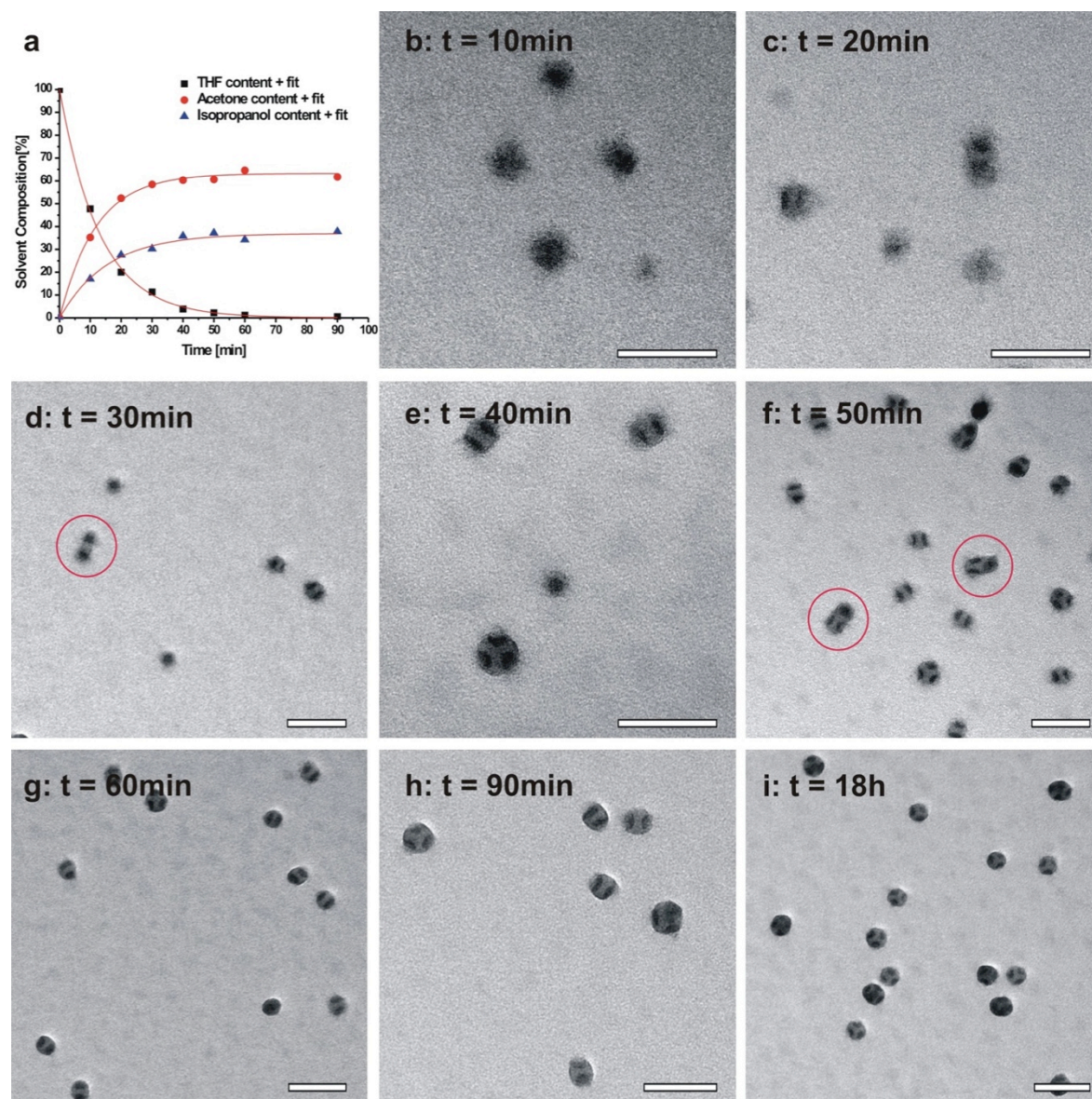


Supplementary Figure S3–3: Structural differences in "hamburger" (BSB), "inverse hamburger" (SBS) and "double burger" (SBS)₂ MCMs as decisive building blocks to understand the polymerization of "double-burger" vs. the aggregation of "hamburger" MCMs. (a) "Hamburger" MCMs possess terminal compartments of PB from which corona chains emanate and are thus incapable of end-to-end growth. Grey-scale analysis clearly shows that "hamburger" MCMs exhibit dark terminal PB compartments after which the intensity (contrast) immediately levels off to the underlying carbon film of the TEM grid (OsO₄ stained; PMMA is not visible due to e-beam degradation; scale bar is 50 nm). (b) Overview of "hamburger" MCMs (scale bar is 100 nm). (c) A contracting corona can only lead to aggregation along the middle compartment of PS, thus favoring side-by-side assembly observed depositing a more concentrated solution on the TEM grid (scale bar is 200 nm). (d–e) Grey-scale analysis of "inverse hamburger" MCMs (scale bar is 50nm) and (f–g) "double-burger" MCMs that clearly show terminal PS compartments after OsO₄ and RuO₄ staining from which no stabilizing corona chains protrude (scale bars are 200 nm and 100 nm in insets). Terminal PS compartments become darker when stained with RuO₄. RuO₄ stains both PS and PB, whereas OsO₄ only stains PB. "Double burgers" form upon dimerization of "inverse hamburger" MCMs. Here, a small step in the grey-scale analysis can be observed before the intensity levels off to the background of the carbon coating, thus confirming the presence of terminal PS compartments. Note also the unusual non-spherical shape of the black polybutadiene compartments. Hence, these combined staining efforts unambiguously demonstrate the structural differences between BSB "hamburger" and SBS "inverse hamburgers" as well as their dimerized (SBS)₂ = SBSBS "double-burger" analogues. (h) Longitudinal end-to-end aggregation of "double-burger" MCMs. See also the extension of the concept of supramicellar polymers to TCD, which provides additional convincing imaging data for the aggregation of "inverse hamburgers" into "double-burgers" and subsequent end-to-end polymerization into colloidal chains (Fig. 3–6d-f in the main article).

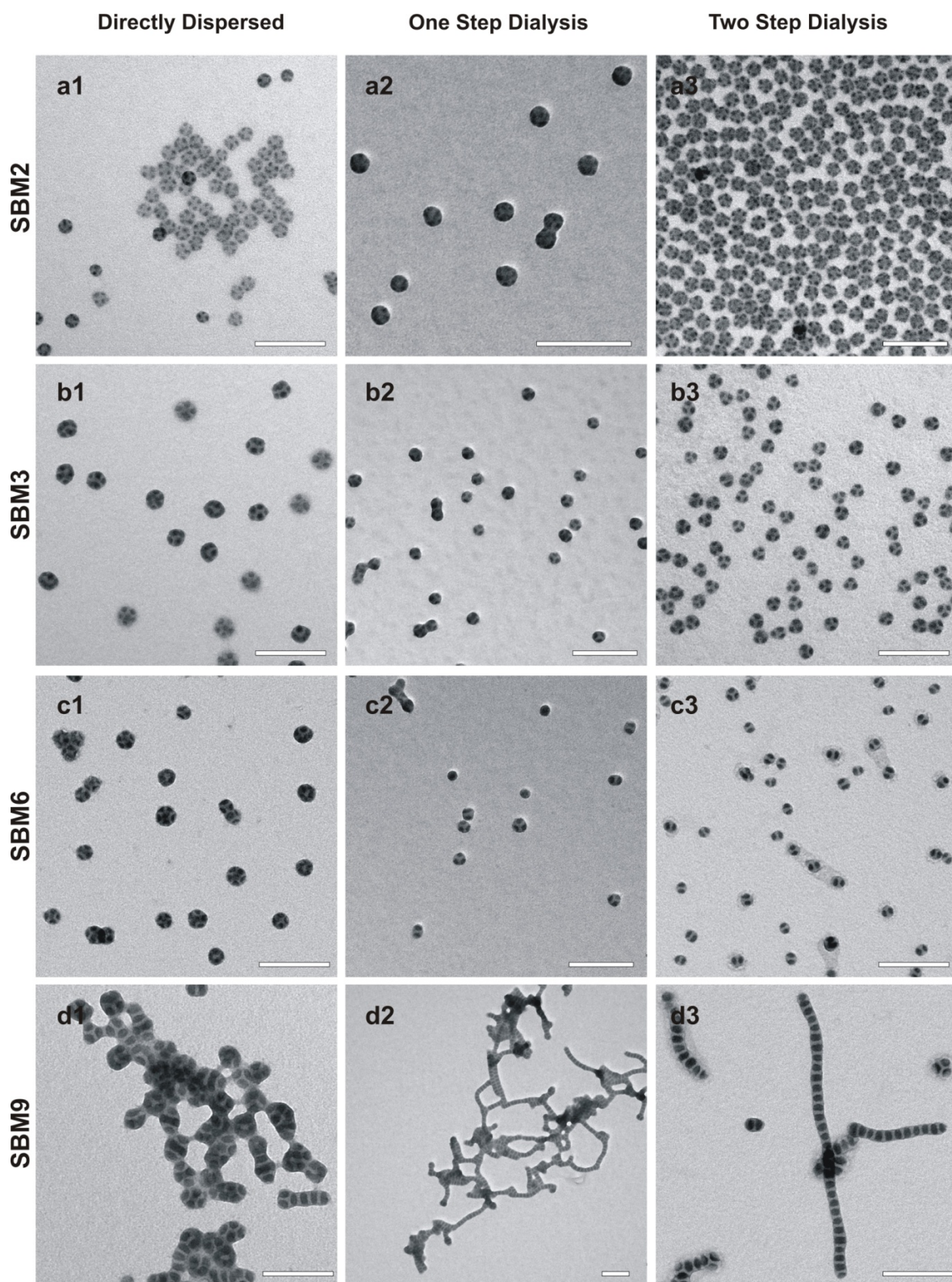
Therein, the pH allows tuning the corona volume and enables the observation of various intermediates via changing the acidity.



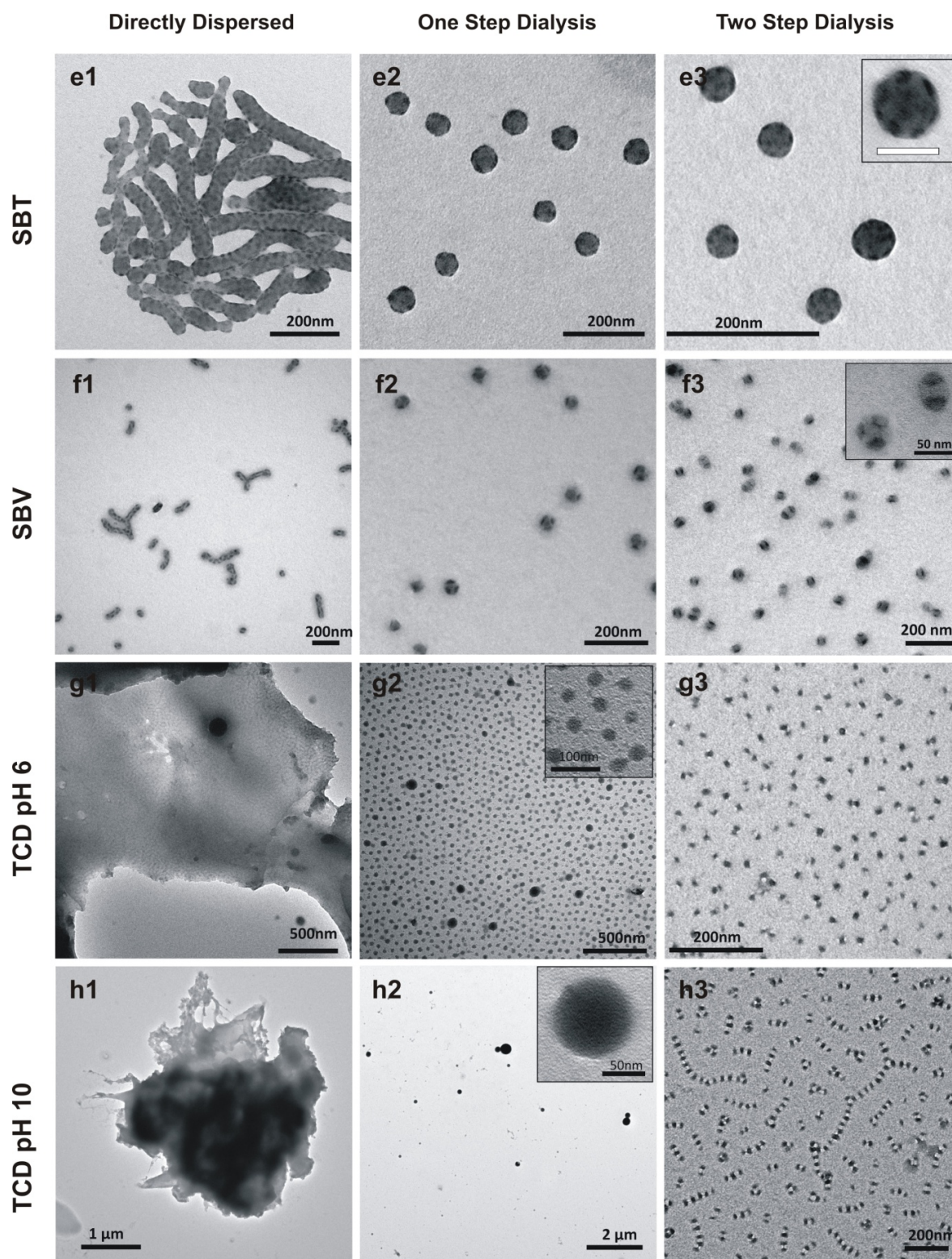
Supplementary Figure S3-4: Supporting DLS for step-growth polymerization of SBM9. (a, c, e) “Double-burger” MCMs are the dominant species according to DLS and TEM in acetone/isopropanol (80/20 v/v). (b, d, f) Colloidal mesoscale polymers formed by the polymerization of “double-burger” MCMs in acetone/isopropanol (50/50 v/v). (a, b) Transition from “double-burger” MCMs in acetone/isopropanol (80/20 v/v) to long segmented chains in acetone/isopropanol (50/50 v/v) observed in TEM (OsO₄ stained; scale bars are 500 nm). (c, d) DLS CONTIN plots at 90° allow following the mesoscale step-growth polymerization of “double-burgers” in-situ in solution and thus, excluding the possibility of colloidal polymers being drying artifacts in TEM. The transition from initial subunits in DMAc to MCMs and their subsequent step-growth polymerization is accompanied by a consecutive increase in hydrodynamic radius. The small $R_{h,app} = 12 \pm 5$ nm of the subunits in DMAc (data not shown) increases about sevenfold to $R_{h,app} = 61 \pm 17$ nm for the state of the “double-burger” MCMs in acetone/isopropanol (80/20 v/v). (e, f) Reduced decay rate, Γ/q^2 , as a function of the squared scattering vector, q^2 , for SBM9 at two different acetone/isopropanol solvent compositions. (e) The angular dependence of the DLS data is very weak, thus confirming near spherical “double-burger” MCMs in acetone/isopropanol (80/20 v/v). (f) Upon a further decrease of the solvent quality, step-growth polymerization into supra-colloidal worms is triggered and leads to higher values for $R_{h,app, q \rightarrow 0} > 1000$ nm. In case of chain-like colloidal assemblies, additional rotational and bending modes contribute to the distribution of relaxation times, resulting in an observation of a dependence of the decay rate, Γ/q^2 , on the squared scattering vector, q^2 . In consequence, the strongly curved plot suggests the presence of long, non-spherical objects in acetone/isopropanol (50/50 v/v).



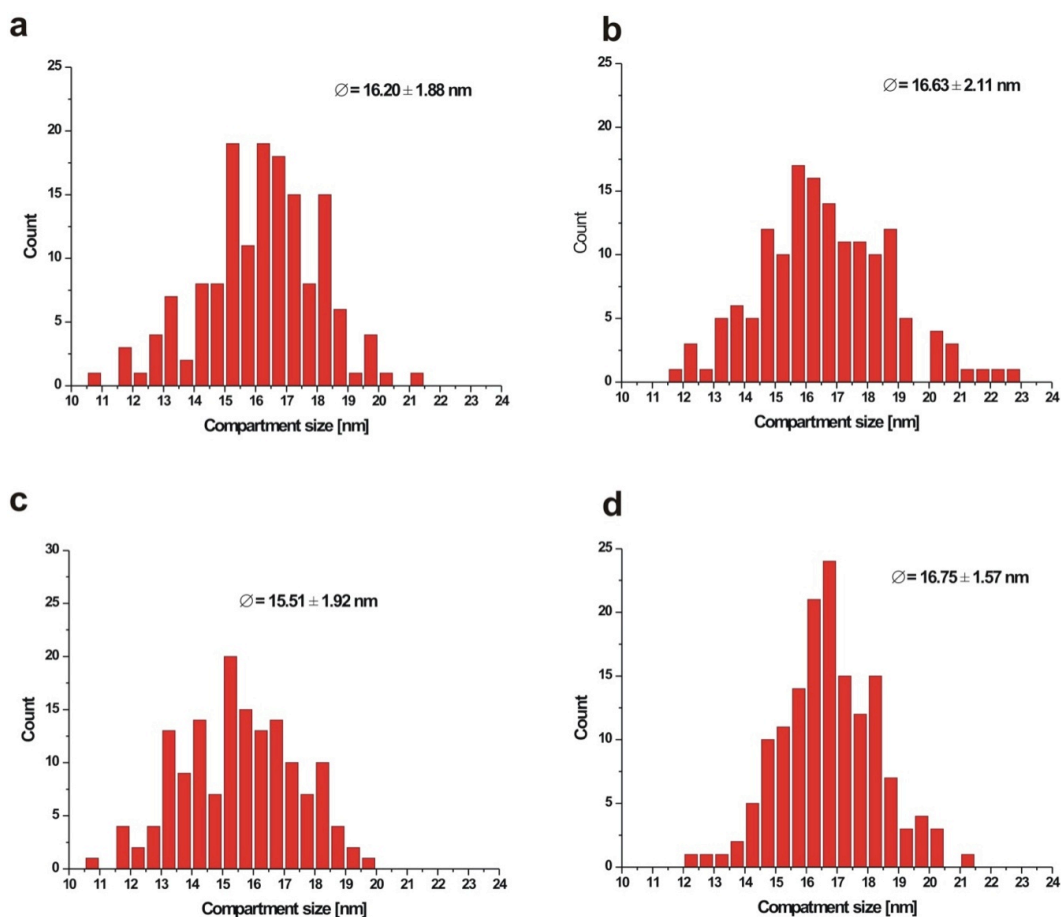
Supplementary Figure S3-5: Kinetic study of SBM3 MCM formation by a one step dialysis from THF into acetone/isopropanol (60/40 v/v). (a) $^1\text{H-NMR}$ study of the time dependent solvent composition. (b-i) TEM micrographs of samples after specific time intervals as indicated within the figure (all samples were OsO_4 stained; scale bar corresponds to 100 nm). The red circles highlight fusion events of subunits during the assembly (see also Supplementary Note 3-1).



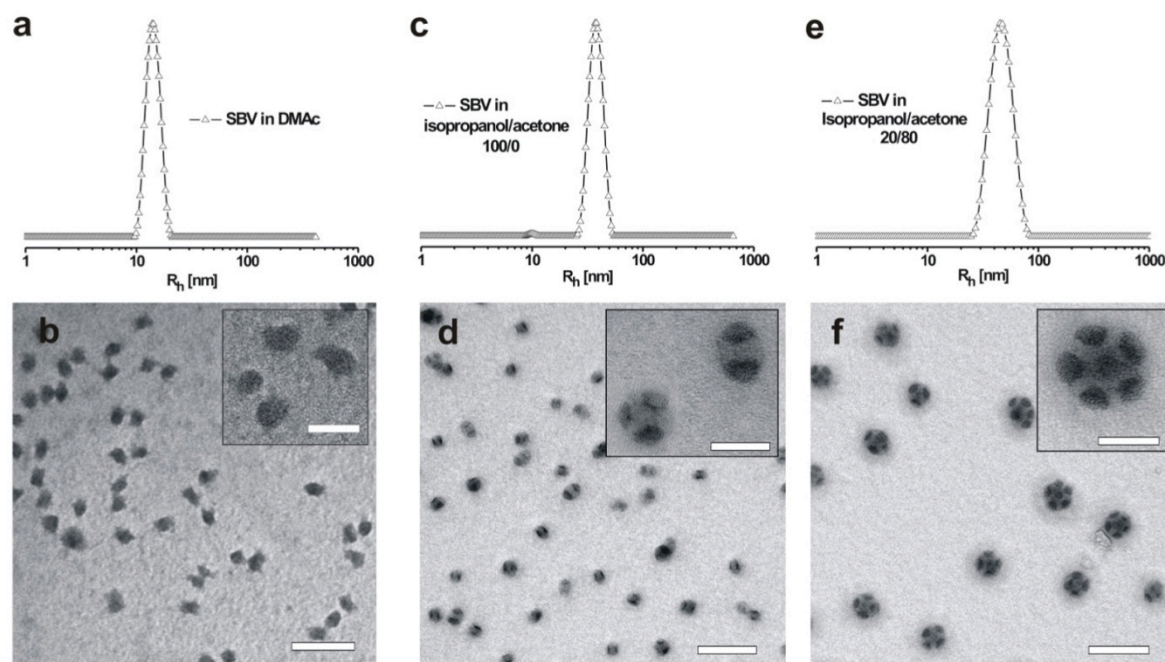
(Supplementary Figure S3–6, continued on the next page)



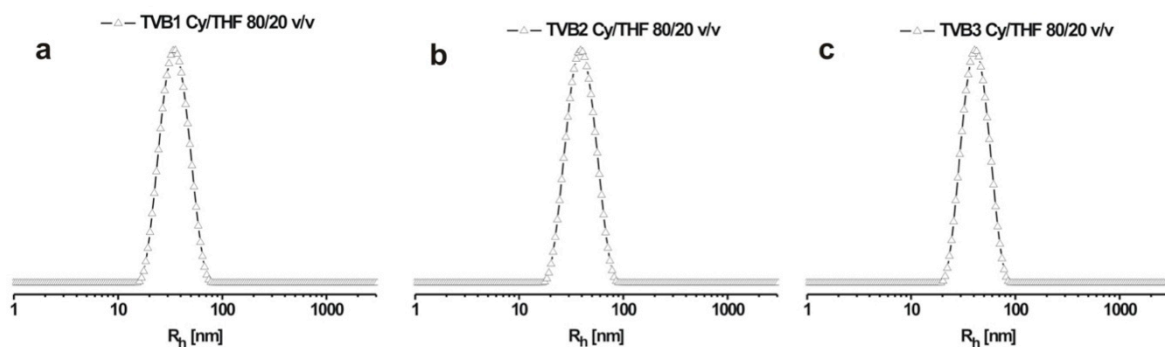
Supplementary Figure S3–6: Terpolymer MCMs directly dispersed, prepared by one step dialysis, and via two step dialysis. (a1–a3) SBM2 "football" MCMs, (b1–b3) SBM3 "clover" MCMs, (c1–c3) SBM6 "hamburger" MCMs and (d1–d3) SBM9 worm-like micelles. (e1–e3) SBT "football" MCMs, (f1–f3) SBV "clover" MCMs, (g1–g3) TCD at pH = 6 oligomers, (h1–h3) TCD at pH = 10 worm-like MCMs (see also Supplementary Note 3–2).



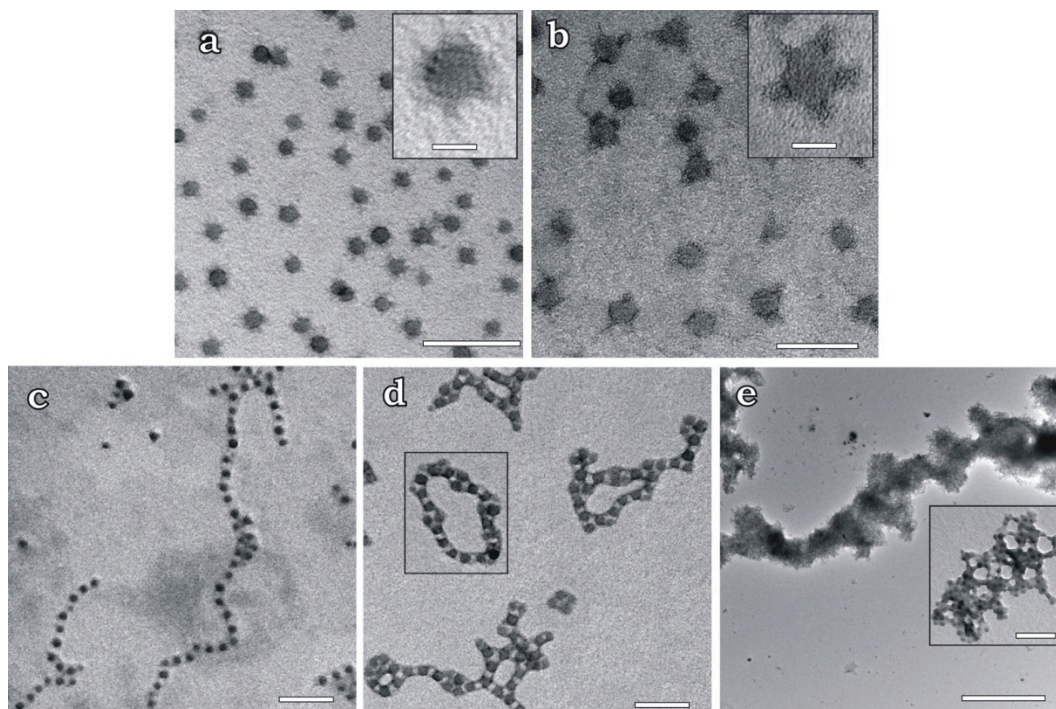
Supplementary Figure S3-7: Statistical evaluation of compartment size distributions of PB patches of SBM3 MCMs during in-situ switching of aggregate morphologies with changing acetone/isopropanol content. (a) Core diameters of 16.2 ± 1.9 nm observed for subunits in acetone/isopropanol 90/10 v/v. (b) Compartment diameters of 16.3 ± 2.1 nm of "hamburger" MCMs observed in 80/20 v/v, (c) 15.5 ± 1.9 nm of "clover" MCMs in 60/40 v/v and (d) 16.8 ± 1.6 nm of "football" MCMs in 50/50 v/v. At least 150 patches were evaluated for each sample. The number average diameters of the PB patches are in the range of 16.1 ± 0.6 nm for all structures, thus nearly constant. Considering the slightly different geometries of the PB domains (spherical in subunits vs. elliptic in MCMs) and the unlike swelling in the various solvent mixtures, the uniformity strongly suggests exchange/assembly of intact subunits. Fusion and fission of PB domains as well as exchange of unimeric polymer molecules would result in larger differences.



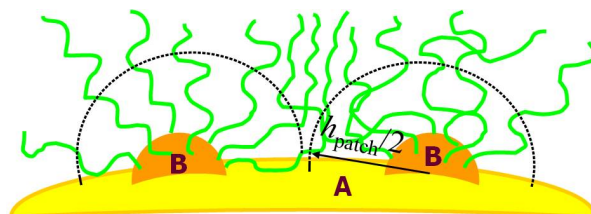
Supplementary Figure S3–8: DLS CONTIN plots of polystyrene-*b*-polybutadiene-*b*-poly(2-vinylpyridine) (SBV) triblock terpolymer measured at an angle of 90° as well as respective TEM images (OsO₄ stained). (a, b) DLS confirms the presence of subunits in DMAc with $R_{h,app} = 16 \pm 2$ nm. (c, d) After dialysis into isopropanol, MCMs with an increased radius of $R_{h,app} = 36 \pm 7$ nm can be found. The slightly asymmetric ratio $V_{PS}/V_{PB} = 1.67$ explains the formation of “hamburger” or “clover” MCMs. Both species are almost equally represented. (e, f) MCMs after dialysis into isopropanol/acetone (20/80 v/v). Addition of acetone leads to corona contraction and to an increased amount of subunits (5-6) per MCM and, in addition, to a larger hydrodynamic radius of $R_{h,app} = 46 \pm 10$ nm. These observations are in good agreement with the results obtained earlier for SBM terpolymers of varying composition.



Supplementary Figure S3–9: CONTIN plots of poly(*tert*-butyl methacrylate)-*b*-poly(2-vinylpyridine)-*b*-polybutadiene (TVB1-3) terpolymer subunits in cyclohexane/THF (80/20 v/v) measured at an angle of 90° . (a) TVB1 with $R_{h,app} = 35 \pm 10$ nm, (b) TVB2 with $R_{h,app} = 39 \pm 8$ nm and (c) TVB3 with $R_{h,app} = 41 \pm 9$ nm. All TVB block terpolymers were synthesized via sequential living anionic polymerization starting with butadiene, followed by the addition of 2-vinylpyridine and *tert*-butyl methacrylate.^[57] We changed the typical acronym sequence from BVT to TVB, as PB acts as the corona in this case. The characteristics of TVB1-3 are summarized in Table S3–1. TVB features a very polar and high T_g middle block, for which MCMs with a PB corona can be formed in non-polar solvents such as hydrocarbons (dodecane). The preceding subunits with P2VP core and *Pt*BMA/PB corona can be created in a solvent mixture cyclohexane/THF (80/20 v/v).



Supplementary Figure S3–10: TEM images of subunits and chain-like polymeric MCMs prepared from TVB terpolymers. All samples were stained with OsO_4 : black P2VP core, grey PB corona patches and PtBMA bright corona patches; scale bars are 200 nm and 25 nm in insets except (e): 5 μm and 200 nm in inset. **(a)** TVB1 subunits with a P2VP core and a patchy corona of PB and PtBMA by direct dispersion in cyclohexane/THF (80/20 v/v). **(b)** TVB1 refined subunits after annealing for 48 h at 50 $^\circ\text{C}$. Interestingly, the corona phase separation of the subunits can be clearly visualized. The micelles exhibit a dark P2VP core and a diffuse grey PB corona before annealing, whereas 3-5 dark PB patches were observed for the annealed sample. This demonstrates enhanced corona phase separation (refinement) by annealing. **(c)** Chain-like MCMs polymers are generated by subsequent dialysis of TVB1 into the final solvent dodecane. The PtBMA patches found for the subunits must significantly rearrange during this process. **(d)** Stronger branched polymeric MCMs obtained for TVB2 and 3D network formation for TVB3 **(e)**. TEM shows worm-like MCMs in all cases despite the much larger asymmetric ratios of $V_{\text{PtBMA}}/V_{\text{P2VP}}$ compared to SBM. This can be explained considering the drastically different polymer/polymer and polymer/solvent interactions. As derived in Eq. 3–3 (main manuscript), the condition $\gamma_{AS} < \gamma_{BS}$ is fulfilled, i.e., the surface tension of P2VP to dodecane is higher than that of PtBMA concluded from the interaction parameters, $\chi_{\text{P2VP,dodecane}} = 0.81 > \chi_{\text{PtBMA,dodecane}} = 0.27$ (calculated from the corresponding solubility parameters using the increment method). In the series of TVB1–3, the increasing PtBMA content leads to more branching points, but the high interfacial tensions prevent spherical growth of subunits and keep the aggregation direction preferably linear. This exemplifies an important design criterion for targeting superstructures.



Supplementary Figure S3–11: Schematic representation of a spherical MCM for the case $V_A \gg V_B$ and scaling analysis for spherical MCMs. Spherical micelles with a patchy multi-compartment core are formed by ABC triblock terpolymers with insoluble A and B blocks if $V_A/V_B \equiv N_A v_A/N_B v_B \gg 1$. The micelle comprises $p \gg 1$ chains and consists of a central core of radius, R_{core} , formed by collapsed A-chains and is decorated by multiple, n , patches formed by collapsed B-chains (see Supplementary Note 3–3).

Supplementary Table S3–1. Terpolymer characteristics and hydrodynamic radii, R_h , of subunits and MCMs.

Code ^a	Polymer ^b	V_A / V_B ^c	$r_c = \frac{N_C}{N_A + N_B}$	R_h , Subunit [nm] ^d	R_h , MCM [nm] ^e
SBM1	S ₃₅₄ B ₁₄₈ M ₃₅₂ ⁸⁰	4.20	0.70	7 ± 4	45 ± 14
SBM2	S ₃₀₆ B ₁₅₁ M ₃₄₀ ⁷⁴	3.57	0.75	10 ± 2	42 ± 11
SBM3	S ₃₃₇ B ₃₃₃ M ₃₆₉ ⁹⁰	1.78	0.54	11 ± 2	36 ± 8
SBM4	S ₆₆₀ B ₆₇₄ M ₃₅₀ ¹⁴⁰	1.72	0.26	14 ± 4	52 ± 14
SBM5	S ₆₁₁ B ₆₃₅ M ₂₉₂ ¹²⁷	1.69	0.23	13 ± 1	54 ± 5
SBM6	S ₂₇₇ B ₃₃₃ M ₄₃₂ ⁹⁰	1.46	0.70	12 ± 4	37 ± 4
SBM7	S ₃₂₅ B ₆₈₁ M ₇₆₄ ¹⁴⁷	0.84	0.76	15 ± 3	33 ± 7
SBM8	S ₃₆₃ B ₇₆₅ M ₃₈₉ ¹¹⁸	0.84	0.35	17 ± 3	>500
SBM9	S ₂₈₃ B ₅₉₆ M ₃₀₄ ⁹²	0.84	0.35	12 ± 5	>1000
SBM10	S ₃₇₄ B ₈₁₉ M ₅₀₉ ¹³⁴	0.80	0.43	14 ± 2	>500
SBM11	S ₁₄₁ B ₃₄₅ M ₁₅₇ ⁴⁹	0.72	0.32	9 ± 3	>>1000
SBM12	S ₂₈₃ B ₇₀₀ M ₃₇₈ ¹⁰⁵	0.71	0.38	12 ± 1	>1000
SBV	S ₃₅₈ B ₃₇₈ V ₅₉₄ ¹²⁰	1.67	0.81	16 ± 2	36 ± 7
SBT1	S ₅₈₀ B ₁₂₄ T ₄₇₂ ¹³⁴	8.23	0.67	14 ± 6	32 ± 4
SBT2	S ₅₂₀ B ₅₃₈ T ₃₄₃ ¹³²	1.70	0.32	12 ± 2	34 ± 6
<i>tSf</i> BT	<i>tS</i> ₄₅₂ / <i>B</i> ₅₁₃ T ₄₆₃ ³⁹²	0.62	0.45	62	>>1000
TVB1	T ₃₈₀ V ₃₀₇ B ₄₄₈ ¹¹⁰	1.77	0.64	35 ± 10	>500
TVB2	T ₆₄₃ V ₂₉₃ B ₄₄₈ ¹⁴⁵	3.00	0.46	39 ± 8	>>1000
TVB3	T ₇₉₀ V ₂₈₆ B ₄₄₈ ¹⁶⁵	3.68	0.40	41 ± 9	>>1000
TCD	T ₂₈₀ C ₁₃₅ D ₂₅₅ ¹¹¹	1.17	0.62	29 ± 7	>1000
<i>Nn</i> BEO	N ₁₇₈ <i>n</i> B ₁₀₅ EO ₁₁₄ ³⁹	1.22	0.40	27	>1000

^a SBM = polystyrene-*block*-polybutadiene-*block*-poly(methyl methacrylate), SBV = polystyrene-*block*-polybutadiene-*block*-poly(2-vinylpyridine), SBT = polystyrene-*block*-polybutadiene-*block*-poly(*tert*-butyl methacrylate), TVB = poly(*tert*-butyl methacrylate)-*block*-poly(2-vinylpyridine)-*block*-polybutadiene, TCD = poly(*tert*-butyl methacrylate)-*block*-poly(2-(*cinnamoyloxy*)ethyl methacrylate)-*block*-poly(2-(*dimethylamino*)ethyl methacrylate), *tSf*BT = Poly(*tert*-butoxy styrene)-*block*-poly(C₆F₁₃C₂H₄S-ethylethylene)-*block*-poly(*tert*-butyl methacrylate) and *Nn*BEO = Poly(N-isopropyl acrylamide)-*block*-poly(*n*-butyl acrylate)-*block*-poly(ethylene oxide).

^b Subscripts denote the degrees of polymerization of the corresponding blocks and superscript is the exact molecular weight in kg/mol determined with ¹H-NMR and GPC (PDI < 1.15).

^c Volume fractions V_A and V_B were calculated via polymer densities.

^d SBM1-12, SBV and SBT subunits measured in DMAc, *tSf*BT in dioxane, TVB1-3 in THF/cyclohexane (80/20 v/v), TCD in isopropanol and *Nn*BEO in water at 25 °C.

^e SBM1-12 measured in acetone/isopropanol (60/40 v/v), SBV in isopropanol, SBT and *tSf*BT in ethanol, TVB1-3 in dodecane, TCD in water pH = 10 and *Nn*BEO in water at 45 °C.

Supplementary Note 3–1**Kinetic Study of MCM Formation by a One Step Dialysis Procedure**

The exact pathway of MCM formation during dialysis from a good solvent for all blocks into a final selective solvent (or mixture) has remained unclear so far - also in the literature. An answer to this question is accompanied by experimental difficulties, i.e., to clearly monitor changes during the dialysis process. Therein, structures continuously evolve with the solvent exchange and crucial intermediates, chain rearrangements and structural transformations can be difficult to identify. Supplementary Figure S3–5 depicts the results for the direct dialysis of SBM3 from the good solvent THF into an acetone/isopropanol mixture (60/40 v/v), where that polymer forms well-defined "clover" MCMs, SB₃, using our controlled two-step process (i.e. DMAc against acetone/isopropanol).

An analysis of the solvent composition via ¹H-NMR revealed a surprisingly fast solvent exchange, practically completed after only 90 min (Supplementary Fig. S3–5a). TEM samples prepared at specific times during this process are shown in Supplementary Figure S5b–i. During this process, distinct species can be identified where again small subunits can be found that assemble into the final MCMs, albeit with a lower quality of the final structure as discussed in detail in Supplementary Figure S3–6.

After 10 min (Supplementary S3–5b, 47 % THF remaining), micelle formation with a strongly THF-swollen PB core and a mixed PS/PMMA corona (subunits) is indicated by the observed aggregates without clearly distinguishable phases. After 20 min (Supplementary Fig. S3–5c, 20 % THF), isolated hamburger MCMs can be identified among a majority of single subunits. The imaged objects are already better defined, originating from an increased selectivity of the solvent mixture and decreased swelling of the blocks PS and PB. At longer dialysis times, subunits appear more developed with PB-core and PS/PMMA-corona. Supplementary Figure S3–5e shows a frequent example of coexisting subunits, "hamburger" MCMs and newly formed "clover" MCMs. We take this as evidence for the assembly of intermediately formed subunits into the final MCM structures. After 50 min subunits are rarely found anymore (Supplementary Fig. S3–5f). "Hamburger" MCMs are the predominant species after 60 min (see Supplementary Fig. S3–5g), whereas more "clovers" can be found after 90 min due to the increasingly diminishing solvent quality (Supplementary Fig. S3–5h). The latter are the dominant fraction after a complete equilibration time of 18 h (Supplementary Fig. S3–5i).

Importantly, compared to the two-step process involving a defined, intermediate dissolution step in DMAc, the fine structure of the MCMs herein is less defined. The fraction of "clover" MCMs is much smaller, demonstrating larger heterogeneity that is unsuitable for further self-assembly to the next higher level. We further comment on a comparison of the various preparation routes in Supplementary Note 3–2.

In summary, direct dialysis from a good solvent for all blocks into the final solvent mixture also illustrates the observation of subunits and their further assembly into final MCMs. The important difference to our two-step, controlled process is that *a defined equilibration in the state of subunits does not occur as the structures continue evolving with the rapid solvent exchange*. The collapse of the middle block as first component in this dialysis procedure is governed by the various interactions (solubility parameters etc.) but is also favored on account of the connection of the PB block on both sides with other polymers, leading to an enhanced tendency for phase-separation vs. e.g. being connected on one side only. On account of the less defined and fast process, the final structures are less defined as compared to our developed two-step, directed self-assembly methodology using a defined intermediate step.

Supplementary Note 3–2

Fine-Structure and Homogeneity of the MCMs Depending on the Preparation Method: Direct Dispersion vs. One Step Dialysis vs. Two Step Dialysis

A well-defined monodisperse structuring of the MCMs is of great importance for colloidal superstructure formation. This section addresses the advantages of our two-step approach vs. previous methods. Therefore, we compare the resulting MCM fine structures of different polymers as a function of the preparation pathway: (a) direct dispersion in the final solvent, (b) dialysis from a good solvent for all blocks into the final solvent (termed: one step dialysis, see Supplementary Fig. S3–5), and (c) step-wise reduction of conformational degrees of freedom using an intermediate step in a selective solvent for both A and C (termed: two step dialysis).

As depicted in Supplementary Figure S3–6 "football" MCMs, as formed by SBM2 (Supplementary Fig. S3–6a1-a3), represent the most reported MCM example in the literature^{[14],[15],[17],[47],[49]} and probably are the thermodynamically most robust morphology. This structure can be obtained for a suitable polymer (SBM2) for all three preparation techniques investigated. The large fraction of the soluble PMMA block helps maintaining dynamics and facilitates their preparation even via direct dissolution.

Significant differences occur in case of SBM3, SBM6, and SBM9, which form uncommon and more labile morphologies. Direct dispersion of the terpolymers only leads to "football" MCMs or even more ill-defined structures (Supplementary Fig. S3–6b1, c1 and d1). The polydispersity of the fine structure and overall size-distribution increases as compared to SBM2. The rather exceptional "clover", "hamburger", or chain-like MCM morphologies are exclusively obtained via the two step dialysis as shown in Supplementary Fig. S3–6b2-d2 and S3–6 b3-d3.

Further evaluation of the inner fine structure reveals important differences between direct dialysis from a common solvent to the two step procedure using DMAc as intermediate solvent. Although qualitatively the same structures can be obtained, the fine structure is

significantly more developed in case of the more controlled two-step approach using the DMAc step. Therein, "clover" and "hamburger" MCMs are almost exclusively observed (Supplementary Fig. S3-6b3 and c3).

Additionally, the one step dialysis procedure results in a higher polydispersity of the aggregates (Supplementary Fig. S3-6b2 and c2). For instance, SBM6 exhibits almost equal fractions of subunits, "hamburger" and "clover" MCMs, thus not corresponding to a well-defined structure formation. Similarly, the worm-like MCMs (Supplementary Fig. S3-6d2) show much higher branching, originating from structural inhomogeneities of the underlying MCM monomers. Hence, quantitative differences between the procedures are evident. These effects are not specific to a particular triblock terpolymer system. Similar behavior can be observed for SBT and SBV polymers (Supplementary Fig. S3-6e1-e3, f1-f3), for which highest homogeneity can again only be obtained for the two step dialysis.

Consequently, homogeneous populations of complex MCM morphologies may not be accessible using direct dispersion or fast one step dialysis, but essentially require a control of the pathway as exercised via our controlled/dedicated process. As expected, this problem is more pronounced for larger fractions of solvophobic blocks, meaning reduced overall dynamics for structural rearrangements.

To further underscore the importance of maintaining dynamics, Supplementary Figure S3-6g1-3 and h1-3 show results obtained for the self-assembly of TCD at pH = 6 and pH = 10 in water. In contrast to the other previously shown polymers in organic solvents, water serves as final solvent for TCD. Due to its unique solvent properties, H₂O suppresses dynamics of solvophobic (here hydrophobic) segments for amphiphilic triblock terpolymers more efficiently than organic solvents in case of solvophobic blocks. Therefore, the kinetic obstacles are more pronounced and even larger differences between the three methods can be observed. Direct dispersion completely fails at both pH values in the observed time frame of one week. The solution stays macroscopically phase-separated and only some micron-scale ill-defined aggregates can be found. Secondly, the one step dialysis (as would commonly be applied to such polymers) leads to nanosized aggregates, but a distinct nanostructuration cannot be observed. The polydispersity of these aggregates increases significantly when using alkaline water (pH = 10) as compared to water with pH = 6. This can again be understood considering the better solubility of the D corona chains upon slight protonation at pH = 6 and the therewith higher dynamics.

In strongest contrast to these methods, the two step dialysis furnishes well-defined nanostructured aggregates whose degree of aggregation into linear chains can be changed by the pH value. Such an unprecedented control is not achievable without distinct and precise control of the self-assembly pathway.

In conclusion, these important results convincingly demonstrate the advantage of an intermediate reduction of the degrees of conformational freedom in a first solvent (e.g.

DMAC), leading to well-defined key subunits and, in turn, drastically improved control over structure and polydispersity of the final MCMs. Moreover, fine structures are accessible with the two step process that remain inaccessible using previous state-of-the-art dispersion methods.

Supplementary Note 3–3

Scaling analysis for spherical MCMs

The corona of the MCM is formed by solvated C chains protruding from the B-domains (patches) into the solution. Even though scaling arguments^{[49],[59-61]} presented below are strictly applicable in the range of $n \gg 1$, the results can be extrapolated to the $n \geq 1$ case. The free energy (in $k_B T$ units) of the MCM can be presented as

$$F = F_{\text{corona}} + F_{\text{core}} + F_{\text{interface}} \quad (\text{S3-1})$$

, where F_{corona} describes repulsive interactions (under good or theta-solvent conditions) between solvated and crowded coronal chains C, whereas F_{core} accounts for the conformational entropy losses in the collapsed core-forming segments: This term is negligibly small as long as the aggregates retain a spherical shape. The last term, $F_{\text{interface}}$, accounts for the excess free energy of the interfaces between collapsed B and A segments and solvent, as well as that of the interfaces between B and A domains:

$$F_{\text{interface}} = F_{AS} + F_{BS} + F_{AB} = \gamma_{AS} S_{AS} + \gamma_{BS} S_{BS} + \gamma_{AB} S_{AB} \quad (\text{S3-2})$$

, where S_{AS}, S_{BS}, S_{AB} are the interfacial areas and the surface tension at the A/S (S=solvent), B/S, and B/A interfaces in $k_B T$ units equals $\gamma_{AS}, \gamma_{BS}, \gamma_{AB}$, respectively.

The equilibrium aggregation number, p , and the number of B-domains (patches) in one MCM can be found from minimization of the free energy of the MCM calculated per chain.

The interfacial free energy (Eq. S2) can be presented in the form

$$F_{\text{interface}} = \gamma_{BS} S_{BS} + (\gamma_{AB} - \gamma_{AS}) S_{AB} + \gamma_{AS} (S_{AS} + S_{AB}) = \Delta F_{\text{interface}} + 4\pi R_{\text{core}}^2 \gamma_{AS} \quad (\text{S3-3})$$

, where

$$4\pi R_{\text{core}}^2 = S_{AS} + S_{AB} = (4\pi)^{1/3} 3^{2/3} (pV_A)^{2/3} \quad (\text{S3-4})$$

is the total interfacial area of the spherical A-core and

$$\Delta F_{\text{interface}} = \gamma_{BS} (S_{BS} - S_{AB} \cos \theta) \quad (\text{S3-5})$$

, where $\cos \theta = (\gamma_{AS} - \gamma_{AB}) / \gamma_{BS}$ is the cosine of the contact angle formed by B-domains with the A/S interface. Here we neglect the curvature of the central A-core as compared to that of the B-patches. This is justified provided $\gamma_{AB} \gg \gamma_{AS} - \gamma_{BS}$ $\gamma_{AB} \gg \gamma_{AS} - \gamma_{BS}$ corresponding to de-wetting of B-domains from the A/S interface. The latter condition implies instability of a laterally uniform core-shell-corona structure with respect to formation of patchy MCMs.

Assuming that each B-domain (one patch) comprises $m = p/n$ chains, Eq. S3–5 can be presented as

$$\Delta F_{\text{interface}} = (2\pi)^{1/3} 3^{2/3} \gamma_{BS} (mV_B)^{2/3} n \left(1 + \frac{\cos\theta}{2}\right)^{1/3} (1 - \cos\theta)^{2/3} \quad (\text{S3-6})$$

The total interfacial free energy can be presented as

$$F_{\text{interface}} = (2\pi)^{1/3} 3^{3/2} \tilde{\gamma}_{BS} (mV_B)^{2/3} n + 6^{2/3} \pi^{1/3} \gamma_{AS} (pV_A)^{2/3} \quad (\text{S3-7})$$

with the notation

$$\tilde{\gamma}_{BS} = \gamma_{BS} (1 - \cos\theta)^{2/3} \left(1 + \frac{\cos\theta}{2}\right)^{1/3} \quad (\text{S3-8})$$

Finally, the interfacial free energy per chain can be presented as

$$\frac{F_{\text{interface}}}{p} \approx \tilde{\gamma}_{BS} m^{-1/3} V_B^{2/3} + \gamma_{AS} p^{-1/3} V_A^{2/3} \quad (\text{S3-9})$$

, where we have omitted numerical factors of the order of unity in the last expression.

The corona contribution to the free energy should be specified separately for starlike and for the crew-cut micelles.

For starlike micelles, $d_{\text{corona}} \equiv R_{\text{micelle}} - R_{\text{core}} \gg R_{\text{core}}$, the free energy of the corona (per chain) can be presented as

$$\frac{F_{\text{corona}}}{p} = m^{1/2} \ln \frac{R_{\text{core}}}{R_B n^{1/2}} + p^{1/2} \ln \frac{R_{\text{micelle}}}{R_{\text{core}} (1 + n^{-1/2})} \quad (\text{S3-10})$$

The first term in Eq. S3–10 describes steric interactions between segments of the C-chains, which are confined between the B-patches within the core region of width $h_{\text{patch}} \sim R_{\text{core}} n^{-1/2}$. Here, we also introduced the characteristic size of a B-patch $R_B \approx (mV_B)^{1/3} \sim R_{\text{core}} n^{-1/2}$. The second term in Eq. S3–10 accounts for steric interactions in the peripheral regions of the corona, i.e., at distances from the core surface exceeding h_{patch} . Remarkably, Eq. S3–10 applies both under good and theta-solvent conditions for the corona chains. The outermost radius of the corona, R_{corona} , is given by

$$R_{\text{corona}} \equiv \begin{cases} 1 N_C^{3/5} \tau_C^{1/5} p^{1/5}, & \text{for good solvent} \\ 1 N_C^{1/2} p^{1/4}, & \text{for near-}\Theta \text{ solvent} \end{cases} \quad (\text{S3-11})$$

Minimization of the free energy of the micelle given by Eqs. S3–1, S3–9, S3–10 with respect to m and p enables us to derive the total aggregation number and the number of patches in the equilibrium spherical starlike MCMs.

The total aggregation number

$$p \equiv (N_A v_A)^{4/5} \gamma_{AS}^{6/5} \ln^{-6/5} (R_{\text{micelle}} / R_{\text{core}}) \quad (\text{S3-12})$$

in spherical starlike MCMs is controlled by the balance of the interfacial energy of the core and the contribution to the free energy of the coronal regions at a distance from the core exceeding the distance between the centers of adjacent patches, h_{patch}

Here, the core radius $R_{core} \equiv (pN_A v_A)^{1/3} \equiv (N_A v_A)^{3/5} \gamma_{AS}^{2/5}$ and the micellar radius are

$$R_{micelle} \equiv \begin{cases} 1N_C^{3/5} \tau_C^{1/5} (N_A v_A)^{4/25} \gamma_{AS}^{6/25}, & \text{for good solvent} \\ 1N_C^{1/2} (N_A v_A)^{1/5} \gamma_{AS}^{3/10}, & \text{for near-}\Theta \text{ solvent} \end{cases} \quad (\text{S3-13})$$

The number of patches (B-domains) is given by

$$n \equiv (N_A v_A / N_B v_B)^{4/5} (\gamma_{AS} / \tilde{\gamma}_{BS})^{6/5} \ln^{-6/5} (R_{micelles} / R_{core}) \quad (\text{S3-14})$$

The number of patches is controlled primarily by the ratio $N_A v_A / N_B v_B$ of volumes of the core-forming blocks and weakly (logarithmically) decreases as a function of length and solvent quality for the corona-forming block C. As stated above, MCMs with multiple B-patches decorating a central A-core are formed by asymmetric terpolymers with $N_A v_A / N_B v_B \gg 1$.

For the crew-cut micelle, $h_{patch} \ll d_{corona} \ll R_{core}$, the first term in Eq. S3-10, corresponding to the contribution from the inter-patch regions, remains the same, whereas in the periphery of the corona the curvature effects are negligible and the distal regions of the corona can be assimilated to a planar polymer brush with the average area C-chain $s \approx R_{core}^2 / p$. Remarkably, at $n \gg 1$ the majority of the monomer units of the C-blocks are located in the distal (quasi-planar) region of the corona. The free energy per chain in a planar brush scales as

$$\frac{F_{brush}}{p} \equiv \begin{cases} N_C \tau_C^{1/3} (s/l^2)^{-5/6}, & \text{for good solvent} \\ N_C (s/l^2)^{-1}, & \text{for near-}\Theta \text{ solvent} \end{cases} \quad (\text{S3-15})$$

and the coronal free energy (per chain) for the crew-cut MCM can be presented as

$$\frac{F_{corona}}{p} \equiv m^{1/2} \ln \frac{R_{core}}{R_B n^{1/2}} + \begin{cases} N_C \tau_C^{1/3} p^{5/18} N_A^{-5/9}, & \text{for good solvent} \\ N_C p^{1/3} N_A^{-2/3}, & \text{for near-}\Theta \text{ solvent} \end{cases} \quad (\text{S3-16})$$

Minimization of the free energy of the micelle given by Eqs. S3-1, S3-9, S3-16 with respect to m and p enables us to find the total aggregation number and the number of patches in the crew-cut MCM. The result is given by

$$p \equiv \begin{cases} (\gamma_{AS} l^2 / N_C \tau_C^{1/3})^{18/11} (N_A v_A)^2 l^{-6}, & \text{for good solvent} \\ (\gamma_{AS} l^2 / N_C)^{3/2} (N_A v_A)^2 l^{-6}, & \text{for near-}\Theta \text{ solvent} \end{cases} \quad (\text{S3-17})$$

$$n \equiv (N_A v_A)^2 (N_B v_B)^{4/5} \tilde{\gamma}_{BS}^{6/5} \begin{cases} (\gamma_{AS} / l^{5/3} N_C \tau_C^{1/3})^{18/11}, & \text{for good solvent} \\ (\gamma_{AS} / l^{-2} N_C)^{3/2}, & \text{for near } \Theta\text{-solvent} \end{cases} \quad (\text{S3-18})$$

Similarly to the case of starlike micelles, the number of patches increases with $V_A / V_B \equiv v_A N_A / v_B N_B$ and decreases with the solvent strength, τ_C , and the length, N_C , of the coronal block. Eqs. S3-17, S3-18 apply as long as $h_{patch} \leq d_{corona}$, i.e., the area of the A-core between the patches is protected by the corona. This is the case provided that

$$\begin{cases} N_C \tau_C^{1/3} \geq (N_B v_B)^{11/15} \gamma_{BS}^{11/10} \gamma_{AS}^{-5/6} l^{-5/3}, & \text{for good solvent} \\ N_C \geq (N_B v_B)^{4/5} \gamma_{BS}^{6/5} \gamma_{AS}^{-1} l^{-2}, & \text{for near-}\Theta \text{ solvent} \end{cases} \quad (\text{S3-19})$$

If condition of Eq. S3–19 is violated, the crew-cut MCMs are expected to be unstable and further aggregation or superstructure formation occurs.

Core morphology

We first consider starlike micelles formed by terpolymers with nearly symmetrical core-forming blocks, $N_A v_A / N_B v_B \approx 1$, (for $N_A v_A / N_B v_B \ll 1$ the collapse of the A-domains does not lead to any significant change in the aggregation number as compared to the “precursor” micelle with a mixed A/C corona; further, this does not lead to aggregation of the precursor micelles. According to Eq. S3–14 the number of B-domains is of the order of unity, though the scaling approach does not enable us to specify the exact number of patches, e.g., to distinguish between $n = 2$ (“double burger”) and $n = 1$ (“inverse hamburger”) cases. Since in the starlike micelle, $d_{\text{corona}} = R_{\text{micelles}} - R_{\text{core}} \gg R_{\text{core}}$, the dominant contribution to the free energy of the corona does not depend on the details of the structure of the compartmentalized core, here we compare the overall interfacial free energies of BAB and ABA structures⁶². For simplicity, we assume that $\gamma_{AS}, \gamma_{BS} \gg \gamma_{AB}$ and, as a result, the compartmentalized core has an overall spherical shape with either one (central) B domain and two A domains or with one central A domain and two B domains.

Then the interfacial free energy can be presented as

$$F_{\text{interface}}^{(ABA)} = \gamma_{AS} S_{AS} + \gamma_{BS} S_{BS} + \gamma_{AB} S_{AB} = 4\pi R_{\text{core}}^2 [\gamma_{BS} + (\gamma_{AB} + \gamma_{AS} - \gamma_{BS})x - \frac{1}{2}\gamma_{AB}x^2] \quad (\text{S3-20})$$

, where $R_{\text{core}} = [3p(V_A + V_B)/4\pi]^{1/3}$ is the core radius and x is the root of the equation

$$x^2 - \frac{1}{3}x^3 = \frac{2}{3} \cdot \frac{V_A}{V_A + V_B} \quad (\text{S3-21})$$

and similarly for the BAB shape of the core. For nearly symmetrical composition, $|(V_A/V_B) - 1| = 1$ the sign of the difference in the free energies, $F_{\text{interface}}^{(ABA)} - F_{\text{interface}}^{(BAB)}$, only depends on the ratio of volumes of insoluble blocks, V_A/V_B and on the combination of interfacial tensions, $(\gamma_{AS} - \gamma_{BS})/\gamma_{AB}$. Specifically, the ABA shape of the core corresponds to lower interfacial free energy than the BAB shape if

$$V_A/V_B \leq [1 + \text{const} \cdot (\gamma_{AS} - \gamma_{BS})/\gamma_{AB}]^{-1} \quad (\text{S3-22})$$

, where the numerical constant is of the order of unity.

Supplementary References:

- [59] Halperin, A. & Alexander, S. Polymeric micelles: Their relaxation kinetics. *Macromolecules* **1989**, 22, 2403-2412.
- [60] Birshstein, T. M. & Zhulina, E. B. Scaling theory of supermolecular structures in block copolymer-solvent systems: 1. Model of micellar structures. *Polymer* **1989**, 30, 170-177.
- [61] Zhulina, E. B. & Borisov, O. V. Scaling theory of 3-miktoarm ABC copolymer micelles in selective solvent. *Macromolecules* **2008**, 41, 5934-5944.

[62] Cates, M. E. & Candau, S. J. Statics and dynamics of worm-like surfactant micelles *J. Phys.: Condens. Matter* **1990**, 2, 6869.

Chapter 4

Guided Hierarchical Co-Assembly of Soft Patchy Nanoparticles

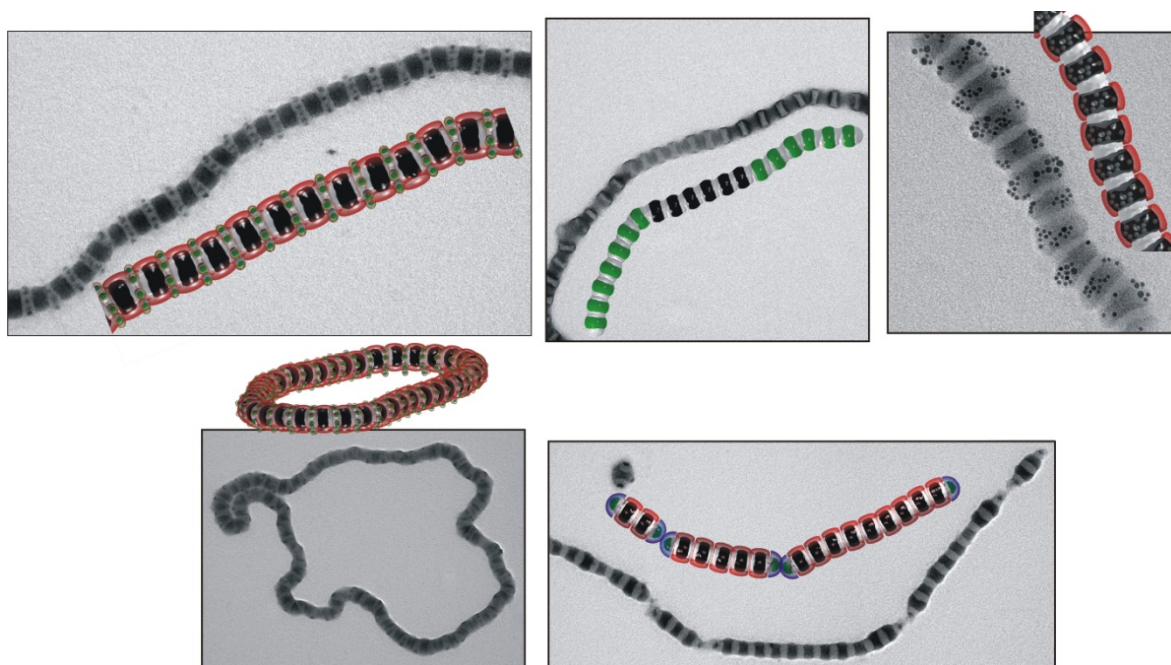
André H. Gröschel^{*}, Andreas Walther¹, Tina I. Löbbling, Felix H. Schacher², Holger Schmalz,
Axel H. E. Müller^{*}

Makromolekulare Chemie II, Universität Bayreuth, D-95440 Bayreuth, Germany

andre.groeschel@uni-bayreuth.de, axel.mueller@uni-bayreuth.de

¹ DWI at RWTH Aachen University – Institute for Interactive Materials Research, 52056 Aachen, Germany

² Institut für Organische Chemie und Makromolekulare Chemie and Jena Center for Soft Matter, Friedrich Schiller Universität Jena, D-07743 Jena, Germany



Published in *Nature* **2013**, DOI:10.1038/nature12610

Abstract

The concept of hierarchical bottom-up structuring commonly encountered in natural materials provides inspiration for the design of complex artificial materials with advanced functionalities^{1,2}. Natural processes have achieved the orchestration of multicomponent systems across many length scales with very high precision^{3,4}, but man-made self-assemblies still face obstacles in realizing well-defined hierarchical structures^{5–11}. In particle-based self-assembly, the challenge is to program symmetries and periodicities of superstructures by providing monodisperse building blocks with suitable shape anisotropy or anisotropic interaction patterns (‘patches’). Irregularities in particle architecture are intolerable because they generate defects that amplify throughout the hierarchical levels. For patchy microscopic hard colloids, this challenge has been approached by using top-down methods (such as metal shading or microcontact printing), enabling molecule-like directionality during aggregation^{12–16}. However, both top-down procedures and particulate systems based on molecular assembly struggle to fabricate patchy particles controllably in the desired size regime (10–100 nm). Here we introduce the co-assembly of dynamic patchy nanoparticles—that is, soft patchy nanoparticles that are intrinsically self-assembled and monodisperse—as a modular approach for producing well-ordered binary and ternary supracolloidal hierarchical assemblies. We bridge up to three hierarchical levels by guiding triblock terpolymers (length scale ~ 10 nm) to form soft patchy nanoparticles (20–50 nm) of different symmetries that, in combination, co-assemble into substructured, compartmentalized materials (>10 μm) with predictable and tunable nanoscale periodicities. We establish how molecular control over polymer composition programs the building block symmetries and regulates particle positioning, offering a route to well-ordered mixed mesostructures of high complexity.

Until now, research on block copolymer self-assembly in solution focused mostly on multicompartment micelles or the crystallization-driven formation of compartmentalized structures bridging one hierarchical level^{17–21}. Only few works consider these nanoscale superstructures to be soft colloidal building blocks (CBBs) that can be self-assembled on higher levels^{22–26}. The central challenge remains to devise patchy CBBs with sufficient precision qualifying as supraparticular tectons; that is, monodisperse in size and modified with defined repulsive and attractive surface patches providing directional interaction patterns²⁷. Equally problematic while operating on the nanoscale are controlled particle positioning (interparticle forces may exceed particle size), the general lack of target-oriented and predictable self-assembly protocols, and convincing visualization of nano-separated multiphase organic materials. Responsive multiblock co-polymers (1–10 nm) are potential candidates for the versatile bottom-up design (geometry, patchiness and dimension) of surface-compartmentalized nanoparticles (20–50 nm) with molecular precision (Fig. 1a). The particles themselves then transmit the information needed for defined higher-level co-assembly into mesoscale structures (0.1–10 μm) of controllable size and periodicity. In contrast with ‘static’, patchy microparticles (hard spheres)^{14,27,28}, these polymer-based nanoparticles are intrinsically self-assembled, soft and ‘dynamic’, offering the attractive feature of assembly or disassembly on demand—from molecules to CBBs and beyond. We recently approached the design of such a system by fabricating near-monodisperse, monovalent and divalent CBBs (‘monomeric units’) by the self-assembly of ABC triblock terpolymers in selective solvents²³. Shaping building-block geometries and understanding both interparticle interactions and aggregation behaviour led us to the hypothesis that the concept of soft nanoparticle self-assembly could be extended to the rational design of supracolloidal co-assemblies by suitable combinations of building blocks. Mixed particle co-assemblies across multiple hierarchical levels open a new level of complexity and have yet to be addressed.

The general design criteria—developed in an experimental approach—for the guided co-assembly of multiple CBBs with distinct valences are few and simple, and should be widely applicable to polymer-decorated particles (Fig. 1a). One essential requirement is tuneable and defined attractive interaction patterns responsive to solvent quality or other external stimuli to favour near-monodisperse structures on different length scales. Modern polymer synthesis provides us with well-defined block co-polymers with a wide range of properties and responses²⁹. We developed a set of ABC triblock terpolymers into which we pre-encoded all parameters necessary for sequential, hierarchical assembly (Fig. 1b). The volume ratio of the core-forming segments, V_A/V_B , determines CBB valence, and the total molecular mass, M_n , controls particle size²³. Thus, $V_A/V_B > 1$ yields monovalent **AB**^C Janus CBBs with one attractive A patch and one repulsive C patch on opposing sides of the B core (we use bold lettering to distinguish CBBs from the underlying polymer chains with regular lettering); $V_A/V_B < 1$ leads to divalent **AB**^C**A** with two attractive A patches on op-

posing sides of the B core and a repulsive C patch emanating radially from the B core. The superscript indicates that the C corona is attached to the B core (Extended Data Table 1).

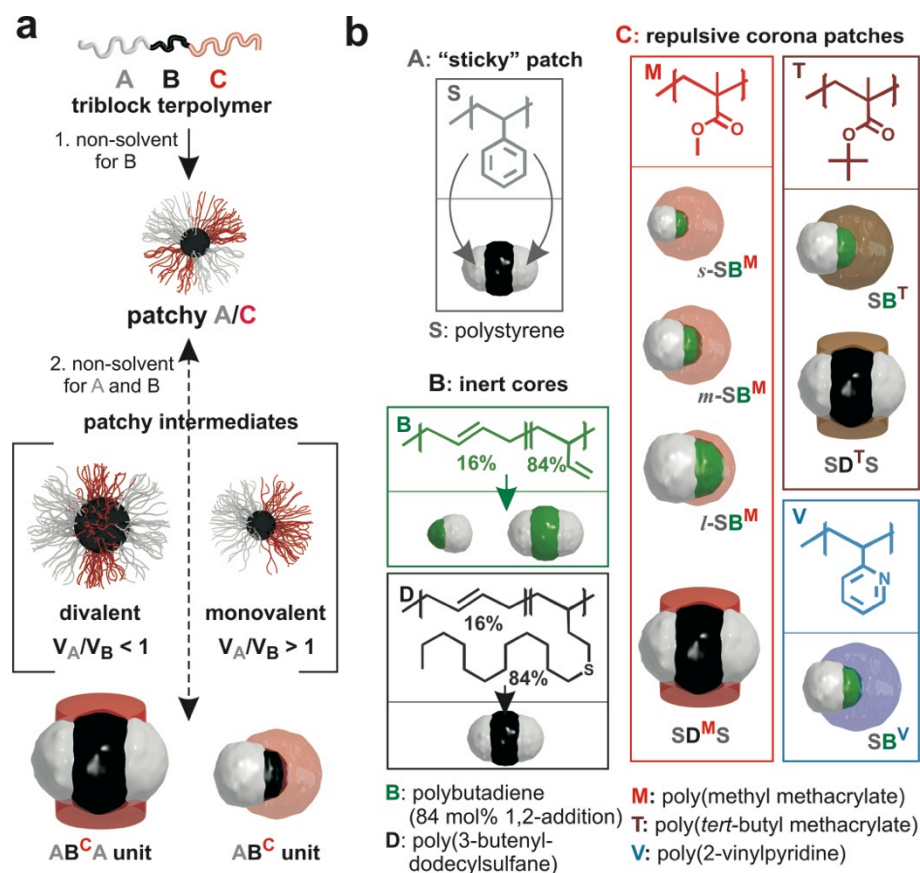


Figure 4-1: Preparation and configuration of soft colloidal building blocks (CBBs). **a**, Dispersion of ABC triblock terpolymers in a non-solvent for B yields B-core particles with A/C corona patches. During transfer into a non-solvent for A and B, these develop into monovalent AB^C and divalent $AB^C A$ units with sticky A patches. **b**, CBBs feature associative ('sticky') polystyrene (S) patches reversibly turned solvophobic on demand, chemically different (inert) polybutadiene (B) or poly(3-butenyldodecylsulfane) (D) core material physically holding the CBBs together, and poly(methyl methacrylate) (M), poly(*tert*-butyl methacrylate) (T) or poly(2-vinylpyridine) (V) as solubilizing/repulsive corona varying in polarity and functionality. Adapted from *Nature*, 2013, doi:10.1038/nature12610. Reprinted with permission from Nature Publishing Group.

From here onwards we replace ABC by the actual block sequences: SBM (polystyrene-*b*-polybutadiene-*b*-poly(methyl methacrylate)) and SDM (polystyrene-*b*-poly(3-butenyldodecylsulfane)-*b*-poly(methyl methacrylate)). Monovalent SB^M and divalent $SD^M S$ CBBs were prepared separately by self-assembly in *N,N*-dimethylacetamide (DMAc), a non-solvent for the middle blocks, B and D (Extended Data Fig. 1). At this stage the S and M patches are still soluble and not yet completely phase-separated, and they reorganize dynamically into fully developed CBBs when the S block is turned insoluble. We trigger this step by changing the solvent to acetone/propan-2-ol (60:40 v/v), leading to particles with essentially different patch arrangements. SB^M and $SD^M S$ thereby act as monomeric units for self-assembly and co-assembly on the next level (transmission electron microscopy (TEM) images in Fig. 2, Level 1, and Extended Data Fig. 2). If kept

separate, both units undergo self-assembly into spherical and linear superstructures to minimize energetically unfavourable S patch/non-solvent interfaces (Fig. 2, Level 2 Self-Assembly), once the solvent quality has been reduced to a critical threshold for the S patches. Small corona volumes, V_M , provide less steric repulsion and promote higher aggregation numbers of SB^M units per spherical $(\text{SB}^M)_x$ cluster or, similarly, higher degrees of polymerization of SD^MS units per $[\text{SD}^M\text{S}]_m$ supracolloidal polymer chain (dimer \rightarrow oligomer \rightarrow polymer)²³.

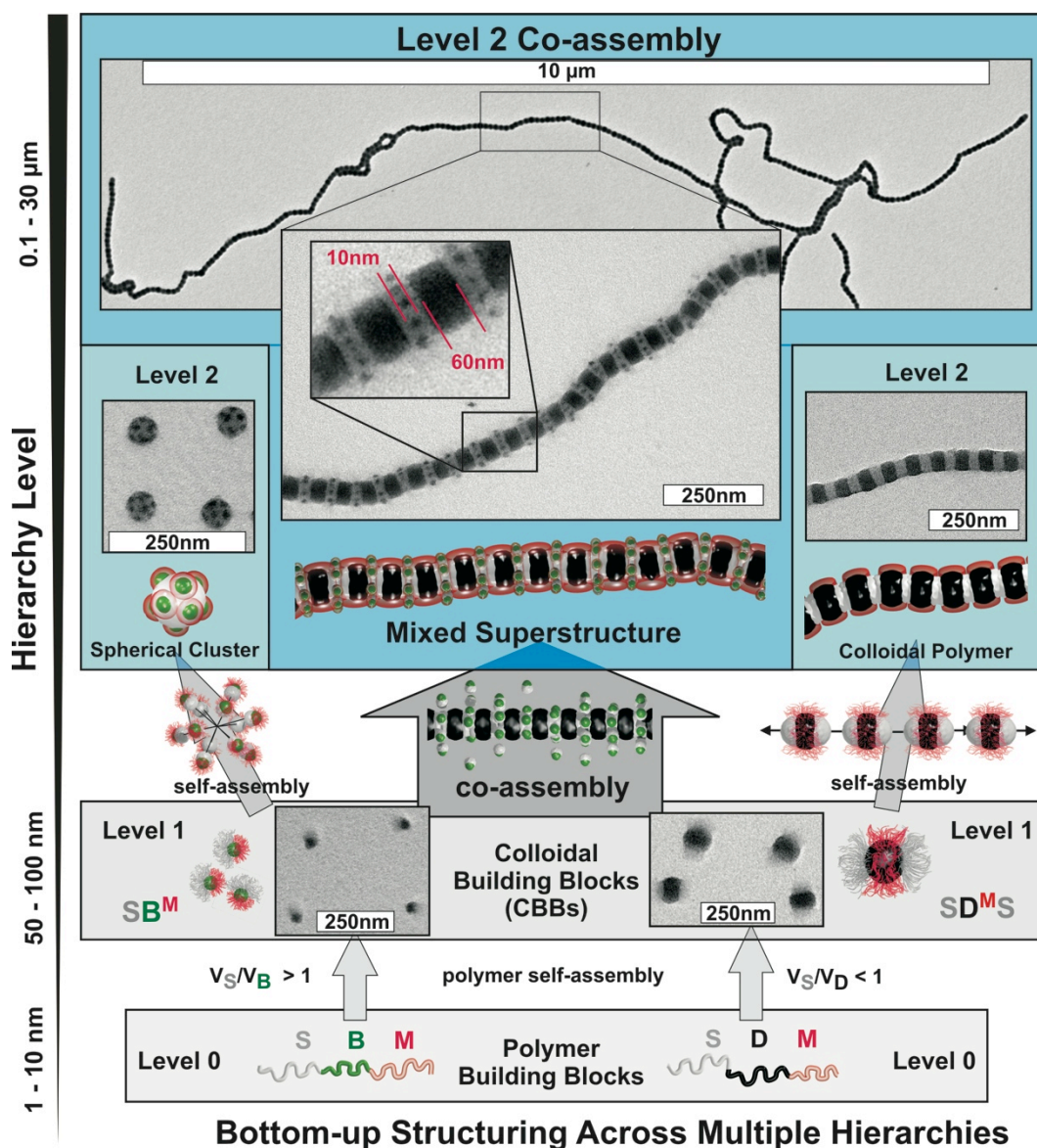


Figure 4-2: Guided co-assembly across multiple hierarchical levels. Level 0: triblock terpolymers are the basic building blocks. Level 1: self-assembly of monovalent $s\text{-SB}^M$ and divalent SD^MS CBBs in dependence on the volume ratios of the core-forming blocks (intermediate CBBs were captured by crosslinking; Extended Data Fig. 2). Level 2 Self-Assembly: $s\text{-SB}^M$ forms spherical $(s\text{-SB}^M)_x$ clusters and SD^MS linear $[\text{SD}^M\text{S}]_m$ supracolloidal polymer chains. Level 2 Co-Assembly: $s\text{-SB}^M$ and SD^MS with mutually attracting S patches co-assemble into mixed superstructures stabilized by the common M corona. (OsO₄ staining: –S– segments grey, B cores dark grey, –D– segments black, and M not visible as a result of degradation by the electron beam). Adapted from *Nature*, 2013, doi:10.1038/nature12610. Reprinted with permission from Nature Publishing Group.

Co-assembly requires at least two CBBs differing in size (10–100 nm), patchiness or chemistry (core/corona). To demonstrate our concept, we mixed two CBBs differing in all three aspects in DMAc in defined particle ratios ($s\text{-SB}^M:\text{SD}^M\text{S} = 8:1$; Fig. 1 and Extended Data Fig. 2)^{9,10} (the prefix ‘s’ in $s\text{-SB}^M$ stands for small). We chose small monovalent $s\text{-SB}^M$ (hydrodynamic radius, $R_h \approx 10$ nm) in combination with much larger divalent SD^MS ($R_h \approx 50$ nm). In DMAc, the core-forming segments (B and D) are immiscible; the two CBB species therefore do not exchange terpolymer chains and so evolve independently. As observed for individual species, changes in solvent quality for the S patch destabilize the SD^MS units and induce aggregation into supracolloidal polymer chains with an $[\text{SD}^M\text{S}]_m$ sequence. On a similar timescale, the $s\text{-SB}^M$ units start to aggregate, yet instead of spherical clusters (self-assemblies), they selectively attach to the newly formed free surface of –S– segments within $[\text{SD}^M\text{S}]_m$, thereby decreasing the –S–/non-solvent interface (Fig. 2, Level 2 Co-Assembly). In the presence of both particles we observe exclusively co-assembly under these conditions. This is surprising, because aggregation of both CBBs is driven solely by a weak non-directional force (solvophobicity) and each CBB is able to form stable populations of spherical and linear superstructures by themselves. Yet the development of $[\text{SD}^M\text{S}]_m$ supracolloidal polymer chains favours the attachment of $s\text{-SB}^M$ units to the –S– segments. Therefore, we associate this phenomenon with a certain level of cooperativity. We chose $s\text{-SB}^M$ units with a particle diameter ($d_{\text{CBB}} \approx 19$ nm) matching the width of the –S– segments of SD^MS ($w \approx 24$ nm) (Extended Data Fig. 2) and indeed found a defined number of seven to nine $s\text{-SB}^M$ units radially covering the –S– segments, which perfectly reflects the original mixing ratio. On exceeding the loading capacity of the –S– segments (for example $s\text{-SB}^M:\text{SD}^M\text{S} = 35:1$), single $s\text{-SB}^M$ CBBs or raspberry-like $(s\text{-SB}^M)_x$ self-assemblies locate in the vicinity of the fully decorated co-assemblies (Extended Data Fig. 3).

Besides suitable particle ratios, the timescales of aggregation during solvent exchange have to correlate to facilitate proper co-assembly. Because the corona volume of the $s\text{-SB}^M$ units affects the critical solvent composition needed for aggregation, we used terpolymers with different lengths of the M block (y stands for s (small), m (medium) or l (large) in Extended Data Table 1 and Extended Data Figs 4 and 5). Divalent SD^MS CBBs self-assemble under solvent conditions in which most $s\text{-SB}^{M(y)}$ prevail as ‘monomeric’ units. Stability against aggregation is best for $s\text{-SB}^{M(l)}$ with the largest M corona. Whereas $s\text{-SB}^{M(m)}$ leads to simultaneous co-assembly, $s\text{-SB}^{M(l)}$ shows a slight delay. However, in both cases about eight units decorate the –S– segments, pointing to a robust process with sufficient dynamics for rearrangements. However, particles with too short a corona, for example $s\text{-SB}^{M(s)}$, are unstable before SD^MS polymerization, and lateral decoration is absent. Instead, fully developed spherical $(s\text{-SB}^{M(s)})_x$ clusters are incorporated into the linear $[\text{SD}^M\text{S}]_m$ superstructure during the step-growth polymerization of SD^MS (Extended Data Fig. 4).

The overall particle size, $x\text{-SB}^M$, of the CBBs (x stands for s (small), m (medium) or l (large)) markedly affects the number of particles attached to each $-S-$ segment of the $[\text{SD}^M\text{S}]_m$ supracolloidal polymer chains (Fig. 3 and Extended Data Fig. 6). The particle diameter of $s\text{-SB}^M$ units, $d_{\text{CBB}} \approx 19$ nm, allows the incorporation of eight particles on average, also slightly enlarging the width of the $-S-$ segments from $w \approx 24$ nm to $w \approx 30$ nm (Figs 2 and 3a). Larger CBBs such as $m\text{-SB}^M$ ($d_{\text{CBB}} \approx 35$ nm) require more space; only one particle is therefore able to attach to each $-S-$ segment (Fig. 3b). As a result of their size and the accompanied volume displacement inside the $-S-$ segments, $m\text{-SB}^M$ units induce strong kinks altering the flexibility and linearity of the co-assembly, which could potentially influence the rheological characteristics and colloidal chain packing. $l\text{-SB}^M$ units substantially exceeding the width of the $-S-$ segments ($d_{\text{CBB}} \approx 47$ nm) are too large for lateral decoration and specifically locate on terminal positions (Fig. 3c). The relative sizes of the monovalent units and the $-S-$ segment of the divalent units govern the location and loading capacity, whereas the size of the stabilizing M patch determines the timescales and extent of co-assembly.

Selective end-capping provides an attractive handle to control the length of the $[\text{SD}^M\text{S}]_m$ supracolloidal polymer chains. Adding $l\text{-SB}^M$ ‘stoppers’ in specific ratios also allows end-functionalization with chemically different CBBs. Without any end-capper, the SD^MS units grow into extended structures in the region of 30 μm long (more than 600 repeating units; Extended Data Fig. 7), reaching scales visible by optical microscopy (Extended Data Fig. 6). Figure 3d–f summarizes the dependence of the length distribution of the co-assemblies on the mixing ratio $\text{SD}^M\text{S}:l\text{-SB}^M$ (Extended Data Fig. 7). The decrease in mean length is evident when comparing the TEM images in Fig. 3d, e, which show mixing ratios of 100:2 and 10:2. Stoichiometric control as known from step-growth polymerizations is corroborated by the linear dependence of the average degree of polymerization on the mixing ratio (Fig. 3f). The deviation from the theoretical values (dashed line) is caused by residual ‘defects’ in the CBBs, because we find a small proportion (less than 1%) of trivalent S_3D^M CBBs that induce branching. Matching patch sizes of CBBs and low corona volumes of the SB^M units are decisive in efficient end-capping: the first effectively prevents the addition of SD^MS monomeric units and the latter causes the SB^M units to interfere directly with SD^MS polymerization. Both factors can be programmed molecularly into the SB^M units by variation of the total molecular mass (particle size) and the fraction of M (onset of aggregation).

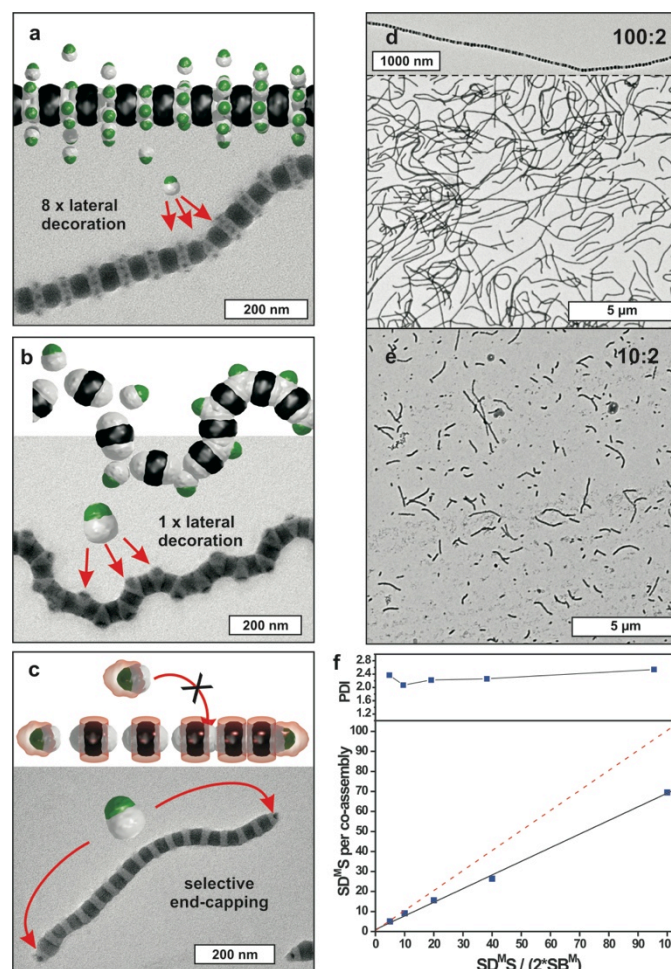


Figure 4-3: Size-selective attachment and control of supracolloidal polymer chain length. **a**, The $-S-$ segments accommodate seven to nine $s-SB^M$ units. **b**, Larger $m-SB^M$ units fit only once and induce strong kinks. **c**, $l-SB^M$ units are too large for lateral decoration and instead act as selective end-cappers. **d**, **e**, Length control of supracolloidal polymer chains by the mixing of 100 (**d**) and 10 (**e**) $SD^M S$ units per 2 $l-SB^M$ end-cappers (Extended Data Fig. 7). Inset shows $[SD^M S]_m$ nanostructure. **f**, Polydispersity indices (PDI; top) and linear dependence of $SD^M S$ repeating units on the mixing ratio (bottom). Adapted from *Nature*, **2013**, doi:10.1038/nature12610. Reprinted with permission from Nature Publishing Group.

Controlled mixing of different CBBs permits the rational design and precise implementation of functionalities within the core and/or corona of the co-assemblies (Fig. 4). We prepare hybrid materials by selectively encapsulating 10 nm maghemite nanoparticles within the $-D-$ segments of $SD^M S$ CBBs on hierarchy level 1 (Fig. 4a). Selective and reversible loading yields a unique advantage compared with top-down approaches that require the synthesis of tailored colloids. The preloaded CBBs then polymerize further to linear chains with alternating D-loaded/S-empty compartments. Nanoparticles with tailored affinities for other phases may allow the preparation of bar-coded distributions, and magnetically responsive co-assemblies may serve as advanced viscosity modifiers or may act as deterministic carrier systems. We also generated co-assemblies comprising five different environments (three core/two corona compartments; Fig. 4b) by mixing $SD^M S$ with SB^T ($T = \text{poly}(t\text{-butyl methacrylate})$), which leads to the already established $[SD^M S]_m$ core sequence, yet now with a segmented M/T corona. In principle, such structures allow us to

control the positioning of nanoparticles along the co-assemblies or to implement predefined responsive folding sites. At this point we emphasize enhanced superstructure stability, because the pristine $[\text{SD}^{\text{M}}\text{S}]_m$ immediately precipitates in ethanol (non-solvent for M) and the $\text{SB}^{\text{T}}/[\text{SD}^{\text{M}}\text{S}]_m$ co-assemblies remain stable (Extended Data Fig. 8).

We extended this approach and designed multiblock co-assemblies by combining two divalent units, $\text{SD}^{\text{M}}\text{S}$ and $\text{SB}^{\text{M}}\text{S}$ (Fig. 4c). Here, several short segments of $[\text{SD}^{\text{M}}\text{S}]_m$ or $[\text{SB}^{\text{M}}\text{S}]_n$ sequences are coupled into multiblock co-assemblies. We suggest that the homogeneity and sequence distribution depend on how synchronized self-assembly and co-assembly occur and that deeper kinetic studies will eventually enable control over the sequence length. In an analogy with polymer architectures, we fabricated telechelic oligomers with terminal functional groups by end-capping $[\text{SD}^{\text{M}}\text{S}]_{10}$ oligomers with SB^{V} ($\text{V} = \text{poly}(2\text{-vinylpyridine})$); Fig. 4d). The number-average length of the telechelics scales with the mixing ratio $\text{SD}^{\text{M}}\text{S}:\text{SB}^{\text{V}}$. The V corona is clearly visible as grey end-cap by TEM (Fig. 4d, central inset). Protonation of the V corona with HCl causes solvophobic attraction and triggers aggregation of the V-termini into extended subdivided superstructures. We emphasize that this process is fully reversible and that it corresponds to a step-growth polymerization on two levels: first for the individual $\text{SD}^{\text{M}}\text{S}$ units, and then chain extension of the telomerized ‘macromonomers’. Combining selective end-capping and lateral decoration yields ternary structures. The addition of SB^{M} units to the $\text{SB}^{\text{V}}\text{-}[\text{SD}^{\text{M}}\text{S}]_{10}\text{-SB}^{\text{V}}$ telechelic oligomers does indeed lead to the decoration of the –S– segments and a final composition of $\text{SB}^{\text{M}}:\text{SD}^{\text{M}}\text{S}:\text{SB}^{\text{V}} = 10:10:2$.

Finally, we bridge three hierarchical levels by co-assembly of SB^{M} and $\text{SD}^{\text{T}}\text{S}$ building blocks into end-capped colloidal molecules with the composition $(\text{SB}^{\text{M}})_N\text{-}[\text{SD}^{\text{T}}\text{S}]_1\text{-}(\text{SB}^{\text{M}})_N$ (where the number of end-caps $N = 1\text{--}5$). The CBB mixing ratio determines the number of end-cappers; for example, $\text{SB}^{\text{M}}:\text{SD}^{\text{T}}\text{S} = 2:1$ gives $(\text{SB}^{\text{M}})_1\text{-}[\text{SD}^{\text{T}}\text{S}]_1\text{-}(\text{SB}^{\text{M}})_1$. These co-assemblies self-assemble spontaneously into triangles and further into two-dimensional networks when cast onto substrates, a necessary two-dimensional confinement tool^{13,30}, and the number of end-caps (SB^{M}) directs the number of nearest neighbours at the network linkages (Fig. 4e). The self-assembly of these colloidal molecules is directed by the M/T corona patches that change their volume on solvent evaporation and develop into attractive M and repelling T patches. For $N = 1$ or 2 the end-cap size allows three or four nearest neighbours, $\{\text{SB}^{\text{M}}\text{-SD}^{\text{T}}\text{S}\text{-SB}^{\text{M}}\}_{4,5}$, whereas for $N = 3\text{--}5$ there is only space for two nearest neighbours and the networks show the onset of distorted kagome lattice formation (Extended Data Fig. 9).

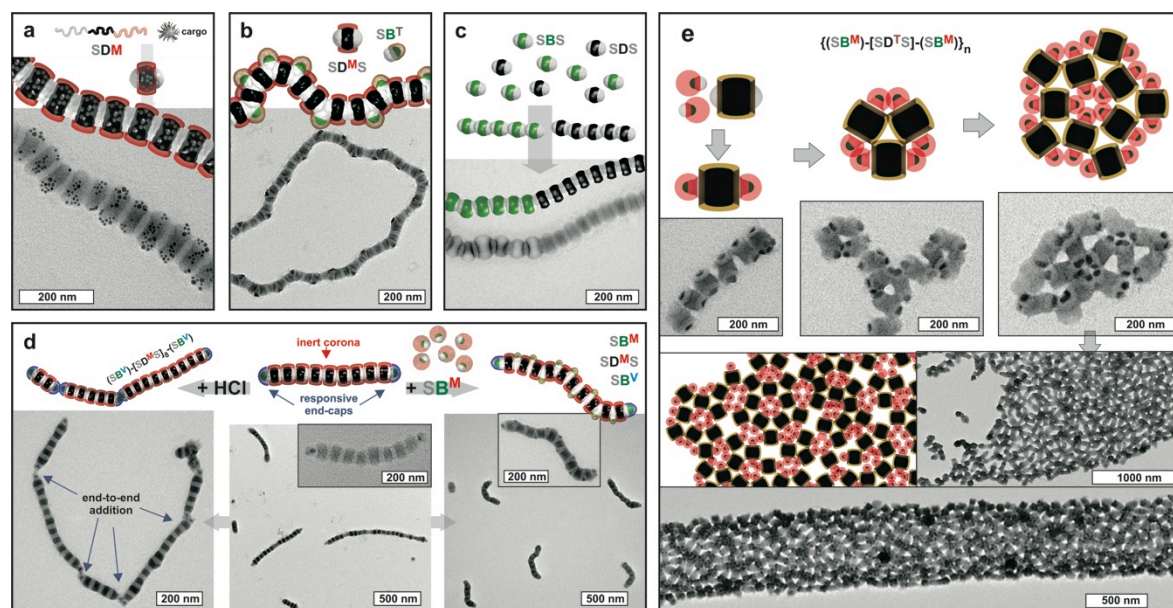


Figure 4-4: Binary and ternary co-assemblies. **a**, Hybrid co-assemblies with maghemite nanoparticles selectively loaded into one core segment. **b**, Core and corona co-assemblies. The $[\text{SD}^{\text{M}}\text{S}]_m$ superstructure is decorated with SB^{T} CBBs, yielding an alternating M/T corona. **c**, Linear multiblock co-assembly composed of $[\text{SD}^{\text{M}}\text{S}]_m/[\text{SB}^{\text{M}}\text{S}]_n$ sequences (M corona omitted for clarity). **d**, SB^{V} end-cappers produce telechelic $[\text{SD}^{\text{M}}\text{S}]_{10}$ oligomers (grey V corona surrounding the SB^{V} end-cap in inset). Protonation with HCl triggers further polymerization, and decoration with SB^{M} units yields ternary co-assemblies. **e**, Multicomponent structuring across three hierarchical levels. In solution, the terpolymers self-assemble into CBBs that co-assemble into colloidal molecules; these finally self-assemble into networks after drop-casting on a substrate. Adapted from *Nature*, **2013**, doi:10.1038/nature12610. Reprinted with permission from Nature Publishing Group.

These hierarchical multicomponent superstructures demonstrate the level of complexity reached through the controlled co-assembly of soft patchy nanoparticles and is in stark contrast to the self-assembly of increasingly complex building blocks (shape and surface pattern). Utilizing proper interacting segments, a wide range of building block combinations is conceivable, from biological origin to inorganic and organic nanoparticles and microparticles. Various self-assembly stimuli can conveniently be implemented by means of functional polymer blocks, for example supramolecular interactions, chemical reactions and environmental triggers (solvent polarity, pH, temperature, light or electrochemistry). Co-assembly opens up avenues to construct new materials, also far from thermodynamic equilibrium, through the tailored spatial organization of functionalities and the control of kinetics. We foresee application possibilities in smart materials, sensing, photonics and nanolithography.

METHODS SUMMARY

Relevant parameters of SBM, SBV and SBT triblock terpolymers^{31–35} are summarized in Fig. 1 and Extended Data Table 1. SBM and SBT were converted to SDM and SDT by thiol-ene click reaction of 1-dodecane thiol to the poly(1,2-butadiene) block. Oleic acid-stabilized magnetite nanoparticles were synthesized as described elsewhere³⁶. All CBBs were prepared in DMAc at a polymer concentration of 0.1 mg ml^{-1} and annealed overnight

at 70 °C. Particle dispersions were mixed in specific particle ratios and 10 ml of solution was co-dialysed (molecular mass cut-off 12,000 – 14,000 g mol⁻¹; Roth) against 5 l of selective solvent or solvent mixture for the corona block (acetone/propan-2-ol for M and V; ethanol for T corona). The solvent exchange was monitored by ¹H-NMR. TEM was performed in bright-field mode on Zeiss CEM 902 and 922 OMEGA electron microscopes operated at 80 kV and 200 kV, respectively. Co-assemblies were deposited by drop-casting (0.05 ml of 0.1 g l⁻¹ dispersion) onto carbon-coated copper grids resting on a filter paper to blot excess solution immediately. Samples were exposed to OsO₄ vapour for 2 h to stain the polybutadiene blocks selectively.

Online Content Any additional Methods, Extended Data display items and Source Data are available in the online version of the paper; references unique to these sections appear only in the online paper.

Received 26 March; accepted 28 August 2013.

- [1] Whitesides, G. M. & Grzybowski, B. Self-assembly at all scales. *Science* **295**, 2418–2421 (2002).
- [2] Studart, A. R. Towards high-performance bioinspired composites. *Adv. Mater.* **24**, 5024–5044 (2012).
- [3] Fratzl, P. & Weinkammer, R. Nature’s hierarchical materials. *Prog. Polym. Sci.* **52**, 1263–1334 (2007).
- [4] Mann, S. Self-assembly and transformation of hybrid nano-objects and nanostructures under equilibrium and non-equilibrium conditions. *Nature Mater.* **8**, 781–792 (2009).
- [5] Glotzer, S. C. & Solomon, M. J. Anisotropy of building blocks and their assembly into complex structures. *Nature Mater.* **6**, 557–562 (2007).
- [6] Quan, Z. & Fang, J. Superlattices with non-spherical building blocks. *Nano Today* **5**, 390–411 (2010).
- [7] Wang, T. *et al.* Self-assembled colloidal superparticles from nanorods. *Science* **338**, 358–363 (2012).
- [8] Grzelczak, M., Vermant, J., Furst, E. M. & Liz-Marzán, L. M. Directed self-assembly of nanoparticles. *ACS Nano* **4**, 3591–3605 (2010).
- [9] Nie, Z. *et al.* Self-assembly of metal-polymer analogues of amphiphilic triblock copolymers. *Nature Mater.* **6**, 609–614 (2007).
- [10] Liu, K. *et al.* Step-growth polymerization of inorganic nanoparticles. *Science* **329**, 197–200 (2010).
- [11] Cui, H., Chen, Z., Zhong, S., Wooley, K. L. & Pochan, D. J. Block copolymer assembly via kinetic control. *Science* **317**, 647–650 (2007).
- [12] Chen, Q. *et al.* Supracolloidal reaction kinetics of Janus spheres. *Science* **331**, 199–202 (2011).
- [13] Chen, Q., Bae, S. C. & Granick, S. Directed self-assembly of a colloidal kagome lattice. *Nature* **469**, 381–384 (2011).
- [14] Wang, Y. *et al.* Colloids with valence and specific directional bonding. *Nature* **491**, 51–55 (2012).
- [15] Kaufmann, T. *et al.* ‘Sandwich’ microcontact printing as a mild route towards monodisperse Janus particles with tailored bifunctionality. *Adv. Mater.* **23**, 79–83 (2010).
- [16] Chen, Q., Bae, S. C. & Granick, S. Staged self-assembly of colloidal metastructures. *J. Am. Chem. Soc.* **134**, 11080–11083 (2012).

- [17] Li, Z., Kesselman, E., Talmon, Y., Hillmyer, M. A. & Lodge, T. P. Multicompartment micelles from ABC miktoarm stars in water. *Science* **306**, 98–101 (2004).
- [18] Wang, X. *et al.* Cylindrical block copolymer micelles and co-micelles of controlled length and architecture. *Science* **317**, 644–647 (2007).
- [19] Schmelz, J., Schedl, A. E., Steinlein, C., Manners, I. & Schmalz, H. Length control and block-type architectures in worm-like micelles with polyethylene cores. *J. Am. Chem. Soc.* **134**, 14217–14225 (2012).
- [20] Gädt, T., Jeong, N. S., Cambridge, G., Winnik, M. A. & Manners, I. Complex and hierarchical micelle architectures from diblock copolymers using living, crystallization-driven polymerizations. *Nature Mater.* **8**, 144–150 (2009).
- [21] Kubowicz, S. *et al.* Multicompartment micelles formed by self-assembly of linear ABC triblock copolymers in aqueous medium. *Angew. Chem. Int. Ed.* **44**, 5262–5265 (2005).
- [22] Gröschel, A. H. *et al.* Facile, solution-based synthesis of soft, nanoscale Janus particles with tunable Janus balance. *J. Am. Chem. Soc.* **134**, 13850–13860 (2012).
- [23] Gröschel, A. H. *et al.* Precise hierarchical self-assembly of multicompartment micelles. *Nature Commun.* **3**, 710, <http://dx.doi.org/10.1038/ncomms1707> (2012).
- [24] Li, Z., Hillmyer, M. A. & Lodge, T. P. Control of structure in multicompartment micelles by blending m-ABC star terpolymers with AB diblock copolymers. *Macromolecules* **39**, 765–771 (2005).
- [25] Fang, B. *et al.* Undulated multicompartment cylinders by the controlled and directed stacking of polymer micelles with a compartmentalized corona. *Angew. Chem. Int. Ed.* **48**, 2877–2880 (2009).
- [26] Rugar, P. A., Chabanne, L., Winnik, M. A. & Manners, I. Non-centrosymmetric cylindrical micelles by unidirectional growth. *Science* **337**, 559–562 (2012).
- [27] Chen, Q., Yan, J., Zhang, J., Bae, S. C. & Granick, S. Janus and multiblock colloidal particles. *Langmuir* **28**, 13555–13561 (2012).
- [28] Sacanna, S., Irvine, W. T. M., Chaikin, P. M. & Pine, D. J. Lock and key colloids. *Nature* **464**, 575–578 (2010).
- [29] Bates, F. S. *et al.* Multiblock polymers: panacea or Pandora's box? *Science* **336**, 434–440 (2012).
- [30] Bowden, N., Terfort, A., Carbeck, J. & Whitesides, G. M. Self-assembly of mesoscale objects into ordered two-dimensional arrays. *Science* **276**, 233–235 (1997).

Acknowledgements We thank O. Ikkala and E. Kumacheva for discussions and comments on the manuscript, and A. Majewski for providing maghemite nanoparticles. This work was supported by Deutsche Forschungsgemeinschaft within Sonderforschungsbereich 840 (TP A1 and A2).

Corresponding Author A.H.G. initiated the project. A.H.G. and T.I.L. performed experiments and collected data. A.H.G., A.W. and A.H.E.M. designed the experiments, discussed results and wrote the manuscript. F.H.S. co-designed experiments, discussed results and commented on the manuscript. H.S. provided polymers, discussed results and commented on the manuscript. A.H.E.M. supervised the project.

Author Information Reprints and permissions information is available at www.nature.com/reprints. The authors declare no competing financial interests. Readers are welcome to comment on the online version of the paper. Correspondence and requests

for materials should be addressed to A.H.E.M. (axel.mueller@uni-mainz.de) or A.H.G. (andre.groschel@aalto.fi).

METHODS

Particle preparation All terpolymers were synthesized by sequential anionic polymerization^{31–35}. Important parameters are summarized in Fig. 1 and Extended Data Tables 1. All solvents used were of analytical grade. Dialysis tubes of regenerated cellulose with a molecular mass cut-off of 12,000–14,000 g mol⁻¹ were purchased from Roth. Oleic acid-stabilized maghemite nanoparticles were synthesized as described elsewhere³⁶. Both polymers, SBM and SBT, were converted to SDM and SDT, respectively, by means of a thiol-ene click reaction of 1-dodecane thiol with the pendant double bonds of poly(1,2-butadiene). In a typical experiment, terpolymer (0.5 g) was dissolved in 20 ml of tetrahydrofuran; 20 ml of 1-dodecane thiol were added and the solution was purged for 15 min with argon. The mixture was irradiated for 24 h with an ultraviolet lamp with a cut-off filter ($\lambda = 300$ nm; $\lambda_{\text{max}} = 360$ nm). After the reaction, the modified terpolymer was precipitated in propan-2-ol, filtered, and washed with excess propan-2-ol to remove remaining 1-dodecane thiol. SBM, SDM, SBT, SDT and SBV triblock terpolymers were dissolved separately in DMAc at an initial polymer concentration of 0.1 mg ml⁻¹ and annealed overnight at 70 °C to guarantee an equilibrated system. At this stage of self-assembly the corona patches were not yet fully developed. To reveal the patches in the developed state (Extended Data Fig. 2), the CBBs were crosslinked while located within the respective superstructure. Therefore, 2 equivalents of the photo-crosslinker 2,4,6-trimethylbenzoyldiphenylphosphineoxide (Lucirin TPO; $\lambda_{\text{max}} \approx 360$ nm), were added to each double bond. Gentle stirring for 2 h ensured a homogeneous distribution of the photo-crosslinker before the samples were irradiated for 1 h with an ultraviolet lamp with a cut-off filter ($\lambda = 300$ nm). Re-dispersion in DMAc as a good solvent for the patches then broke up the superstructures into the respective CBBs.

Self-assembly and co-assembly CBB solutions (0.1 g l⁻¹ in DMAc) were mixed in specific particle ratios to yield 10 ml of a colloidal mixture and co-dialysed against 5 l of selective solvent/solvent mixture for the corona block (acetone/propan-2-ol for the M corona and V corona block, and ethanol for the T corona block). The solvent exchange was monitored by ¹H-NMR. TEM was performed in bright-field mode on Zeiss CEM 902 and LEO 922 OMEGA electron microscopes operated at 80 kV and 200 kV, respectively. Samples were prepared by dropping 0.05 ml of a 0.1 mg ml⁻¹ colloidal suspension onto carbon coated copper grids resting on a filter paper to remove the excess solution immediately. The two-dimensional networks were prepared similarly, except from 0.01 g l⁻¹ colloidal suspension that was allowed to settle on the TEM grid for 30 s before blotting. TEM grids were then exposed for 2 h to OsO₄ vapour to stain the polybutadiene block selectively. The number of polymer chains in each CBB was determined, evaluating at least 250 cores. The

average degree of polymerization of each $[\text{SD}^{\text{M}}\text{S}]_n$ colloidal polymer was determined by counting the black segments of 500 colloidal polymers and plotted as frequency distribution.

Correlating co-assembly with onsets of aggregation We used a CBB ratio of $\text{s-SB}^{\text{M}(\text{y})}:\text{SD}^{\text{M}}\text{S} = 8:1$ for all experiments to ensure that enough monovalent CBBs were present for full decoration of the $-\text{S}-$ segments. $\text{SD}^{\text{M}}\text{S}$ was co-dialysed with three different $\text{s-SB}^{\text{M}(\text{y})}$ units with varying volume of the corona, $\text{M}(\text{y})$ (y stands for s (small), m (medium) or l (large)). The dialysis sequence was from DMAc into acetone/propan-2-ol mixtures. Greater amounts of propan-2-ol led to a contraction of the M corona. $\text{SD}^{\text{M}}\text{S}$ forms extended superstructures irrespective of the propan-2-ol content (also in pure acetone). $\text{s-SB}^{\text{M}(\text{l})}$ CBBs with a large relative volume fraction of the soluble M corona of $r_{\text{M}} = 0.74$ (where $r_{\text{M}} = V_{\text{M}}/(V_{\text{S}} + V_{\text{B}})$) do not co-assemble at low propan-2-ol content (less than 20 vol%) and are only located in the vicinity of polymerized $\text{SD}^{\text{M}}\text{S}$ (Extended Data Fig. 4). The long corona blocks provide steric stabilization by fully covering the CBB. At high propan-2-ol contents (30 vol%), partial co-assembly is observed and quantitative co-assembly only at 40 vol% as a result of progressive contraction of the M corona. Because the $\text{SD}^{\text{M}}\text{S}$ units are already fully polymerized, decoration does not interfere with the growth process (no premature end-capping). $\text{s-SB}^{\text{M}(\text{m})}$ CBBs with $r_{\text{M}} = 0.34$ carry a corona block of moderate length and show partial to quantitative co-assembly over the whole range of solvent mixtures, indicating only a slight difference in onset of aggregation between $\text{SD}^{\text{M}}\text{S}$ and $\text{s-SB}^{\text{M}(\text{m})}$. $\text{s-SB}^{\text{M}(\text{s})}$ CBBs with the shortest corona block, $r_{\text{M}} = 0.15$, show no co-assembly in either of the solvent compositions: at a propan-2-ol contents of only 10 vol% the corona shows insufficient stabilization for the $\text{s-SB}^{\text{M}(\text{s})}$ CBBs, and aggregation into spherical $(\text{s-SB}^{\text{M}(\text{s})})_x$ clusters occurs before polymerization of $\text{SD}^{\text{M}}\text{S}$. The $\text{SD}^{\text{M}}\text{S}$ units still polymerize through these spherical clusters, resulting in randomly distributed bulbs of $(\text{s-SB}^{\text{M}(\text{s})})_x$ clusters along the $[\text{SD}^{\text{M}}\text{S}]_n$ chain.

Calculation of polymer chains in each particle and compartment volumes Because CBBs form dynamically during the self-assembly of triblock terpolymers, one needs to know how many polymer chains are located within one CBB to be able to mix CBBs in the desired ratios for the co-assembly process. We determined the average core diameter of each CBB by TEM (averaged over 250 samples) to calculate the aggregation number of triblock terpolymer chains, N_{agg} , in each CBB. This evaluation is exemplified on monovalent spherical s-SB^{M} and divalent, cylindrical $\text{SD}^{\text{M}}\text{S}$ cores (Extended Data Fig. 2). N_{agg} was then calculated from

$$N_{\text{agg}} = \frac{m_{\text{core}}}{m_{\text{chain}}} = V_{\text{core}} \frac{N_{\text{A}} \rho_{\text{B}}}{M_{\text{B}}^{\text{chain}}}$$

with $V_{\text{core}} = 4/3(\pi R_{\text{core}}^3)$ for spherical SB^{M} and $V_{\text{core}} = w\pi R_{\text{core}}^2$ for cylindrical SD^{MS} ; m_{core} is the mass of the micellar core, $m_{\text{B}}^{\text{chain}}$ is the mass of the middle block, $M_{\text{B}}^{\text{chain}}$ is the molecular mass of the middle block, N_{A} is Avogadro's constant and ρ_{B} is the density of the middle block. We found that this approach yields a good correlation between the ratio of triblock terpolymers and the final composition of CBBs in the co-assemblies. We can calculate the diameter of SB^{M} units combining the calculated volume for the B compartments, V_{B} , from N_{agg} with the volume ratio $V_{\text{S}}/V_{\text{B}}$. The diameter of spherical CBBs, d_{CBB} , is then given by

$$d_{\text{CBB}} = 2 \left(\left(V_{\text{S}} + \frac{1}{2} V_{\text{B}} \right) \frac{3}{4\pi} \right)^{\frac{1}{3}}$$

The volume and surface area of the cylindrical –S– segments are simply determined from TEM data; that is, directly from the colloidal co-assembly as width (w) and height = diameter (d).

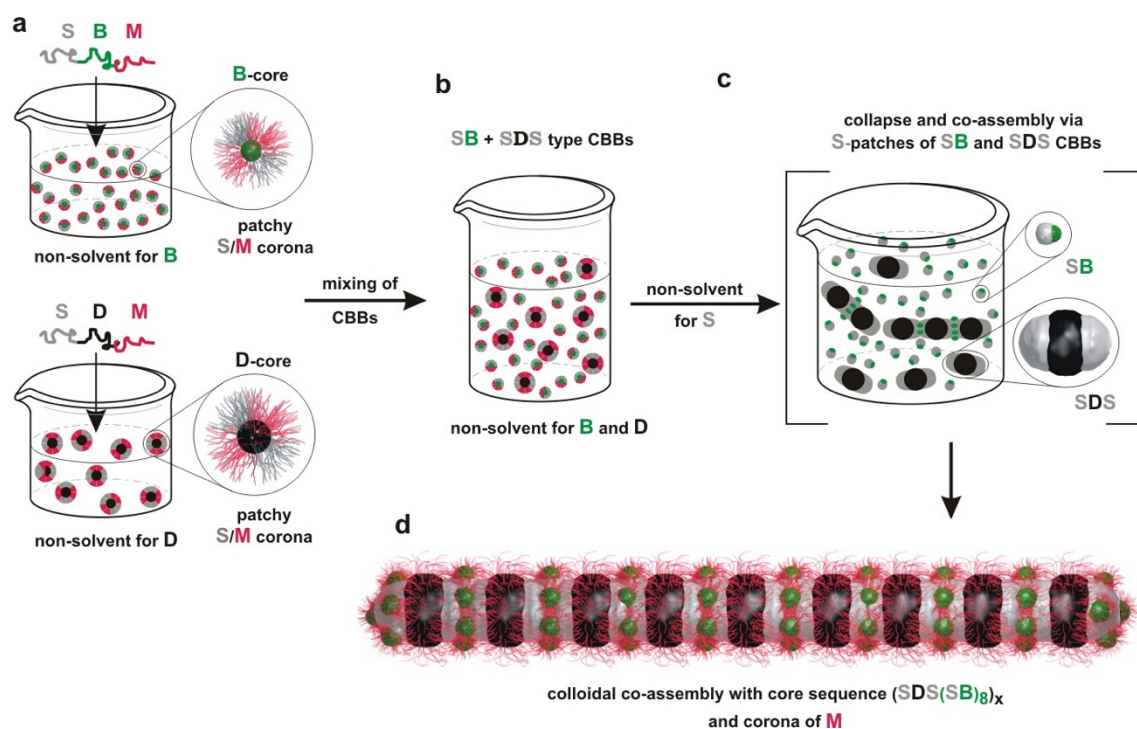
- [31] Auschra, C. & Stadler, R. Synthesis of block copolymers with poly(methyl methacrylate): P(B-*b*-MMA), P(EB-*b*-MMA), P(S-*b*-B-*b*-MMA) and P(S-*b*-EB-*b*-MMA). *Polym. Bull.* **30**, 257–264 (1993).
- [32] Giebeler, E. & Stadler, R. ABC triblock polyampholytes containing a neutral hydrophobic block, a polyacid and a polybase. *Macromol. Chem. Phys.* **198**, 3815–3825 (1997).
- [33] Walther, A., André, X., Drechsler, M., Abetz, V. & Müller, A. H. E. Janus discs. *J. Am. Chem. Soc.* **129**, 6187–6198 (2007).
- [34] Schacher, F., Yuan, J., Schoberth, H. G. & Müller, A. H. E. Synthesis, characterization, and bulk crosslinking of polybutadiene-*block*-poly(2-vinyl pyridine)-*block*-poly(tert-butyl methacrylate) block terpolymers. *Polymer (Guildf.)* **51**, 2021–2032 (2010).
- [35] Ruckdäschel, H. *et al.* Compatibilisation of PPE/SAN blends by triblock terpolymers: correlation between block terpolymer composition, morphology and properties. *Polymer (Guildf.)* **47**, 2772–2790 (2006).
- [36] Majewski, A. P. *et al.* Dual-responsive magnetic core-shell nanoparticles for nonviral gene delivery and cell separation. *Biomacromolecules* **13**, 857–866 (2012).

Supporting Online Material

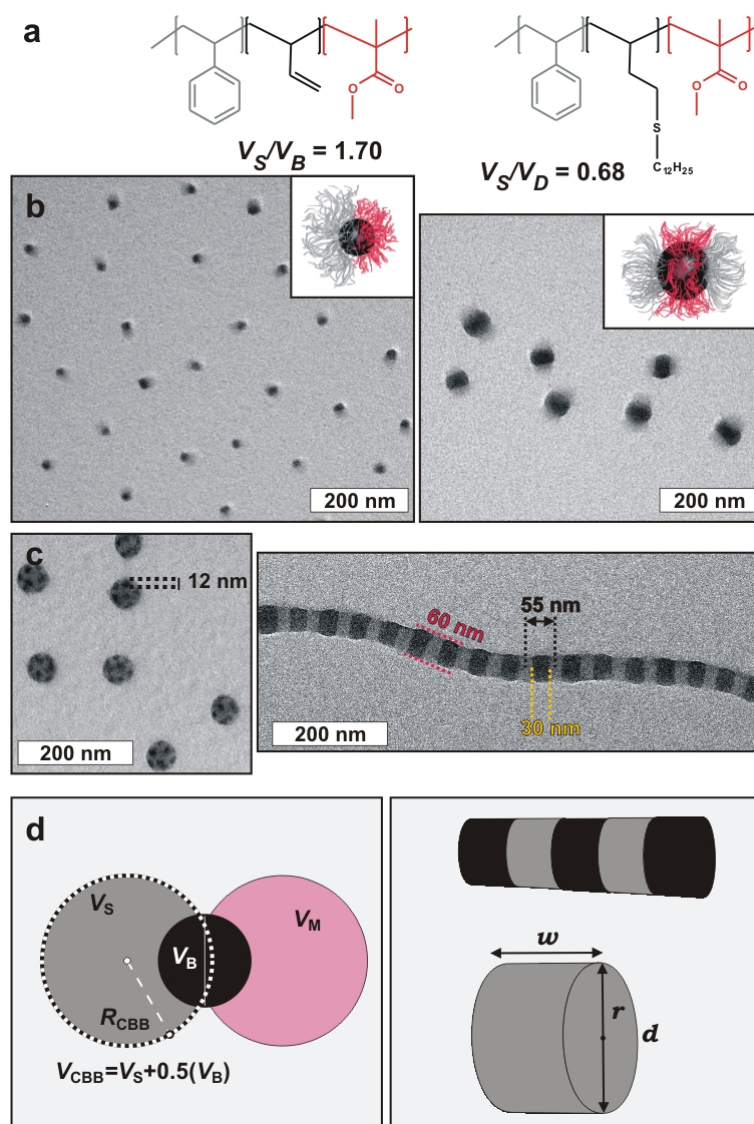
to

Guided hierarchical co-assembly of soft patchy nanoparticles

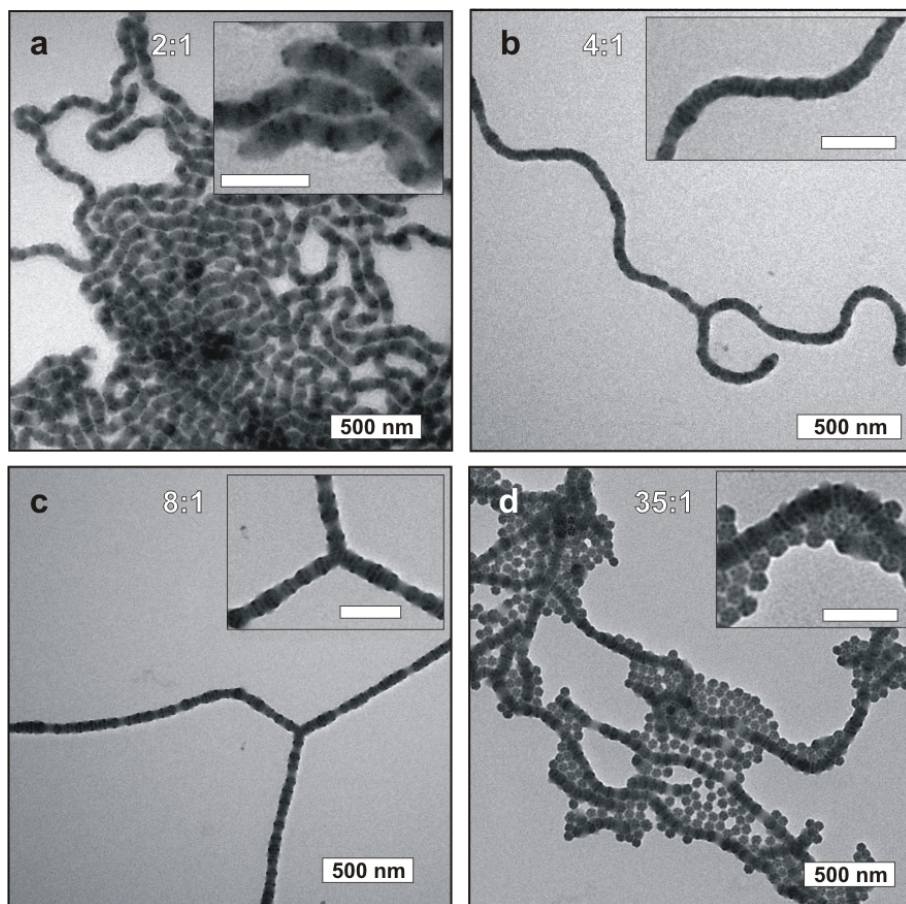
André H. Gröschel*, **Andreas Walther**, **Tina I. Löbbling**, **Felix Schacher**, **Holger Schmalz** and **Axel H. E. Müller***



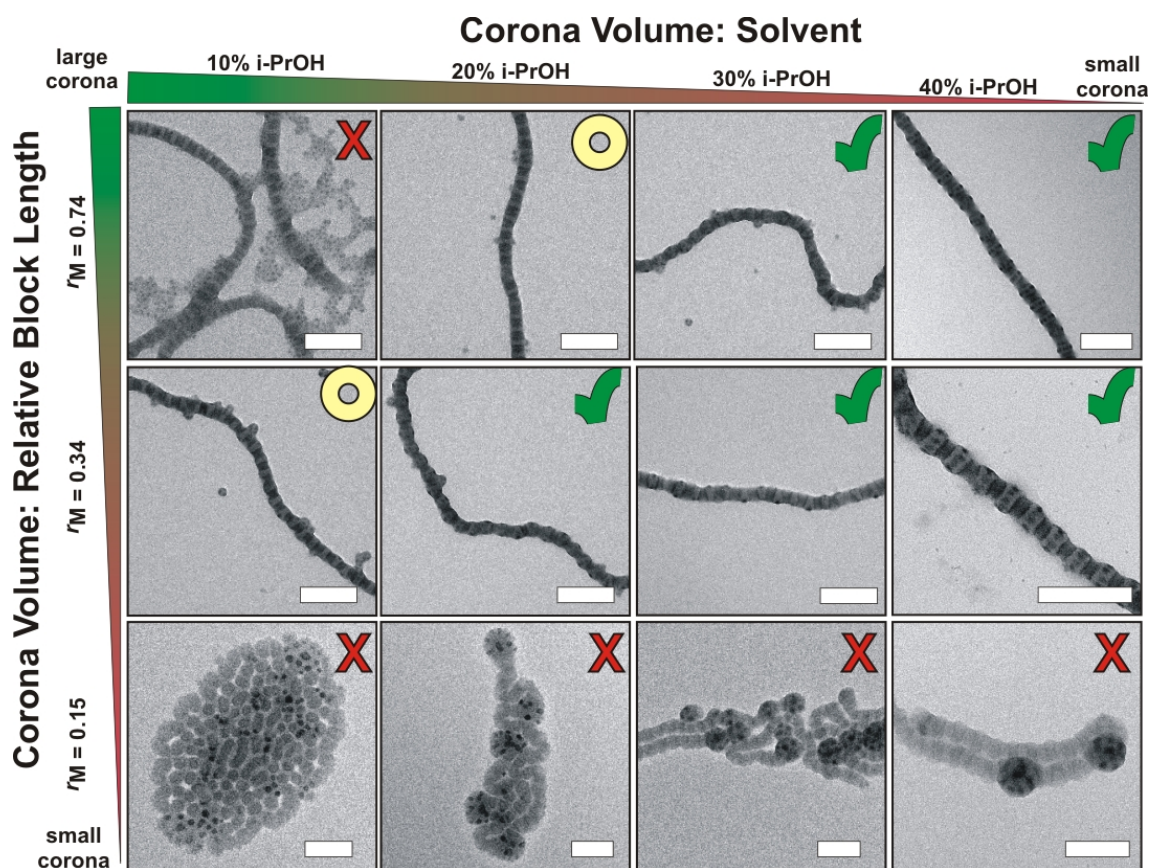
Extended Data Figure 1 | Experimental approach to prepare colloidal co-assemblies exemplified on $s\text{-SB}^M$ and $SD^M S$. **a**, First, the triblock terpolymers are dispersed separately in DMAc as a non-solvent for B and D, equalling bottom-up structuring of CBBs with different cores (B and D), yet identical ‘sticky’ S patch and stabilizing M corona. **b**, Both colloidal dispersions are mixed in specific ratios and stirred overnight to ensure homogeneous distribution. **c**, Co-dialysis into a non-solvent for the S patches induces collapse and aggregation. $SD^M S$ grows into extended linear colloidal polymers decorated by $s\text{-SB}^M$ units (M corona omitted for clarity). **d**, Final colloidal co-assemblies stabilized by the common M corona.



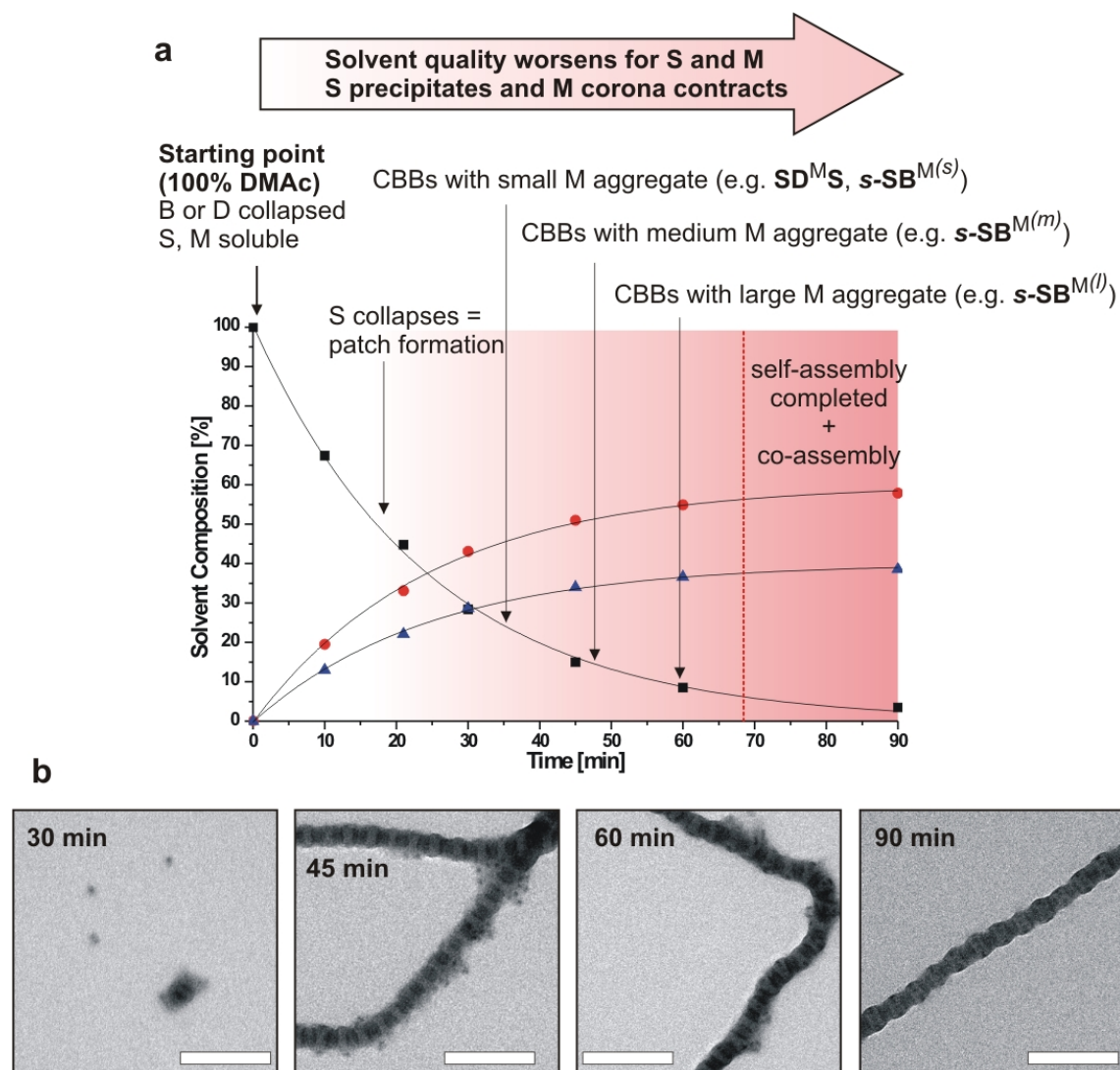
Extended Data Figure 2 | Compartment sizes, polymer chains per CBB and CBB mixing ratios. **a**, SBM with $V_S/V_B = 1.70$ and SDM with $V_S/V_D = 0.68$ result in **b**, monovalent SB^{M} (Janus) and divalent $\text{SD}^{\text{M}}\text{S}$ units, respectively. CBBs are visualized after crosslinking of the remaining double bonds within the particle cores. **c**, Examples of spherical SB^{M} clusters and linear $\text{SD}^{\text{M}}\text{S}$ colloidal polymers. **d**, Diagrams of CBB compartment volumes and surface area of associative patches. We determine the number of SB^{M} units able to attach to the $-\text{S}-$ segments of the $\text{SD}^{\text{M}}\text{S}$ colloidal polymers by calculating the volume and the diameter of the CBBs, assuming a spherical shape of B and S phases and considering the number of polymer chains per patch. The spherical SB^{M} units are composed of (i) the body as the sum of the collapsed S patch (grey) and B core (black) and (ii) the M corona patch. The radius, R_{CBB} , and the volume, V_{CBB} , displaced by the CBB when aggregating into the $-\text{S}-$ segments are estimated by combining the volume of S plus half of the volume of B (the dashed line marks R_{CBB}). These assumptions are valid for the collapsed state, given the unfavourable interactions with the surrounding medium and the minimization of the interfacial energies.



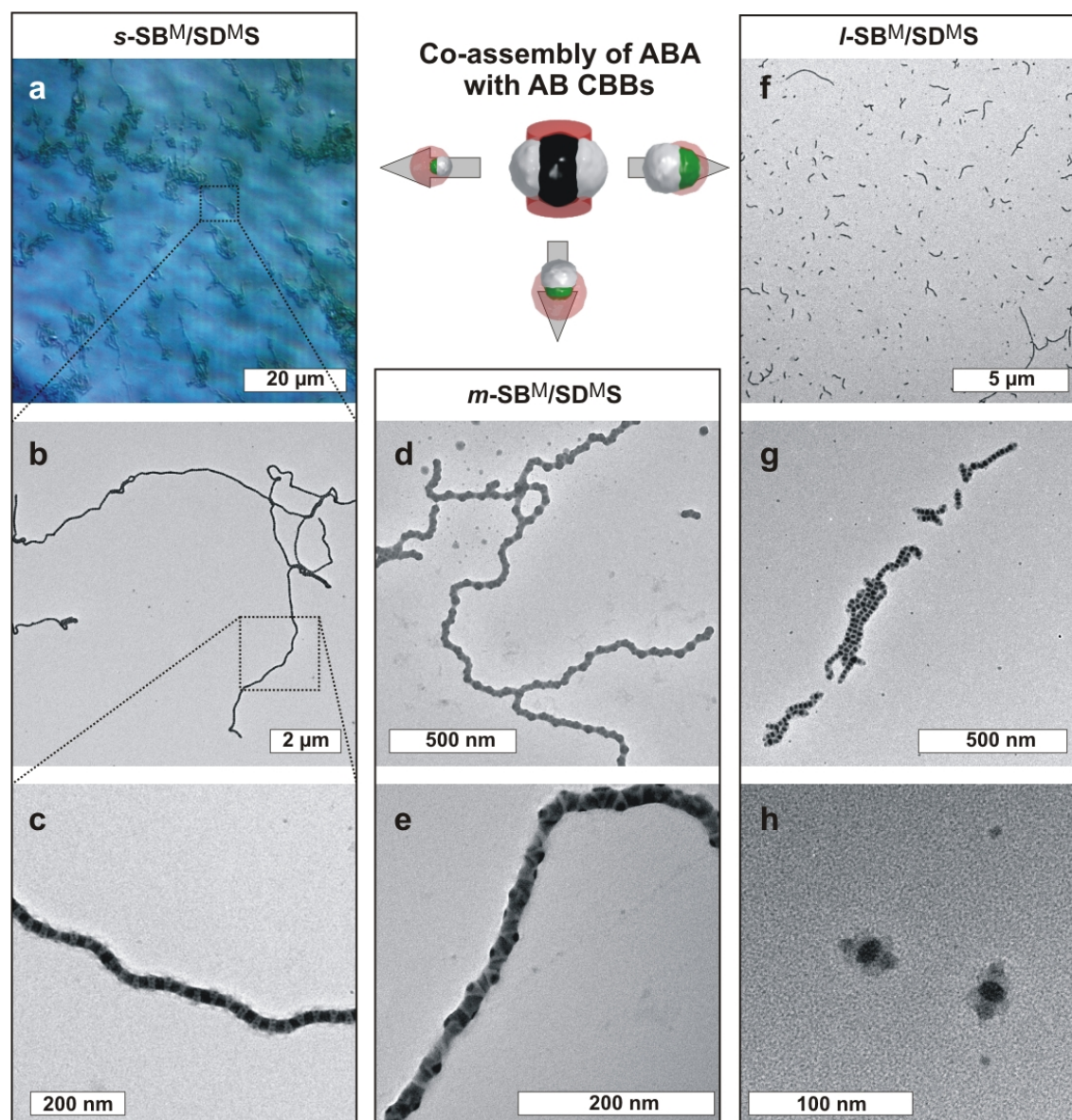
Extended Data Figure 3 | Loading capacity for decoration with spherical CBBs during co-assembly. SD^{MS} and $s\text{-SB}^{\text{M}}$ colloidal co-assemblies with increasing mixing ratios 2:1, 4:1, 8:1 and 35:1 of $s\text{-SB}^{\text{M}}:\text{SD}^{\text{MS}}$ and corresponding co-assembly composition. **a**, At small excess, $s\text{-SB}^{\text{M}}:\text{SD}^{\text{MS}} = 2:1$, the $-S-$ segments are only partly decorated. **b**, **c**, With increasing CBB ratio, the $-S-$ segments of the colloidal polymers are more strongly occupied (4:1) (**b**) and at full capacity in a radial manner (8:1) (**c**). **d**, Above this ratio, no space remains on the colloidal polymer and only then does $s\text{-SB}^{\text{M}}$ start to form homo-clusters (35:1; football-like or raspberry-like homo-clusters adjacent to the colloidal co-assemblies). These observations fit well with our calculations, as a cylinder with $d_{\text{S}} \approx 55$ nm and $w \approx 24$ nm can accommodate up to nine $s\text{-SB}^{\text{M}}$ units with $d_{\text{CBB}} \approx 19$ nm ($pd_{\text{S}} \approx 173$ nm; 173 nm/ 19 nm ≈ 9.1). Scale bars in insets are 200 nm (OsO₄ staining: S grey, B dark grey dots, D black, and M not visible as a result of degradation by the electron beam.)



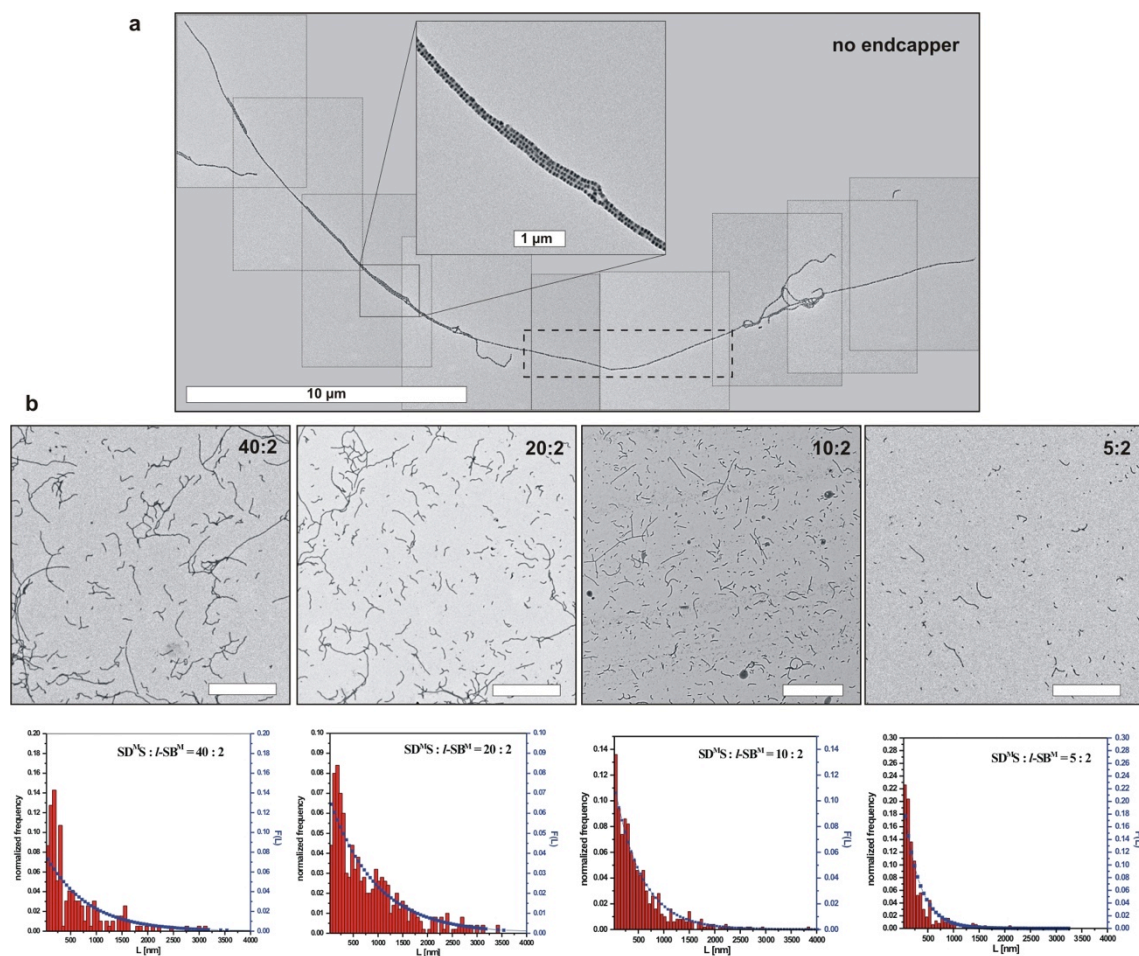
Extended Data Figure 4 | Co-assembly of $s\text{-SB}^{M(y)}$ and SD^MS in dependence on the corona volume of the monovalent $s\text{-SB}^{M(y)}$ units (y stands for s , m or l). Colloidal co-assembly occurs preferentially with matching onsets of aggregation that depend on the corona volume, which is tunable either by decreasing the block length of the corona block, $r_M = V_M/(V_S + V_B)$, $r_M(s\text{-SB}^{M(l)}) = 0.74$, $r_M(s\text{-SB}^{M(m)}) = 0.34$, $r_M(s\text{-SB}^{M(s)}) = 0.15$, or by reducing the solvent quality, here the addition of propan-2-ol from 10 vol% to 40 vol%. Thereby, crosses indicate no co-assembly, circles the onset of co-assembly and tick marks effective and quantitative co-assembly. For detailed discussion see Methods. (OsO₄ staining: S grey, B dark grey dots, D black, and M not visible as a result of degradation by the electron beam.)



Extended Data Figure 5 | Timeline of CBB aggregation and response of CBB constituents on solvent composition. **a**, Co-dialysis of CBBs (here $SD^M S$ and $s-SB^{M(v)}$) from DMAc (squares) into acetone (circles)/propan-2-ol (triangles) mixtures (60:40 v/v) results in a continuous change of a multitude of polymer-polymer interactions as well as polymer block responses to the ternary solvent mixture. With progressing dialysis, DMAc is replaced by acetone/propan-2-ol, affecting the solubility of S/M corona patches. This induces the collapse into S patches and determines the onset of aggregation. Time-dependent 1H -NMR measurements were performed by drawing samples at specific intervals during dialysis to determine the solvent composition. **b**, TEM series exemplifying the timeline of aggregation on $s-SB^{M(l)}$ and $SD^M S$. Up to 30 min, S corona collapses to form S patches, yet both CBBs are still stable due to stabilizing corona; after 30 min, of $SD^M S$ (smaller M corona) aggregate; after 45 min, aggregation of $SD^M S$ proceeds, while $s-SB^{M(l)}$ is still stable (larger M corona, no co-assembly); at 60 min, $s-SB^{M(l)}$ aggregates and co-assembly takes place; up to 90 min, co-assembly is complete. (OsO₄ staining: S grey, B dark grey dots, D black, and M not visible as a result of degradation by the electron beam.)



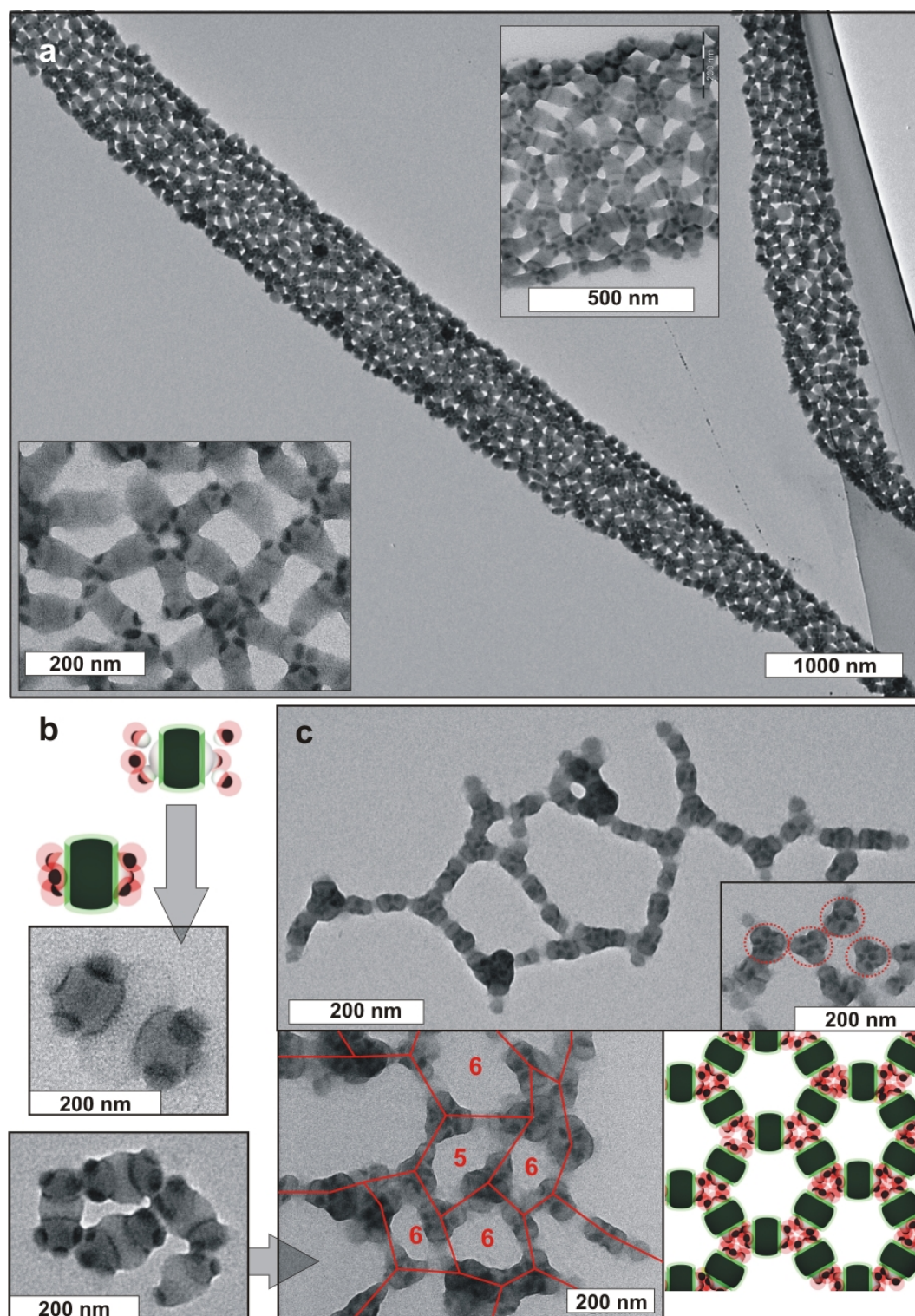
Extended Data Figure 6 | Supporting images of colloidal co-assemblies composed of $SD^M S$ and $s-SB^M$, $m-SB^M$ and $l-SB^M$. **a**, Optical microscopy image of colloidal co-assemblies 30 mm in length. **b**, **c**, TEM images of fully decorated -S- segments with $s-SB^M$. **d**, **e**, Larger $m-SB^M$ units induce kinks due to lateral, alternating decoration and high volume displacement within the -S- segments. **f**, Zoom-out of rod-like colloidal oligomers end-capped with $l-SB^M$. **g**, Magnification of **f**. **h**, The smallest possible co-assembly with $[SD^M S]_1$; that is, two end-caps attached to one $SD^M S$ unit. (OsO₄ staining: S grey, B dark grey dots, D black, and M not visible as a result of degradation by the electron beam.)



Extended Data Figure 7 | Length control of colloidal polymers via end-capping with $I\text{-SB}^M$. **a**, Without any $I\text{-SB}^M$ end-capper added, the SD^M units grow into remarkably extended superstructures several micrometres in length, exceeding 500–600 SD^M repeating units. The inset illustrates the segmented core and some occurrence of branching. The displayed image consists of an overlay of nine separate TEM images, because the superstructure was far too large for magnifications that were still able to resolve the nanostructure. The dashed box marks the part of the colloidal polymer that is shown in Fig. 3d. **b**, TEM images and frequency distributions (red bars) of 500 evaluated colloidal polymers for varying SD^M s to $I\text{-SB}^M$ mixing ratios of 40:2, 20:2, 10:2 and 5:2. We count segments and multiply the resulting average value by the average segment length, $L_n = 55$ nm, to yield the average length of the co-assembly. Data are plotted against the normalized frequency and fitted by a Schulz–Flory frequency distribution (squares), $F(L) = \exp(-L/L_n)/L_n$, showing a continuous decrease in the average length coinciding with the mixing ratio. The similar timescales of onset of aggregation combined with matching sizes of CBBs both promote efficient end-capping.



Extended Data Figure 8 | Stability of $[\text{SD}^{\text{M}}\text{S}]_m$ colloidal polymer versus $\text{SB}^{\text{T}}/[\text{SD}^{\text{M}}\text{S}]_m$ co-assembly in polar solvents. Photograph of two colloidal solutions after dialysis into ethanol. Left: instant precipitation of the $[\text{SD}^{\text{M}}\text{S}]_m$ colloidal homopolymer as a result of complete collapse of the M corona. Right: the $\text{SB}^{\text{T}}/[\text{SD}^{\text{M}}\text{S}]_m$ colloidal co-assembly is stabilized by the soluble T corona patches. Precipitation is not observed even after weeks.



Extended Data Figure 9 | Colloidal molecules and two-dimensional network formation. **a**, Co-assembly of four SB^{M} with one $\text{SD}^{\text{T}}\text{S}$ CBB by means of collapsing S patches in acetone/propan-2-ol (60:40 v/v) yields colloidal molecules with one or two end-caps of the $(\text{SB}^{\text{M}})_2\text{-(SD}^{\text{T}}\text{S)-}(\text{SB}^{\text{M}})_2$ type, permitting three or four nearest neighbours at every linking point in large-area networks. **b**, Co-assembly of six SB^{M} with one $\text{SD}^{\text{T}}\text{S}$ CBB by means of collapsing S patches in acetone/propan-2-ol (60:40 v/v) yields colloidal molecules of the $(\text{SB}^{\text{M}})_3\text{-(SD}^{\text{T}}\text{S)-}(\text{SB}^{\text{M}})_3$ type. **c**, Addition of propan-2-ol until acetone/propan-2-ol reached 20:80 v/v selectively collapses the terminal M corona, allowing two nearest neighbours at every linking point of the network in solution. On some occasions the network takes on the form of a distorted kagome lattice.

Extended Data Table 1 | Characteristics of triblock terpolymers and CBBs

CBB Code [*]	Triblock Terpolymer [†]	$\frac{V_A}{V_B}$ [‡]	$r_C = \frac{V_C}{V_A + V_B}$ [‡]	d_{CBB}^{\S} [nm]	$R_{\text{B-core}}^{\parallel}$ [nm]	V_B^{\parallel} [x10 ³ nm ³]	$N_{\text{agg}}^{\#}$	V_S^{\star} [x10 ³ nm ³]
AB^CA CBBs								
SD^MS	S ₅₆₀ D ₅₈₀ M ₅₄₀ ¹⁹⁵	0.37	0.33	55x24	55x30	71.2	370	26.3
SD^TS	S ₅₁₀ D ₅₄₀ T ₄₆₀ ²⁵⁸	0.36	0.44	60x30	57x38	96.1	385	34.6
SB^MS	S ₅₉₀ B ₂₇₀₀ M ₅₆₀ ²⁶⁵	0.38	0.25	100x31	100x50	394.0	2300	149.7
s-AB^{C(y)} CBBs of similar size, yet decreasing corona length (l), (m), (s)								
s-SB^{M(l)}	S ₃₁₀ B ₁₅₀ M ₃₄₀ ⁷⁴	3.57	0.74	19	5 ± 2	0.5	40	1.9
s-SB^{M(m)}	S ₅₁₀ B ₂₆₀ M ₂₆₀ ⁹⁰	4.20	0.34	28	7 ± 2	1.4	60	5.9
s-SB^{M(s)}	S ₇₀₀ B ₂₇₀₀ M ₁₈₀ ¹⁰⁵	4.50	0.15	29	7 ± 2	1.4	57	6.3
x-AB^C CBBs of different overall size s-, m-, l-								
s-SB^M	S ₃₁₀ B ₁₅₀ M ₃₄₀ ⁷⁴	3.57	0.74	19	5 ± 2	0.5	40	1.9
m-SB^M	S ₅₆₀ B ₅₈₀ M ₅₄₀ ¹⁴³	1.78	0.88	35	11 ± 2	5.6	140	9.9
l-SB^M	S ₆₁₀ B ₆₄₀ M ₂₉₀ ¹⁴⁰	1.72	0.26	47	15 ± 2	14.1	260	24.3
AB CBBs with different nature of the corona								
SB^T	S ₅₁₀ B ₅₄₀ T ₄₈₀ ¹⁵⁵	1.70	0.45	28	9 ± 2	3.1	60	5.2
SB^V	S ₃₆₀ B ₃₈₀ V ₅₉₀ ¹²⁰	1.67	0.95	22	7 ± 2	1.4	54	2.4

* The syntheses and characterization of SBM, SBV and SBT triblock terpolymers were reported in detail previously.^{31–35} Superscripts denote the size of the soluble corona patches in relation to the other CBBs: s, small; m, medium; l, large.

† Subscripts denote the degrees of polymerization of the corresponding blocks, and the superscript is the molecular mass in kg mol⁻¹ determined with combined ¹H-NMR and GPC (polydispersity index, < 1.15) measurements.

‡ Volume fractions V_A , V_B and V_C were calculated from molar volumes and degrees of polymerization.

§ For calculations see Methods. The diameter (d) and width (w) of cylindrical segments of AB^CA units and (AB^CA)_x segments are average values from TEM image analysis.

|| Average of 250 measured particle core radii in TEM image analysis.

¶ Particle core volumes calculated from measured core radii.

Average aggregation number of polymer chains per particle.

☆ Calculated by applying the relation V_S/V_B .

Chapter 5

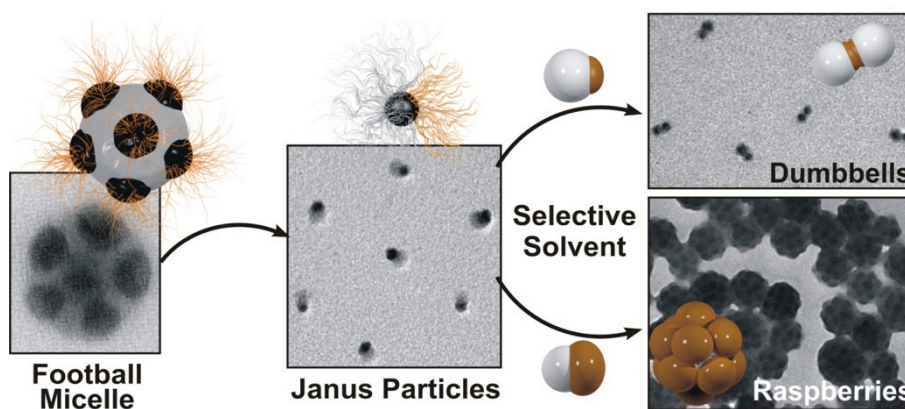
Facile, Solution-Based Synthesis of Soft, Nanoscale Janus Particles with Tunable Janus Balance

André H. Gröschel^{*}, Andreas Walther[‡], Tina I. Löbling, Joachim Schmelz, Andreas Hanisch, Holger Schmalz, Axel H. E. Müller^{*}

Makromolekulare Chemie II, Universität Bayreuth, D-95440 Bayreuth, Germany

andre.groeschel@uni-bayreuth.de, axel.mueller@uni-bayreuth.de

[‡] *DWI at RWTH Aachen University, D-52056 Aachen, Germany*



Published in the *Journal of American Chemical Society* **2012**, 134 (33), 13850–13860.

Abstract

We present a novel, versatile, and simple solution-based routine to produce soft, nanosized Janus particles with tunable structural and physical properties at high volume yield. This process is based on the cross-linking of compartments within precisely defined multicompartment micelles (MCMs), which are themselves formed by the self-assembly of ABC triblock terpolymers. Therein, the C blocks form the stabilizing corona emanating from the B compartments, which in turn reside on an A core. Cross-linking of the B compartments allows to permanently fixate the phase-separated state and dissolution in a good solvent for all blocks breaks up the MCMs into single Janus particles. They now consist of a core of cross-linked B blocks and two phase-separated hemispheres of A and C. The process gives access to unprecedented structural features such as tunable core diameter and control over the Janus balance ranging from dominant A side to equal hemispheres to dominant C side. We demonstrate that this simple one-pot approach can be extended to a range of triblock terpolymers with different block lengths and block chemistries to furnish a library of tailor-made Janus particles with widely tunable physical properties. Such a diversity and simplicity has remained unreachable with our previously developed approach using the controlled cross-linking of bulk morphologies. We show that this new synthetic route can be upscaled to a high volume yield of 10 wt%, thereby enabling large-scale applications. We further demonstrate the effect of the Janus balance on colloidal self-assembly. Janus particles with a dominant hydrophobic and a small hydrophilic patch aggregate into large clusters in water, but merely di- or trimerize in chloroform.

Introduction

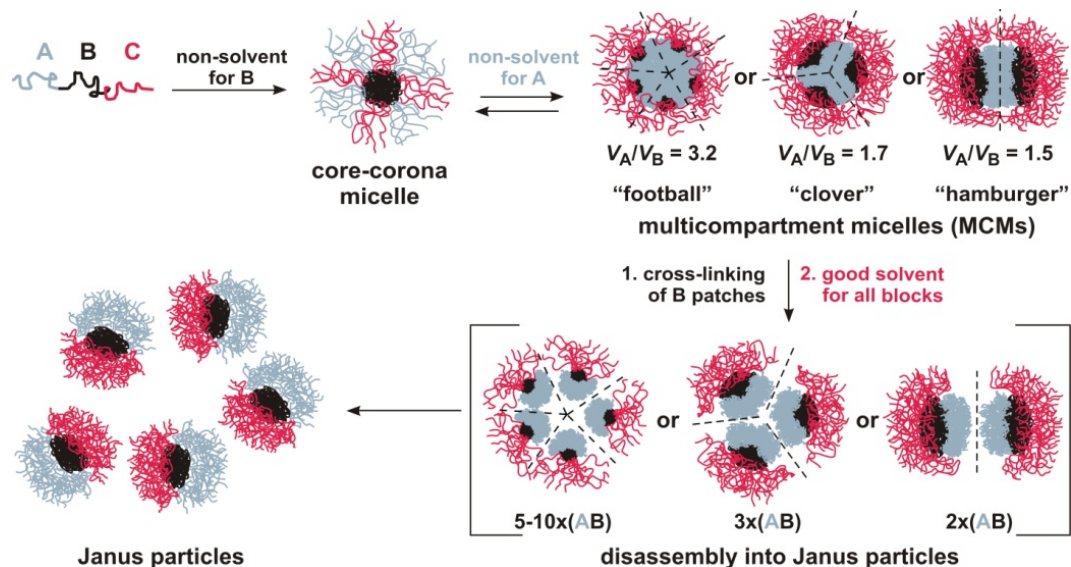
Janus particles (JPs) are non-centrosymmetric spherical, cylindrical, or disk-like colloids consisting of two phase-separated faces or compartments with distinct differences in chemical and/or physical properties.^[1-3] Over the past two decades, JPs have drawn widespread attention in soft matter nanoscience^[4] and materials science,^[5, 6] as nanomotors^[7-11], chemical or optical sensors,^[12-20] for programmable self-assembly,^[21-24] and biomedical applications.^[15-17, 25] Especially their superior affinity toward interfaces, as compared to homogeneous particles, raised considerable interest for applications as future surfactants and for nanostructuring of interfaces.^[3, 26-28] Walther *et al.* showed that one single amphiphilic polystyrene-block-polybutadiene-block-poly(methacrylic acid) (SBMAA) Janus particle with a radius of 10 nm stabilizes ca. $100 \times 100 \text{ nm}^2$ of an oil/water droplet interface and Binks *et al.* theoretically predicted a 2–3 times higher surface activity compared to surface isotropic particles.^[29, 30] The pronounced affinity toward interfaces makes JPs promising key building blocks for many technologically relevant applications, e.g., as surface coatings, stabilizers in emulsion polymerization or compatibilizers in polymer blends.^[1, 3, 31-33] Depending on the nature of the particle, its hemispheres may selectively respond to solvent polarity, pH, electric field, or other stimuli to yield switchable materials. In combination with the surface anisotropy, these responsive properties allow for programmable, colloidal self-assembly, which is currently in focus of soft matter research.^[21, 23, 34-37] The broken-symmetry renders JPs a unique particle class in the portfolio of patchy particles and complex colloids, in which shape and chemical anisotropy is used to impart molecule-like directionality for particle self-assemblies. For instance, very recently, Granick and co-workers reported on the directed self-assembly of amphiphilic, micrometer-sized JPs into nonequilibrium, complex triple helices by selective stimulation of the polyelectrolyte hemisphere with salt and kinetic selection of a self-assembly pathway.^[38] This example unambiguously demonstrates the potential manifesting from the ability to control and understand the self-assembly behavior of JPs.

The influence of the Janus balance, i.e., the relative sizes of both hemispheres, has hardly been addressed so far, which is mainly due to difficulties in developing simple synthetic methods – particularly challenging on the nanoscale. Implementation of JPs with tunable Janus balance would, however, benefit the development and understanding of particle self-assembly into complex materials. Sophisticated self-assembly in selective solvents was already indicated in the early beginnings by Erhardt *et al.*, who showed that SBMAA JPs self-assemble in water into clusters and supermicelles. In recent years, we further developed a comprehensive understanding of how different dimensionalities influence the self-assembly behavior by moving from spherical to cylindrical and disc-shaped JPs.^[34, 39-41] Numerous synthetic strategies have been reported to produce purely inorganic,^[42-45] polymer-inorganic hybrid JPs^[35, 45-48] as well as Janus polymersomes,^[49] microgels,^[47, 50] droplets,^[47, 51, 52] or fibers^[53, 54] in various shapes and geometries, mostly ranging from a few

hundred nanometers to micrometers. However, only few reports were devoted to the synthesis of soft organic JPs on the nanoscale.^[41, 55-61] Up to now, the cross-linking of triblock terpolymer bulk morphologies has been the most capable and efficient method to fabricate polymer-based JPs of controllable size from 10 nm (Janus micelles) to several micrometers (Janus cylinders, tapes, discs and sheets).^[41, 55, 61, 62] Although this method proved to be very successful over the past decade, the necessity of suitable polymer-polymer interaction parameters to enforce bulk segregation to the desired morphology limits the number of applicable polymers. This is especially pronounced for blocks in the weak segregation regime, e.g., for triblock terpolymers with short methacrylate blocks. Beyond that, casting, annealing and cross-linking the bulk morphology can be a time-consuming process with some restrictions in scale-up. Solution-based approaches to nanometer sized JPs comprise template-assisted methods using desymmetrization tools, template-free formation of complex coacervate micelles of oppositely charged polymer blocks or unimolecular intramolecular polyelectrolyte complexation of a suitable triblock terpolymer.^[58-60] However, in most cases tailored polymer block sequences, specific conditions or multistep processes considerably limit the number of materials that can be produced. It still remains a tremendous challenge to develop a versatile and simple method to produce soft, responsive, homogeneous JPs with nanoscale dimensions and tunable physical properties.^[1]

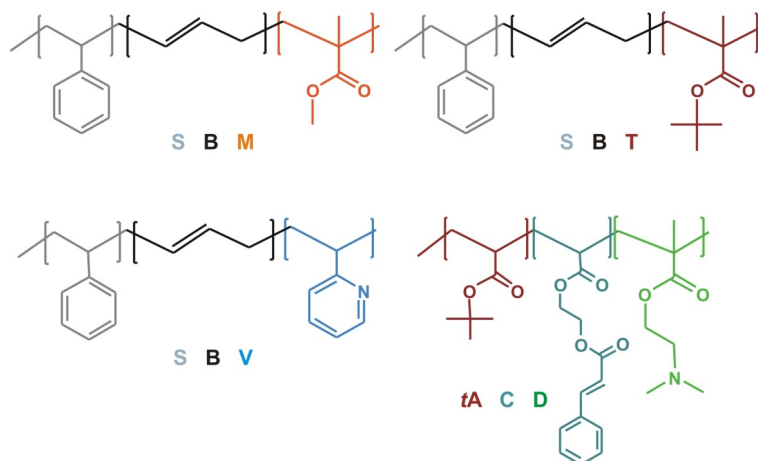
In this report, we demonstrate how to overcome these problems and establish a novel solution-based strategy to prepare a range of chemically and structurally different JPs. We take advantage of our recently developed approach to uniform multicompartment micelles (MCMs)^[63] formed by ABC triblock terpolymers in a step-wise, directed self-assembly process. The MCMs are constituted of cores of the A block, carrying compartments of the B block, and corona chains of the C block emanating from the B compartments (Scheme 5–1). The morphology can be directed to exclusively yield football, clover or hamburger MCMs (multiple, three or two B compartments) by adjusting the volume ratio, V_A/V_B , of the respective blocks. Cross-linking of the B compartments permanently fixates the phase-separated state and JPs are obtained after dissolution of the MCMs in a nonselective solvent. *No additional template or intermediate surface for desymmetrization is needed.* As a unique advantage of this procedure, we can prepare JPs with widely different volume fractions of blocks A and C and thus control the Janus balance. We show that the physical properties of the resulting JPs can be tuned by a number of polymer combinations suitable for this process. We follow the process using scattering and imaging techniques and analyze novel structural features such as tunable core radius and corona composition and its impact on the formation of colloidal superstructures. Finally, we demonstrate rapid synthesis on a larger scale and with high volume yields.

Scheme 5–1: Self-Assembly of ABC Triblock Terpolymers into Multicompartment Micelles and Subsequent Disassembly into Janus Particles. Adapted from *J. Am. Chem. Soc.* **2012**, *134*, 13850-13860. Reprinted with permission from the American Chemical Society.



Results and Discussion

5.1 Synthesis and Characterization of Janus Particles. Homogeneity in both size and fine structure of the MCMs, as uniquely enabled by our directed self-assembly approach,^[63] is decisive to synthesize uniform JPs via cross-linking of the B compartments and subsequent dissolution of the MCMs. We apply this new method to a wide range of triblock terpolymers as summarized in Chart 5–1. We first selected a range of polystyrene-*block*-polybutadiene-*block*-poly(methyl methacrylate) (SBM) triblock terpolymers to derive the effects of varying block weight fractions and overall molecular weight on the structure of the MCMs and the resulting JPs. Polystyrene-*block*-polybutadiene-*block*-poly(*tert*-butyl methacrylate) (SBT; *Pt*BMA acts as a precursor for water-soluble polymethacrylic acid, PMAA) and polystyrene-*block*-polybutadiene-*block*-poly(2-vinylpyridine) (SBV) form JPs with amphiphilic corona hemispheres. Finally, poly(*tert*-butyl acrylate)-*block*-poly(2-cinnamoyloxyethyl acrylate)-*block*-poly(2-(dimethylamino)-ethyl methacrylate) (*t*ACD) features completely different block chemistries. These particles give access to dipolar JPs with anionic and cationic hemispheres after deprotection of *t*A to poly(acrylic acid) and charge-up of D. It may be emphasized that the latter polymer is fully synthesized by controlled radical polymerization (here Atom Transfer Radical Polymerization), which can be easily accomplished with standard lab equipment. This represents some advantage compared to the stringent conditions needed for the anionic polymerization used to synthesize the other triblock terpolymers. The molecular characteristics of the triblock terpolymers such as block lengths, volume ratios, and the corona dimensions are summarized in Table 5–1 and Table S5–1 of the Supporting Information (SI).

Chart 5–1: Chemical Structures of ABC Triblock Terpolymers^a.

^a S = polystyrene, B = polybutadiene, M = poly(methyl methacrylate), T = poly(*tert*-butyl methacrylate), D = poly(2-(dimethylamino)ethyl methacrylate), C = poly(2-cinnamoyloxyethyl acrylate). *tA* = poly(*tert*-butyl acrylate). Adapted from *J. Am. Chem. Soc.* **2012**, *134*, 13850-13860. Reprinted with permission from the American Chemical Society.

Table 5–1: Characteristics of Triblock Terpolymers, Multicompartment Micelles and Janus Particles Used in this Study

Code ^a	Polymer ^c	MCM	$N_{\text{com-partments}}$	$R_{\text{h, MCM}}$ [nm] ^d	$R_{\text{h, JP}}$ [nm] ^e	R_{core} [nm] ^f	f_{core} [wt%]	JB_{A} ^g [mol%]
SBM1	S ₃₁₀ B ₁₅₀ M ₃₄₀ ⁷⁴	football	10-12	42 ± 6	19 ± 3	5.9 ± 1.2	11	47
SBM2	S ₃₄₀ B ₃₃₀ M ₃₆₀ ⁹⁰	clover	3	36 ± 4	25 ± 4	10.9 ± 1.7	20	48
SBM3	S ₆₁₀ B ₆₄₀ M ₂₉₀ ¹²⁷	large football	5-7	54 ± 5	35 ± 3	15.4 ± 2.3	27	68
SBM4	S ₂₈₀ B ₃₃₀ M ₄₃₀ ⁹⁰	hamburger	2	37 ± 4	27 ± 3	10.4 ± 1.7	20	39
SBT ^b	S ₅₁₀ B ₅₄₀ T ₃₅₀ ¹³²	clover	3	34 ± 3	30 ± 4	9.1 ± 1.6	22	59
SBV	S ₃₆₀ B ₃₈₀ V ₅₉₀ ¹²⁰	clover	3	36 ± 4	29 ± 7	6.9 ± 1.3	17	38
<i>tACD</i>	<i>tA</i> ₁₉₀ <i>C</i> ₇₀ <i>D</i> ₁₁₀ ⁵⁹	hamburger/ clover	2-3	36 ± 7	18 ± 3	8.1 ± 1.3	30	63

^a For abbreviations see text and Chart 5–1. ^b Fraction of 1,4-butadiene units ca. 10 mol %; all SBM triblock terpolymers ca. 90 mol %. ^c Subscripts denote the number-average degree of polymerization and superscripts the overall molecular weight in kg/mol determined via combination of GPC using THF as the eluent and PS calibration and ¹H-NMR spectroscopy. ^d MCMs measured at $c = 1$ g/L: SBM1–4 in acetone/isopropanol (70:30 v/v), SBT in ethanol, SBV in isopropanol and *tACD* in pH 6 water. ^e *tACD* JPs were measured in pH 3 water and all others in DMAc at $c = 1$ g/L (see Figure S1 for distributions). ^f Average of 250 JP core radii determined by TEM image analysis. ^g JB_{A} describes the Janus balance as the molar fraction of block A in the corona: $JB_{\text{A}} = DP_{n,\text{A}} / (DP_{n,\text{A}} + DP_{n,\text{C}})$

The detailed mechanism of MCM formation is described in our previous report.^[63] In the following, we shortly discuss the general mechanism to derive SBM JPs from SBM MCMs (Figure 5–1). The SBM triblock terpolymer is dispersed in a nonsolvent for the PB middle block to give core-corona micelles with a PB core and a patchy PS/PMMA corona. Subsequent dialysis of these core-corona micelles into a nonsolvent for both PS and PB initiates

clustering into spherical MCMs. During this step, the corona patches (PMMA/PS) rearrange to minimize the energetically unfavorable PS/nonsolvent interface inducing aggregation along exposed PS patches. Depending on the volume ratio, V_{PS}/V_{PB} , we obtain MCMs with two, three, or multiple PB compartments, which we term “hamburger”, “clover” or “football” MCMs, respectively. Within these MCMs, the phase-separated state is permanently fixated by selective UV-cross-linking of the PB compartments with a photoinitiator. Subsequent redispersion in a good solvent for PS and PMMA breaks up the MCMs and liberates single, core-cross-linked SBM JPs. In a control experiment, we cross-linked the core-corona micelles (in the first selective solvent) prior to dialysis into the second solvent, which merely resulted in ill-defined aggregates. This can be attributed to the frozen, immobilized polymer chains after cross-linking and proves that only a mixed or patchy distribution of PS and PMMA chains is present in the first nonsolvent.^[63-65] Thus, the self-assembly step into MCMs is essential to achieve complete phase separation and symmetry-breaking.

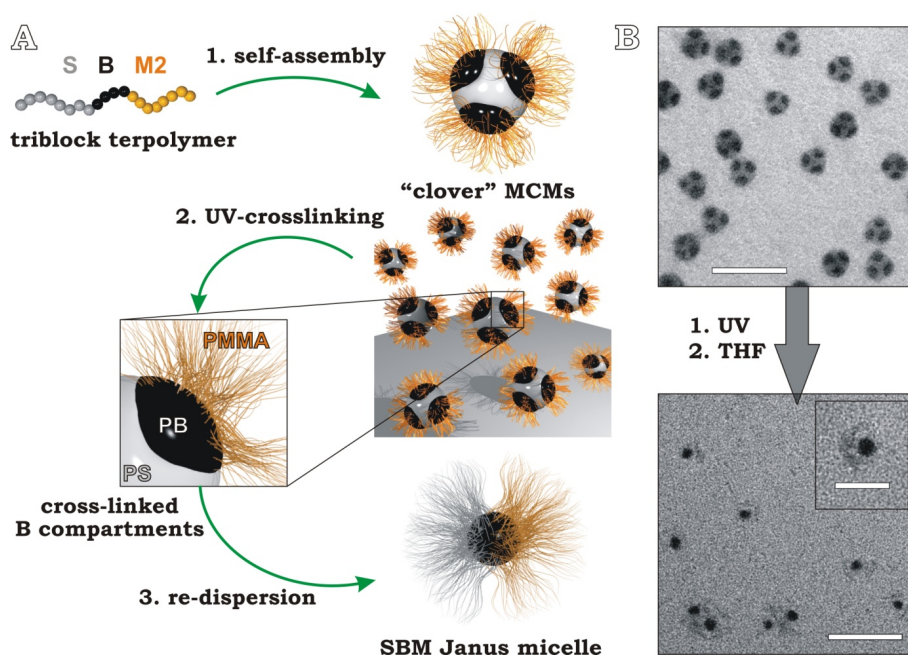


Figure 5–1: (A) JP synthesis via self-assembly of multicompart ment micelles, subsequent cross-linking of the compartments and redispersion in THF. (B) Corresponding TEM images of SBM2 “clover” MCMs and derived JPs. OsO₄ staining: PS grey, PB black and PMMA is invisible due to electron beam degradation. Scale bars are 200 nm and 50 nm in the inset. Adapted from *J. Am. Chem. Soc.* **2012**, *134*, 13850-13860. Reprinted with permission from the American Chemical Society.

Figure 5–1 displays SBM2 “clover” MCMs with a discrete number of 3 PB compartments and very high regularity (over 92 % trimers; Figure 5–1B). These were prepared via dispersion in *N,N*-dimethylacetamide (DMAc) to form micelles with a PB core and a patchy PS/PMMA corona and subsequent dialysis into acetone/isopropanol (70:30 v/v). After addition of a photoinitiator and selective UV-cross-linking of the PB compartments, we obtain single JPs in THF with a cross-linked PB core and hemispheres of PS and PMMA due to disassembly of the former MCMs.

According to ^1H NMR the signals for the double bonds completely disappear while the PS to PMMA signal ratio remains constant (Figure S5–3 [SI]). These findings point to both a tight cross-linking and intact corona hemispheres (i.e., no radical cleavage or side reactions). The successful cross-linking was further confirmed by the detection of defined particles with a hydrodynamic radius of $\langle R_h \rangle_z = 36 \pm 4$ nm (PDI = 1.10) in THF via dynamic light scattering (DLS) (Table S5–1 and Figure S5–2 [SI]). The regular size distribution is corroborated by the corresponding TEM images depicting a very homogeneous population of JPs (Figure 1B). Most importantly, TEM imaging also gives an unambiguous proof of the Janus character, as the PS hemisphere clearly emanates as a gray shadow from only one side of the dark PB cores (OsO₄ staining: PS grey, PB black and PMMA not visible due to electron beam degradation). Note that these gray patches are randomly oriented excluding drying artifacts (see also Figure 5–4B).

5.2 Control of the core size of JPs. Next, we use the series of SBM triblock terpolymers to deduce the relation between PB block length, $DP_{n,\text{PB}}$, and core radius, R_{core} , of the JPs (Figure 5–2). For this purpose, we synthesized JPs from SBM triblock terpolymers (SBM1, SBM2 and SBM3) with increasing block lengths of PB, $DP_{n,\text{PB}} = 150, 330, \text{ and } 640$. The TEM images of MCMs in the center column of Figure 5–2 already illustrate a size increase of the black PB compartments, which then effectively translates into larger core radii of the JPs after cross-linking. An evaluation of 250 PB compartments for each sample yields sizes of $R_{\text{TEM}} = 4.9 \pm 1.0$ nm for SBM1 "football" MCMs ($f_{\text{PB}} \approx 11$ wt%), $R_{\text{TEM}} = 9.9 \pm 1.7$ nm for SBM2 "clover" MCMs ($f_{\text{PB}} \approx 20$ wt%) and $R_{\text{TEM}} = 13.7 \pm 1.9$ nm for SBM3 "large football" MCMs ($f_{\text{PB}} \approx 27$ wt%). Note that especially in bulk morphologies, which have been pursued as source for SBM JPs so far, the weight fraction of the middle block usually cannot exceed 8-10 wt%, as otherwise spheres evolve into cylinders or lamellae.^[66] Hence, nanoscale, soft JPs with such large core fractions (here up to $f_{\text{PB}} = 27$ wt%) can only be obtained with the presented solution approach. This is expected to be an important aspect for instance in Pickering emulsions as the desorption energy from an interface scales with the squared radius of the applied particles ($E \sim R^2$) and better nanoscale Pickering emulsifiers could be obtained by simply increasing the solid core radius, while maintaining the overall dimensions (core plus corona).

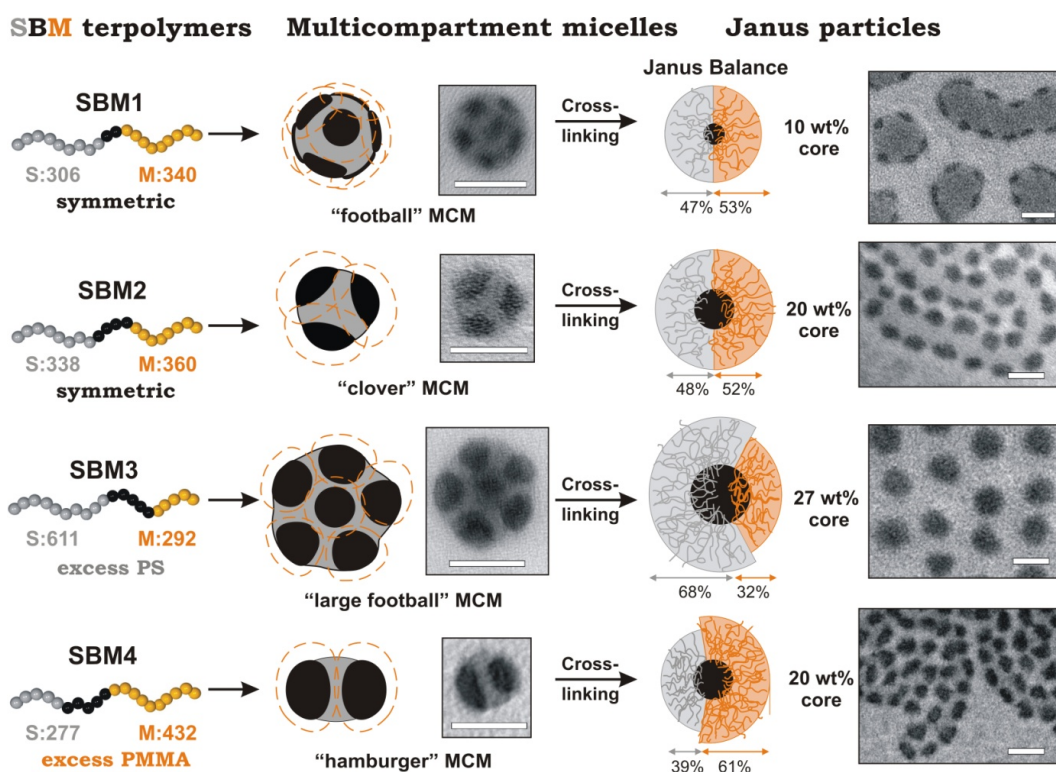


Figure 5–2: Tuning of core size and Janus balance of the JPs. TEM images of JP aggregates obtained from THF solution. OsO₄ staining: PS gray, PB black, and PMMA is not visible due to electron beam degradation. Scale bars are 50 nm. Adapted from *J. Am. Chem. Soc.* **2012**, *134*, 13850-13860. Reprinted with permission from the American Chemical Society.

After cross-linking and redispersion in THF, all JPs exhibit slightly oblate ellipsoidal cores with radii correlating to the initial MCM compartments, as expected. We further evaluated the core radii of SBM JPs on basis of TEM images prepared from THF dispersions. Upon drying on the TEM grid, the particles partly self-assemble into characteristic patterns (Figure S5–4 [SI]). The PB cores are then located as black dots or ellipsoids at the interface between the PMMA-rich (bright) and the PS-rich (gray) phase.

Table 5–2: Relation between Molecular Characteristics of the SBM Triblock Terpolymers and the Dimension of the PB Compartments in MCMs and the JPs Cores

Code ^a	Polymer ^b	M_{PB}^{chain} [kg/mol]	$DP_{n,PB}$	$R_{PB,MCM}^c$ [nm]	R_{core}^c [nm]	$N_{agg,app}^d$
SBM1	S ₃₁₀ B ₁₅₀ M ₃₄₀	8.1	150	4.9 ± 1.0	5.9 ± 1.2	47 ± 28
SBM2	S ₃₄₀ B ₃₃₀ M ₃₆₀	18.0	330	9.9 ± 1.7	10.9 ± 1.5	174 ± 81
SBM3	S ₆₁₀ B ₆₄₀ M ₂₉₀	34.3	640	13.7 ± 1.9	15.1 ± 1.9	257 ± 115

^a For abbreviations see text and Chart 5–1. ^b Subscripts denote the number-average degree of polymerization. ^c Determined from TEM of the Janus particles cast from THF solution. ^d According to eq. 5–1 in the Supporting Information.

SBM3 preferably orients with one side to the hydrophobic carbon coating of the copper grid due to favorable interactions with excess PS. The formation of these patterns does, however, not obstruct the evaluation of the sizes of the PB cores as summarized in Table

5–2 (average values of 250 core radii; see Figure S5–5 [SI] for distributions). The core radii of our JP's follow a power law dependence on the PB block length with an exponent of $x = 0.73 \pm 0.10$, which is in accordance with theoretical expectations for micelles intermediate between the star-like and crew-cut regime. Details are given in the Supporting Information in Figure S5–6 and Figure S5–7.

5.3 Control of the Janus balance. A characteristic feature of JPs, decisive for interfacial activity and self-assembly, is the ratio of surface phase-separation/compartmentalization, termed Janus balance, JB .^[67] Recent studies showed that the free energy upon particle adsorption to water/oil interfaces can be significantly altered via the Janus balance.^[30] In fact, very little effort has so far been devoted to understanding the influence of the JB on the type of self-assembled superstructure. This is to some extent due to the difficulties of tailoring this ratio with synthetic means. In our approach, we have a convenient molecular handle, encoded by precise macromolecular engineering, to distinctly manipulate this balance by modifying the A and C block lengths accordingly. In our MCM-based JPs, both patches have an identical number of polymer chains by definition. The ratio of monomer units of both polymer chains is, at first approximation, sufficient to describe the symmetry or asymmetry of the two corona hemispheres. The contribution of one patch to the JB is then expressed by eq 5–1:

$$JB_A = \frac{DP_{n,A}}{DP_{n,A} + DP_{n,C}} \quad (5-1)$$

For instance, SBM2 JPs have symmetrical patches and we can quantify the contribution of the PS block to the Janus balance as $JB_{PS} = 48\%$ (or vice versa $JB_{PMMA} = 52\%$). Assuming equal swelling of both corona blocks, equal volumes of both hemispheres are expected. On the contrary, SBM3 ($DP_{n,PS} = 610$, $DP_{n,PMMA} = 290$) and SBM4 ($DP_{n,PS} = 280$, $DP_{n,PMMA} = 430$) are triblock terpolymers with asymmetric end blocks. SBM3 has a $JB_{PS} = 68\%$ and thus a dominant patch of PS, whereas SBM4 JPs with a $JB_{PS} = 39\%$ have a dominant PMMA patch. Figure 5–2 schematically depicts the distribution and ratios of both patches.

5.4 Self-Assembly of Asymmetric PS-PB-PMAA (SBMAA) Janus Particles. JPs with equally sized patches (symmetric hemispheres) are expected to form the same equilibrium superstructures if brought into selective solvents for either side, because the conditions for aggregation are, in principle, identical in both cases. It stands to reason that asymmetric JPs will behave differently and self-assemble into clusters whose shape and size is strongly dependent on the patch size ratio (Janus balance) and the selective solvent. In the previous chapter we determined the Janus balance of SBM3 JPs to be $JB_{PS} = 68\%$ corresponding to a dominant PS patch. To enhance the solvent selectivity of the patches, we hydrolyzed the hydrophobic PMMA side to yield very hydrophilic poly(methacrylic acid) (PMAA). Self-assembly of the now strongly amphiphilic SBMAA3 JPs was then triggered by dialysis

from THF, which is a solvent for both PS and PMAA, into either chloroform (selective for PS) or water pH 10 (selective for PMAA) (Figure 5–3).

We observe concentration-dependent self-assembly of the SBMAA3 JPs via the solvophobic PS patches, when dialyzed from THF into alkaline solutions. The TEM image series in Figure 5–3A shows a progressive increase in cluster size as a function of the JP concentration. Below a critical aggregation concentration, $cac \approx 0.05$ g/L,^[34] single JPs are the dominant species in TEM. DLS corroborates this finding as the $\langle R_h \rangle_z = 50$ nm is in good agreement with the R_h obtained for single SBM3 JPs in THF ($\langle R_h \rangle_z = 49$ nm). The Janus character is clearly visible from the gray PS shadow emanating from only one side of the black PB core (OsO₄ staining).

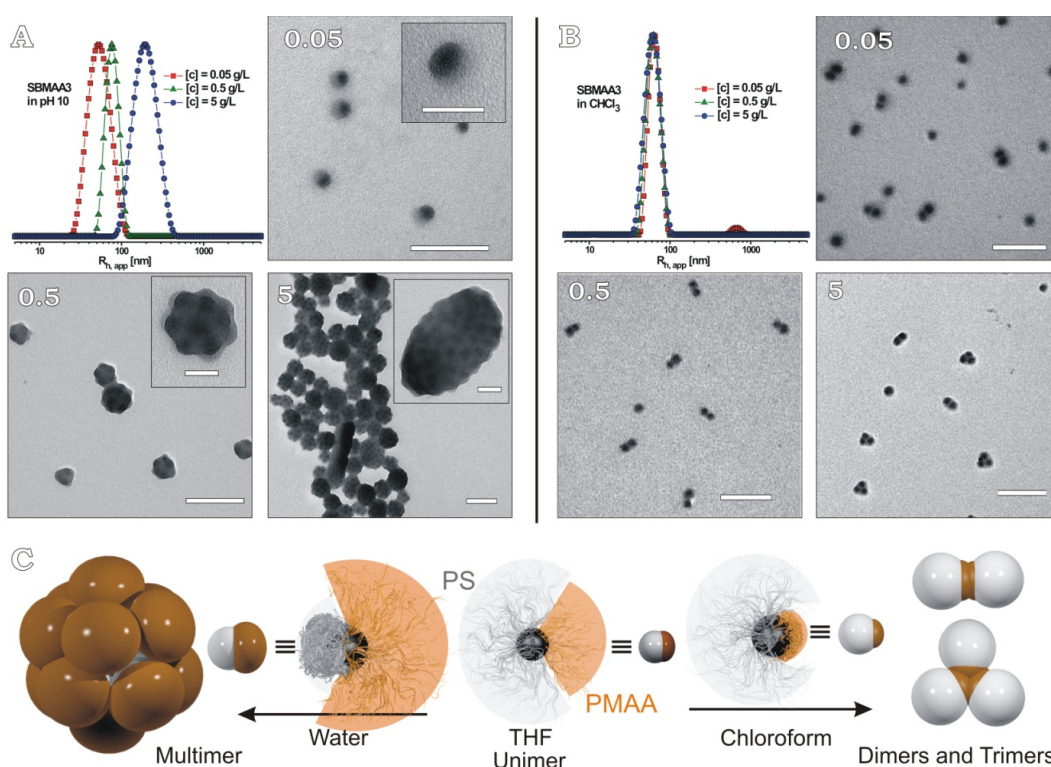


Figure 5–3: Self-assembly of SBMAA3 JPs in water and chloroform: (A) DLS size distributions and respective TEM images of clusters obtained after dialysis into water pH 10 at $c = 0.05$ g/L, 0.5 g/L and 5 g/L. (B) DLS size distributions and respective TEM images of unimers to trimers in chloroform at $c = 0.05$ g/L, 0.5 g/L and 5 g/L (OsO₄ staining: PS grey, PB black, PMMA not visible. Scale bars are 100 nm and 50 nm in insets). (C) Schematic clustering of asymmetric JPs in dependence of the corona size in chloroform and water pH 10. Here also PS is grey and PB is black. Adapted from *J. Am. Chem. Soc.* **2012**, *134*, 13850-13860. Reprinted with permission from the American Chemical Society.

Considering the number of polymer chains per JP ($N_{\text{agg,app}} \approx 260$ for SBMAA3, Table 5–2 and [SI]) a molecular weight of several million g/mol ($M_{\text{SBMAA3}} \approx 3.2 \cdot 10^6$ g/mol) is easily achieved for the JPs, and thus, the molar concentration at 0.05 g/L is only $c \approx 1.6 \cdot 10^{-8}$ mol/L. This low concentration reduces the probability of two JPs to aggregate during dialysis before the PMAA corona is progressively swelling and extended enough to provide complete shielding of the hydrophobic core (now PB+PS) against further aggrega-

tion. We observed a related behavior also in earlier studies on SBMAA Janus discs with much larger PS surfaces compared to those of the JPs here, where a substantial part of the Janus disks had PS surfaces unfavorably exposed to water.^[40] Complete coverage of the hydrophobic core by PMAA chains can, in fact, be visualized via selective staining of the PMAA corona chains with uranyl acetate ($\text{UO}_2(\text{OAc})_2$) (see Figure S5–8 [SI]). Consequently, the Janus balance is inverted during the solvent exchange. If the concentration during dialysis is above the cac and two or more JPs are in close proximity or even in contact, the solvophobic PS patches undergo enough “effective” collisions and aggregate to minimize the disfavored PS/water interaction. At higher concentrations of 0.5 g/L, a fraction of JPs self-assemble into clusters consisting of 10 – 20 JPs reminiscent of their prior “football” MCM morphology (Figure 5–2). DLS measurements confirm clustering with an increase of the hydrodynamic radius to $\langle R_h \rangle_z = 89$ nm. At a concentration of 5 g/L much larger aggregates are found with slightly elliptical shape and a cluster size typically exceeding 50 JPs ($\langle R_h \rangle_z = 194$ nm). Note, that z-averaged hydrodynamic radii obtained by DLS overestimate larger particles and thus do not adequately represent the number-averaged size increase deduced from TEM. The polydispersity of these aggregates also increases with concentration, but individual JPs can no longer be found at 5 g/L.

To rationalize this behavior in terms of equilibrium or non-equilibrium self-assembly, one has to consider the time scales of dialysis and self-assembly, as well as the length scales of the JPs and corona arms and their dynamic changes. During solvent exchange, there is an interplay between the kinetics of particles colliding sufficiently often to form clusters and reach near-equilibrium aggregates, and the process of increasing swelling of PMAA and collapse of PS due to the continuous infiltration of water, arresting the growth potentially prematurely. The frequency of particle collisions per time is essentially controlled by their molar concentration, which is partly very low, thus requiring long equilibration times. The process of collapse and extension of solvophobic and solvophilic arms acts on a similar time scale for all concentrations but is decisive to induce kinetic control. In fact, the length scales of the JPs herein are peculiar, because the corona chains are sufficiently long to reach around the particle core, thus leading to an in situ change (here inversion) in Janus balance. Such a phenomenon cannot be expected for solid JPs with short ligands or large colloids grafted with polymers, in which the dimensions of the corona can be neglected compared to those of the solid core. Therefore, we deal with a complex self-assembly process, in which dynamic changes of the Janus balance and concentration-dependent reaction kinetics interact. Growth into near-equilibrium self-assemblies for a given Janus balance may only occur in a narrow window of solvent conditions and requires sufficient time. Here, this window rapidly closes due to continuously increasing water content, and rapid changes in the Janus balance hamper dynamics, efficient collisions, and further growth. Hence, the measured aggregates represent intermediate structures trapped in a non-

equilibrium state. This is underscored by the fact that dilution of the large aggregates found at, e.g., 5 g/L does not lead to breakup into smaller clusters or individual micelles.

In contrast, when we dialyze the JPs from THF into chloroform, we only observe unimers to trimers in DLS and TEM (Figure 5–3B), almost independent of the concentration. Unlike in water, the hydrodynamic radius does not change, because the Janus balance does not undergo drastic changes during dialysis and the collapsed PMAA patch is completely protected by the much larger, expanded PS corona (Figure 5–3C). In concentration dependent DLS measurements the hydrodynamic radii remain constant at $\langle R_h \rangle_z = 60$ nm. Unimers, dimers and trimers are the dominant species in TEM, which aggregate via the collapsed PMAA patch. The weaker solvophobic forces and the minor changes in Janus balance probably allow for an easier equilibration and the formation of near-equilibrium self-assemblies.

5.5 Generalization of the concept. Another intriguing feature of the presented approach is the easy access to a multitude of chemistries in the corona hemispheres that so far remained inaccessible for a number of desired polymeric nanoscale JPs. Above, we already established the preparation of various SBM JPs. Next, we demonstrate the general applicability of our concept on the preparation of PS-PB-*Pt*BMA (SBT), PS-PB-P2VP (SBV) and *Pt*BA-PCEA-PDMAEMA (*t*ACD) JPs, following the same general protocol as described for SBM triblock terpolymers, except for the choice of solvents (Figure 5–4).

PS-PB-*Pt*BMA (SBT) was first dispersed in DMAc as the nonsolvent for PB and annealed for 24 h at 70 °C. Except for the good solubility of *Pt*BMA in alcohols, SBT terpolymers are very similar in structure and polarity to those of SBM. Since PS is insoluble in alcohols, ethanol as a single solvent is sufficient to form stable "clover" MCMs with $\langle R_h \rangle_z = 34 \pm 6$ nm (Figure 5–4A). The SBT used here has almost identical block ratios ($V_{PS}/V_{PB} = 1.7$) as SBM2 and, as expected, the MCMs also contain three compartments with an abundance of > 92%. After cross-linking, the JPs were redispersed in DMAc yielding $\langle R_h \rangle_z = 30 \pm 9$ nm (Figure S5–1, [SI]) with a core radius of $R_{TEM} = 9.1 \pm 1.6$ nm in TEM (Figure 5–4B). According to the block lengths, we obtain JPs with a dominant PS patch ($JB_{PS} = 59\%$) The Janus character is clearly visible as the gray PS patch exclusively emanates from one side of the black PB core (OsO₄ stained). The unfavorable interfacial tensions in the SBT system prevent a lamella–sphere bulk morphology even for very small fractions of PB^[41] and, hence, SBT JPs are one example of an end block combination unique to this solution-based process.

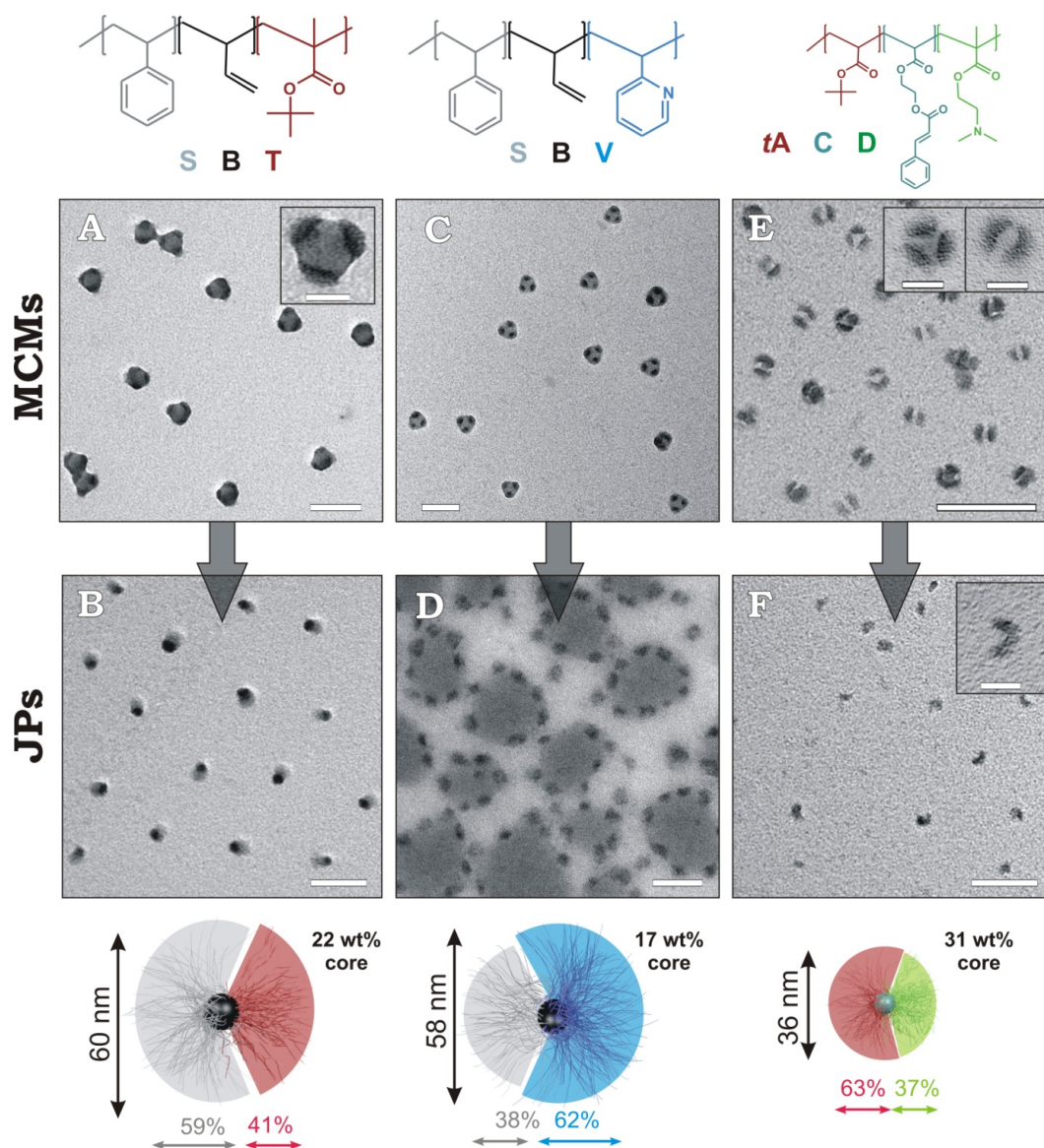


Figure 5-4: MCMs and resulting JPs after crosslinking: (A, B) SBT "clover" MCMs in ethanol and JPs in DMAc. (C, D) SBV "clover" MCMs in isopropanol and JPs in DMAc (A-D: OsO₄ staining: PS grey, PB black, P2VP dark grey and PtBMA not visible). (E, F) tACD "clover" and "hamburger" MCMs at pH 6 and JPs at pH 3 (RuO₄ staining: PCEA black, PtBA bright grey and PDMAEMA not visible). All scale bars are 100 nm and 25 nm in the insets. Adapted from *J. Am. Chem. Soc.* **2012**, *134*, 13850-13860. Reprinted with permission from the American Chemical Society.

The amphiphilic triblock terpolymer PS-PB-P2VP (SBV) was dispersed in DMAc as the nonsolvent for PB, annealed for 24 h at 70 °C and then dialyzed into isopropanol (selective for P2VP). Self-assembly occurs via the insoluble PS patches into "clover" MCMs (Figure 5-4C). The cross-linked JPs were redispersed in DMAc and measured with DLS ($\langle R_h \rangle_z = 29 \pm 7$ nm, Figure S5-1, [SI]) and TEM ($R_{\text{TEM}} = 6.9 \pm 1.3$ nm, Figure 5-4D). Again both corona blocks (PS and P2VP) are soluble in DMAc and JPs are identified in TEM, arranged in a circular fashion. It is evident that the black dots correspond to the PB core located at the interface of the dark gray P2VP and the bright gray PS phase. The JPs tend to aggregate along the P2VP patches upon drying on the TEM grid. The circular aggregation pattern may be attributed to the strong amphiphilic nature and the dominant P2VP

patch with $JB_{P2VP} = 62\%$. P2VP broadens the scope of JPs as it can be protonated or quaternized and easily gives access to hybrid materials by coordinating metals or semiconductor NPs. It may further serve in the buildup of inter-polyelectrolyte complexes with polyanions or anionic hemispheres of other JPs on the way to controlled colloidal self-assembly.

Finally, “clover” and “hamburger” MCMs of *Pt*BA-PCEA-PDMAEMA (*t*ACD) with $\langle R_h \rangle_z = 36 \pm 14$ nm were prepared by direct dispersion in isopropanol (selective for *t*A and D) to form PCEA core micelles with a patchy *Pt*BA/PDMAEMA corona and subsequent dialysis into water (pH = 6, selective for PDMAEMA). From earlier investigations we know that the PDMAEMA block poorly phase-separates in bulk from other poly(meth)acrylates. Yet, in solution this problem can be overcome as polymer-polymer interactions (bulk) are substituted by easily adjustable polymer-solvent interactions. RuO_4 selectively stains the aromatic groups of PCEA and mostly 2–3 black PCEA compartments per MCM are clearly visible in TEM (Figure 5–4E). The cinnamoyl moieties of the PCEA block provide an attractive, additive-free cross-linking chemistry, as they are able to dimerize under UV-irradiation at a wavelength of $\lambda_{max} = 300$ nm.^[68, 69] After cross-linking, we imaged *t*ACD JPs in pH 3 (Figure 5–4F) with a core radius of $R_{TEM} = 8.1 \pm 1.3$ nm (both, PCEA and *Pt*BMA are collapsed) and an $\langle R_h \rangle_z = 18 \pm 3$ nm in DLS. According to the block lengths, we obtain JPs with a dominant *Pt*BA patch ($JB_{PtBA} = 63\%$). The *t*ACD triblock terpolymer is a precursor for the fabrication of ampholytic, dipolar JPs responsive to changes in pH and temperature and at the same time exclusively composed of (meth)acrylate blocks synthesized via sequential ATRP.

5.6 Scale-up. The demonstrated solution-based process is not only of academic significance, but also very attractive for fast and large-scale synthesis as needed in technological applications. SBM triblock terpolymers are, in fact, already commercially available and their self-assembly is triggered solely by solvents that could be retrieved after precipitation of the JPs. Exemplified on SBM2, we demonstrate additional efforts to increase the volume yield and simplify production (Figure 5–5). For reasons of simplicity we will focus on the MCM homogeneity as a measure of the final quality of the JPs.

Figure 5–5A shows SBM2 “clover” MCMs prepared via our dedicated two-step process furnishing most homogeneous MCMs. This typically involves dispersion in DMAc at a concentration of 1 g/L followed by dialysis into acetone/isopropanol (70:30 v/v). Controlled solvent transitions help to reduce kinetic barriers and facilitate the structural evolution from random coil to uniform MCMs. However, SBM2 MCMs can also be prepared faster in a single-step dialysis procedure, directly from THF into acetone/isopropanol (70:30 v/v), which leads to MCMs of good quality (Figure 5–5B). Further details on this “direct dialysis” approach can be found in our previous publication.^[63] Benefits of this ap-

proach are utilization of THF as the starting solvent and the very fast replacement of THF with acetone/isopropanol, practically completed within one hour (Figure 5–5F).

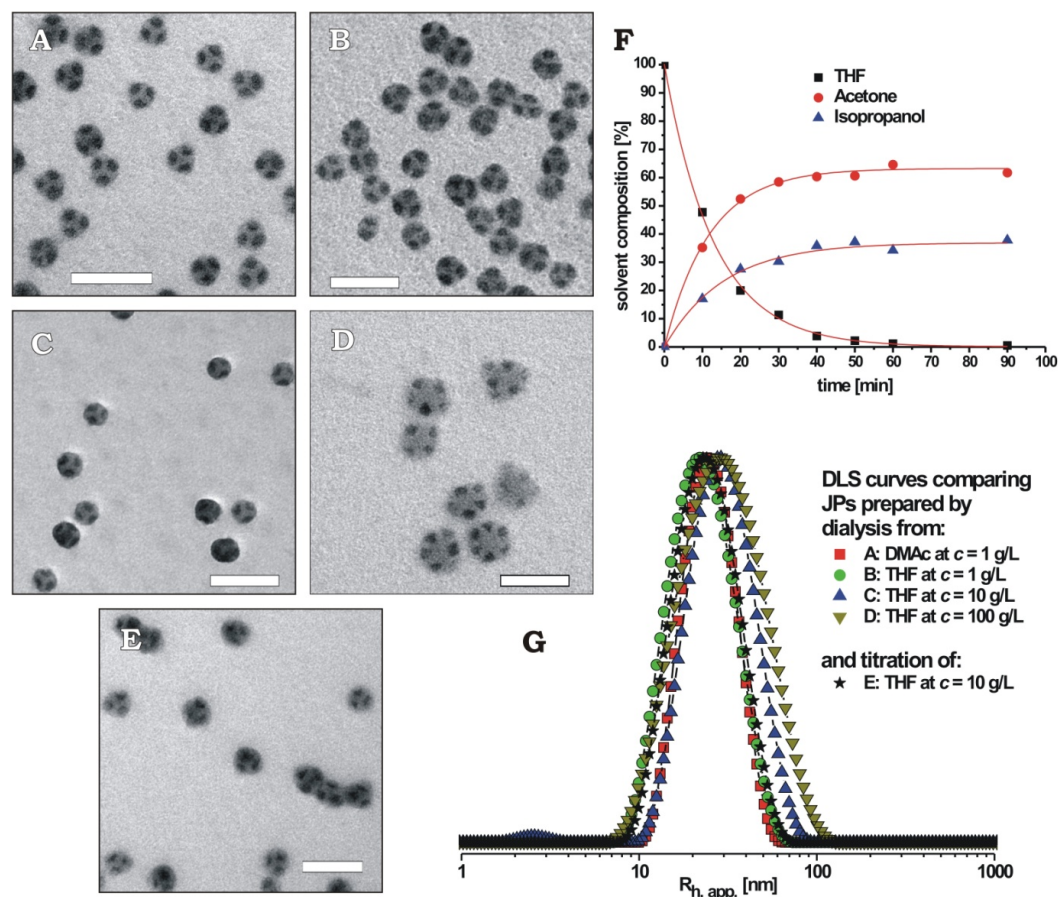


Figure 5–5: Influence of preparation protocol on MCM homogeneity: (A) SBM2 MCMs prepared via two-step dialysis at $c = 1$ g/L. (B–D) SBM2 MCMs prepared via direct dialysis of (B) 1 g/L, (C) 10 g/L and (D) 100 g/L THF solutions against acetone/isopropanol (70/30 v/v). (E) SBM2 MCMs prepared via addition of acetone/isopropanol (70/30 v/v) to a 10 g/L SBM2 solution in THF (OsO₄ staining: PS grey, PB black and PMMA not visible due to electron beam degradation). Scale bars are 100 nm). (F) ¹H-NMR monitoring of the solvent composition during direct dialysis of 50 ml of a 1g/L solution of SBM2 in THF into 5 L acetone/isopropanol (70/30 v/v). (G) Intensity weighted DLS size distributions of JPs prepared under different conditions (A)–(E) and measured in DMAc at $c = 1$ g/L after crosslinking. Adapted from *J. Am. Chem. Soc.* **2012**, *134*, 13850–13860. Reprinted with permission from the American Chemical Society.

More importantly, the maximum output within a single production cycle can be considerably increased using very high concentrations. Although Figure 5–5D shows a higher number of compartments per MCM, the overall process is not disturbed as the blocks still show complete phase separation. This allows us to synthesize SBM2 JPs of reasonable quality by "direct dialysis" at significant concentrations of 10 wt% (100 g/L). Alternatively, dialysis can be avoided completely by direct addition of an excess of nonsolvent to a concentrated solution of the triblock terpolymer in THF. Such a titration method is commonly used to study micelle formation of block copolymers^[70] and yields SBM2 MCMs of acceptable quality by adding 18 mL acetone/isopropanol (70:30 v/v) to 2 mL of a 10 g/L SBM2 solution in THF at a rate of 1 mL/min equaling a final concentration of 1 g/L (Figure 5–5E).

In Figure 5–5G we compare the DLS size distributions of JPs originating from MCMs prepared by the two-step dialysis, direct dialysis at concentrations of 1, 10 and 100 g/L and the described titration experiment to assess the quality of the JPs. The distributions of hydrodynamic radii reveal an excellent consistency and demonstrate that nearly identical JPs can be prepared while raising the concentration by two orders of magnitude and under accelerated and simplified preparation conditions. We observe a slight broadening of the distribution, potentially caused by the slightly less homogeneous PB compartments of the MCMs upon increasing concentration. Only direct dispersion of the triblock terpolymers in the final solvent or solvent mixture would be faster, but this method is typically not applicable to triblock terpolymers due to the long dissolution times for solvophobic blocks and the often resulting ill-defined structures.^[63]

In summary, applying these improvements, the entire production cycle can be reduced to only a few hours. Fast solvent exchange or even simple solvent addition combined with the possibility to use concentrated solutions of up to 100 g/L make this procedure a meaningful candidate for production of tunable terpolymer-based JPs on a larger scale and further transfer into technologies.

Conclusion

We demonstrated a straightforward, solution-based approach to prepare Janus particles with widely tunable structural and physical properties by cross-linking uniform compartments of spherical multicompartment micelles (MCMs). The MCMs were derived from linear ABC triblock terpolymers in selective solvents by a step-wise self-assembly process. Templates or interfaces for de-symmetrization are unnecessary. The core size of the Janus particles can be controlled by the length of the triblock terpolymer middle block. Further, we demonstrated that the concept applies to a range of triblock terpolymers and we expect validity to most polymers chemistries. Our method satisfies the need for the development of rapid and simple synthetic methods allowing functionality and responsiveness to be easily expanded, promoting the creation of comprehensive libraries. Most importantly, the Janus balance (i.e., the relative volumes of the corona hemispheres) can be controlled by synthetically adjusting the lengths of the outer blocks of the triblock terpolymers as they directly translate into the JP corona. We showed that the self-assembly of asymmetric Janus particles in selective solvents for the respective hemispheres leads to either a concentration-dependent cluster growth, when the majority of the corona is switched insoluble, or to an almost concentration-independent persistence of unimers, dimers and trimers when the minority of the corona is switched insoluble. The underlying complexity of this process is caused by competing dynamic changes of the Janus balance due to high volume ratios of corona to core, polymer dynamics that are influenced by the solvophobicity (from dynamic to frozen), and concentration-dependent reaction kinetics. The demonstrated self-assembly behavior and the question of non-equilibrium vs. near-equilibrium self-assembly provides

an intriguing glimpse into the emerging research field of self-assembly of patchy soft nanoobjects. Comprehensive studies on self-assembly of such asymmetric JPs with dynamic coronas are currently pursued by us and will be reported in due course. This solvent-based, template-free approach will be a vital step towards further technological breakthroughs of Janus particles, as it is simple, versatile and, in particular, scalable. This methodology brings about the necessary tools to tailor their size and Janus balance and, in combination with macromolecular engineering, gives access to highly functional and responsive corona hemispheres. This can profoundly assist in a further understanding of the complex self-assembly of Janus particles and their use in applications.

Associated Content

Supporting Information

Methods and Materials, full Experimental Section, polymer Characteristics and further details on synthesis and characterization of the block copolymers using $^1\text{H-NMR}$, DLS, and TEM. This material is available free of charge via the Internet at <http://pubs.acs.org>.

Author Information

Corresponding Authors

andre.groeschel@uni-bayreuth.de (A.H.G.), axel.mueller@uni-bayreuth.de (A.H.E.M.)

Notes

The authors declare no competing financial interest.

Acknowledgements

This work was supported by the *Deutsche Forschungsgemeinschaft* within SFB 840 (TP A1 and A2) and Mu896/39-1. We thank Markus Müllner for helpful discussions.

References

- [1] F. Wurm, A. F. M. Kilbinger, *Angew. Chem., Int. Ed.* **2009**, *48*, 8412-8421.
- [2] J. Du, R. K. O'Reilly, *Chem. Soc. Rev.* **2011**, *40*, 2402-2416.
- [3] A. Walther, A. H. E. Müller, *Soft Matter* **2008**, *4*, 663-668.
- [4] P.-G. de Gennes, *Angew. Chem., Int. Ed.* **1992**, *31*, 842-845.
- [5] A. Perro, S. Reculosa, S. Ravaine, E. Bourgeat-Lami, E. Duguet, *J. Mater. Chem.* **2005**, *15*, 3745-3760.
- [6] A. G. Vanakaras, *Langmuir* **2005**, *22*, 88-93.
- [7] R. A. Pavlick, S. Sengupta, T. McFadden, H. Zhang, A. Sen, *Angew. Chem., Int. Ed.* **2011**, *50*, 9374-9377.
- [8] Y. Wang, R. M. Hernandez, D. J. Bartlett, J. M. Bingham, T. R. Kline, A. Sen, T. E. Mallouk, *Langmuir* **2006**, *22*, 10451-10456.
- [9] Y. Hong, D. Velegol, N. Chaturvedi, A. Sen, *Phys. Chem. Chem. Phys.* **2010**, *12*, 1423-1435.
- [10] S. J. Ebbens, J. R. Howse, *Langmuir* **2011**, *27*, 12293-12296.
- [11] L. Baraban, D. Makarov, R. Streubel, I. Mänch, D. Grimm, S. Sanchez, O. G. Schmidt, *ACS Nano* **2012**, *6*, 3383-3389.
- [12] I. Kretzschmar, J. H. Song, *Curr. Opin. Colloid Interface Sci.* **2011**, *16*, 84-95.

- [13] T. Nisisako, T. Torii, T. Takahashi, Y. Takizawa, *Adv. Mater.* **2006**, *18*, 1152-1156.
- [14] T. Kaufmann, M. T. Gokmen, C. Wendeln, M. Schneiders, S. Rinnen, H. F. Arlinghaus, S. A. F. Bon, F. E. Du Prez, B. J. Ravoo, *Adv. Mater.* **2011**, *23*, 79-83.
- [15] H. Takei, N. Shimizu, *Langmuir* **1997**, *13*, 1865-1868.
- [16] M. Himmelhaus, H. Takei, *Sens. Actuators, B* **2000**, *63*, 24-30.
- [17] C. J. Behrend, J. N. Anker, B. H. McNaughton, M. Brasuel, M. A. Philbert, R. Kopelman, *J. Phys. Chem. B* **2004**, *108*, 10408-10414.
- [18] R. M. Erb, N. J. Jenness, R. L. Clark, B. B. Yellen, *Adv. Mater.* **2009**, *21*, 4825-4829.
- [19] S.-N. Yin, C.-F. Wang, Z.-Y. Yu, J. Wang, S.-S. Liu, S. Chen, *Adv. Mater.* **2011**, *23*, 2915-2919.
- [20] C. J. Behrend, J. N. Anker, R. Kopelman, *Appl. Phys. Lett.* **2004**, *84*, 154-156.
- [21] S. Jiang, Q. Chen, M. Tripathy, E. Luijten, K. S. Schweizer, S. Granick, *Adv. Mater.* **2010**, *22*, 1060-1071.
- [22] S. Whitelam, S. A. F. Bon, *J. Chem. Phys.* **2010**, *132*, 074901-074908.
- [23] S. K. Smoukov, S. Gangwal, M. Marquez, O. D. Velev, *Soft Matter* **2009**, *5*, 1285-1292.
- [24] L. Hong, A. Cacciuto, E. Luijten, S. Granick, *Nano Lett.* **2006**, *6*, 2510-2514.
- [25] J. R. Millman, K. H. Bhatt, B. G. Prevo, O. D. Velev, *Nature Mater.* **2005**, *4*, 98-102.
- [26] A. Walther, M. Hoffmann, A. H. E. Müller, *Angew. Chem., Int. Ed.* **2008**, *47*, 711-714.
- [27] T. M. Ruhland, A. H. Gröschel, A. Walther, A. H. E. Müller, *Langmuir* **2011**, *27*, 9807-9814.
- [28] N. Glaser, D. J. Adams, A. Böker, G. Krausch, *Langmuir* **2006**, *22*, 5227-5229.
- [29] B. P. Binks, P. D. I. Fletcher, *Langmuir* **2001**, *17*, 4708-4710.
- [30] R. Aveyard, *Soft Matter* **2012**, *8*, 5233-5240.
- [31] A. B. Pawar, I. Kretzschmar, *Macromol. Rapid Commun.* **2010**, *31*, 150-168.
- [32] S.-H. Kim, S. Y. Lee, S.-M. Yang, *Angew. Chem., Int. Ed.* **2010**, *49*, 2535-2538.
- [33] A. Walther, K. Matussek, A. H. E. Müller, *ACS Nano* **2008**, *2*, 1167-1178.
- [34] R. Erhardt, M. Zhang, A. Böker, H. Zettl, C. Abetz, P. Frederik, G. Krausch, V. Abetz, A. H. E. Müller, *J. Am. Chem. Soc.* **2003**, *125*, 3260-3267.
- [35] X. Y. Ling, I. Y. Phang, C. Acikgoz, M. D. Yilmaz, M. A. Hempenius, G. J. Vancso, J. Huskens, *Angew. Chem., Int. Ed.* **2009**, *48*, 7677-7682.
- [36] L. Cheng, G. Zhang, L. Zhu, D. Chen, M. Jiang, *Angew. Chem., Int. Ed.* **2008**, *47*, 10171-10174.
- [37] L. Nie, S. Liu, W. Shen, D. Chen, M. Jiang, *Angew. Chem., Int. Ed.* **2007**, *46*, 6321-6324.
- [38] Q. Chen, J. K. Whitmer, S. Jiang, S. C. Bae, E. Luijten, S. Granick, *Science* **2011**, *331*, 199-202.
- [39] A. Walther, M. Drechsler, S. Rosenfeldt, L. Harnau, M. Ballauff, V. Abetz, A. H. E. Müller, *J. Am. Chem. Soc.* **2009**, *131*, 4720-4728.
- [40] A. Walther, M. Drechsler, A. H. E. Müller, *Soft Matter* **2009**, *5*, 385-390.
- [41] A. Walther, X. André, M. Drechsler, V. Abetz, A. H. E. Müller, *J. Am. Chem. Soc.* **2007**, *129*, 6187-6198.
- [42] F. Liang, K. Shen, X. Qu, C. Zhang, Q. Wang, J. Li, J. Liu, Z. Yang, *Angew. Chem., Int. Ed.* **2011**, *50*, 2379-2382.
- [43] C.-C. Lin, C.-W. Liao, Y.-C. Chao, C. Kuo, *ACS Appl. Mater. Interfaces* **2010**, *2*, 3185-3191.
- [44] S. Ye, R. L. Carroll, *ACS Appl. Mater. Interfaces* **2010**, *2*, 616-620.
- [45] K. D. Anderson, M. Luo, R. Jakubiak, R. R. Naik, T. J. Bunning, V. V. Tsukruk, *Chem. Mater.* **2010**, *22*, 3259-3264.
- [46] B. Liu, W. Wei, X. Qu, Z. Yang, *Angew. Chem., Int. Ed.* **2008**, *47*, 3973-3975.

- [47] R. F. Shepherd, J. C. Conrad, S. K. Rhodes, D. R. Link, M. Marquez, D. A. Weitz, J. A. Lewis, *Langmuir* **2006**, *22*, 8618-8622.
- [48] D. M. Andala, S. H. R. Shin, H.-Y. Lee, K. J. M. Bishop, *ACS Nano* **2012**, *6*, 1044-1050.
- [49] D. A. Christian, A. Tian, W. G. Ellenbroek, I. Levental, K. Rajagopal, P. A. Janmey, A. J. Liu, T. Baumgart, D. E. Discher, *Nature Mater.* **2009**, *8*, 843-849.
- [50] S. Seiffert, M. B. Romanowsky, D. A. Weitz, *Langmuir* **2010**, *26*, 14842-14847.
- [51] Z. Nie, W. Li, M. Seo, S. Xu, E. Kumacheva, *J. Am. Chem. Soc.* **2006**, *128*, 9408-9412.
- [52] S. Lone, S. H. Kim, S. W. Nam, S. Park, J. Joo, I. W. Cheong, *Chem. Commun.* **2011**, *47*, 2634-2636.
- [53] J.-H. Jung, C.-H. Choi, S. Chung, Y.-M. Chung, C.-S. Lee, *Lab Chip* **2009**, *9*, 2596-2602.
- [54] Y. Srivastava, M. Marquez, T. Thorsen, *Biomicrofluidics* **2009**, *3*, 012801.
- [55] R. Erhardt, A. Böker, H. Zettl, H. Kaya, W. Pyckhout-Hintzen, G. Krausch, V. Abetz, A. H. E. Müller, *Macromolecules* **2001**, *34*, 1069-1075.
- [56] K. V. Butsele, C. A. Fustin, J. F. Gohy, R. Jérôme, C. Jérôme, *Langmuir* **2009**, *25*, 107-111.
- [57] Y. Li, E. Themistou, J. Zou, B. P. Das, M. Tsianou, C. Cheng, *ACS Macro Lett.* **2012**, *1*, 52-56.
- [58] S. Zhang, Z. Li, S. Samarajeewa, G. Sun, C. Yang, K. L. Wooley, *J. Am. Chem. Soc.* **2011**, *133*, 11046-11049.
- [59] I. K. Voets, A. de Keizer, P. de Waard, P. M. Frederik, P. H. H. Bomans, H. Schmalz, A. Walther, S. M. King, F. A. M. Leermakers, M. A. Cohen Stuart, *Angew. Chem., Int. Ed.* **2006**, *45*, 6673-6676.
- [60] L. Cheng, G. Hou, J. Miao, D. Chen, M. Jiang, L. Zhu, *Macromolecules* **2008**, *41*, 8159-8166.
- [61] Liu, V. Abetz, A. H. E. Müller, *Macromolecules* **2003**, *36*, 7894-7898.
- [62] A. Wolf, A. Walther, A. H. E. Müller, *Macromolecules* **2011**, *44*, 9221-9229.
- [63] A. H. Gröschel, F. H. Schacher, H. Schmalz, O. V. Borisov, E. B. Zhulina, A. Walther, A. H. E. Müller, *Nat. Commun.* **2012**, *3*, 710.
- [64] B. Fang, A. Walther, A. Wolf, Y. Xu, J. Yuan, A. H. E. Müller, *Angew. Chem. Int. Ed.* **2009**, *48*, 2877-2880.
- [65] J. Schmelz, M. Karg, T. Hellweg, H. Schmalz, *ACS Nano* **2011**, *5*, 9523-9534.
- [66] R. Stadler, C. Auschra, J. Beckmann, U. Krappe, I. Voight-Martin, L. Leibler, *Macromolecules* **1995**, *28*, 3080-3097.
- [67] S. Jiang, S. Granick, *J. Chem. Phys.* **2007**, *127*, 161102.
- [68] J. Ding, G. Liu, *Macromolecules* **1998**, *31*, 6554-6558.
- [69] A. Lendlein, V. P. Shastri, *Adv. Mater.* **2010**, *22*, 3344-3347.
- [70] A. Walther, A. S. Goldmann, R. S. Yelamanchili, M. Drechsler, H. Schmalz, A. Eisenberg, A. H. E. Müller, *Macromolecules* **2008**, *41*, 3254-3260.

Supporting Information

to

**Facile, Solution-Based Synthesis of Soft, Nanoscale
Janus Particles with Tunable Janus Balance**

**André H. Gröschel^{*}, Andreas Walther, Tina I. Löbbling, Joachim Schmelz,
Andreas Hanisch, Holger Schmalz, Axel H. E. Müller^{*}**

Materials and Methods

Materials

The preparation and characterization of SBM, SBV, and SBT triblock terpolymers were reported in detail previously.^[41, 71-73] Relevant terpolymer specifics are summarized in Table 5–1 and Table S5–1. All solvents used were of analytical grade. Dialysis tubes of regenerated cellulose with a MWCO of 12,000 – 14,000 g/mol were purchased from Roth, equilibrated in deionized water for 30 min and washed with excess dioxane before use. Copper(I)bromide (99%, Aldrich), ethyl 2-bromopropionate (2-EBP 99%, Aldrich), *N,N,N',N',N'*-pentamethyldiethylenetriamine (PMDETA 99%, Aldrich), 2-hydroxyethyl acrylate (HEA-OH 99%, Aldrich) and triethylamine (TEA, 99%, Aldrich) were used as received. 2-(dimethyl-amino)ethyl methacrylate (DMAEMA 99%, Aldrich) and *tert*-butyl acrylate (*t*BA 99%, Aldrich) were passed through a column filled with silica to remove the stabilizer. The solvents and other used chemicals were of analytical grade and used without further purification.

Synthesis of poly(*tert*-butyl acrylate)-*block*-poly(2-(cinnamoyloxyethyl acrylate)-*block*-poly(2-(dimethylamino)ethyl methacrylate)

Synthesis of trimethylsilyloxyethyl acrylate (HEA-TMS). To a 200 mL round bottom flask equipped with a stir bar HEA-OH (16.16 g, 0.14 mol), TEA (21.08 g, 0.21 mol) and 50 mL of dichloromethane were added and cooled down to 0 °C. After drop-wise addition of chlorotrimethylsilane (22.76 g, 0.21 mol) the reaction mixture was stirred at 0 °C for another 2 h and then at room temperature over night. After that, the mixture was filtered two times to remove the salt, which in turn was washed with excess cyclohexane. After evaporation of the solvents, protected HEA-TMS was recovered by distillation under reduced pressure.

Synthesis of PtBA Homopolymer. In a typical ATRP reaction 2-EBP (496 mg, 2.74 mmol), CuBr (393 mg, 2.74 mmol) and *t*BA (70.00 g, 547 mmol) were added to a round bottom flask, sealed with a rubber septum and equipped with a stir bar and purged with argon for 30 min. PMDETA (474 mg, 2.74 mmol) was kept and purged with argon in a separate flask. After the flask was placed in an oil bath and heated up to 50 °C, PMDETA was added via gas-tight argon flushed syringe. Periodically, aliquots were removed via a gas-tight syringe for GPC and ¹H-NMR analysis. After 5 h the reaction was stopped by rapid cooling to room temperature and stirring under air. The crude product was diluted with cyclohexane and passed through a column filled with silica to remove the catalyst. After evaporation of the solvents, THF was added to the flask and the polymer was then precipitated into 5 L methanol/water mixture (70:30 v/v), collected by vacuum filtration and dried at 60 °C under vacuum for one day. The resultant PtBA ($M_{n,GPC} = 24,000$ g/mol; PDI = 1.13) was collected as a white powder.

*Synthesis of PtBA-*b*-P(HEA-TMS) diblock copolymer.* Bromine end-functionalized PtBA was used as the macroinitiator to synthesize PtBA-*b*-P(HEA-TMS). In a typical reaction PtBA-Br macroinitiator (12.00 g, 0.50 mmol), CuBr (71.7 mg, 0.50 mmol), HEA-TMS (20.00 g, 106.4 mmol) and 32.5 mL anisole were placed in a round bottom flask, sealed with a rubber septum and equipped with a stir bar and purged with argon for 30 min. In a separate flask PMDETA (86.7 g, 0.50 mmol) was diluted with 1 ml anisole and also purged with argon. After the flask was placed in an oil bath and heated up to 90 °C, the polymerization was initiated by adding PMDETA to the reaction mixture via gas-tight argon flushed syringe. Periodically, 0.1 mL aliquots were removed via a gas-tight syringe for GPC and ¹H-NMR analysis. The reaction was stopped after 1180 min by cooling the reaction mixture down to room temperature and stirring under air. The crude product was diluted with cyclohexane and passed through a column filled with silica to remove the catalyst. After evaporation of the cyclohexane, the diblock copolymer was dissolved in THF and purified by dialysis against 5 L THF for 2 days, changing the solvent one time after 24 h. After evaporation of the THF PtBA-*b*-P(HEA-TMS) diblock copolymer was dis-

solved in 1,4-dioxane, freeze-dried and collected as a white solid: ($M_{n,GPC} = 32,000$ g/mol; PDI = 1.12).

Synthesis of *PtBA-b-P(HEA-TMS)-b-PDMAEMA* triblock terpolymer. Bromine end-functionalized *PtBA-b-P(HEA-TMS)* was used as the macroinitiator to synthesize *PtBA-b-P(HEA-TMS)-b-PDMAEMA*. In a typical reaction *PtBA-b-P(HEA-TMS)-Br* macroinitiator (1.0 g, 0.030 mmol), CuCl (2.7 mg, 0.030 mmol) and DMAEMA (1.43 g, 9.10 mmol) were placed in a round bottom flask together with 7 ml anisol, sealed with a rubber septum and equipped with stir bar and purged with argon. In a separate flask PMDETA (4.7 mg, 0.03 mmol) was also purged with argon. After the flask was placed in an oil bath and heated up to 60 °C, the polymerization was initiated by adding PMDETA to the reaction mixture via an argon flushed gas-tight syringe. Periodically, 0.1 mL aliquots were removed via a gas-tight syringe for GPC and ¹H-NMR analysis. The reaction was stopped after 28 h by cooling the reaction mixture down to room temperature und stirring under air. The crude product was diluted with cyclohexane and passed through a column filled with silica to remove the catalyst. After evaporation of the cyclohexane, THF was added to the flask. The polymer was then dialyzed against 5 L ethanol for 2 days, changing the solvent one time after 24 h. The resultant *PtBA-b-P(HEA-TMS)-b-PDMAEMA* ($M_{n,GPC} = 72,000$ g/mol; PDI = 1.28) was dissolved in 1,4-dioxane and freeze-dried.

Conversion of *PtBA-b-P(HEA-TMS)-b-PDMAEMA* to *PtBA-b-PCEA-b-PDMAEMA*. The P(HEA-TMS) block was converted to PCEA by selective acidic hydrolysis of the TMS-groups followed by esterification with cinnamoyl chloride. For this purpose the terpolymer (0.75 g, 0.24 mmol) was dissolved in a mixture of 15 mL THF and 15 mL methanol containing 1 mL acetic acid as catalyst. The mixture was stirred for 4 h at room temperature and quantitative removal of the TMS protective group was confirmed by ¹H-NMR analysis. The solvents were removed by evaporation and the newly formed hydroxyl groups of the PHEA block were reacted with a 4-fold excess of cinnamoyl chloride in dry pyridine at room temperature for 48 h. The resultant *PtBA-b-PCEA-b-PDMAEMA* was purified by dialysis against 5 L ethanol for two days.

Methods

Preparation of precursor micelles. SBM, SBV and SBT terpolymers were dissolved in *N,N'*-dimethylacetamide (DMAc) and *t*ACD in isopropanol. All polymer solutions were prepared at an initial concentration of $c = 1$ g/L. The as-prepared micellar solutions of SBM, SBV and SBT were annealed overnight at 70 °C and *t*ACD at 50 °C to guarantee an equilibrated system. The resulting precursor micelles were investigated by dynamic light scattering (DLS) and transmission electron microscopy (TEM).

Self-assembly of core-corona micelles into MCMs. In all cases, 5 mL of the core-corona micelles (1 g/L) were dialyzed into 5 L of selective solvent for the corona block. The solvent exchange was monitored by ¹H-NMR. Micellar solutions of SBM terpolymers were

dialyzed into acetone/isopropanol mixtures, SBT terpolymer into ethanol, SBV into isopropanol and *t*ACD into water pH 6. The resulting structures were investigated by both DLS and TEM.

Crosslinking of the compartments. In order to permanently fix the phase separated state, 2 equivalents of the photo-crosslinker, 2,4,6-trimethylbenzoyldiphenylphosphineoxide (Lucirin TPO[®]; $\lambda_{max} \approx 360$ nm), per double bond were added to the solution. Stirring for 2 h ensured homogeneous distribution of the photo-crosslinker before the sample was irradiated for 1 h using a UV-lamp with a cut-off filter of $\lambda = 300$ nm. Re-dispersion in THF as a good solvent for all blocks then broke up the MCMs into single JPs.

Hydrolysis of SBM3 Janus micelles. The Janus micelles were dissolved in 1,4-dioxane ($c = 10$ g/L) in a sealed Schott glass and the PMMA ester groups were hydrolyzed with 3 eq. KOH per PMMA unit using 18-crown-6 as a phase transfer catalyst (molar ratio [18-crown-6]/[KOH] = 5/1). The reaction was carried out at 110 °C for 5 days. Finally the solution was precipitated into 1 M hydrochloric acid, and washed with water, before the residue was dried under vacuum (maximum 50 °C).

Instrumentation

Dynamic Light Scattering (DLS) was performed at a scattering angle of 90° or multiple angles ranging from 30°-150° in 10° steps on an ALV DLS/SLS-SP 5022F equipment consisting of an ALV-SP 125 laser goniometer, an ALV 5000/E correlator, and a He–Ne laser operating at a wavelength of $\lambda = 632.8$ nm. The CONTIN algorithm was applied to analyze the obtained correlation functions. Apparent hydrodynamic radii were calculated according to the Stokes–Einstein equation. All CONTIN plots are intensity-weighted. Prior to the light scattering measurements, all sample solutions were filtered twice through a 5 μ m PTFE-membrane. The dynamic viscosities of acetone/isopropanol mixtures were calculated according to Ubbelohde,

$$\eta = \nu\rho = K(t - \nu)[w_1\rho_1 + (1 - w_1)\rho_2],$$

, where ν is the kinematic viscosity, K is the viscometer constant, t is the measurement time, ν is the Hagenbach capillary correction factor, w_1 is the weight fraction of acetone and, ρ_i are the corresponding densities.

Transmission Electron Microscopy (TEM) was performed in bright-field mode on Zeiss CEM 902 and LEO 922 OMEGA electron microscopes operated at 80 kV and 200 kV, respectively. The samples were prepared by placing one drop of the polymer solution (0.01 g/L) onto carbon-coated copper grids. Excess solvent was instantly absorbed by a filter paper. For selective staining, the TEM specimens were exposed to RuO₄ vapor for 15 min (stains aromatics: PS, P2VP, PCEMA), OsO₄ vapor for 3 h (stains double bonds: PB) or I₂ vapor for 3 h (stains amines: P2VP).

Polymer Characteristics

Table S5–1: Molecular characteristics of the employed triblock terpolymers

Code ^a	Polymer ^c		$\frac{V_A}{V_B}$ ^d	r_C ^e	N_{patches}	R_h MCM [nm] ^f	R_h JP [nm] ^g	R_h JP [nm] ^h
SBM1	S ₃₁₀ B ₁₅₀ M ₃₄₀	S ₄₃ B ₁₁ M ₄₆ ⁷⁴	3.57	0.75	10-12	42 ± 5	42 ± 9	19 ± 6
SBM2	S ₃₄₀ B ₃₃₀ M ₃₆₀	S ₄₀ B ₂₀ M ₄₀ ⁹⁰	1.78	0.54	3	36 ± 8	36 ± 6	23 ± 7
SBM3	S ₆₁₀ B ₆₄₀ M ₂₉₀	S ₅₀ B ₂₇ M ₂₃ ¹²⁷	1.69	0.23	5-7	54 ± 5	49 ± 6	35 ± 5
SBM4	S ₂₈₀ B ₃₃₀ M ₄₃₀	S ₃₂ B ₂₀ M ₄₈ ⁹⁰	1.46	0.70	2	37 ± 4	38 ± 7	26 ± 8
SBT ^b	S ₅₁₀ B ₅₄₀ T ₃₅₀	S ₄₀ B ₂₂ T ₃₈ ¹³²	1.67	0.67	3	34 ± 6	36 ± 8	30 ± 9
SBV	S ₃₆₀ B ₃₈₀ V ₅₉₀	S ₃₁ B ₁₇ V ₅₂ ¹²⁰	1.67	0.81	3	36 ± 7	49 ± 6	29 ± 7
<i>t</i> ACD	<i>t</i> A ₁₉₀ C ₇₀ D ₁₁₀	T ₄₁ C ₃₀ D ₂₉ ⁵⁹	1.65	0.43	2-3	36 ± 7	18 ± 3	---

^a For abbreviations see Chart 5–1 in the main text;

^b 1,4-butadiene content ca. 10 mol%, otherwise 90 mol%;

^c Subscripts in the left column denote the number-average degree of polymerization, subscripts in the right column denote the weight fraction and superscript is the overall molecular weight in kg/mol;

^d Volume ratio of the core forming blocks;

^e Molar ratio of the coronal to the core blocks $r_C = N_C / (N_A + N_B)$;

^f MCMs measured in solvents of preparation at a concentration of 1 g/L: SBM1-4 in acetone/isopropanol (70/30 v/v), SBT in ethanol, SBV in isopropanol and *t*ACD in water pH 6.

^g Janus particles measured in THF at a concentration of 1 g/L. *t*ACD JPs were measured in water pH 3.

^h Janus particles measured in DMAc at a concentration of 1 g/L.

Dynamic Light Scattering of Janus micelles after crosslinking and re-dispersion in DMAc

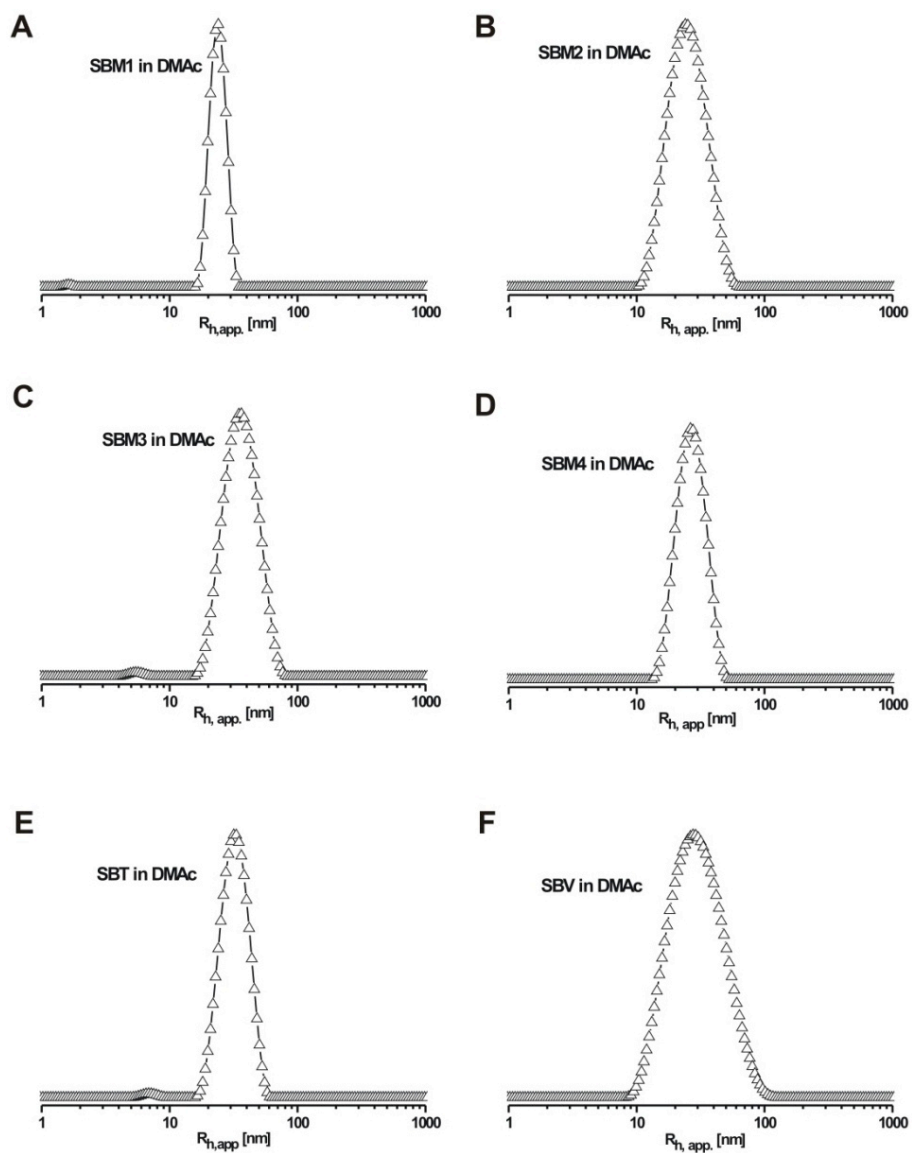


Figure S5-1: Size distributions of SBM1-4, SBT and SBV JPs after redispersion in DMAc

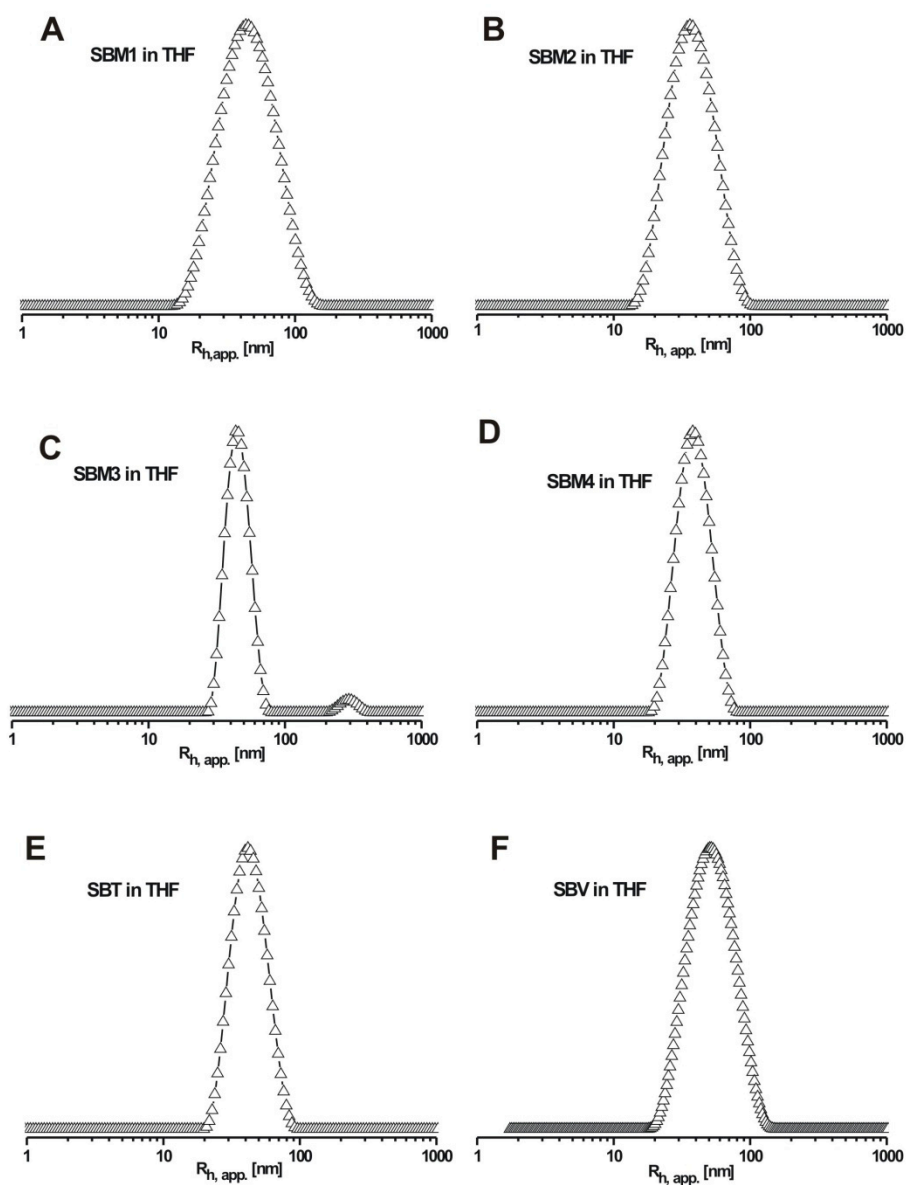
^1H NMR of crosslinked SBM2 Janus particles before and after crosslinking

Figure S5-2: Size distributions of SBM1-4, SBT and SBV JPs after re-dispersion in THF

Dynamic Light Scattering of Janus micelles after crosslinking and re-dispersion in THF

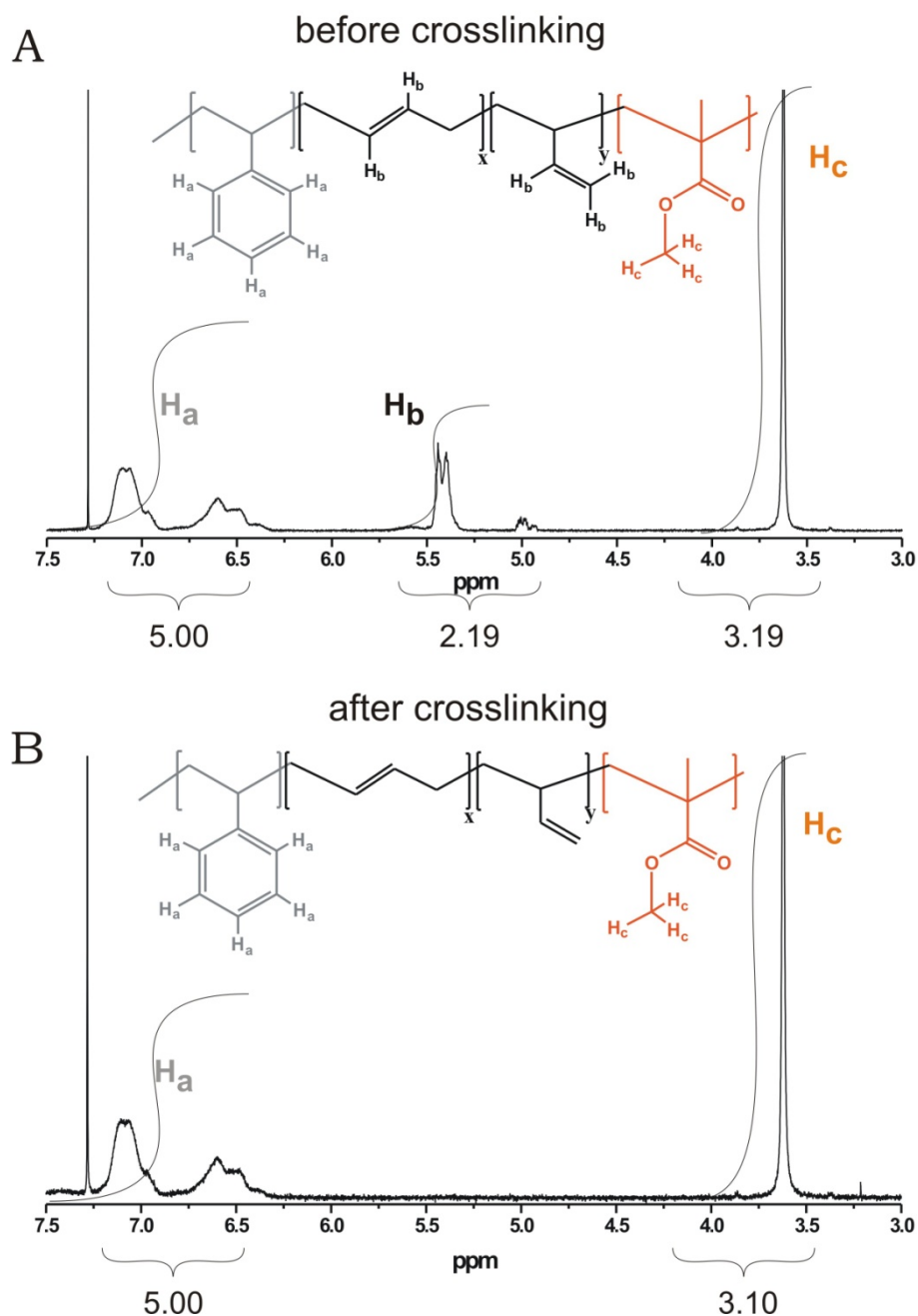


Figure S5–3: ^1H NMR spectra of: (A) SBM2 triblock terpolymer; (B) JPs without any indication of remaining PB at $\delta = 5.2\text{--}5.6$ after crosslinking. Before and after crosslinking, the ratio of intensities $I_{\text{PS}}/I_{\text{PMMA}}$ are identical with $I_{\text{PS}} = 5.0$ at $\delta = 6.4\text{--}7.2$ and $I_{\text{PMMA}} = 3.2$ at $\delta = 3.6$ before and $I_{\text{PS}} = 5.0$ and $I_{\text{PMMA}} = 3.1$ after crosslinking, which corresponds to 50 mol% of each repeating unit in both cases.

Comparison of JPs prepared via the bulk and the solution route

Visualization of the Janus character is challenging, especially in the case of nanometer-sized ones. Even in good solvents the high surface activity can lead to aggregation or preferential orientation towards surfaces such as the carbon coating of the TEM copper grid. A simple way to prove the typical Janus micelle character is the comparison with micelles prepared via the well documented cross-linking of lamella-sphere bulk morphologies as exemplified on SBM1 (Figure S5–4A, B).^[55] Films of SBM1 were cast from THF (100 mg/ml) with slow solvent evaporation over a period of at least one week. The thin films (< 1 mm) were cross-linked with S₂Cl₂ vapor for two days and re-dispersed in THF under vigorous stirring for another week. TEM samples prepared by applying one drop of a 0.01g/L solution of JPs in THF on a carbon coated copper grid showed Janus micelles that, upon drying, again form aggregation patterns reminiscent of the lamella-sphere morphology (Figure S5–4C). Although these aggregation patterns vary with local concentration of micelles the observed arrangements are almost identical to those prepared via the solvent-based process (Figure S5–4D, E).

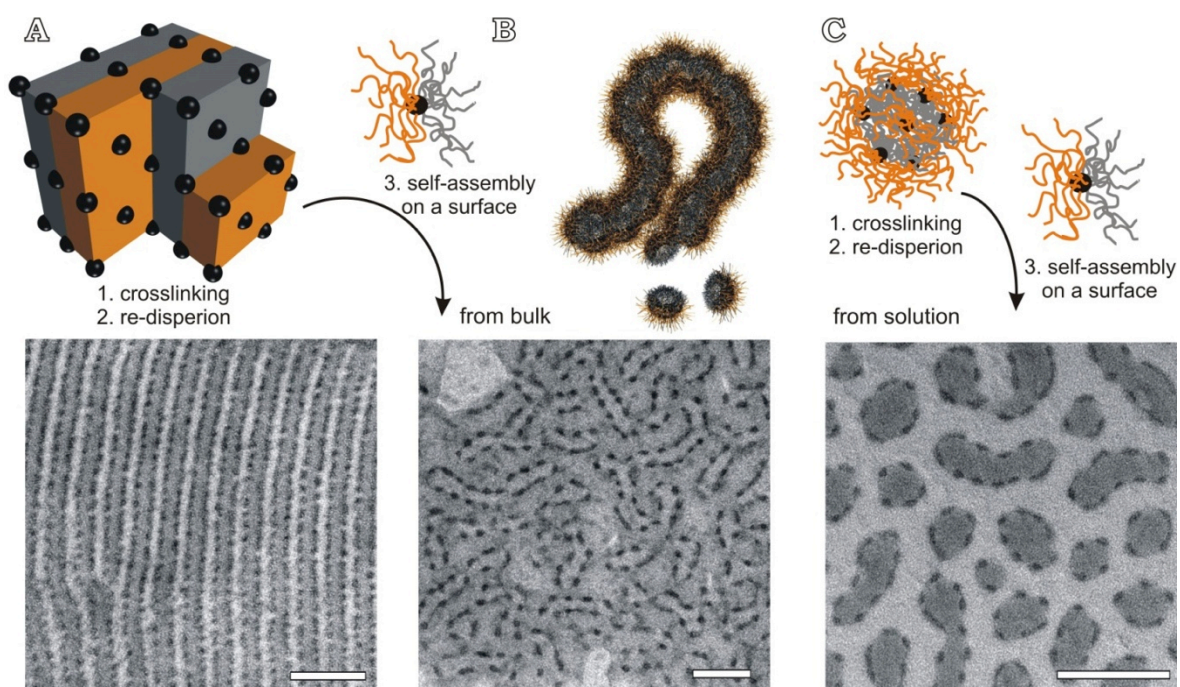


Figure S5–4: Bulk morphology route and solution-based approach to JPs and the self-assembly behavior on surfaces: (A) Schematic representation of lamella-sphere (*ls*) bulk morphology and TEM image of the SBM1 bulk morphology. (B) Janus micelle after cross-linking of the PB phase and re-dispersion in THF. Schematic of proposed self-assembly pattern of Janus micelles on surfaces and self-assembly of Janus micelles found on carbon coated TEM grids. (C) Self-assembly of SBM1 in acetone/isopropanol (70/30 v/v) and almost identical aggregation pattern of Janus micelles in TEM. (Scale bars correspond to 200 nm; color code from selective staining with OsO₄: PS grey, PB black and PMMA not visible due to electron beam degradation).

Aggregation number of block terpolymer chains per JP core

The aggregation number for a sphere can be estimated from the core radius determined in TEM and eq. 5–1:

$$N_{agg} = \frac{m_{core}}{m_{PB}^{chain}} = V_{core} \frac{N_A \rho_{PB}}{M_{PB}^{chain}}, \quad V_{core} = \frac{4}{3} \pi R_{core}^3 \quad (5-1)$$

, where m_{core} is the mass of the micellar core; m_{PB}^{PB} is the mass of an individual PB chain, N_A is the Avogadro constant, ρ_{PB} is the density of PB, V_{core} is the volume of the micellar core, and M_{PB}^{chain} is the molecular weight of an individual PB chain.

Thus, with $M_{PB} \sim DP_{PB}$,

$$R_{core} : (N_{agg} DP_{PB})^{1/3} \quad (5-1a)$$

Since the contribution of the staining agent, OsO_4 , is neglected, the N_{agg} values are only apparent. The aggregation numbers were calculated using an average value of 250 core radii measured in TEM as depicted in Figure S5–5.

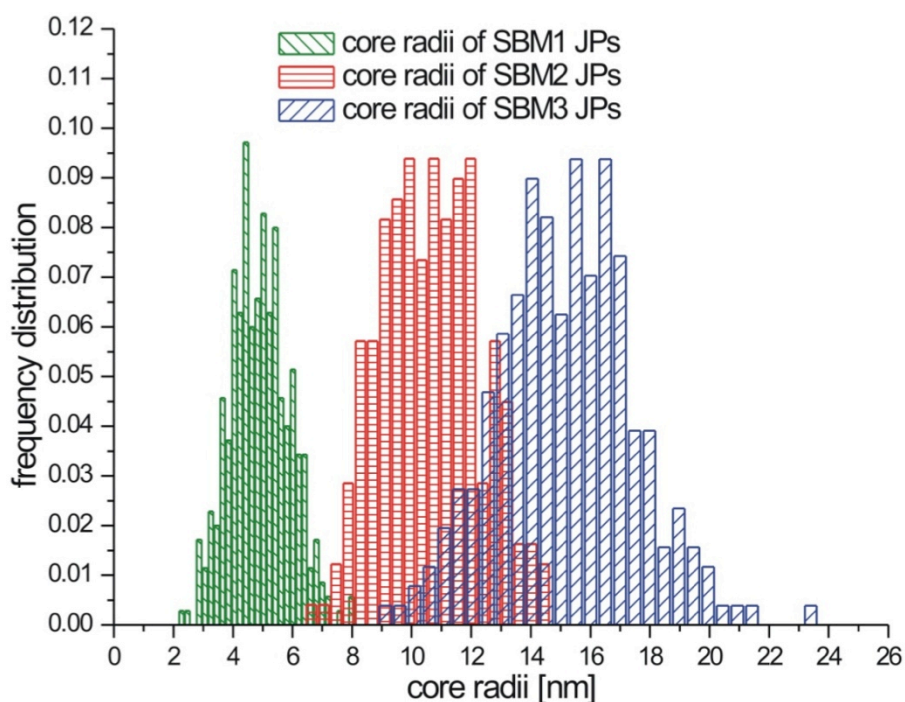


Figure S5–5: Frequency distributions of the core radii of SBM1, SBM2 and SBM3 JPs. At least 250 core radii were measured in TEM for each sample.

A theoretical approach for diblock copolymer micelles with a solvophobic B and a solvophilic A block states that the dependence of N_{agg} on the DP of the solvophilic blocks can be neglected.^[74] Thus, for terpolymers with a solvophobic PB and two solvophilic blocks PS and PMMA these considerations can be adjusted to yield equation 2 as an approximation:

$$N_{agg} : DP_{PB}^x \quad (5-2)$$

Here, the exponent x can adapt values from 0.8 to 2 for the limiting cases of star-line and crew-cut micelles.

Insertion of eq. 5–2 into eq. 5–1a renders

$$R_{core} : DP_{PB}^{(x+1)/3} \quad (5-3)$$

A double-logarithmic plot in Figure S5–6 according to equation 1 renders $x = 1.2 \pm 0.3$, indicating that the micelles are between the star-like and crew-cut regimes. Using this value of the exponent we obtain for our JP's

$$R_{core} : DP_{PB}^{0.733} \quad (5-4)$$

Thus, the exponent for R_{core} vs. $DP_{n,PB}$ is between 0.6 and 0.9.

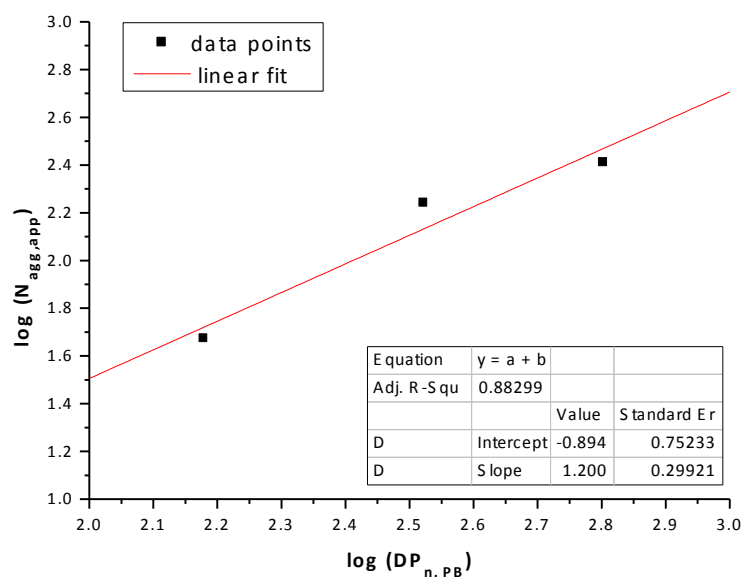


Figure S5–6: Double logarithmic plot of aggregation number vs. degree of polymerization

The double logarithmic plot of R_{core} vs. $DP_{n,PB}$ confirms these conclusions as the slope is calculated to $x = 0.67 \pm 0.07$

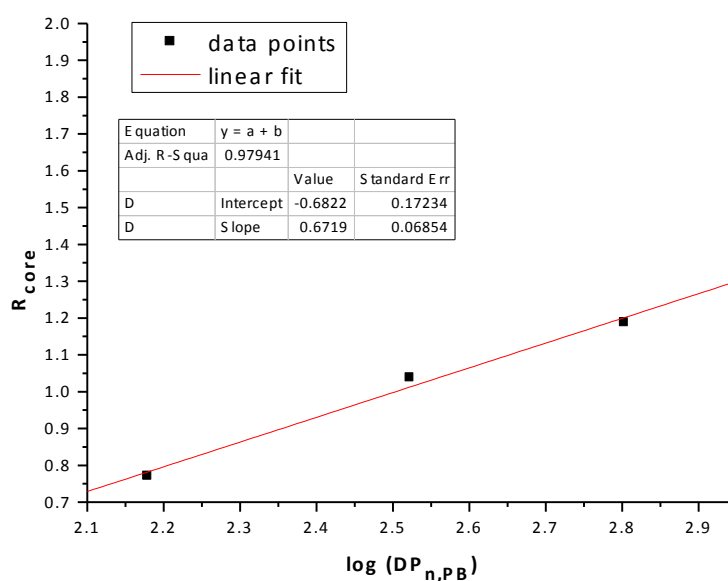


Figure S5–7: Double logarithmic plot of core radii vs. degree of polymerization

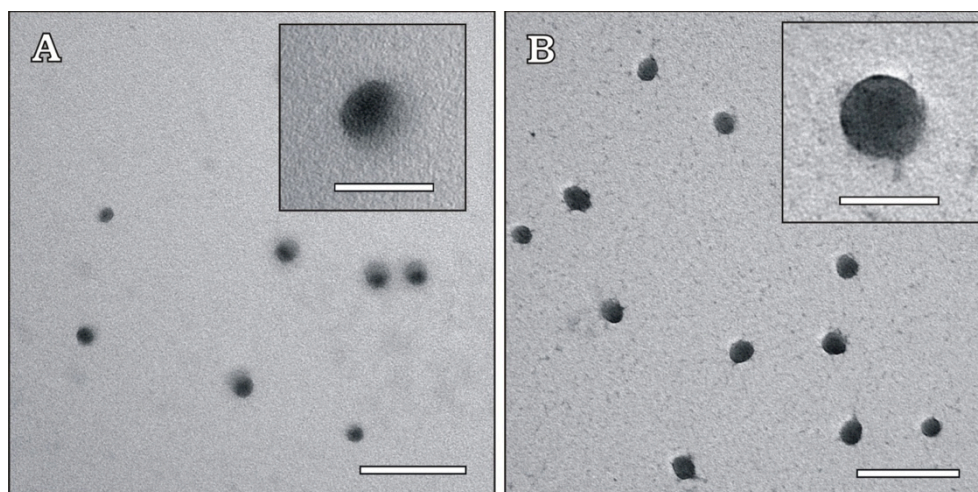
PMAA corona distribution of SBMAA3 JPs in water pH 10

Figure S5–8: SBMAA3 JPs after dialysis from THF into water pH 10 at a concentration $c = 0.05$ g/L. **(A)** OsO_4 staining renders PB black, PS grey and PMAA is visible. The Janus character is clearly visible. **(B)** Staining with uranylacetate $\text{UO}_2(\text{OAc})_2$ only visualizes the PMAA corona. The homogeneous coloring and the spherical appearance of the micelle supports a complete coating of the JP with PMAA chains.

References

- [71] C. Auschra & R. Stadler. Synthesis of block copolymers with poly(methyl methacrylate): P(B-*b*-MMA), P(EB-*b*-MMA), P(S-*b*-B-*b*-MMA) and P(S-*b*-EB-*b*-MMA). *Polym. Bull.* **1993**, *30*, 257-264.
- [72] E. Giebeler & R. Stadler. ABC triblock polyampholytes containing a neutral hydrophobic block, a polyacid and a polybase. *Macromol. Chem. Phys.* **1997**, *198*, 3815-3825.
- [73] H. Ruckdäschel *et al.* Compatibilisation of PPE/SAN blends by triblock terpolymers: Correlation between block terpolymer composition, morphology and properties. *Polymer* **2006**, *47*, 2772-2790.
- [74] E. B. Zhulina & O. V. Borisov. Theory of Block Polymer Micelles: Recent Advances and Current Challenges. *Macromolecules* **2012**, *45*, 4429-4440.

Chapter 6

Janus Micelles as Effective Supracolloidal Dispersants for Carbon Nanotubes

André H. Gröschel^{*†}, Tina I. Löbbling[‡], Petar D. Petrov¹, Markus Müllner[‡], Christian Kuttner², Florian Wieberger³, and Axel H. E. Müller^{*†}

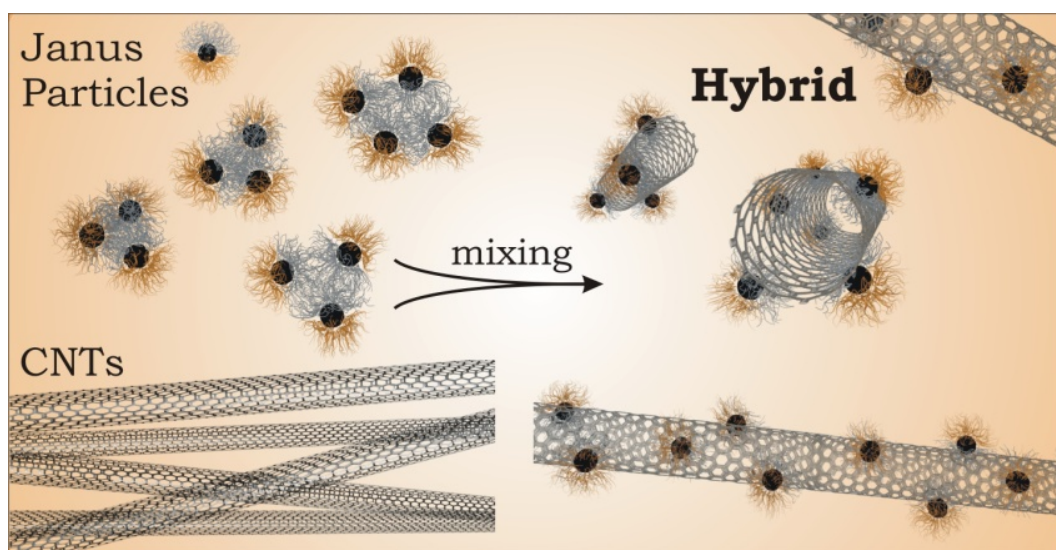
Makromolekulare Chemie II, Universität Bayreuth, D-95440 Bayreuth, Germany.

andre.groeschel@uni-bayreuth.de; axel.mueller@uni-bayreuth.de

¹ *Institute of Polymers, Bulgarian Academy of Sciences, Sofia 1113, Bulgaria.*

² *Physikalische Chemie II, Universität Bayreuth, D-95440 Bayreuth, Germany.*

³ *Makromolekulare Chemie I, Universität Bayreuth, D-95440 Bayreuth, Germany.*



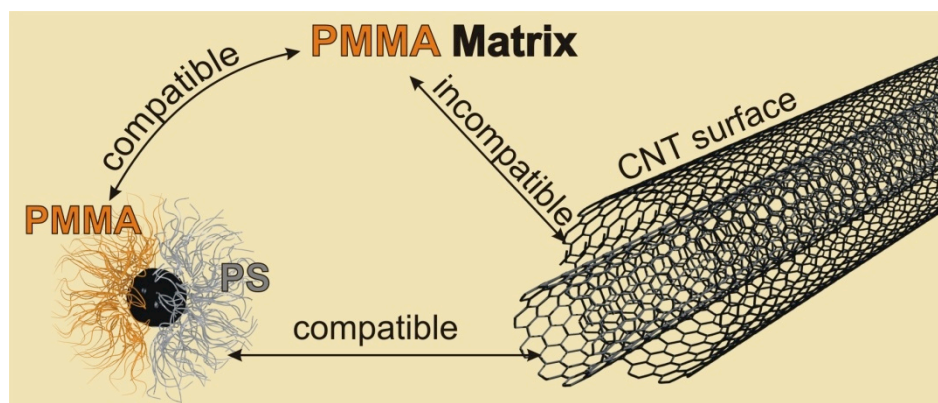
Published in *Angew. Chem. Int. Ed.* **2013**, 52 (13), 3602-3606; *Angew. Chem.* **2013**, 125 (13), 3688-3693.

Supracolloidal Hybrids: Soft polymer-based Janus micelles provide excellent stabilization for multi-walled carbon nanotubes in a variety of solvents, including water. The size ratio of stabilizing to adsorbing patch (Janus balance) is decisive for substantial physisorption and stabilization. The supracolloidal interaction preserves the structural integrity of the nanotubes, essential for maintaining many appealing properties.

Carbon nanotubes (CNTs) undoubtedly pose exceptional materials in nanotechnology and materials science.^[1,2] Their outstanding strength, robustness and electrical and thermal conductivity render them very attractive fillers for numerous innovative composites.^[3-6] A uniform distribution of CNTs in the target medium, e.g., solvent or polymer matrix, is often mandatory to fully harness the desired properties and to enhance CNT processability. However, the high cohesion energy (π -stacking) combined with a low solubility parameter promotes extreme bundling to minimize interactions with the surrounding medium.^[6, 7] It is therefore necessary to stabilize each CNT with a surface coating either via covalent attachment (grafting to/from) or physisorption.^[8-14] Covalent attachments provide very good stabilization, yet this “anchoring” also interrupts the conjugated π -system lowering the CNT properties. Physisorbed moieties are better suited as they show excellent stabilization, while maintaining the structural integrity of the CNTs. Non-covalent dispersants range from pure organic compounds to surfactants^[15-17] and block copolymers^[18-22], and recently, even block copolymer micelles.^[23, 24] Organic solvents have the disadvantage that the CNTs cannot be transferred into other media without coagulation and precipitation. Surfactants and amphiphilic block copolymers can be tailored to match any solvent, but often require a high dispersant-to-CNT weight ratio to form stable dispersions.^[18] In comparison to that, block copolymer micelles have similar stabilizing properties, while requiring lower dispersant/CNT ratios.^[23] These developments mirror that the trend is clearly shifting towards more sophisticated compatibilizers unifying strong adsorption to the CNTs paired with enhanced stabilization, preferably in many different media. Janus particles of various topologies^[25-29] are well-known for their strong affinity towards interfaces,^[30-32] outstanding performance as “giant surfactants” in emulsion polymerization, and as compatibilizers in polymer blends.^[33, 34] The strong interfacial affinity originates from the Pickering effect^[35] and the two strictly phase-separated corona patches.

Here, we demonstrate that polymer-based Janus micelles (JMs) facilitate the dispersion of multi-walled carbon nanotubes (MWNTs) in a variety of solvents, including water. JMs selectively adsorb to the MWNTs with a π -stacking patch, while stabilizing the formed supracolloidal hybrid in the chosen medium through steric repulsion with a solvophilic patch (Scheme 6–1). The non-invasive physisorption preserves the conjugated structure of the MWNTs, essential for maintaining its attractive properties. We recently developed a large-scale approach allowing the functional design of nanoscale JMs^[36, 37] with respect to size, corona chemistry and Janus balance (JB), all decisive for MWNT dispersion as summarized in Table 1. The overall size of the JMs can be tailored from 20 – 100 nm, matching the outer diameter of MWNTs, typically in the range of 10 – 100 nm. Larger particles (> 100 nm) may attach to several tubes causing network formation and precipitation. Matching sizes are essential to enhance particle-particle interaction as recently demonstrated for a biomimetic composite, where a genetically engineered “Janus-like” protein, hydrophobin, facilitates extremely strong supramolecular interaction between nanofibrillated

cellulose and graphene.^[38] The tasks of the corona hemispheres can be tailored to meet application needs, simply by choosing the proper ABC triblock terpolymer. Beyond that, we systematically vary the rarely addressed Janus balance, i.e. the size ratio of both corona patches, from dominant adsorbant to dominant stabilizer and show its critical impact on the effectiveness of the dispersant.



Scheme 6–1. JMs compatibilizing between MWNTs and medium. Adapted from *Angew. Chem. Int. Ed.* **2013**, 52, 3602-3606. Reprinted with permission from Wiley-VCH Verlag GmbH & Co. KGaA.

Table 6–1. Characteristics of used Janus Micelles

Code	Polymer ^[a]	R_h [nm] ^[b]	d_{core} [nm] ^[c]	JB_{PS} [%] ^[d]
SBM1	S ₆₁₀ B ₆₄₀ M ₂₉₀ ¹²⁷	35 ± 3	31 ± 5	68
SBM2	S ₃₄₀ B ₃₃₀ M ₃₆₀ ⁹⁰	25 ± 4	22 ± 4	48
SBM3	S ₂₈₀ B ₃₃₀ M ₄₃₀ ⁹⁰	27 ± 3	21 ± 3	39
SBT	S ₅₈₀ B ₁₂₀ T ₄₇₀ ¹³⁴	29 ± 2	10 ± 2	55
SBV	S ₃₆₀ B ₃₈₀ V ₅₉₀ ¹²⁰	29 ± 7	14 ± 3	38

[a] Subscript denotes the number-average degree of polymerization and superscript the molecular weight in kg/mol. [b] Hydrodynamic radii in THF at $c = 1$ g/L. [c] Average from TEM image analysis of 250 cores.^[41] [d] Janus balance, $JB_{PS} = DP_{n,PS}/(DP_{n,PS} + DP_{n,C})$ with C = PMMA, PtBMA or P2VP.

The experimental approach to JM/MWNT hybrids is straightforward and will be exemplified on polystyrene-*block*-polybutadiene-*block*-poly(methyl methacrylate) (SBM) JMs with a cross-linked B-core, a dominant S- and a minor M-patch ($JB_{PS} = 68$ %). Pristine, untreated MWNTs were dispersed in acetone together with SBM1 JMs at a weight ratio of 50:50 w/w to yield a final MWNT concentration of 0.05 g/L. Acetone is a good solvent for M, a near- Θ solvent for S and a non-solvent for the MWNTs. Thus, the MWNTs entangle into strongly interacting bundles (sedimentation), whereas the solvophobic S-patches cause clustering of JM (Figure 6–1A). This setup was sonified to disassemble the MWNTs and the JM-clusters. After treatment, re-assembly induces adsorption of JMs onto the MWNTs surface to minimize energetically unfavorable solvent/solvophobic interfaces. Thereby, the M-patches provide steric repulsion, suppressing rebundling of the MWNTs and promote the formation of a stable dispersion. A dense coating of JMs on to the MWNTs is evident from the substantial amount of spherical particles residing on the surface as visualized by

transmission and scanning electron microscopy (TEM, SEM) and atomic force microscopy (AFM, Figure 6–1B). Raman spectroscopy proves that the CNT surface is not affected by this supracolloidal attachment and in IR measurements both materials contribute to the spectrum (Figures S6–1-3).

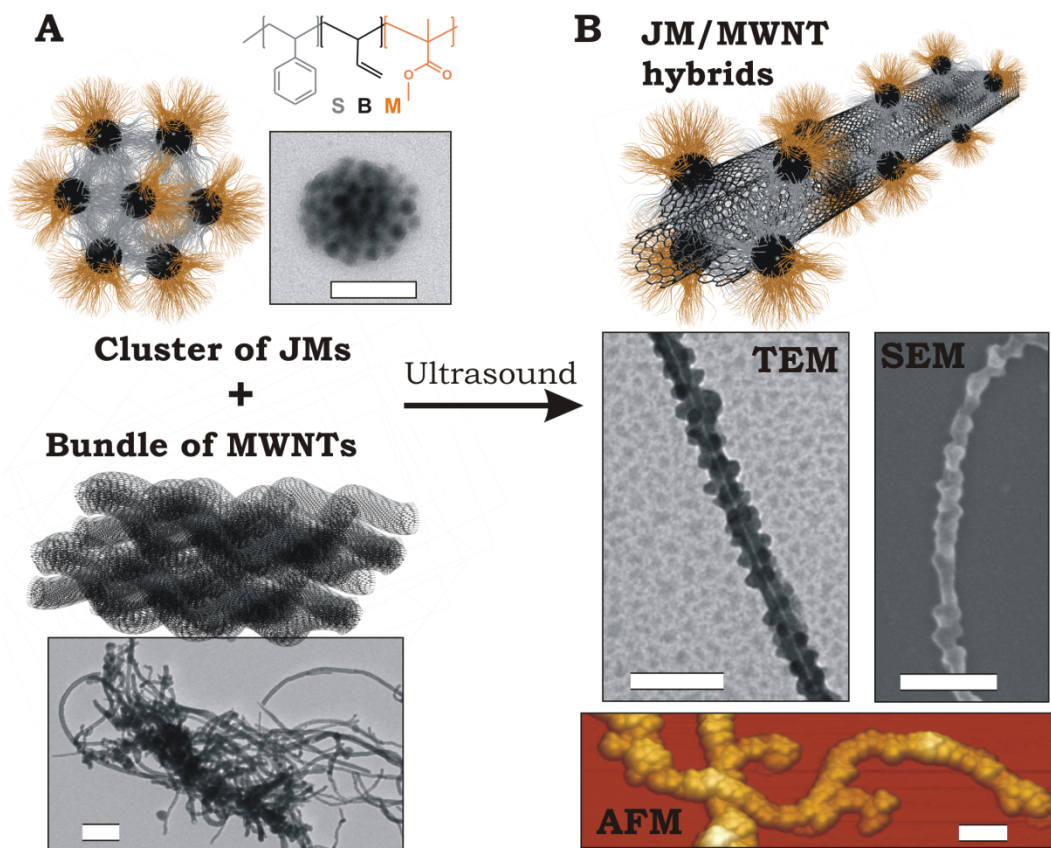


Figure 6–1. General preparation procedure. A) Schematics and TEM images of starting materials in acetone. B) Supracolloidal re-assembly (scale bars are 200 nm). Adapted from *Angew. Chem. Int. Ed.* **2013**, *52*, 3602-3606. Reprinted with permission from Wiley-VCH Verlag GmbH & Co. KGaA.

Surprisingly, the JMs selectively attach to the MWNTs instead of re-assembling with each other, irrespective of JM concentration or Janus balance. At a JM/MWNT ratio of 33:66 w/w, the JMs fully attach to the MWNTs and we do not identify any of the former clusters or residual JMs (Figure 6–2A). Dense packing is not observed yet, because there is still enough space for the JMs to evenly distribute along the MWNT surface. At a ratio of 50:50 w/w, SBM1 forms a dense multilayer packing, but still no residual JMs are found (Figure 6–2B). However, an excess of JMs (90:10 w/w) results in quantitative coverage, multilayer formation and growth of JM clusters from the surface (Figure S6–4). Only then, a fraction of the JMs simply re-assemble into the former raspberry-like shape. We attribute the strong and selective affinity of the JMs towards the solvent/MWNT-interface to (i) the Pickering effect,^[35] (ii) π -stacking of the polystyrene hemisphere facing towards the sp^2 -hybridized carbon surface, but mostly, to (iii) minimization of unfavorable interfacial energies. In good solvents such as THF (or less polar), JMs do not attach to the MWNTs but are evenly scattered on the TEM grid as the driving force for surface energy minimization

is greatly reduced. Reversible switching between the adsorbed and desorbed state underlines the supracolloidal nature of the interaction (Figure S6–5).

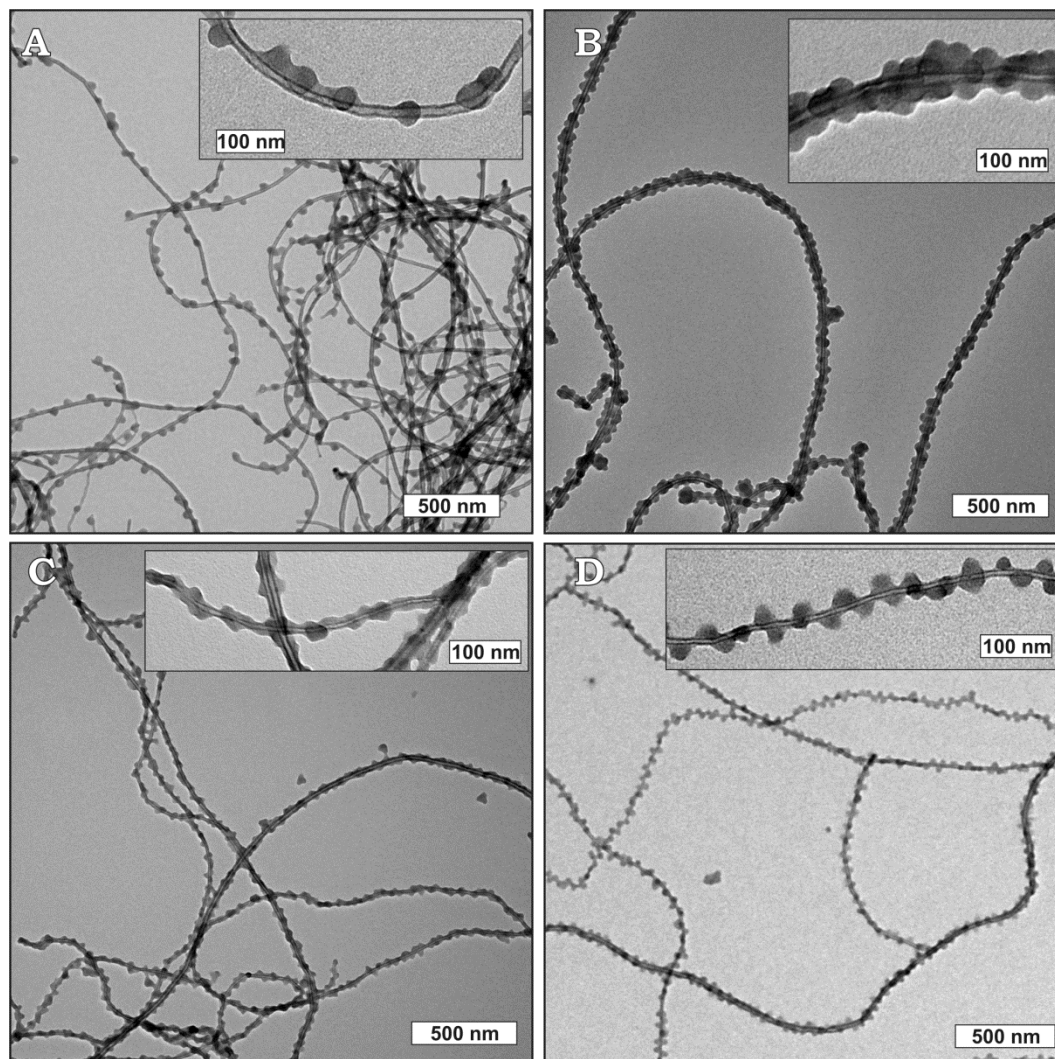


Figure 6–2. Adsorption pattern of SBM1 at A) 20:80 w/w and B) at 50:50 w/w, of C) SBM2 and D) SBM3. Adapted from *Angew. Chem. Int. Ed.* **2013**, *52*, 3602–3606. Reprinted with permission from Wiley-VCH Verlag GmbH & Co. KGaA.

In recent works, we and others showed that the Janus balance is a key element determining the aggregation behavior of JMs in selective solvents.^[36, 39, 40] Here, we demonstrate its fundamental influence on the quantity of adsorbed JMs on a set of SBM JMs ranging from dominant adsorbing (SBM1, $JB_{PS} = 68\%$) to equal-sized (SBM2, $JB_{PS} = 48\%$) to dominant stabilizing patch (SBM3, $JB_{PS} = 39\%$). The adsorption behavior is visualized qualitatively in TEM (Figures 6–2B–D, S6–4–7) and followed quantitatively via thermogravimetric analysis (TGA) (Figures 6–3, S6–8, 9). As long as the surface is not saturated ($< 50:50$ w/w), we observe quantitative adsorption corroborated by the linear relationship in Figure 6–3 (also no residual JMs in Figure 6–2B–D). At a constant weight ratio of 66:33 w/w, the amount of adsorbed JMs decreases from SBM1 to SBM3. SBM1 has the largest adsorbing S-patch and the smallest repulsive M-corona both promoting

dense packing. After adsorption, the “sticky” S-patch attracts other JMs inducing a cascading effect as every newly attached JM generates an additional hydrophobic surface. Even at very high JM content (83:17 w/w), we determine almost quantitative adsorption in TGA (≈ 70 wt.-%) realized by multilayer coating and cluster growth from the MWNT surface (Figures S6–4, 8, 9). SBM2 on the other hand, displays an adsorption limit at ≈ 45 wt.-% reached at 50:50 w/w, also indicated by the less dense coating as compared to SBM1 (Figure 2C). The larger stabilizing M-corona occupies more volume and blocks surface area for other JMs. These effects become more distinct for SBM3 (Figure 6–2D). Here, the surface uptake reaches saturation at ≈ 35 wt.-% as the M-corona requires too much space for all JMs to be accommodated. In TEM the space between the particles is occupied by PMMA (not visible due to e-beam degradation) and therefore not accessible for other JMs. Repulsive interactions of the solvated M-corona prevent complete coverage. In both TEM and SEM, JMs are evenly spaced on the MWNT surface, reminiscent of helical packing (Figure 6–2D, S6–7), where the JM-JM interparticle spacing is defined by the excluded volume of the M-corona. The motif of helical wrapping of CNTs is not uncommon and has been reported for several polymers.^[11]

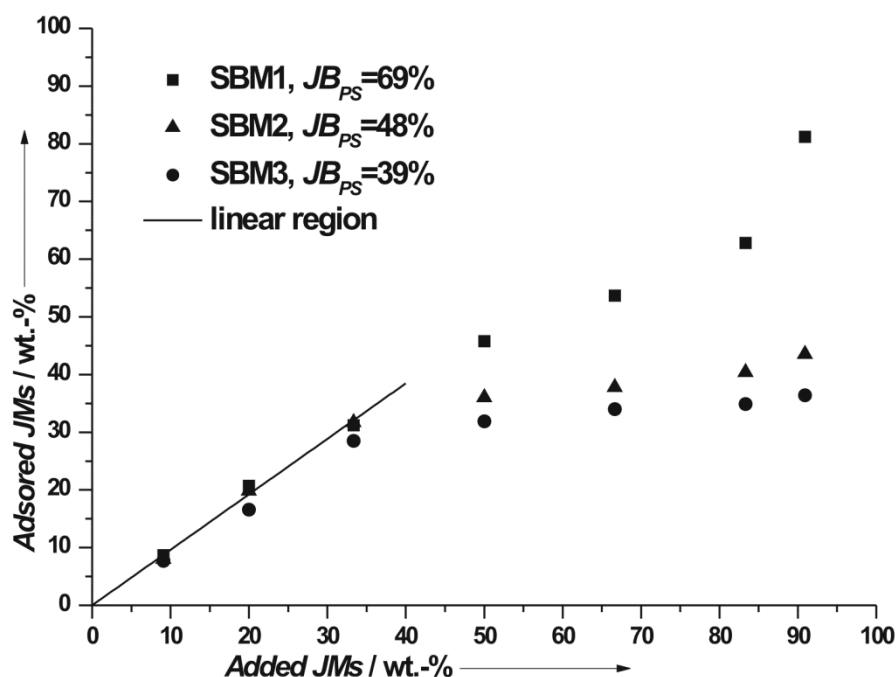


Figure 6–3. Adsorption efficiency of SBM1-3 JMs in dependence of their Janus balance determined by thermogravimetric analysis. Adapted from *Angew. Chem. Int. Ed.* **2013**, 52, 3602-3606. Reprinted with permission from Wiley-VCH Verlag GmbH & Co. KGaA.

The striking advantage of JMs is the possibility to combine and spatially divide different chemical environments within one single particle. We designed several JMs with one patch, matching the demands of increasingly polar solvents, while continued to use the S-patch that already proved its extraordinary affinity towards MWNTs. We first exchange the PMMA-patch (suitable for blending with poly(styrene-*co*-acrylonitrile) or PMMA)

with poly(*tert*-butyl methacrylate) (T) that is stable in ethanol (Figure 6–4A). We chose PS-*b*-PB-*b*-PtBMA (SBT) JMs with a very small B-core ($d \approx 10$ nm) to demonstrate control of the size of the JMs that are only visible as regularly spaced small black dots on the MWNTs surrounded by a dark gray coating (S, selectively stained with RuO₄). PS-*b*-PB-*b*-P2VP (SBV) JMs with a pH-responsive poly(2-vinyl-pyridine) (V) patch allow stabilization of MWNTs in acidic water. Cryogenic TEM imaging gives a clear picture of the JM distribution around the MWNTs and rules out drying artifacts (Figure 6–4B). P2VP is an attractive functional corona that allows the entire supracolloidal hybrid to undergo reversible precipitation/redispersion cycles with a sharp transition at pH 4 and it is also well-known to coordinate metal anions (e.g. AuCl₄⁻, TiO₂²⁻). JMs with a poly(methacrylic acid) (MAA) patch (SBMAA, obtained via hydrolysis of SBM),^[41] form stable dispersions in neutral and basic water (Figure 6–4C). This hybrid shows a precipitation/redispersion transition at pH ~5 and PMAA is known to coordinate metal cations (e.g. Ag⁺, Cd²⁺). Surprisingly, the stability of the SBMAA/MWNT hybrids follows an inverse trend to the adsorbed mass of JMs and increases from SBMAA1 to SBMAA3 (Figure 6–4D). Although MWNTs have a lower bulk density than water ($\delta_{\text{MWNTs}} \approx 0.22$ g/cm³), the SBMAA1 coating induces sedimentation due to insufficient stabilization ($JB_{\text{PS}} = 68$ %) as compared to the increased total weight of the hybrid. Stabilization enhances for SBMAA2 and peaks for SBMAA3, clearly demonstrating that not the amount of attached JMs is decisive for stability, but rather the contribution of each JM to hybrid stabilization, i.e., a Janus balance in favor of the stabilizing MAA-patch.

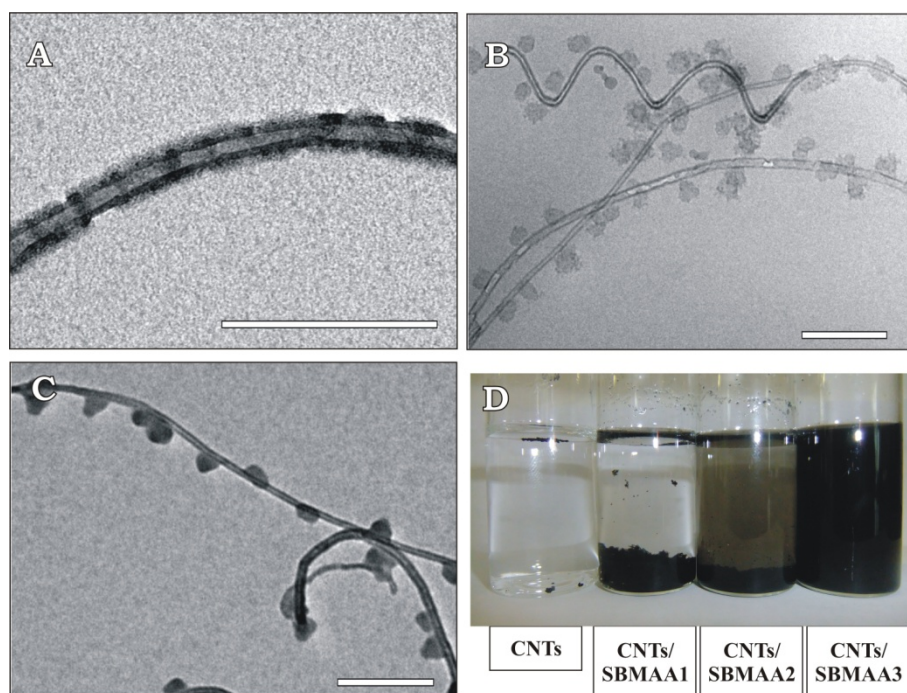


Figure 6–4. JM/MWNT hybrids (50:50 w/w) in protic solvents. A) SBT JMs in ethanol, B) SBV JMs in water pH 3 (cryo-TEM) and C) SBMAA3 JMs in water pH 10. D) MWNT dispersions in water pH10: pristine, stabilized by SBMAA1, SBMAA2 and SBMAA3 (scale bars are 200 nm). Adapted from *Angew. Chem. Int. Ed.* **2013**, 52, 3602-3606. Reprinted with permission from Wiley-VCH Verlag GmbH & Co. KGaA.

In conclusion, we demonstrated that Janus micelles are well suited as supracolloidal dispersants for carbon nanotubes. They exhibit (i) amphiphilic character and (ii) tunable surface patches; (iii) the supracolloidal attachment preserves CNTs properties, while (iv) low dispersant/tube weight ratios (10:90 w/w) are sufficient for stabilization. In the dried state, the JMs act as a glue for the CNTs and the hybrid material approaches the bulk density of the glassy polymers ($\delta \approx 1.15\text{-}1.50 \text{ g/cm}^3$), making handling safer and dosing easier. In contrast, pristine disentangled CNTs exhibit a very low density and become easily airborne. The quantitative coating allows precipitation, drying, long-time storage and redispersion in any medium, matching the stabilizing corona. The Janus balance determines the quantity of adsorbed JMs and thus controls adsorption patterns from multilayered to helical. The direct visualization of adsorption patterns should aid the design of future CNT dispersants. A number of other attractive stabilizing patches are currently pursued by us, such as pH- and temperature-responsive poly(2-(dimethylamino)ethyl methacrylate), technologically relevant and degradable poly(ϵ -caprolactone) or biocompatible poly(ethylene oxide).

ASSOCIATED CONTENT

Supporting Information

Supporting information and experimental details for this article is available on the WWW under <http://www.angewandte.org> or from the authors.

AUTHOR INFORMATION

Corresponding Author

andre.groschel@uni-bayreuth.de; axel.mueller@uni-bayreuth.de

Notes

The authors declare no competing financial interests.

Present Addresses

[†]MM is currently working in the Department of Chemical & Biomolecular Engineering at the University of Melbourne, Australia. AHG is currently working at Molecular Materials, Department of Applied Physics, Aalto University, Finland, E-mail: andre.groschel@aalto.fi; AHEM is currently working at Institute of Organic Chemistry, Johannes Gutenberg University Mainz, Germany, E-mail: axel.mueller@uni-mainz.de;

Author Contributions

AHG conceived the project, designed the experiments and wrote the manuscript. PDP and TIL performed some of the experiments and was involved in discussions. MM performed AFM measurements and helped discussing the results. FW performed SEM measurements. AHEM co-designed the experiments and was involved in writing the manuscript.

ACKNOWLEDGMENT

This work was supported by the Deutsche Forschungsgemeinschaft within SFB 840 (TP A1) and Mu896/39-1. We thank Andreas Fery for his support in analyzing the JM-MWNT interaction.

REFERENCES

- [1] R. H. Baughman, A. A. Zakhidov, W. A. de Heer, *Science* **2002**, *297*, 787-792.
- [2] G. Sahoo, S. Rana, J. W. Cho, L. Li, S. H. Chan, *Progr. Polym. Sci.* **2010**, *35*, 837-867.
- [3] S. J. Kang, C. Kocabas, T. Ozel, M. Shim, N. Pimparkar, M. A. Alam, S. V. Rotkin, J. A. Rogers, *Nature Nanotech.* **2007**, *2*, 230-236.
- [4] Z. Han, A. Fina, *Progr. Polym. Sci.* **2011**, *36*, 914-944.
- [5] Z. Spitalsky, D. Tasis, K. Papagelis, C. Galiotis, *Progr. Polym. Sci.* **2010**, *35*, 357-401.
- [6] L. Hu, D. S. Hecht, G. Grüner, *Chem. Rev.* **2010**, *110*, 5790-5844.
- [7] E. Nativ-Roth, R. Shvartzman-Cohen, C. Bounioux, M. Florent, D. Zhang, I. Szleifer, R. Yerushalmi-Rozen, *Macromolecules* **2007**, *40*, 3676-3685.
- [8] N. Roy, R. Sengupta, A. K. Bhowmick, *Progr. Polym. Sci.* **2012**, *37*, 781-819.
- [9] T. Akasaka, F. Wudl, S. Nagase, *Chemistry of Nanocarbons*, John Wiley & Sons, **2010**, 1-48.
- [10] D. Tasis, N. Tagmatarchis, A. Bianco, M. Prato, *Chem. Rev.* **2006**, *106*, 1105-1136.
- [11] A. Hirsch, *Angew. Chem.* **2002**, *114*, 1933-1939; *Angew. Chem. Int. Ed.* **2002**, *41*, 1853-1859.
- [12] D. Tasis, N. Tagmatarchis, V. Georgakilas, M. Prato, *Chem. Europ. J.* **2003**, *9*, 4000-4008.
- [13] N. Karousis, N. Tagmatarchis, D. Tasis, *Chem. Rev.* **2010**, *110*, 5366-5397.
- [14] J.-M. Thomassin, D. Vuluga, M. Alexandre, C. Jérôme, I. Molenberg, I. Huynen, C. Detrembleur, *Polymer* **2012**, *53*, 169-174.
- [15] M. R. Diehl, S. N. Yaliraki, R. A. Beckman, M. Barahona, J. R. Heath, *Angew. Chem.* **2002**, *114*, 363-366; *Angew. Chem. Int. Ed.* **2002**, *41*, 353-356.
- [16] C. A. Furtado, U. J. Kim, H. R. Gutierrez, L. Pan, E. C. Dickey, P. C. Eklund, *J. Am. Chem. Soc.* **2004**, *126*, 6095-6105.
- [17] K. K. Kim, S. M. Yoon, J. Y. Choi, J. Lee, B. K. Kim, J. M. Kim, J. H. Lee, U. Paik, M. H. Park, C. W. Yang, K. H. An, Y. Chung, Y. H. Lee, *Adv. Funct. Mater.* **2007**, *17*, 1775-1783.
- [18] V. C. Moore, M. S. Strano, E. H. Haroz, R. H. Hauge, R. E. Smalley, J. Schmidt, Y. Talmon, *Nano Lett.* **2003**, *3*, 1379-1382.
- [19] N. Sluzarenko, B. Heurtefeu, M. Maugey, C. Zakri, P. Poulin, S. Lecommandoux, *Carbon* **2006**, *44*, 3207-3212.
- [20] J. Zou, L. Liu, H. Chen, S. I. Khondaker, R. D. McCullough, Q. Huo, L. Zhai, *Adv. Mater.* **2008**, *20*, 2055-2060.
- [21] V. A. Sinani, M. K. Gheith, A. A. Yaroslavov, A. A. Rakhnyanskaya, K. Sun, A. A. Mamedov, J. P. Wicksted, N. A. Kotov, *J. Am. Chem. Soc.* **2005**, *127*, 3463-3472.
- [22] S. Soll, M. Antonietti, J. Yuan, *ACS Macro Lett.* **2012**, *1*, 84-87.
- [23] H.-I. Shin, B. G. Min, W. Jeong, C. Park, *Macromol. Rapid Commun.* **2005**, *26*, 1451-1457.
- [24] P. D. Petrov, G. L. Georgiev, A. H. E. Müller, *Polymer* **2012**, *53*, 5502-5506.
- [25] R. Erhardt, A. Böker, H. Zettl, H. Kaya, W. Pyckhout-Hintzen, G. Krausch, V. Abetz, A. H. E. Müller, *Macromolecules* **2001**, *34*, 1069-1075.
- [26] A. Walther, M. Drechsler, S. Rosenfeldt, L. Harnau, M. Ballauff, V. Abetz, A. H. E. Müller, *J. Am. Chem. Soc.* **2009**, *131*, 4720-4728.
- [27] F. Wurm, A. F. M. Kilbinger, *Angew. Chem.* **2009**, *121*, 8564-8574; *Angew. Chem. Int. Ed.* **2009**, *48*, 8412-8421.

- [28] D. Hirsemann, S. Shylesh, R. A. De Souza, B. Diar-Bakerly, B. Biersack, D. N. Mueller, M. Martin, R. Schobert, J. Breu, *Angew. Chem.* **2012**, *124*, 1376-1380; *Angew. Chem. Int. Ed.* **2012**, *51*, 1348-1352.
- [29] A. Walther, A. H. E. Müller, *Soft Matter* **2008**, *4*, 663-668.
- [30] A. Walther, X. André, M. Drechsler, V. Abetz, A. H. E. Müller, *J. Am. Chem. Soc.* **2007**, *129*, 6187-6198.
- [31] N. Glaser, D. J. Adams, A. Böker, G. Krausch, *Langmuir* **2006**, *22*, 5227-5229.
- [32] T. M. Ruhland, A. H. Gröschel, A. Walther, A. H. E. Müller, *Langmuir* **2011**, *27*, 9807-9814.
- [33] A. Walther, M. Hoffmann, A. H. E. Müller, *Angew. Chem.* **2008**, *120*, 723-726; *Angew. Chem. Int. Ed.* **2008**, *47*, 711-714.
- [33] A. Walther, K. Matussek, A. H. E. Müller, *ACS Nano* **2008**, *2*, 1167-1178.
- [35] B. P. Binks, P. D. I. Fletcher, *Langmuir* **2001**, *17*, 4708-4710.
- [36] A. H. Gröschel, F. H. Schacher, H. Schmalz, O. V. Borisov, E. B. Zhulina, A. Walther, A. H. E. Müller, *Nat. Commun.* **2012**, *3*, 710.
- [37] A. H. Gröschel, A. Walther, T. I. Löbbling, J. Schmelz, A. Hanisch, H. Schmalz, A. H. E. Müller, *J. Am. Chem. Soc.* **2012**, *134*, 13850-13860.
- [38] P. Laaksonen, A. Walther, J.-M. Malho, M. Kainlauri, O. Ikkala, M. B. Linder, *Angew. Chem.* **2011**, *123*, 8847-8850; *Angew. Chem. Int. Ed.* **2011**, *50*, 8688-8691.
- [39] S. Jiang, S. Granick, *J. Chem. Phys.* **2007**, *127*, 161102-161104.
- [40] S. Jiang, S. Granick, *Langmuir* **2008**, *24*, 2438-2445.
- [41] R. Erhardt, M. Zhang, A. Böker, H. Zettl, C. Abetz, P. Frederik, G. Krausch, V. Abetz, A. H. E. Müller, *J. Am. Chem. Soc.* **2003**, *125*, 3260-3267.

Supporting Information

to

Janus Micelles as Effective Supracolloidal Dispersants for Carbon Nanotubes

André H. Gröschel^{*†}, Tina I. Löbling[†], Petar D. Petrov¹, Markus Müllner[†], Christian Kuttner², Florian Wieberger³, and Axel H. E. Müller^{*†}

Makromolekulare Chemie II, Universität Bayreuth, D-95440 Bayreuth, Germany.

andre.groeschel@uni-bayreuth.de; axel.mueller@uni-bayreuth.de

¹ *Institute of Polymers, Bulgarian Academy of Sciences, Sofia 1113, Bulgaria.*

² *Physikalische Chemie II, Universität Bayreuth, D-95440 Bayreuth, Germany.*

³ *Makromolekulare Chemie I, Universität Bayreuth, D-95440 Bayreuth, Germany.*

1. Experimental Section

Materials

The preparation and characterization of SBM, SBV and SBT triblock terpolymers were reported in detail previously.^[1-5] Relevant terpolymer specifics are summarized in Tables S1. Multi-walled carbon nanotubes were purchased from Aldrich (carbon content > 95 %, average diameter $d=20-30$ nm, 0.5-200 μm length, produced *via* CoMoCAT[®] Catalytic Chemical Vapor Deposition (CVD) Method). All solvents used were of analytical grade.

Methods

Preparation of Janus Micelles (JMs). To demonstrate the readily accessible large-scale synthesis, we prepared solutions of SBM, SBV and SBT terpolymers (1g) in THF (10ml) at a concentration of $c = 100$ g/L. The highly concentrated polymer solutions were dialyzed into 1 L of selective solvent for the corona block to yield spherical multicompartment micelles. This step breaks the symmetry by phase separation of block A (core) and C (corona). The solvent exchange was monitored by ¹H-NMR. Micellar solutions of SBM terpolymers were dialyzed into acetone/isopropanol mixtures, SBT terpolymer into ethanol, SBV into isopropanol. In order to permanently fixate this phase separated state, we added 0.5 equivalents photo-crosslinker, 2,4,6-trimethylbenzoyldiphenyl-phosphineoxide (Lucirin TPO[®]; $\lambda_{max} \approx 360$ nm) per double bond to the solution. Stirring for 2 hours ensured homogeneous distribution of the photo-crosslinker before the sample was irradiated for 1 hour using a

UV-lamp with a cut-off filter of $\lambda = 300$ nm. Precipitation in methanol (or MilliQ water for SBV) removed the cross-linker and yielded Janus micelles. The overall procedure takes over night and can be modified to produce JMs on a 100 g scale. As stable dispersions with MWNTs are already obtained at ratios of 10:90 w/w this can be used to prepare 1 kg of hybrid material equalling 100 kg composite with 1 wt% filler content.

Preparation of JM/MWNT hybrids. JMs and MWNTs were dispersed in acetone, JMs at varying concentrations $c = 0.05, 0.1$ and 0.5 g/L, and MWNTs at a fixed concentration $c = 0.05$ g/L. The JM and MWNT solutions were mixed to yield JM/MWNT weight ratios of 10:90, 20:80, 33:66, 50:50, 66:33, 83:17 and 90:10 w/w. The mixtures underwent ultrasonic treatment using a Branson model-250 digital sonifier, equipped with 1/8 in. diameter tapered microtip, for 10 min with 10 % amplitude (200 watt) and a pulse/pause sequence of 30s/10s.

Hydrolysis of SBM JMs to SBMAA. The JMs were dissolved in 1,4-dioxane ($c = 10$ g/L) in a sealed Schott glass and the PMMA ester groups were hydrolyzed with 3 eq. KOH per PMMA unit using 18-crown-6 as a phase transfer agent (molar ratio [18-crown-6]/[KOH] = 5/1). The reaction was carried out at 110 °C for 5 days. Finally the solution was precipitated into 1 M hydrochloric acid, and washed with water, before the residue was dried under vacuum (maximum 50 °C).

Transmission Electron Microscopy (TEM) was performed in bright-field mode on Zeiss CEM 902 and LEO 922 OMEGA electron microscopes operated at 80 kV and 200 kV, respectively. The samples were prepared by placing one drop of the polymer solution (0.01 g/L) onto carbon-coated copper grids. Excess solvent was instantly absorbed by a filter paper.

Sample preparation for additional measurements. 10 mg of MWNTs were sonified together with JMs in acetone for 20 min, filtered to remove excess JMs (e.g., for high JM contents) and washed with acetone. After drying of the residue, 8-10 mg of hybrid was used for the measurements.

Thermogravimetric Analysis (TGA) were carried out on a Mettler Toledo TGA/SDTA 851e to study the thermal properties at a heating rate of 10 °K/min in N_2 from 25 to 800 °C.

Raman spectroscopy. The Raman data was acquired using a confocal Raman microscope (LabRAM Division, HORIBA Jobin Yvon) equipped with an objective from Olympus (100x, NA = 0.9) and a linear polarized laser (He-Ne, $\lambda = 632.8$ nm). The Raman scattering was detected by a Peltier-cooled CCD camera (-70 °C, Synapse), behind a grating spectrometer. All spectra were accumulated from three measurements with the laser focused at the sample surface.

Attenuated Total Reflection Infrared (ATR-IR) spectra were recorded on a Digilab Excalibur Series with an ATR unit MIRacle from Pike Technology.

2. Raman spectroscopy of supracolloidal JM/MWNT interaction

Apart from the radial breathing modes (RBM) the Raman spectra of MWNTs show three characteristic frequency bands: D(defect)-band (1320 cm^{-1}), G(raphene)-band ($1570 - 1600\text{ cm}^{-1}$), and G'-band (2635 cm^{-1}). The D-band is a result of photon-defect interactions.^[6] For MWNTs, the G-band can be differentiated for the longitudinal (G-) and the circumferential (G+) stretching of the nanotube.^[7] The G-/G+ ratio suggests that the studied CNT sample has a multi-wall configuration.^[8] The G'-band is an overtone which is related to photo-second photon interactions. These peaks are characteristic of MWNTs and graphite sheets. Figure S1 shows overview spectra comparing neat and SBM modified MWNTs.

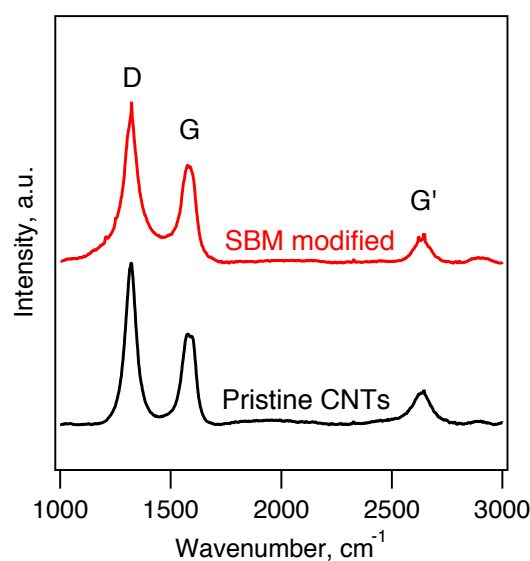


Figure S6-1. Raman spectra of pristine (black) and modified CNTs (red). For clarity a low resolution grating (600 g mm^{-1}) was used.

The ratio of the D-band to the G-band intensity (I_D/I_G) is a sensitive measure of the defect concentration, which is commonly used for MWNTs samples.^[8,9] The D/G bands are presented in Figure S2. By fitting the data for three Voigt signals, the G-/G+ signals can be distinguished. A comparison of the Raman data can be found in Table S1. We found that the I_D/I_G -band ratio, which is related to the defect concentration, did not change noticeably upon modification (<2%). Considering the area ratio $A_D/(A_G+A_{G+})$ the data suggests an apparent decrease of the defect density, which is due to a contribution of the polymer (additional vibrations/ cm^{-1} : $\nu(\text{CC})$ alicyclic, aliphatic chain $600-1300\text{ cm}^{-1}$; aromatic ring chain 1600 cm^{-1} , 1500 cm^{-1} ; $\delta(\text{CH}_3)$ 1380 cm^{-1} ; $\delta(\text{CH}_2)$ $\delta(\text{CH}_3)$ asym. $1400-1470\text{ cm}^{-1}$; $\nu(\text{C=O})$ $1680-1820\text{ cm}^{-1}$). The specific signals could not be distinguished from the MWNTs bands.

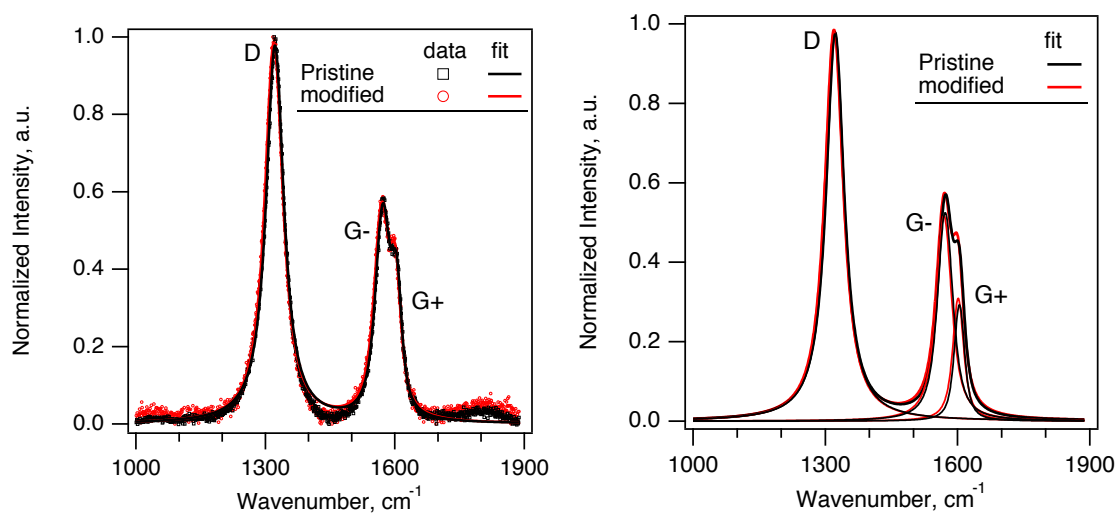


Figure S5-2. Raman spectra of G/D-band regime measured at high resolution (grating: 1800 g mm⁻¹). The fitting was based on three Voigt signals (D, G-, and G+).

Table S6-1. Comparison of Raman data.

	D [cm ⁻¹]	G- [cm ⁻¹]	G+ [cm ⁻¹]	I_{G+}/I_{G-}	I_D/I_{G-}	$A_D/(A_{G-}+A_{G+})$
Pristine	1320	1570	1600	0.56	1.86	1.86
modified	1320	1570	1600	0.60	1.89	1.67

3. IR-Spectroscopy of JM, pristine MWNTs and purified hybrid

After sonication treatment and removal of excess micellar solution we find a contribution of both materials to the characteristic signals within the hybrid.

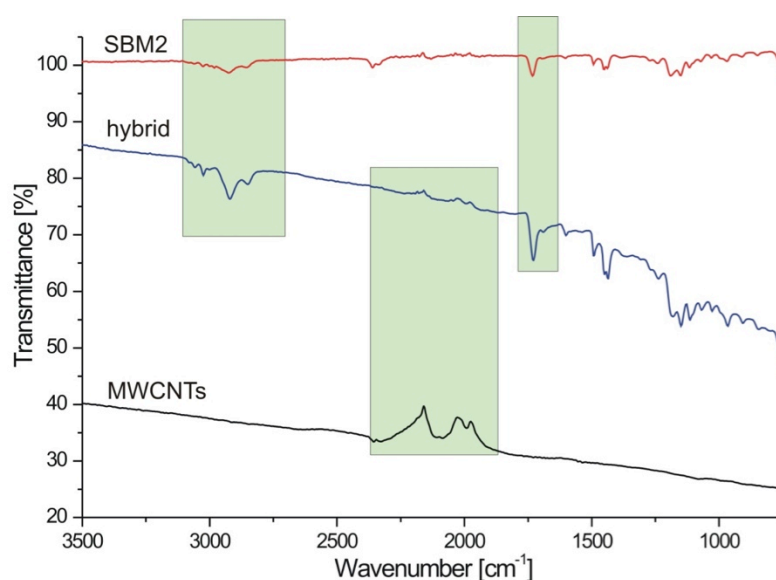


Figure S6-3. IR-spectra of SBM2 (red), pristine MWNTs (black) and hybrid (blue). The characteristic features of both materials are highlighted and can be found within the hybrid material. The characteristic adsorption band for CH₂ (3200-2800 cm⁻¹), the MWNT (2300-1800 cm⁻¹) and -COO- of PMMA (1750 cm⁻¹).

4. Magnified adsorption pattern of SBM1-3 at weight ratios 50:50, 66:33 and 90:10.

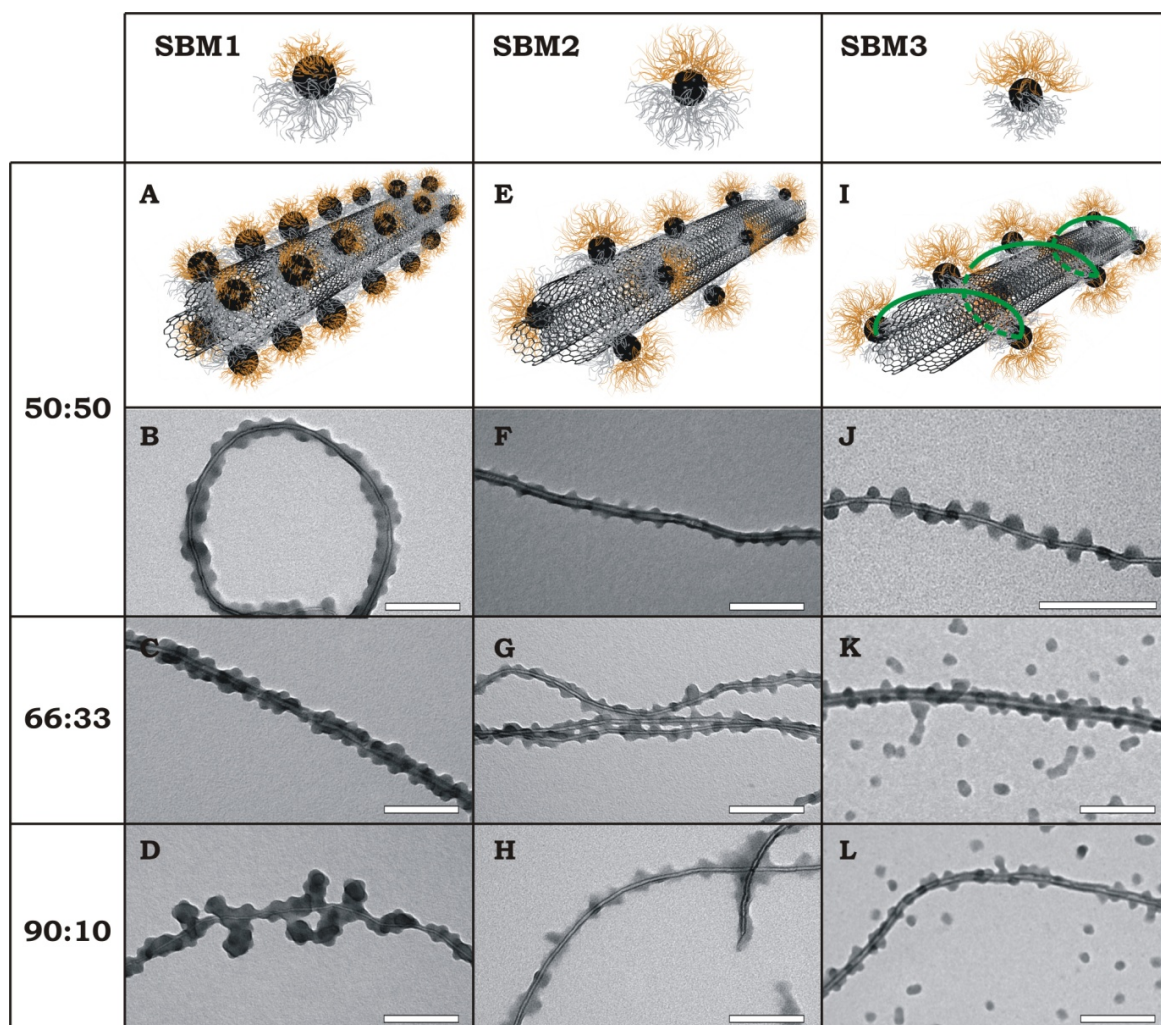


Figure S6-4. JM/MWNT hybrids at varying weight ratios 50:50, 66:33 and 90:10 and differing Janus balance. A-D) The adsorption pattern goes from statistical to dense to multilayer coating for SBM1 with JM clusters observed only at high weight ratios (D). E-H) SBM2 displays less dense coating and I-L) SBM3 adsorption pattern with regular spacing. Already at a moderate weight ratio of 66:33 a large fraction of the JMs cannot adsorb to the MWNTs.

5. Reversible supracolloidal adsorption/desorption of SBM1

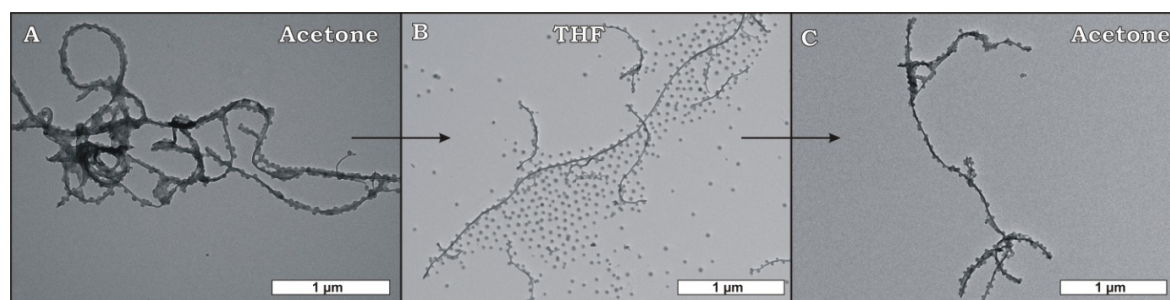


Figure S6-5. Supracolloidal adsorption/desorption of SBM1 onto MWNTs in selective solvents at a weight ratio of 50:50. A) Dense coating after 20 min sonication in acetone. Full consumption of the JMs and no residual micelles in the background. B) The TEM image shows the sample from (A) after drying, redispersion in THF and sonication for 20 min. Some JMs are still attached to the surface, yet the major part has detached and is located in the vicinity. C) The TEM image shows the sample from (B) after drying, redispersion in acetone and sonication for 20 min. The JMs are again quantitatively attached to the surface and no residual JMs are in the vicinity.

6. TEM overviews of SBM1-3 at a weight ratio of 66:33.

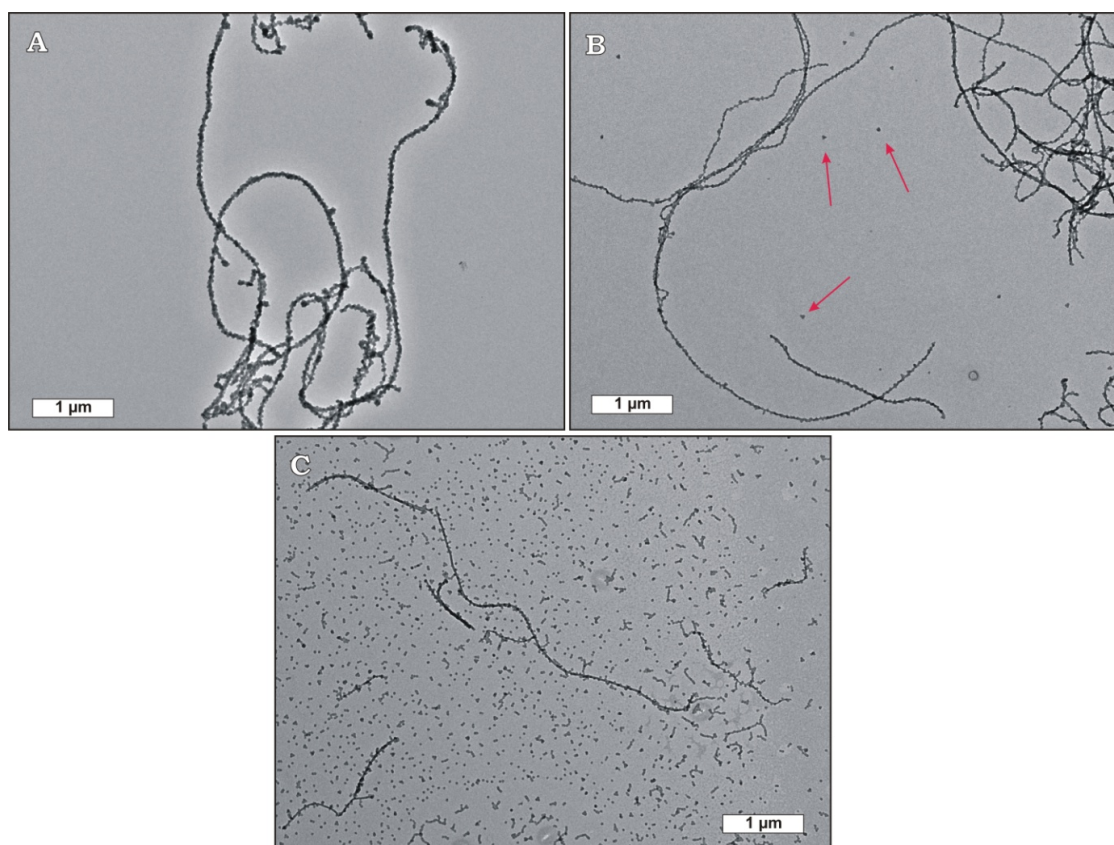


Figure S6-6. Overviews of MWNTs coated with SBM1-3 at a weight ratio of 66:33. A) MWNTs coated with SBM1 show full consumption of the JMs with no residual micelles in the background. B) For SBM2 the surface is also completely covered with JMs, but at this weight ratio already small micellar clusters are visible (red arrows). C) Due to the large swollen repulsive corona, SBM3 JMs require more space and at this weight ratio a large amount cannot attach to the surface of the MWNTs.

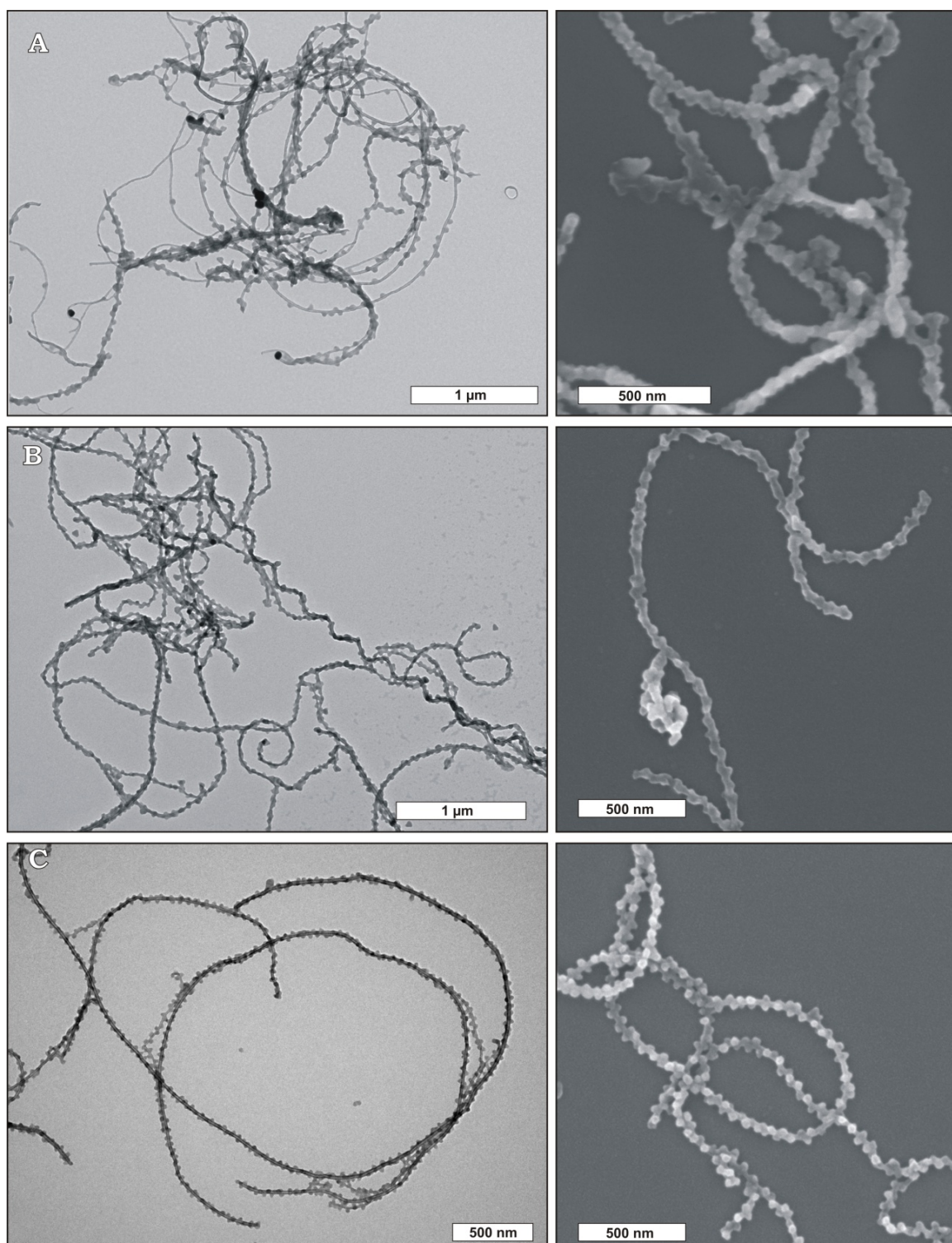
7. TEM and SEM overviews of SBM1-3 at a weight ratio of 50:50.

Figure S6-7. Overviews of MWNTs coated with SBM1-3 at a weight ratio of 50:50. A-C) MWNTs coated with SBM1 show full consumption of the JMs with no residual micelles in the background. B) For SBM2 the surface is also completely covered with JMs, but at this weight ratio already small micellar clusters are visible (red arrows). C) Due to the large swollen repulsive corona, JMs SBM3 require more space and already at this weight ratio a large amount cannot attach to the surface of the MWNTs.

8. Thermogravimetric (TGA) measurements

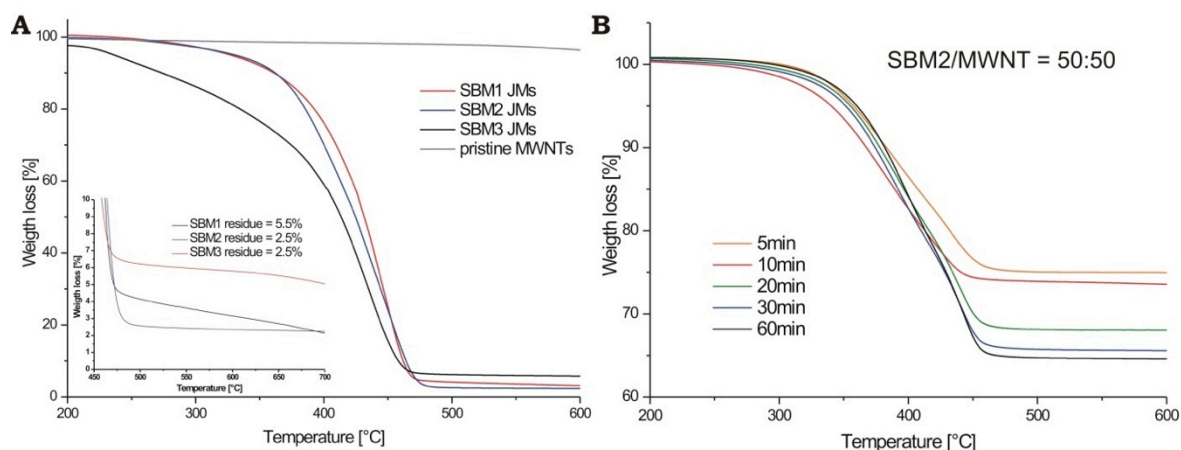


Figure S6-8. A) TGA of starting materials. B) Influence of sonication time on adsorbed mass. We observe a clear increase with sonication time, which we attribute to the progressing disentanglement of the long and length-disperse MWNTs (0.5-200 μm) and the larger produced surface area.

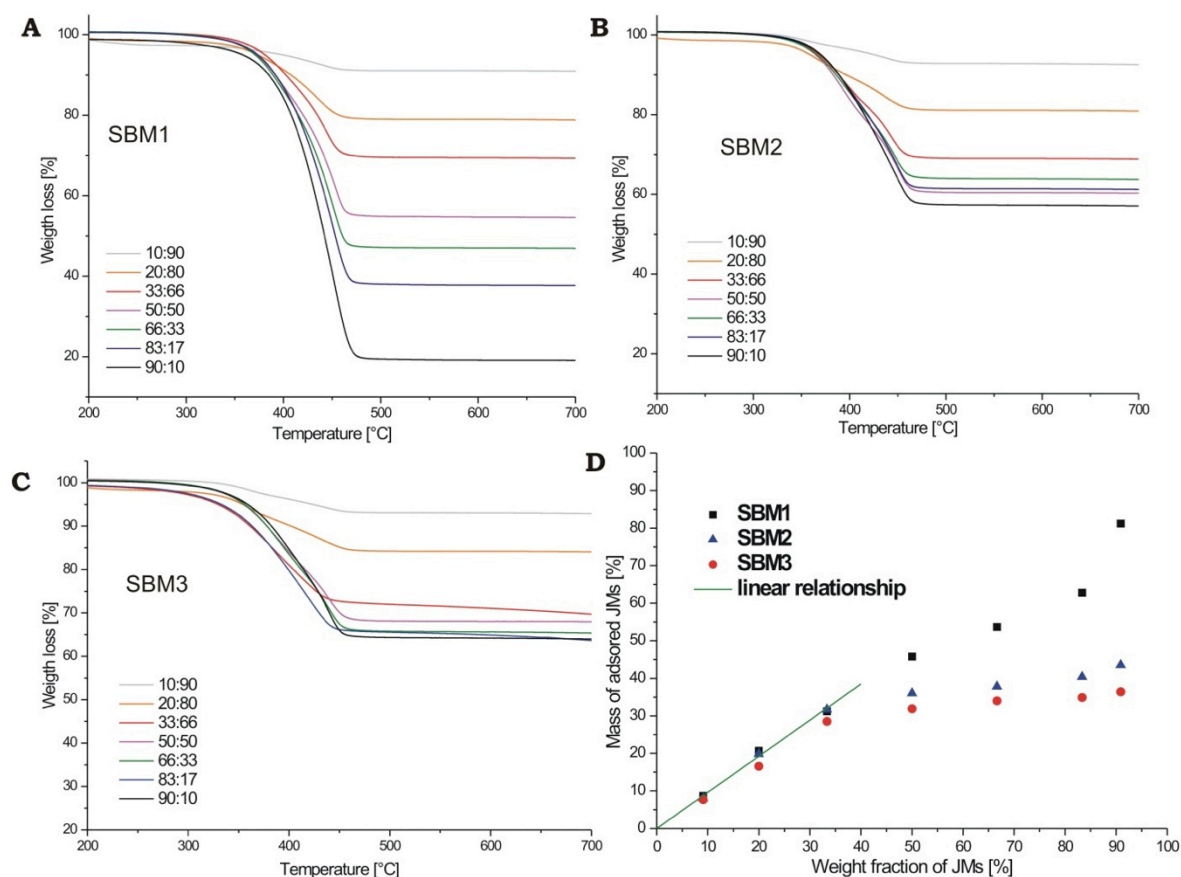


Figure S6-9. Quantitative determination of adsorbed mass in dependence of mixing ratios 10:90, 20:80, 33:66, 50:50, 66:33, 83:17 and 90:10. A) SBM1, B) SBM2 and C) SBM3. D) Comparison of adsorption behaviour of SBM1-3. All JMs exhibit a linear region (quantitative adsorption) until surface saturation is reached. The larger the stabilizing corona patch, the sooner complete coverage of the MWNTs is reached expressed by asymptotic approximation of the maximum loading limit: $\approx 70\text{wt}\%$ for SBM1, $\approx 45\text{wt}\%$ for SBM2, $\approx 35\text{wt}\%$ for SBM3. The excessively large weight fraction ($\approx 85\text{wt}\%$) of adsorbed SBM1 at 90:10 w/w is attributed to the formation of large JM clusters alongside with MWNT coating.

9. Supporting References

- [1] C. Auschra, R. Stadler, *Polym. Bull.* **1993**, *30*, 257-264.
- [2] E. Giebeler, R. Stadler, *Macromol. Chem. Phys.* **1997**, *198*, 3815-3825.
- [3] A. Walther, X. André, M. Drechsler, V. Abetz, A. H. E. Müller, *J. Am. Chem. Soc.* **2007**, *129*, 6187-6198.
- [4] F. Schacher, J. Yuan, H. G. Schoberth, A. H. E. Müller, *Polymer* **2010**, *51*, 2021-2032.
- [5] H. Ruckdäschel *et al.*, *Polymer* **2006**, *47*, 2772-2790.
- [6] F. Tuinstra, J. L. Koenig. *J. Chem. Phys.* **1970**, *53*, 1126-1130.
- [7] R. Graupner, *J. Raman Spectrosc.* **2007**, *38*, 673-683.
- [8] M. S. Dresselhaus; G. Dresselhaus; R. Saito; A. Jorio, *Phys. Rep.* **2005**, *409*, 47–99.
- [9] J. Maultzsch *et al.*, *Appl. Phys. Lett.* **2002**, *81*, 2647-2649.

List of Publications:

1. Hirao, A.; Matsuo, Y.; Oie, T.; Goseki, R.; Ishizone, T.; Sugiyama, K.; **Gröschel, A. H.**; Müller, A. H. E.
Facile synthesis of triblock co- and terpolymers of styrene, 2-vinylpyridine, and methyl methacrylate by a new methodology combining living anionic diblock copolymers with a specially designed linking reaction,
Macromolecules **2011**, *44*, 6345-6355.
2. Schütz, M. R.; Kalo, H.; Lunkenbein, T.; **Gröschel, A. H.**; Müller, A. H. E.; Wilkie, C.A.; Breu J.
Shear stiff, surface modified mica-like nanoplatelets: A novel filler for polymer nanocomposites,
J. Mater. Chem. **2011**, *21*, 12110-12116.
3. Ruhland, T.; **Gröschel, A. H.**; Walther, A.; Müller, A. H. E.
Janus cylinders at liquid-liquid interfaces,
Langmuir **2011**, *27*, 9807-9814.
4. Wieberger, F.; Forman, D.C.; Neuber, C.; **Gröschel, A. H.**; Böhm, M.; Müller, A.H.E.; Schmidt, H.-W.; Ober, C.K..
Tailored star-shaped statistical teroligomers via ATRP for lithographic applications,
J. Mater. Chem. **2012**, *22*, 73-79.
5. **Gröschel, A. H.**; Schacher, F. H.; Schmalz, H.; Borisov, O. V.; Zhulina, E. B.; Walther, A.; Müller, A. H. E.
Precise hierarchical self-assembly of multicompartement micelles,
Nat. Commun. **2012**, *3*, 710-717.
6. Hanisch, A.; **Gröschel, A. H.**; Schacher, F. H.; Förtsch, M.; Drechsler, M.; Müller, A. H. E.
Worms, beehives and woodlice - Evolution of multicompartement micelles from new ABC Miktoarm-star-terpolymers,
Pol. Mater. Sci. Technol. **2012**, 95.
7. **Gröschel, A. H.**; Walther, A.; Löbbling, T. I.; Schmelz, J.; Hanisch, A.; Schmalz, H.; Müller, A. H. E.
Facile, large-scale synthesis of soft, nanosized Janus particles with widely tunable properties,
J. Am. Chem. Soc. **2012**, *134* (33), 13850–13860.
8. Müllner, M.; Lunkenbein, T.; Schieder, M.; **Gröschel, A. H.**; Miyajima, N.; Förtsch, M.; Breu, J.; Caruso, F.; Mueller, A. H. E.
Template-directed mild synthesis of anatase hybrid nanotubes within cylindrical core-shell-corona polymer brushes,
Macromolecules **2012**, *45* (17), 6981-6988.
9. **Gröschel, A. H.**; Löbbling, T. I.; Petrov, P. D.; Müllner, M.; Kuttner, C.; Wieberger, F.; Müller, A. H. E.
Janus micelles as effective supracolloidal dispersants for carbon nanotubes,
Angew. Chem. Int. Ed. **2013**, *52* (13), 3602-3606; *Angew. Chem.* **2013**, *125* (13), 3688-3693.
10. **Gröschel, A. H.**; Walther, A.; Löbbling, T. I.; Schacher, F. H.; Schmalz, H.; Müller, A. H. E.
Guided hierarchical co-assembly of soft patchy nanoparticles,
Nature **2013**, doi:10.1038/nature12610

List of Conference Contributions

Oral Presentations

1. July 2010 in Glasgow, Scotland at the **Macro2010: 43rd IUPAC World Polymer Congress**: Polymer based ampholytic Janus discs
2. July 2010 in Prague, Czech Republic at the **74th PMM conference**: Multicompartment micelles and hierarchical superstructures from linear triblock terpolymers
3. March 2011 in Beer Sheva, Israel at the **9th Stadler Minerva Student Symposium**: Precise hierarchical self-assembly of multicompartment micelles
4. January 2012 in Doha, Qatar at the **14th IUPAC conference on Polymers and Organic Chemistry**: Controlled colloidal (co-)polymerization

Poster Presentations

1. 2009 in Bayreuth, Germany at the **Bayreuth Polymer Symposium '09**: Synthesis and phase behavior of linear poly(*tert*-butyl methacrylate)-*b*-poly(cinnamoyloxyethyl methacrylate)-*b*-poly(2-(dimethylamino)ethyl methacrylate) triblock terpolymer
2. 2009 in Houffalize, Belgium at the **CRP meeting**: Cationic block copolymers by AR-GET ATRP: Organogelation triggered by charge introduction
3. 2010 in Prague, Czech Republic at the **24th Conference of the European Colloid and Interface Society**: Shell-compartmentalized and multicompartment micelles from linear triblock terpolymers
4. 2011 in Bayreuth, Germany at the **Bayreuth Polymer Symposium '11**: Precise hierarchical self-assembly of multicompartment micelles
5. 2011 in Bonn, Germany at the **1st Bonn Humboldt Award Winners' Forum 'Frontiers in Macromolecular and Material Science'**: Precise hierarchical self-assembly of multicompartment micelles

Acknowledgements

Mastering a thesis is a comprehensive journey, leading through ups and downs both physically and mentally. It goes without saying that this undertaking was not the work of one, but rather a joint project of much collaboration each of which a unique experience and some even a push into the right direction. I would like to take the opportunity and thank all the people I was fortunate to work with.

First and foremost, I would like to express my deep gratitude to Prof. Dr. Axel H.E. Müller for several reasons. Most importantly for letting me work in the highly motivated group of MC2, where I was allowed to pursue ideas and projects not supervised by a firm hand, but in a fruitful, respectful and kind working atmosphere. I owe him a lot of gratitude for the many possibilities to present my work to the science community on renowned conferences. His inspiring attitude and versatile interest in many research fields rubbed off onto the working group and induced a self-dynamic and dedicated environment that evolved into thriving research atmosphere for all members. He left it to everyone, to decide for himself how much supervision one wanted to claim or to be left to one's own device and to learn to take responsibility and be independent. I am very thankful that I could not only gather invaluable experience in the most important aspects of research, collaboration and management, but also getting to know the world of academia first hand. I felt drawn into this world bit by bit, which is to a great part the credit of Prof. Müller.

To my collaborator, desk neighbour, closest friend, girlfriend and roommate Tina Löbling, I owe countless thanks, as she gave me a new beautiful place to live and more importantly a place in her heart. With her cheerful and kind personality she made every day bright and entertaining even when projects looked grim and experiments hopeless. Especially to the end of my work she was a constant support helping to master everyday life just as well as practical work in the laboratory. I am very much looking forward into our mutual future as a team in life as in academic activities.

I want to acknowledge many other people I had the privilege to meet and work with during my time in Bayreuth. Markus Müllner was my hood-neighbour for almost three years and the many common interests in chemistry and even more importantly enjoying life with all its aspects, opportunities and events will bring us together from time to time. Felix Schacher marked a cornerstone in my life I can clearly remember as if it just happened. He gave me push into the right direction, namely entering MC2 and becoming a polymer chemist, at a time I didn't have the overview to make that decision by myself. Andreas Walther for the many, many, many times he gave me valuable advice, for all the collaborations and especially for guiding me and introducing me to my new boss. He was a constant teacher during my studies, my diploma and my PhD, and it appears that he is and always will be at least one step ahead of me. Within the group of MC2 and other groups, there are many people that came and left, and left a deep impression. All of them were a part of my life and I want to thank all of them in no particular order: Sandrine Tea and André Pfaff, the always good-humoured Jiayin Yuan, Alexander Schmalz, Alexander (Sascha) Yakimansky, Joachim Schmelz, Klaus Kreger, my GPC mentor Sabine Wunder and the GPC

magician Marietta Böhm, my lab mates Stephan Weiß and Thomas Ruhland, Alexander Majweski, Felix Plamper, Christopher Synatschke, Youyong Xu, Markus Drechsler, Eva Betthausen, Christian Neuber, Francesca Bennet, Marina Krekhova, Kerstin Küspert, Anuj Mittal, the Spanish connection Ramón Novoa-Carballal and Lourdes Pastor-Pérez, Holger Schmalz, my next tenant Zhicheng Zheng, Markus Burkhardt, Bing Fang, the strongest cocktail Sergey Nosov & Pierre-Eric Millard, Shohei Ida, Andrea Wolf, Karina Möller, my neighbours Daniela Pirner and Moritz Tebbe, Stefan Reinicke, Anja Goldmann, Manuela Schumacher, Ainhoa Tolentino Chivite, Markus Ruppel, Michael Witt, the barbeque division of the AC terrace Daniel Kunz, Marko Schmidt, Axel Herrmann, Patrick Feicht, the network gaming community Andreas Ringk, Florian Wieberger, Robin Pettau, Tristan Kolb, Florian Richter, Andreas Haedler, Christian Probst, Christian Schneider my former roommates Julian Lang, Markus Weiß, Bertram Barnickel, my colleges during studies Markus Retsch, Michael Möller, Bertram Barnickel, Sandra Breyer, André Wicklein, Christina Görmer, Tine Schödel, Dominik Erhardt, Eva Max, Anne Horn, Marc Schrunner and many others...

I owe special thanks to my family for always being there for me in difficult times and providing me with a safe haven to relax. In particular my mother Anita having things in mind when I sometimes could not keep a level head, my brother Sebastian for his life welcoming attitude and especially, my father Klaus who was the main reason I grew up to become who I am now. From the early beginnings of grammar school to university he always provided me with everything I needed, with both advisory support and financially, and he was an inspiration forming not only my character but also my perception of life.

And finally Bayreuth/Bayreuth University for being such a nice place to study and for providing so many opportunities to get distracted from work.

Erklärung

Die vorliegende Arbeit wurde von mir selbst verfasst und ich habe dabei keine anderen Hilfsmittel und Quellen verwendet als die Angegebenen.

Ferner habe ich nicht versucht anderweitig, mit oder ohne Erfolg, eine Dissertation einzureichen oder mich der Doktorprüfung zu unterziehen.

Bayreuth, den 15.10.2013

André H. Gröschel